

AD-A171 418

AN INVESTIGATION OF THE ELECTRODE KINETICS AND
ELECTROCHEMISTRY OF REFRAC (U) EIC LABS IN NORWOOD MA
S H WHITE ET AL JUL 86 C-674(F) ARO-19554 3-M5-5

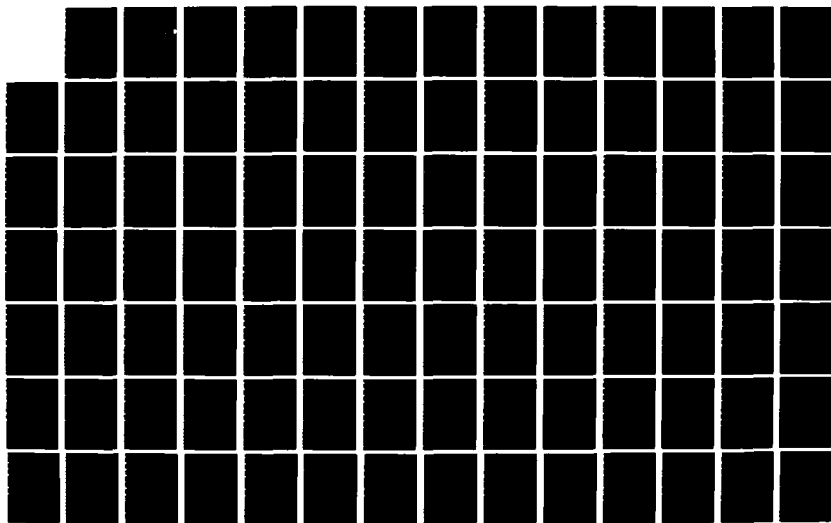
1/2

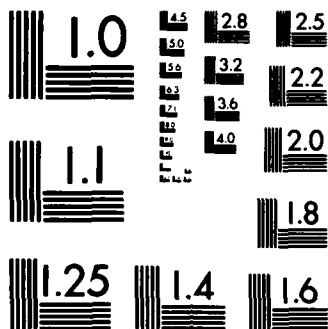
UNCLASSIFIED

DAAG29-82-C-0015

F/G 13/8

NL





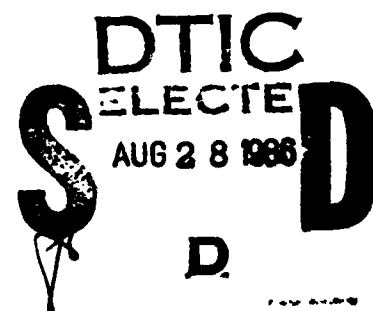
MICROCOPY RESOLUTION TEST CHART
NATIONAL BUREAU OF STANDARDS-1963-A

AD-A171 410

AN INVESTIGATION OF THE ELECTRODE KINETICS AND
ELECTROCHEMISTRY OF REFRACTORY METAL DEPOSITION

FINAL REPORT

April 26, 1982 - June 30, 1985



S. H. White and U. M. Twardoch

EIC Laboratories, Inc.
111 Downey Street
Norwood, Massachusetts 02062

CONTRACT NO. DAAG29-82-C-0015

Prepared for

U.S. Army Research Office
P.O. Box 12211
Research Triangle Park, NC 27709

July, 1986

Approved for Public Release;
Distribution Unlimited

The view, opinions, and/or findings contained in this report are those of the authors and should not be construed as an official Department of the Army position, policy, or decision, unless so designated by other documentation.

DTIC FILE COPY

UNCLASSIFIED

SECURITY CLASSIFICATION OF THIS PAGE (When Data Entered)

AD-A171410

REPORT DOCUMENTATION PAGE		READ INSTRUCTIONS BEFORE COMPLETING FORM
1. REPORT NUMBER ARO/9554.3ms-S	2. GOVT ACCESSION NO. N/A	3. RECIPIENT'S CATALOG NUMBER N/A
4. TITLE (and Subtitle) AN INVESTIGATION OF THE ELECTRODE KINETICS AND ELECTROCHEMISTRY OF REFRACTORY METAL DEPOSITION		5. TYPE OF REPORT & PERIOD COVERED Final Report 26 Apr 82 to 30 Jun 85
		6. PERFORMING ORG. REPORT NUMBER C-674(F)
7. AUTHOR(s) Sydney H. White and Urszula M. Twardoch		8. CONTRACT OR GRANT NUMBER(s) DAAG29-82-C-0015
9. PERFORMING ORGANIZATION NAME AND ADDRESS EIC Laboratories, Inc. 111 Downey Street Norwood, MA 02062		10. PROGRAM ELEMENT, PROJECT, TASK AREA & WORK UNIT NUMBERS N/A
11. CONTROLLING OFFICE NAME AND ADDRESS U.S. Army Research Office Post Office Box 12211 Research Triangle Park, NC 27709		12. REPORT DATE JULY 1986
		13. NUMBER OF PAGES 168
14. MONITORING AGENCY NAME & ADDRESS (if different from Controlling Office)		15. SECURITY CLASS. (of this report) UNCLASSIFIED
		15a. DECLASSIFICATION/DOWNGRADING SCHEDULE N/A
16. DISTRIBUTION STATEMENT (of this Report) Approved for public release; distribution unlimited.		
17. DISTRIBUTION STATEMENT (of the abstract entered in Block 20, if different from Report) N/A		
18. SUPPLEMENTARY NOTES The view, opinions, and/or findings contained in this report are those of the authors and should not be construed as an official Department of the Army position, policy, or decision, unless so designated by other documentation.		
19. KEY WORDS (Continue on reverse side if necessary and identify by block number) Molten salts, Solution electrochemistry, Chromium electrocrystallization, Molybdenum electrocrystallization, Pulse plating, Refractory metal plating		
20. ABSTRACT (Continue on reverse side if necessary and identify by block number) Electrochemical methods represent important ways in which the refractory metal coatings can be applied to the more active metals and alloys to take advantage, at the new surface, of their superior properties to provide erosion and corrosion protection. Currently, of the refractory metals, only chromium can be plated from aqueous solution, albeit in a form that is not entirely free of cracks and pores. These aberrations in the coating can lead to protection failure under severe conditions. The remaining metals can be plated from		

DD FORM 1 JAN 73 1473

EDITION OF 1 NOV 65 IS OBSOLETE

UNCLASSIFIED

SECURITY CLASSIFICATION OF THIS PAGE (When Data Entered)

20. ABSTRACT (Cont.)

molten fluoride electrolytes at temperatures in excess of 700°C. It is clear that less severe operating conditions are required for the plating of these metals, to take advantage of their properties in coatings upon as wide a range of materials as possible. The plating process involves the transport of ionic species, established in an ionic medium, to the solution electrode interface at which these species undergo electron transfer reactions and ligand removal to form metal atoms at favored sites. The aggregation of these atoms into clusters of nuclei, their growth into crystallites, and the accumulation of crystallites into a coherent polycrystalline metal coating, represents the final stages of the complex process of metal plating. This program of work has explored some aspects of each of these contributing processes to develop a scientific basis for the design of new plating baths and techniques which can be operated for chromium and molybdenum at substantially lower temperatures.

Molybdenum is a metal of particular interest since fluoride plating baths are not entirely satisfactory because of the high temperature and the concomitant instability of the solutions. The low melting zinc chloride - alkali metal chloride mixtures were explored as alternative electrolytes for molybdenum (III) solutions for plating. It was found that because of the acidity of the zinc chloride, in the Lewis sense, the solution chemistry of Mo(III) involves the formation of metal-metal bonded complexes which modify the reduction pathways in such a way that only lower oxidation states are reached within the electrochemical window of the zinc chloride containing electrolytes at temperatures between 270-400°C. By raising the basicity of the melt and employing a cation combination which ensures a wider electrochemical window, the problems associated with the solution chemistry of molybdenum are reduced. In the LiCl-KCl eutectic mixture, it has been shown that the solutions of Mo(III) involve an equilibrium between a monomer and a dimer species (of the chloride bridging type). The equilibrium constant has been determined from cyclic voltammetric and potential step measurements. The formation and growth of nuclei from these melts was studied briefly and the nucleation rates as well as the surface interaction energy between molybdenum and gold were determined. The results of this chemistry suggest ways by which the plating of molybdenum from these melts can be successful. The electroplating of molybdenum was demonstrated by using pulsed currents.

The solution chemistry of chromium (II) and (III) in halide melts is considerably simpler than the case of molybdenum. It has been suggested that such solutions provide an improved deposit quality which for specialized applications might justify the additional difficulties associated with employing a molten salt electrolyte. From a fundamental point of view, the chromium system offers a test bed for exploring the processes of nucleation and growth of metal from a molten salt electrolyte. The influence of temperature, substrate composition, and electrolyte composition have been explored for the deposition of chromium from Cr(II) containing solutions in bromide and chloride electrolytes. The measurements have been made both by potential step and current step methods. The values obtained for the nucleation rates, from classical theory, are in reasonable agreement from the two methods as are the surface interaction energies. The results of this study of chromium again indicate how coherent deposits of the metal might be formed and plating experiments have shown that under pulsed current conditions coherent deposits can be obtained at temperatures as low as 335°C.

TABLE OF CONTENTS

<u>Section</u>		<u>Page</u>
1.0	INTRODUCTION.	1
2.0	EXPERIMENTAL.	5
2.1	Materials.	5
2.2	Solvent Preparation.	5
2.3	Experimental Apparatus and Electrochemical Cells	7
2.3.1	General	7
2.3.2	Electrodes.	7
2.4	Electrochemical Techniques	14
2.4.1	General	14
2.4.2	Pulse Plating	14
2.5	Electrochemical Procedures	18
2.5.1	General	18
2.5.2	Fundamental Studies	18
2.5.3	Plating Studies	18
3.0	RESULTS AND DISCUSSION.	20
3.1	Program Overview	20
3.2	Solution Chemistry of Chromium in Alkali Metal Halide Melts	20
3.2.1	Solutions of Cr(II) in Lithium Chloride - Potassium Chloride Eutectic Mixture . . .	20
3.2.2	Solutions of Cr(III) in Lithium Bromide - Potassium Bromide - Caesium Bromide Eutectic Mixture.	32
3.2.3	Solutions of Cr(II) in Lithium Bromide - Potassium Bromide - Caesium Bromide Eutectic Mixture.	43
3.2.4	Discussion of Chromium Solution Chemistry	50
3.3	Electronucleation and Growth of Chromium on Different Substrates	56
3.3.1	Potential Step Measurements	56
3.3.2	Discussion of Potential Step Results. . .	69



1	<input checked="" type="checkbox"/>
2	<input type="checkbox"/>
3	<input type="checkbox"/>

Availability Codes	
Dist	Avail and/or Special
A-1	

TABLE OF CONTENTS
(Continued)

<u>Section</u>	<u>Page</u>
3.3.3 Current Step Measurements.	95
3.3.4 Discussion of Galvanostatic Results.	95
3.4 Solution Chemistry of Molybdenum in Alkali Metal Chloride Containing Melts	107
3.4.1 Electrochemistry of Molybdenum in Zinc Chloride - Potassium Chloride Mixtures	107
3.4.2 Electrochemistry of Molybdenum in Lithium Chloride - Potassium Chloride Eutectic Mixture.	128
3.5 Electrocrystallization of Molybdenum from Lithium Chloride-Potassium Chloride Eutectic Mixture at 450°C	132
3.5.1 Discussion	138
4.0 PLATING OF CHROMIUM AND MOLYBDENUM FROM LOWER MELTING HALIDE ELECTRODES.	139
5.0 REFERENCES	150

LIST OF FIGURES

		<u>Page</u>
Fig. 1	Preelectrolysis between a graphite anode and a tungsten cathode at 2.2V for the ternary alkali bromide eutectic (LiBr-KBr-CsBr).	8
Fig. 2	Background cyclic voltammograms acquired on gold electrodes at 0.1 Vs ⁻¹ in four solvents: LiBr-KBr-CsBr; LiCl-KCl; ZnCl ₂ -KCl(2:1); ZnCl ₂ -KCl(1:1) at 320°C and 450°C.	9
Fig. 3	Cooling curve for ternary bromide eutectic mixture LiBr-KBr-CsBr.	10
Fig. 4	Vacuum line and auxiliary gas lines.	11
Fig. 5	Electrochemical and plating cells.	12
Fig. 6	Various electrode designs.	15
Fig. 7	Typical cell inserts	16
Fig. 8	Pulsed current waveform and circuit diagram for generation of current pulses and capture of resultant potential time transients	17
Fig. 9	Normal pulse voltammograms for reduction and oxidation of Cr(II) ions in LiCl-KCl eutectic mixture at 425°C . .	21
Fig. 10	Plot of log {(i _L /i)-1} vs. potential for the oxidation of Cr(II) in LiCl-KCl solution at 425°C.	22
Fig. 11	Voltammogram illustrating the redox behavior of Cr(II) ions in molten LiCl-KCl.	24
Fig. 12	Current reversal chronopotentiograms for the oxidation and reduction of Cr(II) in LiCl-KCl eutectic at 425°C on a gold electrode and on a chromium coated copper electrode.	25
Fig. 13	Change in Cr(II) ion concentration after electrolytic generation of Cr(II) as measured by a Cr ²⁺ /Cr indicator electrode in LiCl-KCl at 425°C	29
Fig. 14	Cyclic voltammograms acquired at a scan rate of 0.5 V/s for the electro-oxidation of Cr(II) in LiCl-KCl eutectic at 425°C on Pt and gold electrodes	31

LIST OF FIGURES
(Continued)

	<u>Page</u>
Fig. 15	Differential pulse voltammograms acquired on a gold electrode in a solution of CrBr_3 in LiBr-KBr-CsBr at 381°C 33
Fig. 16	Normal pulse voltammograms for the electroreduction of Cr(III) in LiBr-KBr-CsBr eutectic mixture at 374°C on a gold electrode. 34
Fig. 17	Cyclic voltammograms for the LiBr-KBr-CsBr eutectic and the eutectic with an addition of nominally 7.88×10^{-3} molal CrBr_3 35
Fig. 18	Cyclic voltammograms acquired at a gold electrode in a solution of 7.9×10^{-3} molal CrBr_3 in LiBr-KBr-CsBr eutectic at 381°C 36
Fig. 19	Current time transient acquired at gold electrode for the electroreduction of Cr(III) in LiBr-KBr-CsBr eutectic mixture at 377°C for the potential step -600 mV and -1.5V from the rest potential 0.543V vs. Ag/Ag(I) reference electrode. 39
Fig. 20	The influence of temperature on the voltammetric reduction peak on gold for Cr(II) ions in the ternary alkali bromide eutectic acquired at 50 mVs^{-1} 44
Fig. 21	Comparison of Cr(II) ion reductions relative to the solvent window at three different temperatures in the ternary bromide eutectic. 45
Fig. 22	Influence of switching potential on the deposition and stripping of Cr on gold from ternary bromide melt at 450°C and scan rate of 1 Vs^{-1} 46
Fig. 23	Plots of the peak current for the reduction of Cr(II) ions in the ternary alkali metal bromide melt at five different temperatures as a function of the square root of the scan rate. 47
Fig. 24	The influence of sweep rate on the development of the prepeak during the reduction of Cr(II) on a gold substrate in the ternary alkali bromide eutectic at 293°C 48

LIST OF FIGURES
(Continued)

		<u>Page</u>
Fig. 25	Analysis of prepeak for the reduction of Cr(II) in the ternary alkali bromide eutectic at 295°C, gold substrate.	49
Fig. 26	Potential time analysis of galvanostatic transient for Cr deposited on chromium coated copper.	54
Fig. 27	Cyclic voltammograms illustrating overpotential deposition of Cr and the influence of switching potential on "nucleation crossover effect" in the return current sweep for nickel and copper substrates in LiCl-KCl containing 13 mM Cr(II) at 450°C.	55
Fig. 28	Cyclic voltammogram acquired on Pt electrode in LiCl-KCl containing 24 mM of Cr(II) at 100 mVs ⁻¹	57
Fig. 29	Current time transients from potential step experiments for the deposition of chromium on a platinum substrate from a solution of Cr(II) ions in LiCl-KCl eutectic mixture (450°C)	58
Fig. 30	Current time transients from potential step experiments for the deposition of chromium on a gold substrate from a solution of Cr(II) ions in LiCl-KCl eutectic mixture (425°C)	58
Fig. 31	Chronoamperogram for the reduction of Cr(II) ions on a copper substrate; plot of i vs. $t^{-1/2}$ for data showing diffusion control	74
Fig. 32	Current time ^{1/2} plots of potential step transients showing linear region for and induction times for platinum substrate in LiCl-KCl eutectic at 450°C	77
Fig. 33	Current time ^{1/2} plots of potential step transients showing linear region for gold substrate in LiCl-KCl eutectic at 450°C	78
Fig. 34	Current time ^{1/2} plots of potential step transients showing linear region and induction times for copper substrate in LiCl-KCl eutectic at 450°C.	79
Fig. 35	Current time ^{1/2} plots of potential step transients showing linear region and induction times for copper substrate in LiCl-KCl eutectic at 425°C.	83

LIST OF FIGURES
(Continued)

		<u>Page</u>
Fig. 36	A plot showing the dependence of N_{sat} on overpotential for reduction of Cr(II) on platinum in LiCl-KCl containing Cr(II) at 24 mM.	84
Fig. 37	Plots of the arrested nucleus density as a function of measured overpotential according to the classical nucleation theory.	86
Fig. 38	Comparison of data of Vargas with the present work . . .	87
Fig. 39	Plot of steady state nucleation rate for chromium deposition on platinum substrate in LiCl-KCl-Cr(II) 24 mM at 450°C as a function of applied overpotential according to atomistic theory.	91
Fig. 40	Plot of the steady state nucleation rate vs. the overpotential for the deposition of chromium metal on gold and platinum substrates according to the atomistic theory	92
Fig. 41	Cyclic voltammograms acquired at 100 mVs ⁻¹ illustrating the differences in overpotential required at gold and platinum to initiate the reduction of Cr ²⁺ ions to chromium metal on these different substrates in LiCl-KCl at 450°C	93
Fig. 42	Plots of "induction time" τ' as a function of overpotential for deposition of chromium on gold and platinum at 450°C in LiCl-KCl-Cr(II).	94
Fig. 43	Current reversal chronopotentiogram for the reduction of Cr(II) ions at a platinum electrode in LiCl-KCl containing $24 \times 10^{-3}\text{M}$ Cr(II) at 450°C.	96
Fig. 44	Double pulse galvanostatic transients for a gold substrate in LiCl-KCl containing $24 \times 10^{-3}\text{M}$ Cr(II) at 450°C	99
Fig. 45	Double pulse galvanostatic transients recorded for the reduction of Cr(II) at a copper electrode at LiCl-KCl containing $47 \times 10^{-3}\text{M}$ Cr(II) at 450°C.	100
Fig. 46	Comparison of nucleation kinetics for the deposition of Cr on different substrates at 450°C in LiCl-KCl.	102

LIST OF FIGURES
(Continued)

	<u>Page</u>
Fig. 47 Temperature dependence on nucleation kinetics for the deposition of chromium on gold from the ternary bromide eutectic mixture at different temperatures.	103
Fig. 48 Cyclic voltammetric background of a molten 2:1 ZnCl_2 -KCl mixture of 320°C at scan rate 0.1 V/s on platinum, gold and glassy carbon electrodes	108
Fig. 49 Cyclic voltammograms acquired at scan rate 0.1 V/s on a platinum electrode in molten ZnCl_2 -KCl (2:1) mixture at 320°C.	111
Fig. 50 Cyclic voltammetric backgrounds acquired at scan rate 0.1 V/s on a platinum electrode in molten ZnCl_2 -KCl mixtures.	112
Fig. 51 Cyclic voltammetric backgrounds acquired at scan rate 0.1 V/s for a gold electrode at temperature 320°C in ZnCl_2 -KCl mixtures.	113
Fig. 52 Cyclic voltammetric backgrounds acquired at a scan rate of 1 V/s on a gold electrode in ZnCl_2 -KCl (2:1) mixture at temperature 320°C.	115
Fig. 53 Cyclic voltammograms acquired at a scan rate of 1 V/s at molybdenum electrode in molten ZnCl_2 -KCl (2:1) mixture at 320°C to different anodic potential	116
Fig. 54 Multicyclic voltammograms acquired at molybdenum electrode in molten ZnCl_2 -KCl (2:1) at 320°C of scan rates of 1 V/S, 0.1 V/s and 0.01 V/s.	118
Fig. 55 Cyclic voltammograms acquired at gold electrode at scan rate 0.1 V/s in a 1:1 ZnCl_2 -KCl melt at temperature 320°C containing K_3MoCl_6 at concentrations of 0.028 mol/kg and 0.129 mol/kg	119
Fig. 56 Cyclic voltammograms acquired at 0.1 V/s on a gold electrode for solutions of K_3MoCl_6 in molten ZnCl_2 -KCl mixtures.	120
Fig. 57 Cyclic voltammograms of 0.129 molal K_3MoCl_6 in 1:1 ZnCl_2 -KCl melt acquired at gold electrode at scan rate 0.1 V/s at temperatures of 320°C and 400°C.	121

LIST OF FIGURES
(Continued)

	<u>Page</u>
Fig. 58 Cyclic voltammograms obtained at different initial scan directions and rates at a gold electrode in a solution of 0.129 molal K_3MoCl_6 in 1:1 $ZnCl_2$ -KCl melt at 400°C. .	124
Fig. 59 Current reversal chronopotentiogram acquired at gold electrode in LiCl-KCl containing 0.0197 molal K_3MoCl_6 at 450°C, current pulses $\pm 70 \text{ mA cm}^{-2}$	129
Fig. 60 Cyclic voltammograms acquired on gold electrodes in LiCl-KCl containing K_3MoCl_6 at 550°C	130
Fig. 61 Current time transients acquired at gold electrode (0.43 cm^2) in molten LiCl-KCl mixture at 450°C for the reduction of Mo(III) at different overpotentials vs. Mo^{3+}/Mo	134
Fig. 62 Plot of $i_m^2 t_m$ vs. applied overpotential for molybdenum metal deposition on a gold substrate in LiCl-KCl eutectic mixture at 450°C.	136
Fig. 63 Current maximum from potential step measurements as a function of $t_m^{-1/2}$ for Mo deposition on a gold substrate from LiCl-KCl at 450°C	137
Fig. 64 SEM of chromium deposit from the ternary alkali metal bromide melt at 340°C.	142
Fig. 65 SEM of cross section of chromium deposition on stainless steel obtained from bromide melt at 340°C; nuclei formed and grown on copper substrate during 10 current pulses	143
Fig. 66 Ten potential time curves acquired during the galvanostatic pulsing of a copper substrate to deposit Cr metal nuclei from a ternary bromide melt at 335°C. . . .	144
Fig. 67 Micrographs of molybdenum deposit on nickel.	148
Fig. 68 Robinson backscattered electron image of cross section of a molybdenum deposit on nickel from LiCl-KCl bath at 450°C	149

LIST OF TABLES

<u>Table</u>		<u>Page</u>
1	SUMMARY OF THE ELECTROCHEMISTRY OF REFRACTORY METALS IN MOLTEN FLUORIDE MELTS	2
2	MATERIALS USED IN EXPERIMENTAL WORK	6
3	CYCLIC VOLTAMMETRIC DATA ON GOLD ELECTRODES AT 7 mM Cr (II) AT 425°C.	26
4	CHRONOPOTENTIOMETRIC DATA ON GOLD ELECTRODES AT 7 mM Cr (II) AT 425°C.	27
5	CYCLIC VOLTAMMETRIC DATA ON GOLD ELECTRODES AT 7 mM Cr (II) AT 425°C 17-24 HOURS AFTER DATA TAKEN IN TABLE 3	28
6	ANODIC/CATHODIC CYCLIC VOLTAMMETRY DATA FOR Cr ²⁺ (24 mM) IN LiCl-KCl AT 450°C.	30
7	ANALYSIS OF CYCLIC VOLTAMMETRIC DATA FOR REV/SOL BOTH OX AND RED IN SOLUTION	37
8	ANALYSIS OF CYCLIC VOLTAMMETRIC DATA FOR REV/SOL BOTH OX AND RED IN SOLUTION	38
9	ANALYSIS OF REPRESENTATIVE DOUBLE STEP CHRONOAMPEROMETRIC DATA FOR THE REDUCTION OF Cr (III) TO Cr (II) IN ALKALI METAL BROMIDE MELT AT 382°C	40
10	ANALYSIS OF REPRESENTATIVE CHRONOAMPEROMETRIC DATA FOR THE REDUCTION OF Cr (III) TO Cr (0) IN THE ALKALI METAL BROMIDE MELT AT 382°C	41
11	SUMMARY OF CHRONOAMPEROMETRIC AND COULOMETRIC RESULTS FOR LiBr-KBr-CsBr EUTECTIC AT 385°C	42
12	SUMMARY OF THE ELECTROCHEMISTRY OF CHROMIUM	51
13	POTENTIAL STEP RESULTS FOR PLATINUM SUBSTRATE (0.23 cm ²) IN LiCl-KCl EUTECTIC AT 450°C - FIRST CONCENTRATION CHROMIUM II	60
14	POTENTIAL STEP RESULTS FOR PLATINUM SUBSTRATE (0.23 cm ²) IN LiCl-KCl EUTECTIC AT 450°C - SECOND CONCENTRATION CHROMIUM II	61

LIST OF TABLES
(Continued)

<u>Table</u>	<u>Page</u>
15 POTENTIAL STEP RESULTS FOR PLATINUM SUBSTRATE (0.23 cm ²) IN LiCl-KCl EUTECTIC AT 450°C - THIRD CONCENTRATION CHROMIUM II	62
16 MEASUREMENTS OF $CAD^{1/2}$ FOR THE PLATINUM ELECTRODE (0.23 cm ²) AND THE CALCULATED VALUES OF $i_m^2 t_m$ PREDICTED FOR INSTANTANEOUS AND PROGRESSIVE NUCLEATION	63
17 POTENTIAL STEP RESULTS FOR GOLD SUBSTRATE IN LiCl-KCl EUTECTIC AT 425°C	64
18 POTENTIAL STEP RESULTS FOR GOLD SUBSTRATE IN LiCl-KCl EUTECTIC AT 450°C	65
19 POTENTIAL STEP RESULTS FOR GOLD SUBSTRATE IN LiCl-KCl EUTECTIC AT 450°C	66
20 MEASUREMENTS OF $CAD^{1/2}$ FOR GOLD ELECTRODES IN DIFFERENT HALIDE SOLVENTS AND THE CALCULATED VALUES OF $i_m^2 t_m$ PRE- DICTED FOR INSTANTANEOUS AND PROGRESSIVE NUCLEATION	67
21 POTENTIAL STEP RESULTS FOR GOLD SUBSTRATE IN THE TERNARY ALKALI METAL BROMIDE EUTECTIC AT 292°C.	68
22 POTENTIAL STEP RESULTS FOR COPPER SUBSTRATE IN LiCl-KCl EUTECTIC AT 425°C	70
23 POTENTIAL STEP RESULTS FOR COPPER SUBSTRATE IN LiCl-KCl EUTECTIC AT 425°C	71
24 POTENTIAL STEP RESULTS FOR NICKEL SUBSTRATE IN LiCl-KCl EUTECTIC AT 450°C	72
25 MEASUREMENTS OF $CAD^{1/2}$ FOR COPPER AND NICKEL ELECTRODES IN LiCl-KCl EUTECTIC AND THE CALCULATED VALUES OF $i_m^2 t_m$ PREDICTED FOR INSTANTANEOUS AND PROGRESSIVE NUCLEATION.	73
26 TIME DEPENDENCE OF EARLY PART OF GROWTH TRANSIENT FOR Cr DEPOSITION ON PLATINUM SUBSTRATE IN LiCl-KCl AT 450°C.	80
27 POTENTIAL STEP RESULTS - ANALYSIS AS i VS. $t^{3/2}$ OF INITIAL PORTION OF GROWTH TRANSIENT ON PLATINUM SUB- STRATE IN LiCl-KCl EUTECTIC AT 450°C.	82

LIST OF TABLES
(Continued)

<u>Table</u>	<u>Page</u>
28 SURFACE ENERGIES AND NUCLEATION RATE FROM POTENTIAL STEP DATA ACCORDING TO CLASSICAL NUCLEATION THEORY	88
29 COMPARISON OF RESULTS OF CLASSICAL NUCLEATION THEORY FOR DEPOSITION OF CHROMIUM ON A PLATINUM SUBSTRATE IN LiCl-KCl AT 450°C. PLOT OF $\ln A N_0$ vs. η^{-2}	89
30 TYPICAL CHRONOPOTENTIOMETRIC DATA FOR CHROMIUM (II) REDUCTION ON COPPER AT 425°C.	97
31 REPRESENTATIVE GALVANOSTATIC DATA FOR THE REDUCTION OF Cr(II) IONS ON DIFFERENT SUBSTRATES IN ALKALI HALIDE MELTS BETWEEN 295 and 450°C	98
32 GALVANOSTATIC RESULTS FOR CHROMIUM DEPOSITION ON DIFFERENT SUBSTRATES AS A FUNCTION OF MELT COMPOSITION AND TEMPERATURE	104
33 INFLUENCE OF TEMPERATURE ON THE NUCLEATION PROCESS FOR CHROMIUM DEPOSITION ON GOLD IN THE TERNARY BROMIDE MELT . . .	105
34 THE INFLUENCE OF SUBSTRATE COMPOSITION UPON THE NUCLEATION OF Cr METAL FROM LiCl-KCl SOLUTIONS AT 450°C	106
35 TYPICAL CYCLIC VOLTAMMETRIC DATA FOR THE ANODIC FORMATION OF THE PASSIVATION FILM AND CATHODIC REDUCTION OF THAT FILM IN MOLTEN ZnCl ₂ -KCl MIXTURE AT Pt ELECTRODE.	109
36 TYPICAL CYCLIC VOLTAMMETRIC DATA FOR THE REDUCTION AND REOXIDATION PROCESSES IN MOLTEN ZnCl ₂ -KCl AT GOLD ELECTRODE AT SCAN RATE 0.1 V/S.	114
37 TYPICAL CYCLIC VOLTAMMETRIC DATA FOR THE PRE-CATHODE PROCESS AT GOLD ELECTRODE IN MOLTEN ZnCl ₂ -KCl (2:1) MIXTURE AT 320°C.	114
38 CYCLIC VOLTAMMETRIC DATA FOR THE ANODIC OXIDATION OF THE MOLYBDENUM ELECTRODE IN MOLTEN ZnCl ₂ -KCl (2:1) AT 320°C .	114
39 REPRESENTATIVE NUMERICAL DATA FOR THE FIRST REDUCTION PEAK (c) OF THE VOLTAMMOGRAMS ACQUIRED IN A SOLUTION OF K ₃ MoCl ₆ IN MOLTEN ZnCl ₂ -KCl (2:1) ON A GOLD ELECTRODE	123
40 CYCLIC VOLTAMMETRIC DATA FOR THE OXIDATION AND CORRESPONDING REDUCTION PROCESS OF THE SOLUTION OF K ₃ Mo ₃ Cl ₂ IN MOLTEN ZnCl ₂ -KCl (1:1) AT 400°C AT GOLD ELECTRODE.	125

LIST OF TABLES
(Continued)

<u>Table</u>	<u>Page</u>
41 REPRESENTATIVE NUMERICAL DATA FOR THE SECOND REDUCTION PROCESS OF THE VOLTAMMOGRAMS ACQUIRED IN A SOLUTION OF K_3MoCl_6 IN MOLTEN $ZnCl_2-KCl$ (1:1) IN GOLD ELECTRODE	126
42 REPRESENTATIVE NUMERICAL VOLTAMMETRIC DATA ACQUIRED AT A GOLD ELECTRODE IN MOLTEN $LiCl-KCl$ MIXTURE CONTAINING K_3MoCl_6 . a) 5.06×10^{-3} mol/Kg at $550^\circ C$. b) 19.7×10^{-3} mol/Kg at $450^\circ C$	131
43 EQUILIBRIUM CONSTANTS DETERMINED FOR THE MONOMER DIMER EQUILIBRIUM INVOLVING $Mo(III)$ SPECIES IN $LiCl-KCl$ EUTECTIC. .	133
44 POTENTIAL STEP RESULTS FOR GOLD SUBSTRATE IN $LiCl-KCl$ EUTECTIC AT $450^\circ C$	135
45 ELECTROPLATING EXPERIMENTS - CHROMIUM DEPOSITION FROM A LITHIUM CHLORIDE-POTASSIUM CHLORIDE-CHROMOUS CHLORIDE SOLN (0.27 wt %) AT $450^\circ C$	140
46 ELECTROPLATING EXPERIMENTS - CHROMIUM DEPOSITION FROM A LITHIUM BROMIDE-POTASSIUM BROMIDE-CESIUM BROMIDE- CHROMIUM(II) BROMIDE SOLUTION AT $335 \pm 5^\circ C$	141
47 COMPARISON OF CONDITIONS FOR THE ELECTRODEPOSITION OF CHROMIUM FROM DIFFERENT ELECTROLYTES	146
48 ELECTROPLATING EXPERIMENTS - MOLYBDENUM DEPOSITION FROM A LITHIUM CHLORIDE-POTASSIUM CHLORIDE-POTASSIUM HEXA- CHLOROMOLYBDATE SOLUTION AT $455^\circ C$	147

1.0 INTRODUCTION

The refractory metals, i.e., those transition metals belonging to Groups IV-VIB of the periodic table are known as "super metals" because they offer useful mechanical and chemical properties which enable them to be used under conditions where other metals fail. Thus they, together with their alloys are commonly used in extreme conditions such as those associated with high acidity, high radioactivity, high temperatures, and where erosion is severe. Of particular interest are conditions where high temperatures, erosion and corrosion coexist. The ability to form protective coating of these metals and alloys becomes paramount. There are numerous methods which include chemical vapor deposition, plasma spraying, metallizing and electroplating for the production of coating. Electroplating is particularly attractive because it also enables thick deposits (electroforms) of these materials to be produced.

Electrodeposition of metals from molten salts has been practiced successfully on an industrial scale for the winning of, for example, aluminum, magnesium, calcium, lithium, and sodium (1). Titanium, tantalum, and niobium (2) have also been electrodeposited in dendritic form in large scale operations. Electroplating, on the other hand, requires coherent metal formation, a severe restriction which has limited success to but a few metals which include the refractory metals, the precious metals, and aluminum. Union Carbide, in the 1960s, announced a generalized process for electroplating refractory metals from molten fluoride electrolytes (2,4). Table 1 shows the operating temperatures, metal ion oxidation states and reduction pathways for these processes (2-4). Molten alkali fluorides have a number of advantages as electrolytes. They are good solvents with good complexing properties which enable the refractory metal cations to be stabilized in solution in a variety of oxidation states. High solute precursor concentrations are thereby achievable, leading to a wide range of plating conditions. The alkali fluoride solvents possess high conductivities which minimize IR losses at the high rates of metal deposition possible. The molten fluoride electrolyte acts as a fluxing agent to remove scale from work pieces within the electrolyte. The wide electrochemical window in alkali fluoride solvents provides a versatile electrolyte both suitable for the electrodeposition in coherent form of all nine of the refractory elements at moderate cost (4). On the other hand, the molten fluoride electrolyte baths possess a number of disadvantages amongst which are the following. The operation of the electrolyte baths requires temperatures in excess of 600°C, see Table 1, which limits the choice of materials for the construction of the plating cells and for the substrates available as cathodes. In addition, composite materials which undergo thermally induced transformations may be excluded even though they are solid at the plating bath temperature. The electrolyte can be modified by atmospheric contamination, and the plating process is sensitive to impurities such as oxide and chloride ions (5). When lithium

TABLE 1

SUMMARY OF THE ELECTROCHEMISTRY OF REFRACTORY
METALS IN MOLTEN FLUORIDE MELTS

Group	T°C	Element	Mean Valency	Reduction Sequence
Group IV	-	Ti	3	$Ti^{3+} \rightarrow Ti$
	700	Zr	4	$Zr^{4+} \rightarrow Zr$
	700	Hf	4	$Hf^{4+} \rightarrow Hf$
Group V	600/800	V	3	$V^{3+} \rightarrow V$
	600	Nb	4	$Nb^{4+} \rightarrow Nb^{+} \rightarrow Nb$
	600/800	Ta	5	$Ta^{5+} \rightarrow Ta^{2+} \rightarrow Ta$
Group VI	700/1000	Cr	3?	$Cr^{3+} \rightarrow Cr^{2+} \rightarrow Cr$
	700	Mo	3.3	$Mo^{3+} \rightarrow Mo$
	700	W	4.5	$W^{4+} \rightarrow W$

containing electrolytes are used, cleanup of the plated article can be a problem because of the low solubility of the fluoride salt, and finally, fluorides and their vapors are toxic.

Prior to and subsequent to the development of the Union Carbide process, many electrolyte compositions have been considered for electroplating of the refractory metals. Oxyanionic melts have been examined (6-8), but the ease of reducibility of the oxyanion, the strong probability for oxygen contamination, through oxidation of the metal during reduction of the oxyanion and the formation of anodic oxide films, limit the usefulness of these melts. On the other hand, early work had shown that in the case of tungsten, complex mixture of borates and tungstates could lead to the formation of coherent tungsten plates (6). Recent results for molybdenum and tungsten (8) have suggested that molybdates and tungstates can be employed as precursors for metal formation from halide electrolytes. Liquid organic salts such as the quaternary 'onium salt represent another alternative solvent group for plating baths. These have been considered either as a component in a mixture with aluminum halides (9,10) or in the pure state. The aluminum chloride based melts appear to favor cluster compound formation (11) and are good solvents for such syntheses (12). So far, experiments have failed to produce coherent metal deposits of the refractory metals from these melts (13).

The present research has focused upon two fundamental aspects of the electroplating of the refractory metals - chromium and molybdenum:

- Electrolyte composition and the association solution chemistry and reduction pathways to metal.
- The mechanisms and kinetics associated with the electrocrystallization of these two metals.

At the same time, an attempt has been made to use the information gained in the studies to develop current pulsed plating for these metals.

In the case of electrolyte composition, the cation and anion components of the electrolyte determine the electrochemical range of stability of the electrolyte and hence the suitability for the reduction of the refractory metal ion component. In addition, the cations and anions play a major role in determining the stability of the metal precursor and the charge requirement for the electroreduction process. It is well known that the pure refractory metal compounds in high oxidation states exhibit high volatility and disproportionation chemistry (14). In their lower oxidation states, these compounds are often complex and involve metal-metal bonded species (15) which may undergo disproportionation or polymerization. The behavior of such species in molten electrolyte solutions is not well known and is a major task which will have to be addressed in order to improve the design of alternate plating baths. The successful use of fluoride electrolytes as plating baths probably arises from the strong complexing power of the fluoride ions which results in simpler solution chemistry in these electrolytes.

The initial phase of the work attempted to develop compositions of zinc chloride-potassium chloride for the deposition of molybdenum at temperatures considerably below those required in the fluoride process. It turns out that these melts apparently favor the formation of intermediates which modify the pathway to metal in such a way that the reduction of the solvent cations (Zn^{+2}) occurs prior to molybdenum metal formation. Under these circumstances, attention was turned toward the use of low melting alkali halide mixtures which perhaps offer the best alternative, low temperature of operation, solvents for the development of electroplating baths for the refractory metals (VIA), and studies in both chloride and bromide mixtures are reported.

In the case of the metal electrocrystallization mechanisms, it is important to know both the reduction pathway to metal (Table 1), and the kinetics of the reduction of the metal ion to coherent metal. It turns out that the electrochemistries of chromium and molybdenum involve increasingly complex reduction pathways which enable different aspects of the metal forming processes to be examined. The electroreduction of $Cr(II)$ ions to metal provides a relatively simple example of metal formation from the solution complex $CrCl_4^{-2}$. In contrast, the reduction of molybdenum occurs from $Mo(III)$ ions which exist in two forms in solution, and consequently the reduction process is complicated by the presence of a preceding chemical equilibrium. The results of potential step experiments in this work show that the growth of depositing molybdenum metal nuclei reflects

the presence of this preceding reaction. In conjunction with results from other studies (16), it is also clear that the solution chemistry in the form of cation composition plays a role. Previous work with liquid metal electrodes, where electrocrystallization processes are absent, has shown that in molten salts at around 450°C the exchange current density for the charge transfer process is greater than 1 A cm⁻² (17). The results from the studies of chromium phase formation show that the initial nucleation process depends upon the nature of the substrate and the temperature.

These studies have identified the importance of the metal electrocrystallization processes in refractory metal deposition which extends the recent results for silver, cobalt, and copper deposition in molten salts. These results are particularly relevant to the understanding and design of electroplating and forming of the refractory metals and are the first of their kind for these metals. The details of these processes and their relationships to the control of the physical properties of the deposit, including grain size hardness as well as diffusion and reaction overvoltages, remains to be fully quantified and should be an important aspect of fundamental studies in the area of refractory metal plating in the future.

2.0 EXPERIMENTAL

2.1 Materials

Table 2 summarizes the chemical compounds and materials, their sources, and qualities used in this study. The solvents for use in the studies reported here were prepared from the salts in Table 2. Their compositions are as follows:

ZnCl ₂ :KCl	mp. 262°C
mol% 71 :29	
ZnCl ₂ :KCl	mp. 250°C
mol% 51.5 :48.5	
LiCl :KCl	mp. 365°C
mol% 59 :41	
LiBr :KBr :CsBr	mp. 236°C
mol% 56 :19 :25	

2.2 Solvent Preparation

The solvents were prepared in 300-500 gram batches using some or all of the following unit operations whose detail has been discussed previously (18).

- Vacuum desiccation of each individual salt prior to makeup of the appropriate mixture.
- Stepwise vacuum drying of the mixture to just below the melting point.
- Melting under appropriate hydrogen halide atmosphere and subsequent treatment of the liquid with the acid gas to remove oxide, hydroxide and water.
- Displacement of hydrogen halide by argon.
- Preelectrolysis between tungsten cathode and graphite anode under reduced pressure to remove trace metal ion impurities.
- Filtration to remove solid matter.
- Inert gas transfer of cooled product from filtration apparatus to dry box. Storage in sealed individual bottles.

The series of operations was carried out in a Pyrex vessel on a vacuum line (19). Preelectrolysis was carried out at a constant voltage which

TABLE 2
MATERIALS USED IN EXPERIMENTAL WORK

<u>Chemical</u>	<u>Quality</u>	<u>Source</u>
<u>Salts</u>		
LiCl	Certified	Fisher
KCl	ACS Certified	Fisher
ZnCl ₂	ACS Reagent	Aldrich
LiBr	Purified	Fisher
KBr	ACS Certified	Fisher
CsBr	99%	Alfa
AgCl	Certified	Fisher
AgBr	5N Grade	Cerac
K ₃ MoCl ₄		Climax
	Reagent	Paltz
CrCl ₂	Anhydrous	Alfa
CrBr ₃	>99%	Cerac
<u>Metals and Carbons</u>		
Chromium	Aluminothermic	
Molybdenum	3N7 sheet	Alfa
Tungsten	3N8 sheet	Alfa
Platinum	4N sheet/wire	Alfa
Gold	100% sheet/wire	Johnson Matthey
Silver	100% wire	Johnson Matthey
Copper	5N sheet/wire	Alfa
Nickel	200 shim	Shop Aid Inc.
Stainless Steel	304 shim	Shop Aid Inc.
Vitreous carbon	3mm rod V25	Le Carbone
Graphites	6 mm rod Spec pure	Johnson Matthey
<u>Gases</u>		
Argon	UHP	Airco
Hydrogen chloride	Electronic Grade	Airco
Hydrogen bromide		Airco

was selected to be compatible with the cation composition of the melt but give as wide a voltage span as possible (18,20). A typical current time curve for the preelectrolysis of the ternary bromide melt is shown in Figure 1. Typical background cyclic voltammograms on gold electrodes for the four purified solvents are shown in Figure 2. The melting point of the ternary bromide melt was measured and the cooling curve is shown in Figure 3.

2.3 Experimental Apparatus and Electrochemical Cells

2.3.1 General

The gas lines and vacuum system are shown schematically in Figure 4. The cells were connected to the vacuum/gas lines via a flexible stainless steel tube fitted with Pyrex cup joints. The header for the purification cell C was a Pyrex top hat with four #7 Ace thread joints which carried the bubbler, breaker and preelectrolysis electrodes sealed with viton "O" rings backed by Teflon bushes (18). Rotary pumps enabled pressures to be reduced to less than 10 microns.

The electrochemical cells were heated in furnaces with wire wound resistance elements either fed by two adjustable 10 ampere variacs or a Eurotherm temperature controller and power supply. The temperatures were monitored with chromel alumel thermocouples either mounted near the furnace elements for control or in the cells for temperature measurement. The thermocouples were calibrated and supplied by Omega.

Two cell designs were used in this program of study and are illustrated in Figure 5. The cell for the electrochemical measurements consisted of a 75 mm diameter silica envelope 30-50 cm long and capped with a water cooled header which made an "O" ring seal to the tube. Electrodes were introduced into the cell through #7 Ace screw thread adapter joints sealed with viton "O" rings. The electrolyte was contained in an alumina crucible. In the case of the plating experiments, cell (B) was used. The outer Pyrex vessel, closed at one end, was 120 mm in diameter and 45 cm long with a flange to accommodate the Pyrex cell cap. It was provided with a central tower held in a 24 mm Cajon adapter to enable cathodes to be introduced into the cell without exposing the electrolyte to the atmosphere. The electrolyte bath was contained in an alumina crucible (McDaniel 99.9%), 85 mm diameter and 160 mm high. Inert gas could be introduced and maintained in the cathode tower assembly as well as the main cell compartment.

2.3.2 Electrodes

Counter Electrodes. In the case of plating experiments, the counter electrodes were of the metal to be plated. Molybdenum sheet was used to form an anode which was held with a steel screw on a molybdenum holder supported on a stainless steel rod, mounted in a 7 mm Pyrex tube. Irregular size pieces of chromium were spot welded to a thick platinum-rhodium wire supported in a 7 mm Pyrex tube. In the basic electrochemical experiments,

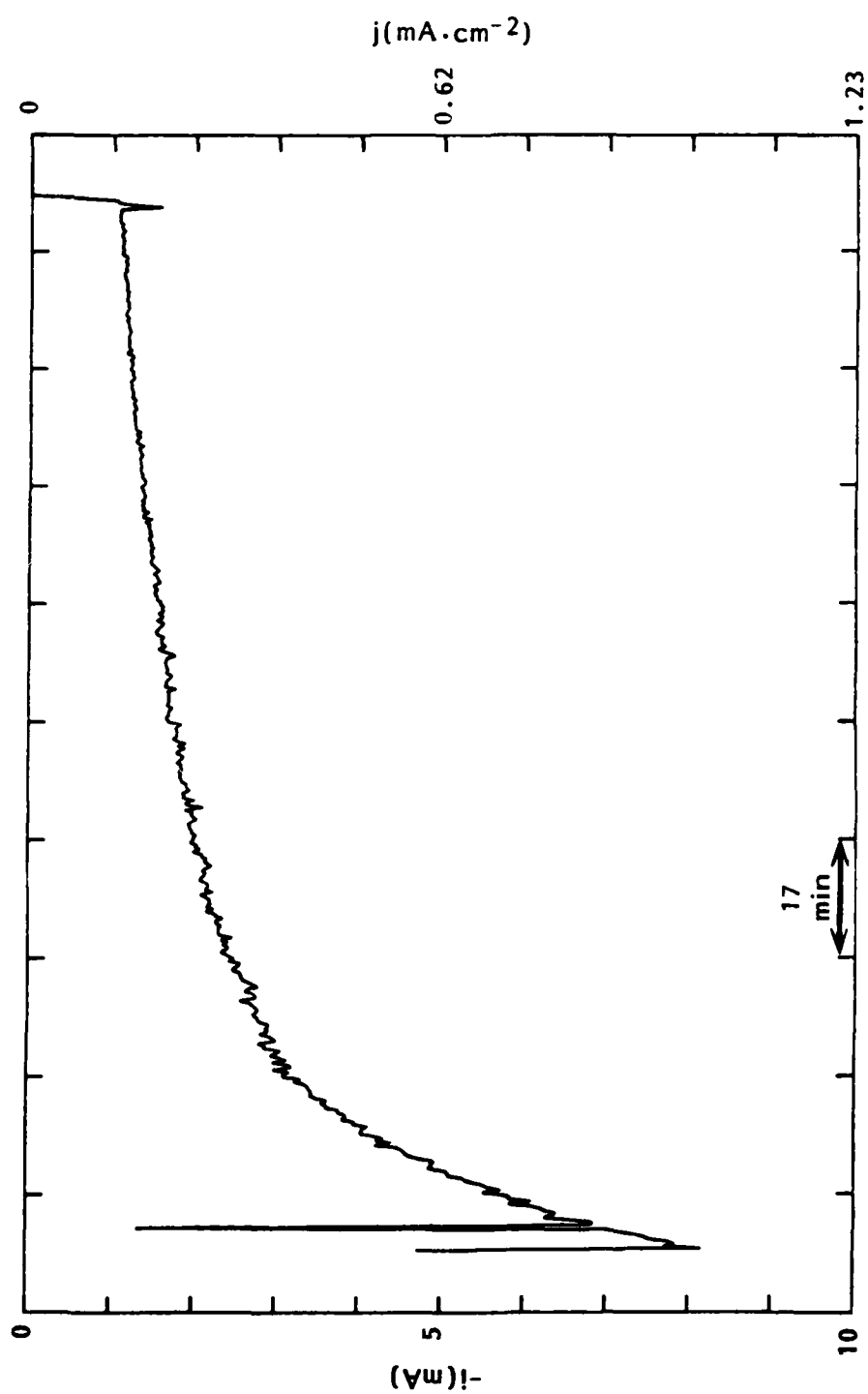


Fig. 1. Preelectrolysis between a graphite anode and a tungsten cathode (area 8.1 cm^2) at 2.2 V for the ternary alkali bromide eutectic (LiBr-KBr-CsBr).

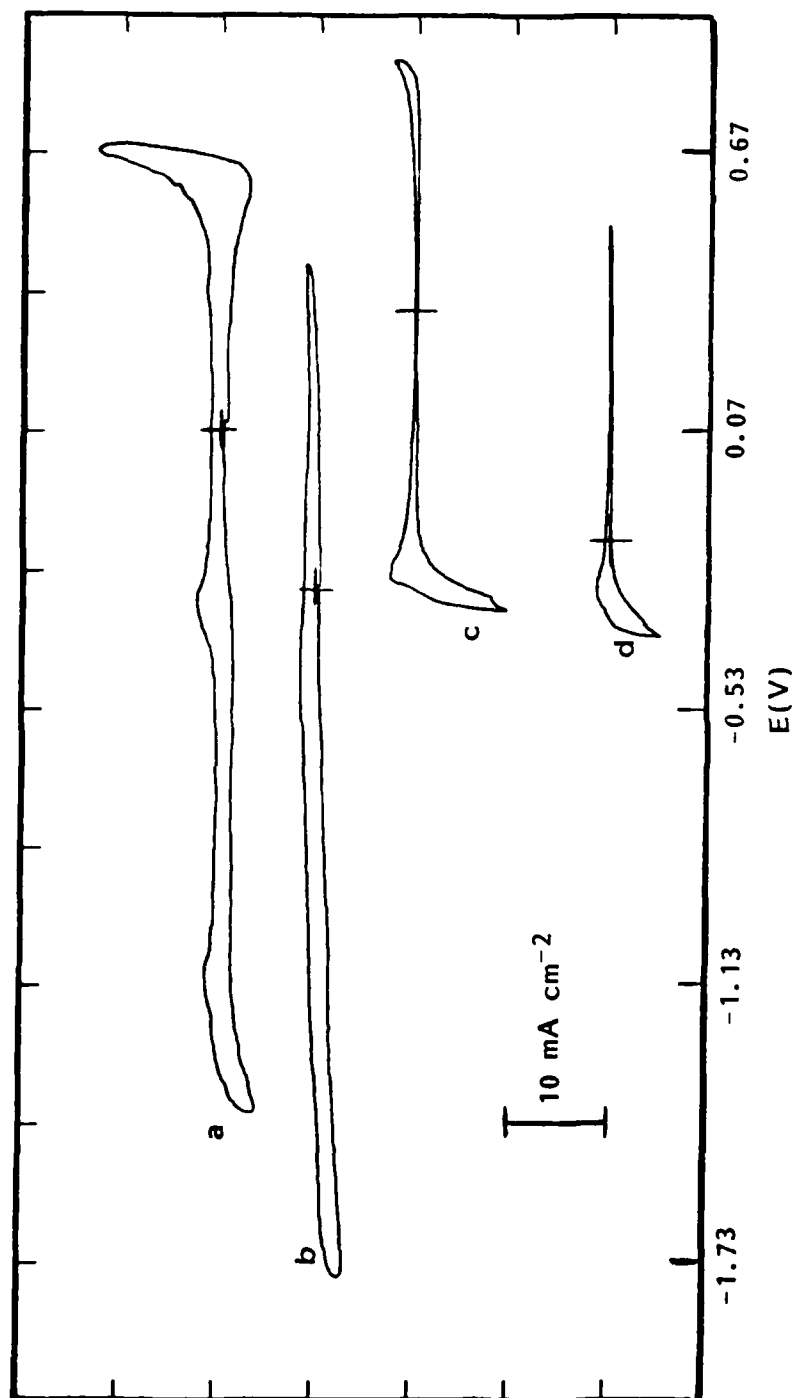


Fig. 2. Background cyclic voltammograms acquired on gold electrodes at 0.1 V s^{-1} in the four solvents: (a) LiBr-KBr-CsBr ; (b) LiCl-KCl ; (c) $\text{ZnCl}_2\text{-KCl (2:1)}$; (d) $\text{ZnCl}_2\text{-KCl (1:1)}$ at 320°C (a,c,d) and 450°C (b).

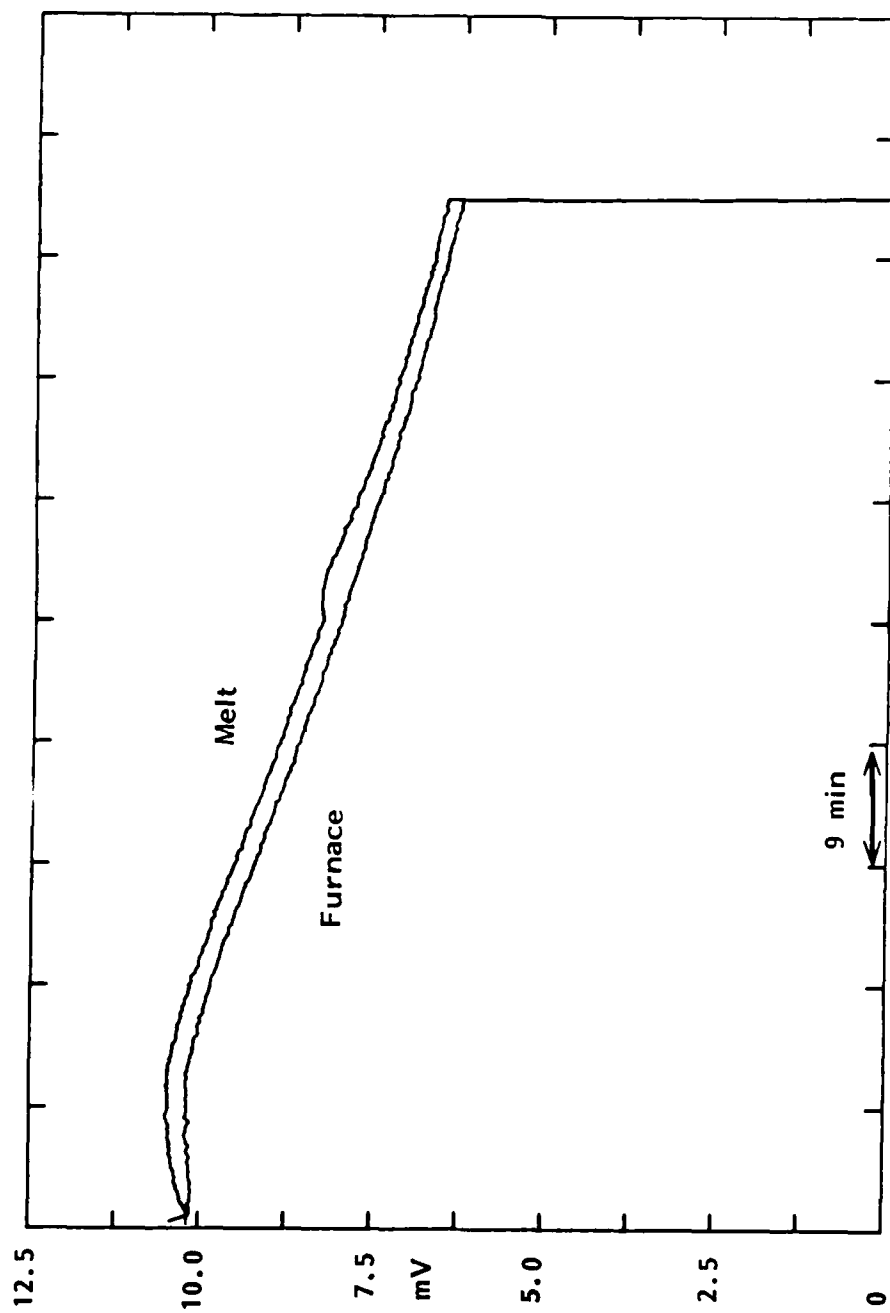


Fig. 3. Cooling curve for ternary bromide eutectic mixture LiBr-KBr-CsBr.

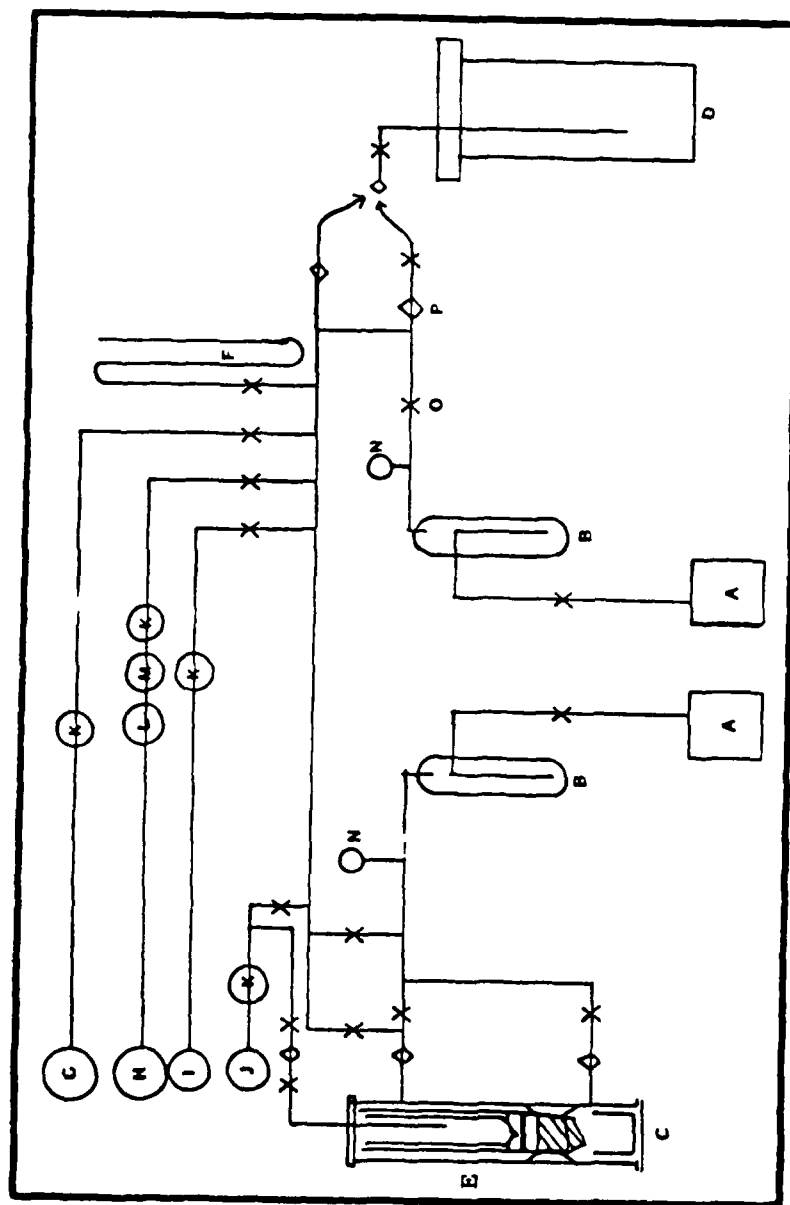


Fig. 4. Vacuum line and auxiliary gas lines.

Glossary

- | | |
|--------------------------|--|
| A - Rotary Pump | I - Oxygen Tank |
| B - Cold Trap | J - Hydrogen Halide |
| C - Purification Cell | K - Molecular Sieve Tower |
| D - Electrochemical Cell | L - Sofnalite Tower |
| E - Filtration Section | M - Copper Deoxygenating Tower Furnace |
| F - Manometer | N - Thermocouple Vacuum Gauge |
| G - Carbon Dioxide Tank | O - Rotoflow (Teflon) Stopcocks |
| H - Argon Tank | P - Greasless Ball Joint |

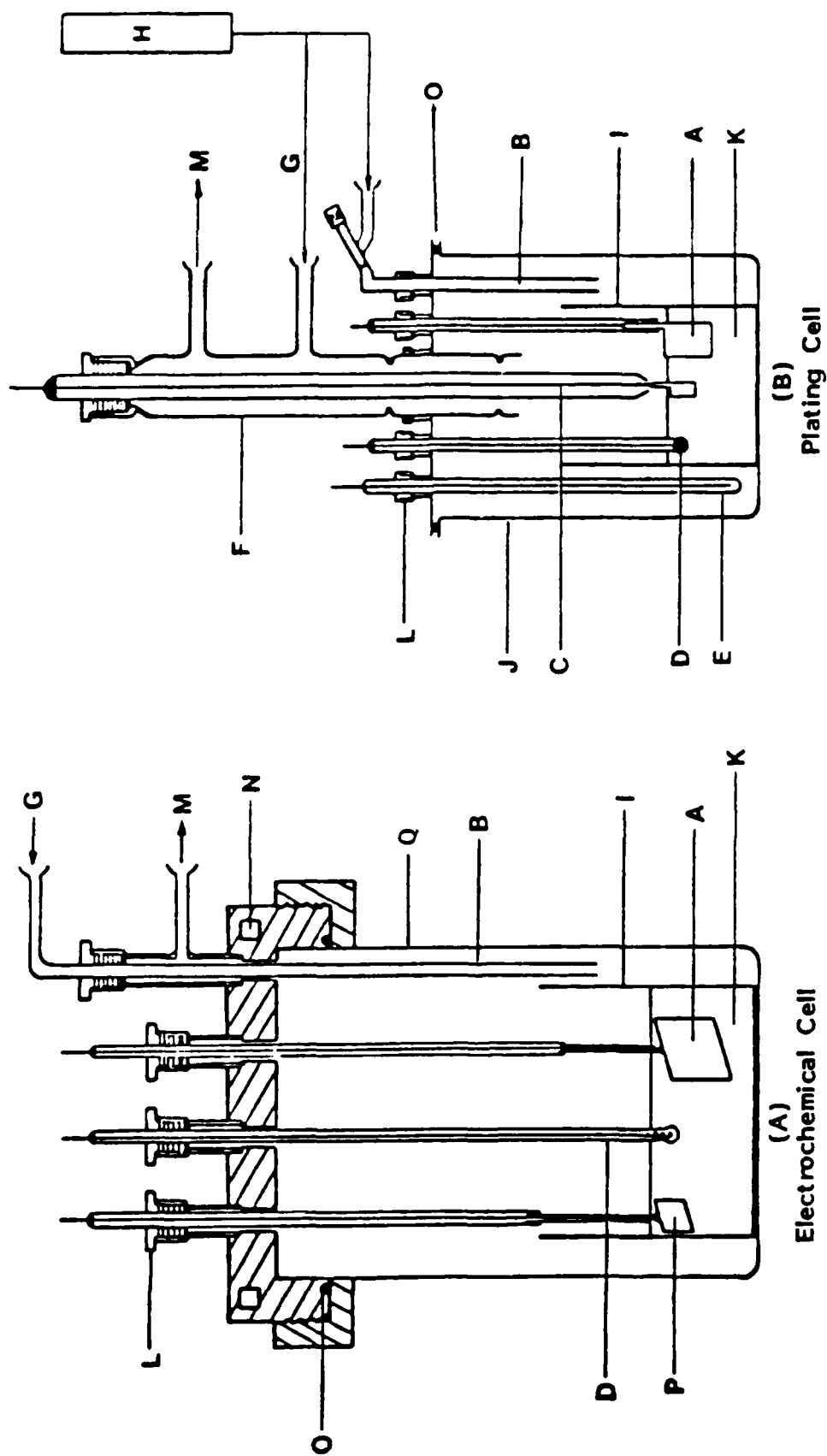


Fig. 5. Electrochemical and plating cells. A, Anode; B, Bubbler; C, Cathode Assembly; D, Reference Electrode; E, Thermocouple; F, Cathode Exchange Tower; G, Gas In; H, Argon Supply; I, Al_2O_3 Crucible; J, Pyrex Envelope; K, Ace Thread Adapter; L, Electrolyte; M, Gas Outlet; N, Water Colling; O, "O" Ring Seal; P, Microelectrode; Q, Silica Envelope.

large gold flag electrodes were used. A spectroscopically pure graphite rod, mounted on a stainless steel support rod in a separate Pyrex counter compartment was used as a cathode during the anodic generation of Cr(II) ions.

Working Electrodes. Working electrodes were made of gold, platinum, vitreous carbon, molybdenum, copper, nickel, tungsten, and stainless steel. For plating experiments, only the latter five metals were used in the form of 1-2 cm² coupons screwed to a stainless steel or molybdenum support which in turn was threaded onto a stainless steel (3/16th) rod mounted in a 14 mm Pyrex tube. The microelectrodes for basic studies were flags, spheres, or cylinders of the appropriate metal. They were made by sealing the metal wire in an alumina capillary leaving a small protruding spherical bead of the metal. For planar electrodes, a small flag of the metal (<0.5 cm²) was attached to a minimum of protruding metal. This procedure is easily achieved with platinum and gold, but for the other metals, it is a question of trial and error until a satisfactory electrode is obtained. Molybdenum was also sealed into Pyrex to form simple cylindrical electrodes. Planar vitreous carbon electrodes were made by sealing 3 mm diameter pieces into Pyrex at around 600°C under vacuum after first treating the vitreous carbon (VC) to prolonged heating at 900°C under reduced pressure to remove trapped gases. The Pyrex tube was attached to a silica thermal treatment section via a graded seal and possessed a Pyrex side arm for the vacuum connection. These procedures are modifications of those published by other authors (21,22). The sealed end was cut and polished to provide a scratch free surface. The contact between the vitreous carbon and the silver lead wire was made using fine graphite powder.

Gold and platinum electrodes were cleaned by electrocycling in sulfuric acid (23). The copper and nickel electrodes for basic studies were degreased in acetone/chloroform, washed in distilled water, and electropolished using the procedures given in Smithells (24). In the plating experiments, electrodes were degreased and washed in distilled water and dried by evacuation. All geometric electrode areas were determined with the optical microscope and compared with those (Au,Pt,VC) measured chronopotentiometrically with a solution of thallium nitrate in 1M potassium nitrate at 25°C. The diffusion coefficient of Tl⁺ used in the calculation of the area is that reported by Wolfe and Caton (25).

Reference Electrodes. The silver/silver (I) redox couple was used (19). The appropriate silver salt was dissolved in the solvent by mixing the components together in a small Pyrex tube, sealed under vacuum, and melted to form the solution. The sample was quenched and handled subsequently in the dry box to make individual reference electrodes. The concentrations of Ag⁺ in the reference electrodes used were:

Acid zinc chloride melt	AgCl = 0.16 molal
Basic zinc chloride melt	AgCl = 0.16 molal
Standard lithium chloride melt	AgCl = 0.163 molal
Standard lithium bromide melt	AgBr = 0.141 molal

The potentials in the figures are quoted with respect to the appropriate reference electrode. The electrode was made by containing about 0.5-1 gram of the silver (I) solution in a Pyrex bulk. A silver lead wire was introduced to run from the inside of the bulb to the upper end of the 7 mm Pyrex tube where it was sealed with epoxy cement (see Figure 6).

Auxiliary reference electrodes were also used in the form of the chromium or molybdenum metal dipping into the electrolyte solutions of their respective ions under study. Quasi-reference electrodes of gold or platinum sheet were used to reduce the effect of the relatively high impedance of the glass bulk of the silver electrode in the potentiostatic circuitry experienced, particularly at the lower temperatures (<450°C).

Other Inserts. A number of other inserts were used which include an addition tube, a gas bubbler and gas outlet assembly and thermocouple sheath. These, together with the electrodes, are illustrated in Figures 6 and 7.

2.4 Electrochemical Techniques

2.4.1 General

The electrochemical instrumentation was based upon the Amel 551 fast rise time potentiostat (0.1 μ s at full load) modulated by a PAR 175 waveform generator. The current or voltage transients were recorded on a Bascom-Turner 8120 series microprocessor controlled recorder and stored on floppy discs for further analysis. Cyclic voltammetry and chronopotentiometry were carried out in this mode. Normal pulse voltammetry and differential pulse voltammetry were employed in a limiting manner using a PAR 174a polarograph.

Single and double potential step and galvanostatic step measurements were also performed using the Amel/PAR 175 combination. The transients were again recorded with the Bascom-Turner 8120. Data from the BT could be transported to and from the Apple. The analysis of this data was performed using BT software and also with software developed for the Apple II+ computer.

2.4.2 Pulse Plating

Only pulsed current plating has been attempted in this study. In principle, the PAR 175 can be used to generate a pulsed current waveform, as shown in Figure 8a from the Amel 551 potentiostat using a known resistance in the control loop. The control of the duty cycle is limited to $t_{off}/t_{on} = 11$. Consequently, the pulses were generated using a second PAR 175 to control the period while the first controlled the current amplitude and pulse length. Figure 8b shows the circuit used in conjunction with a PAR 173/176 potentiostat current follower. The circuit also shows the BT 8120 connected to acquire records of the potential response of the cathode during pulse plating. This data acquisition was controlled

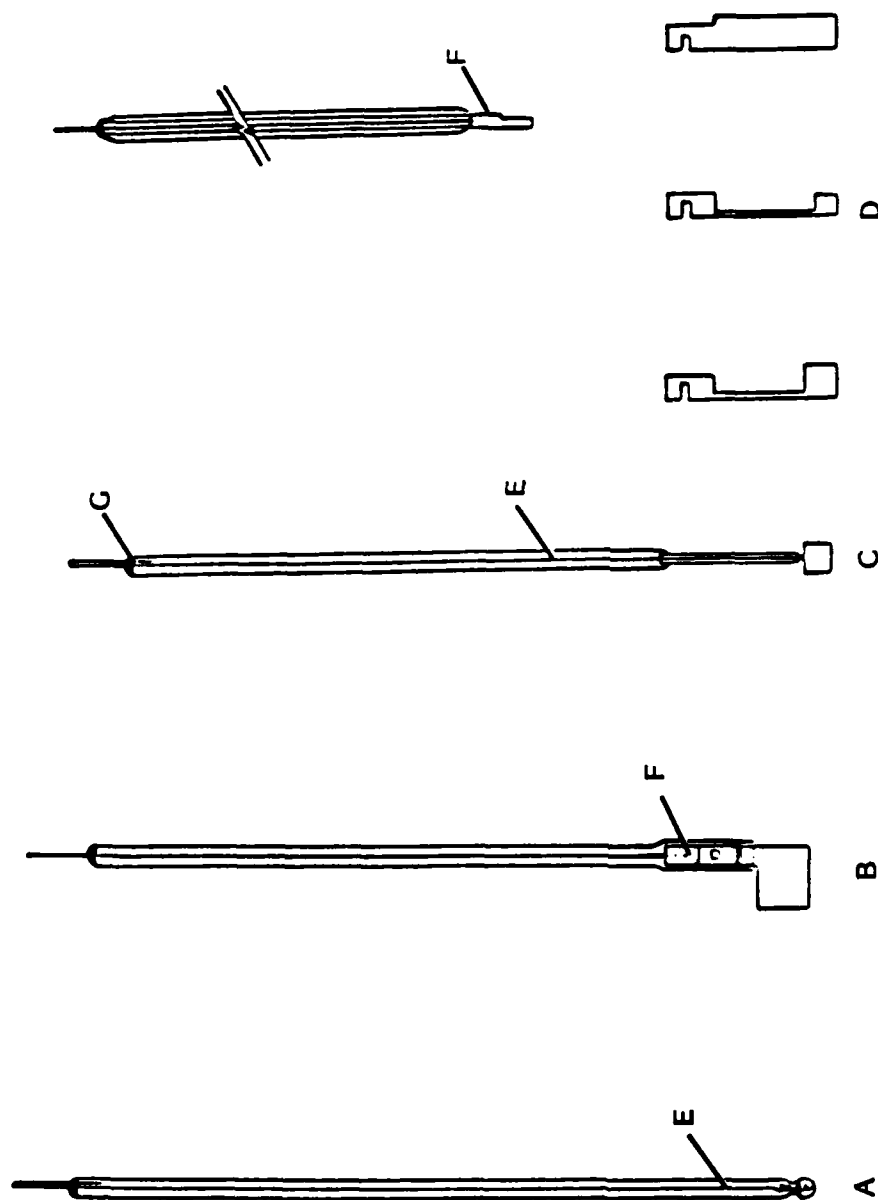


Fig. 6. Various electrode designs. A, Reference Electrode; B, Molybdenum Anode; C, Working (micro) Electrode; D, Cathode Forms for Plating; E, Silver Wire; F, Molybdenum Holder; G, Epoxy Resin Seal; H, Planar Flag Electrode.

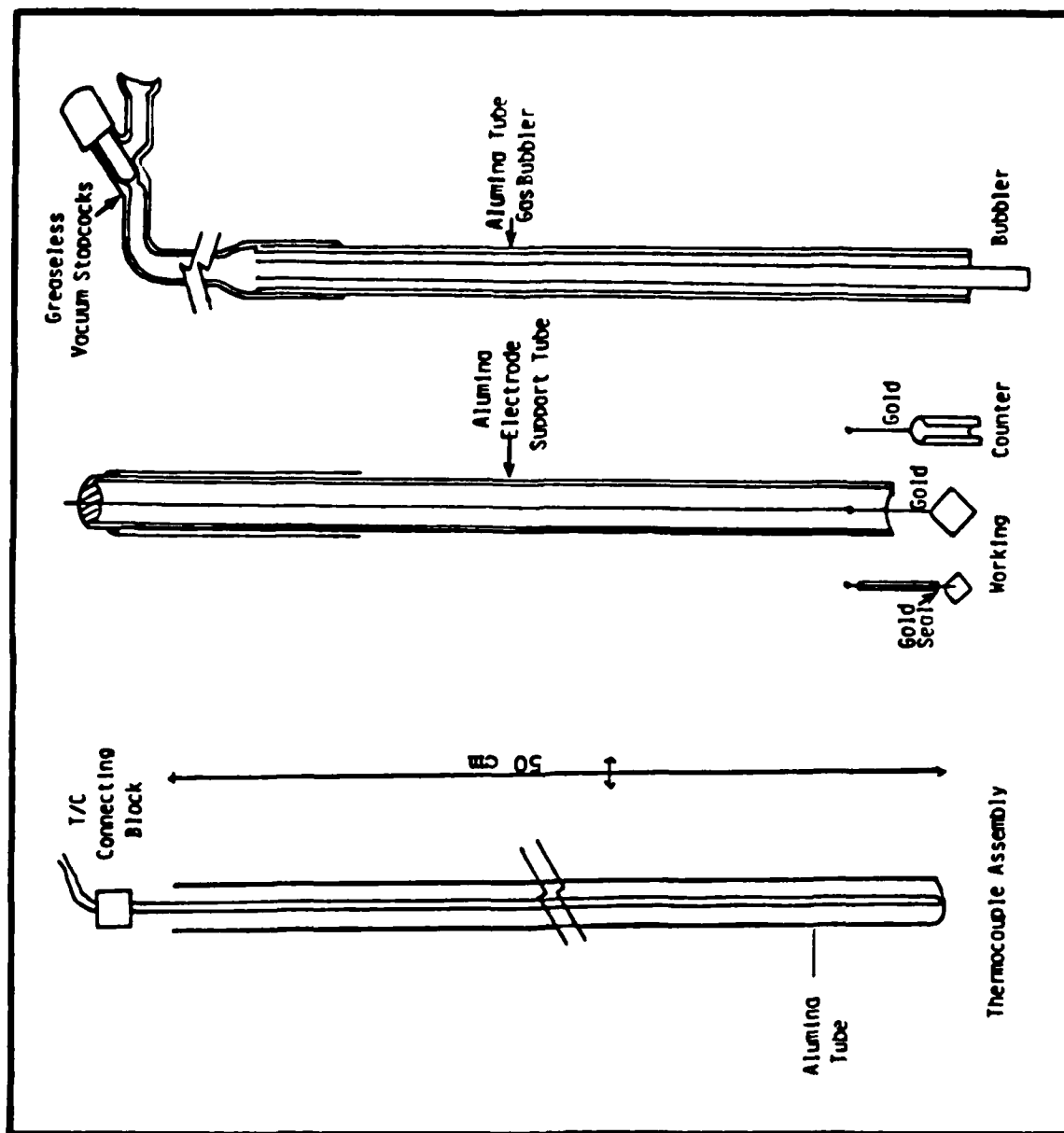


Fig. 7. Typical cell inserts.

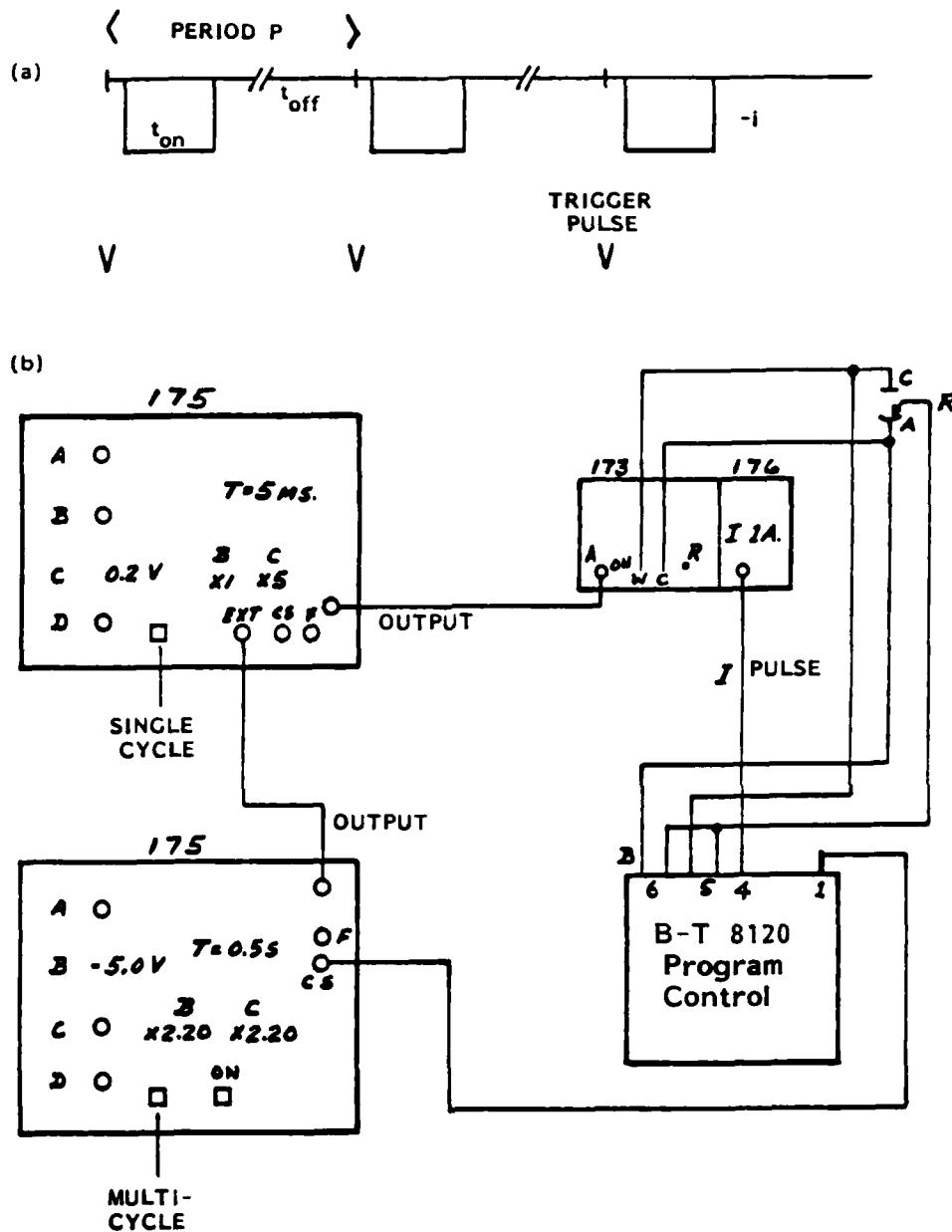


Fig. 8. (a) Pulsed current waveform and (b) circuit diagram for generation of current pulses and capture of resultant potential time transients.

via a keystroke program written for this purpose. In some experiments, the following data was acquired:

- First 14 consecutive pulses.
- Pulses after 1 min, 5 min, 15 min, 30 min, and 60 min.
- Thereafter, a pulse every 60 min until the end of the plating.

The data were stored on disc and could be plotted and examined at the end of the experiment.

2.5 Electrochemical Procedures

2.5.1 General

The cell components, made of Pyrex, silica and ceramics, which came into contact with the experimental reagents were cleaned with 50% H_2SO_4 -50% HNO_3 mixture to degrease and clean their surfaces. Such components were subsequently soaked in distilled water and rinsed until clean before drying in the oven. Metal parts such as brass cell heads were cleaned with 50% nitric acid, washed with water, acetone and finally rinsed with distilled water and air dried. Each electrode assembly was tested for vacuum tightness and to remove any moisture.

2.5.2 Fundamental Studies

The cells were assembled and transferred to the dry box via the evacuable port. Solvents were weighed in the dry box and mixed where appropriate with solutes. Alternatively, pellets of solute were prepared, weighed, and loaded into the addition tube. Reference electrodes were also prepared using dry box techniques prior to introduction into the cell. The cell was removed from the dry box, introduced into the furnace at 50°C , attached to the vacuum line, and pumped down to $<10\text{ }\mu\text{m}$. In some experiments the cells were heated to the salt melting point under vacuum, but in others the cell was filled with argon before the salt was melted. In the case of the chromium/chloride system, chromium (II) ions were introduced by anodic dissolution at constant potential. The electrodes were lowered into the cell as required, all potentials being monitored via the reference electrode. The electrodes were connected to a control panel and could be switched into circuit as required by the particular experiment.

2.5.3 Plating Studies

Because of the size of the plating cell, different procedures were necessary. The purified melt was loaded into the large alumina crucible in the dry box. The crucible was covered with aluminum foil and quickly transferred from the box into the assembled plating cell. The cell was evacuated backfilled with argon, and placed in the furnace and heated slowly to the operational temperature. The solution chemistry was checked

by running voltammograms prior to carrying out the plating experiments. Generally, several DC runs were made prior to pulse plating. The individual cathodes were cleaned, measured, and weighed before being attached to the cathode holder. The cathode unit was then placed in a separate tube, evacuated, and backfilled with argon before being placed into the top of the cathode entry port. This ensured minimal transfer of air into the cell by the large cathode support tube. The electrode was attached to the pulse generator circuit, Figure 8, set with the appropriate plating waveform, and the electrode was lowered into the electrolyte to a known depth. The time of immersion was noted and the electroplating was carried out. In some cases, data was collected for the potential response of the cathode during the plating. The electrode was finally raised above the melt and cooled as it was slowly raised up the tower. The electrode was removed under a fast flow of inert gas. The deposit was washed and characterized by a visual inspection, low power microscopic examination, electron microscopy, and electron dispersive X-ray analysis.

3.0 RESULTS AND DISCUSSION

3.1 Program Overview

The course of this work was required to take a number of related but distinct directions. The overall goal was the advancement of the understanding of the electrochemistry of refractory metals, particularly chromium and molybdenum in molten halide solvents. Two specific goals were initially envisaged which required the investigation of zinc chloride melts as low temperature media for molybdenum plating. In parallel with this, the nature of the early stages of chromium deposition were to be examined in view of the importance of chromium plating for high temperature erosion control. As the work developed, other goals were required which included the study of molybdenum electrochemistry in LiCl-KCl, the development of a solvent with a lower operating temperature than the LiCl-KCl currently being assessed for chromium plating, as well as the application of pulsed current plating for molybdenum and chromium. The results of this fundamental program of work are presented in the order of solution chemistry, electrocrystallization effects, and plating for the two metals of interest.

3.2 Solution Chemistry of Chromium in Alkali Metal Halide Melts

3.2.1 Solutions of Cr(II) in Lithium Chloride - Potassium Chloride Eutectic Mixture

The behavior of Cr(II) ions in this solvent system was investigated at 425 and 450°C. Because the oxidation of Cr(II) is rather anodic, the solution chemistry is best explored with noble metal electrodes such as platinum and gold as well as vitreous carbon. Solutions of Cr(II) ions in the eutectic solvent were prepared by anodic dissolution using alumino-thermic quality chromium. The oxidation as well as the reduction of Cr(II) ions are readily observed in this solvent. Figure 9 shows normal pulse voltammograms acquired on a gold electrode for the redox processes of these ions in dilute solution. The reduction process shows a limiting current, but the foot of the wave is somewhat distorted on the gold electrode and no qualitative results were obtained. The oxidation process shows a limiting current with a half wave potential of 0.26V vs. the Ag/Ag(I) reference electrode used at 425°C. At 450°C, the difference in the standard potentials for Ag/Ag(I) and Cr(III)/Cr(II) is 0.22V. The potential dependence of the current is consistent with the relationship:

$$E = E_1 - RT/nF \ln[(i_L/i) - 1] \quad [1]$$

as shown in Figure 10 where the log term is plotted as a function of the potential (E). A one electron process is deduced from the slope of this plot consistent with the reaction:

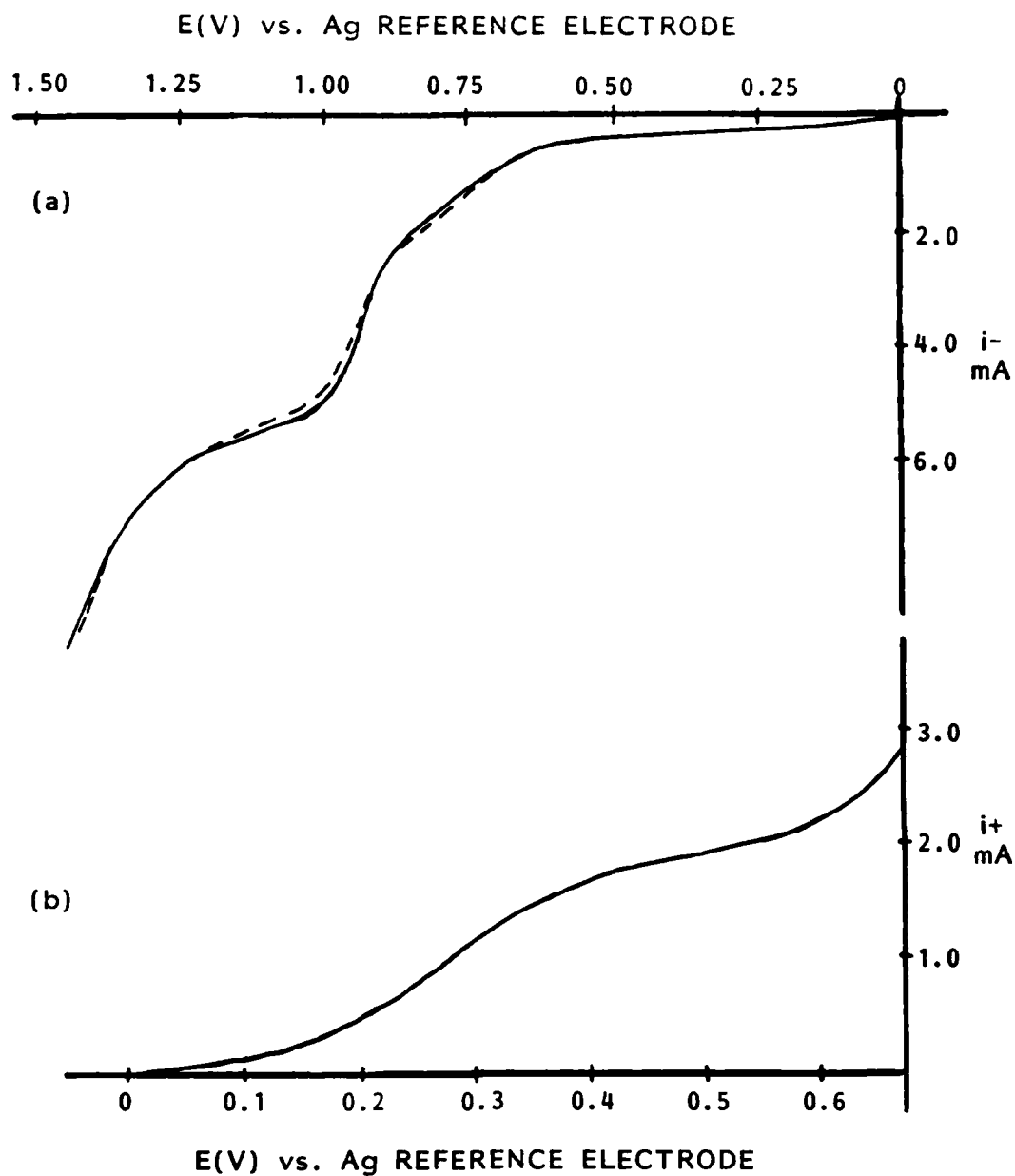


Fig. 2. Normal pulse voltammograms for (a) reduction and (b) oxidation of Cr(II) ions in LiCl-KCl eutectic mixture at 425°C. Gold microelectrode (0.4 cm²), (---) reverse scan.

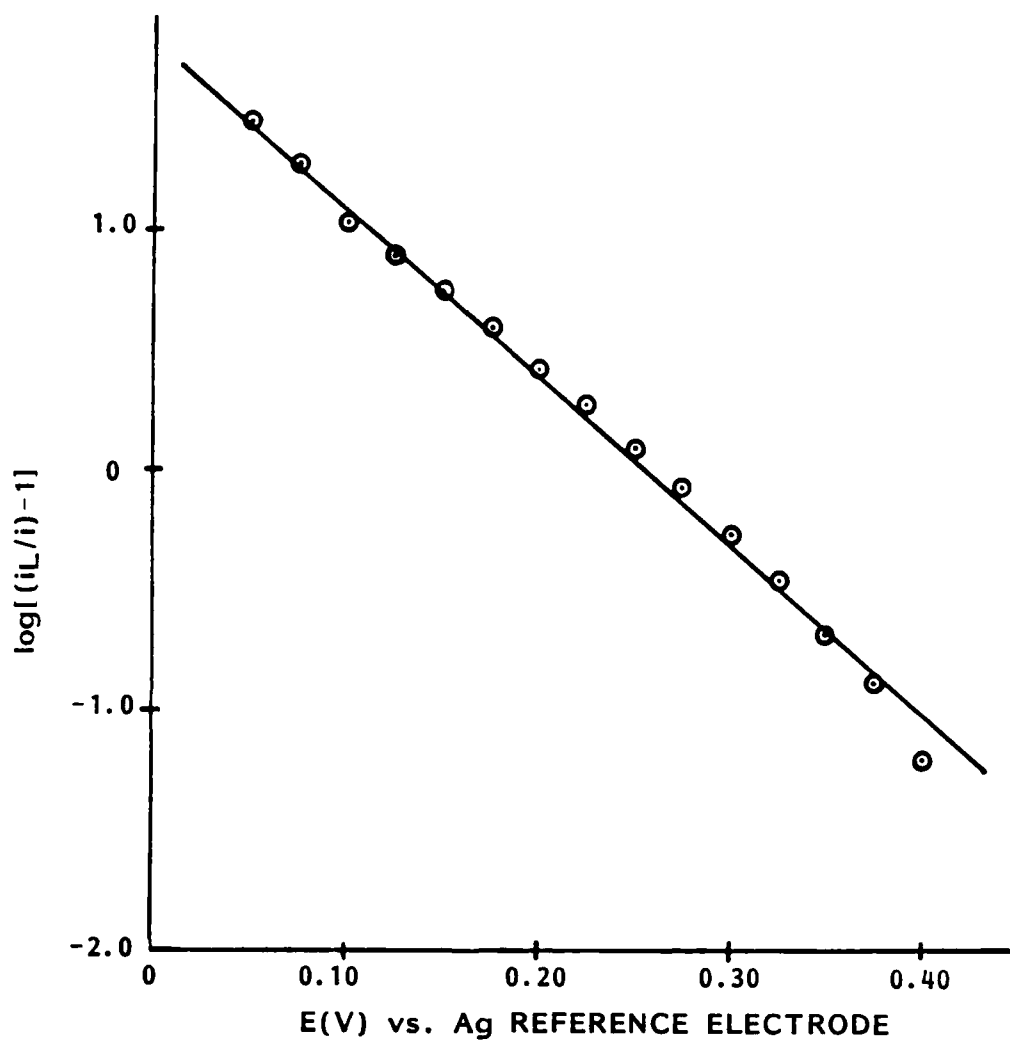


Fig. 10. Plot of $\log\{(i_L/i)-1\}$ vs. potential for the oxidation of Cr(II) in LiCl-KCl solution at 425°C. (RT/nF) measured -0.146V; $(RT/nF) = (0.139/n)$ V.

$$\text{Cr}^{+3} = \text{Cr}^{+6} - e \quad [2]$$

The diffusion coefficient for Cr(II) ions was calculated from the limiting current expression:

$$i_L = [nFACD^{1/2}]/[\pi\Delta t]^{1/2} \quad [3]$$

where Δt for the PAR 174A is 0.04 seconds. The diffusion coefficient is determined to be $1.25 \times 10^{-5} \text{ cm}^2\text{s}^{-1}$.

Cyclic voltammetric and chronopotentiometric measurements from the rest potential showed both cathodic and an anodic response corresponding to the reduction and oxidation of Cr(II) ions in the melt. Figures 11 and 12 illustrate typical voltammograms and chronopotentiograms obtained at low concentrations. Tables 3 and 4 show some results obtained on gold electrodes from such measurements. The results obtained some 17 hours after those in Table 3 are illustrated in Table 5 for the cathodic and anodic processes. Figure 13 shows the change in concentration with time after electrolysis as determined from the Cr/Cr(II) electrode potentials and the Nernst equation, assuming that the temperature coefficient determined by Yang and Hudson (26) are appropriate to account for the temperature differences between 450°C and 425°C. In any event, the relative concentration changes are demonstrated. Although such changes occur at the higher concentrations, the magnitudes of the concentration changes are less.

Table 6 compares cyclic voltammetric data acquired on platinum and gold electrode substrates at 450°C at higher concentrations of Cr(II) ions. Integration of the voltammograms using the Bascom-Turner 8120 recorder enabled the charge to the peak for the anodic process to be calculated for a reversible process involving a soluble product. The charge is given by:

$$Q_p = 0.437 \times nFCA \times [DRT/vnF]^{1/2} \quad [4]$$

Table 6 shows the values of $Q_p v^{1/2}$ obtained for the cases of gold and platinum electrodes. In the case of the reduction process at these two electrodes, the ratio of forward to reverse charge as well as the charge to the peak potential were evaluated and are given in Table 6. The integral of the voltammetric current expression given by Delahay (27) for the process in which metal is deposited, assuming unit activity is:

$$Q_p = 0.8325 \times nFAC[D E_p/v]^{1/2} \quad [5]$$

where at 450°C

$$E_p = E_p - E_1 = 0.8540RT/nF = 0.053/n \quad [6]$$

The anodic process on platinum shows evidence for a prepeak even at low scan rates. The response on gold shows no evidence for a prepeak. Figure 14 illustrates a typical response for these electrodes.

REDOX OF CHROMOUS CHLORIDE

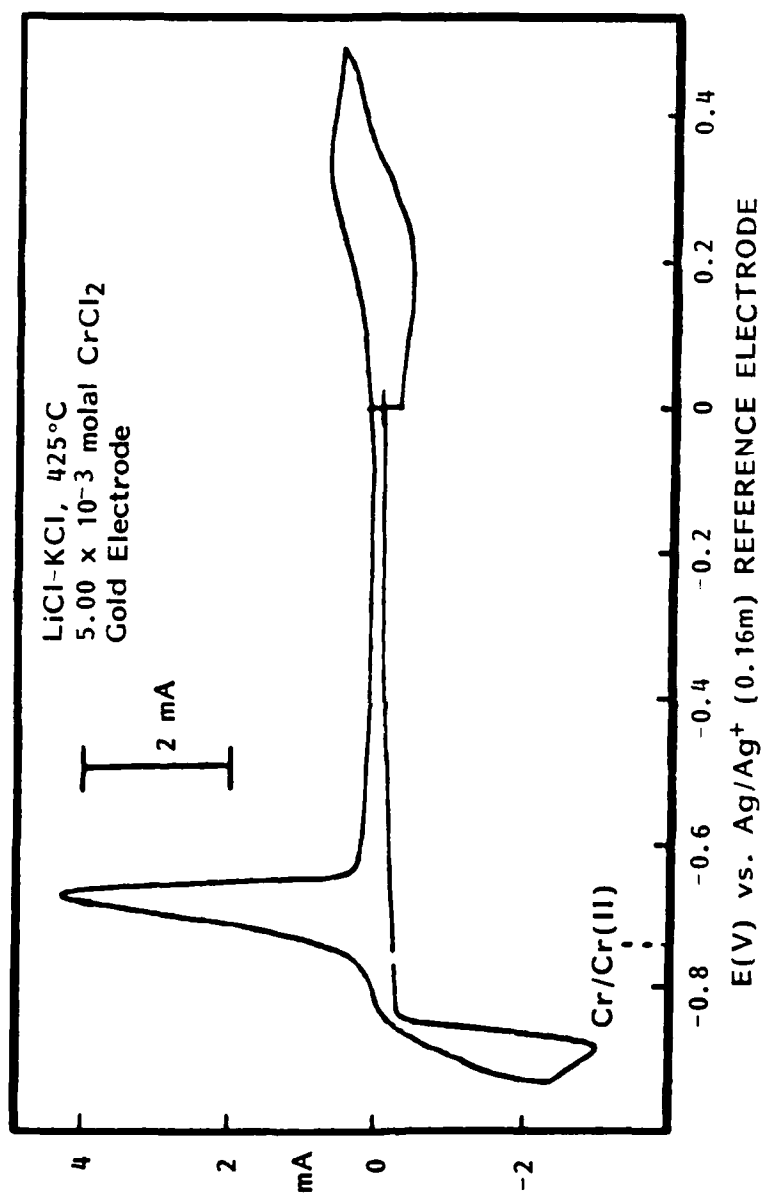


Fig. 11. Voltammogram illustrating the redox behavior of Cr(II) ions in molten LiCl-KCl.

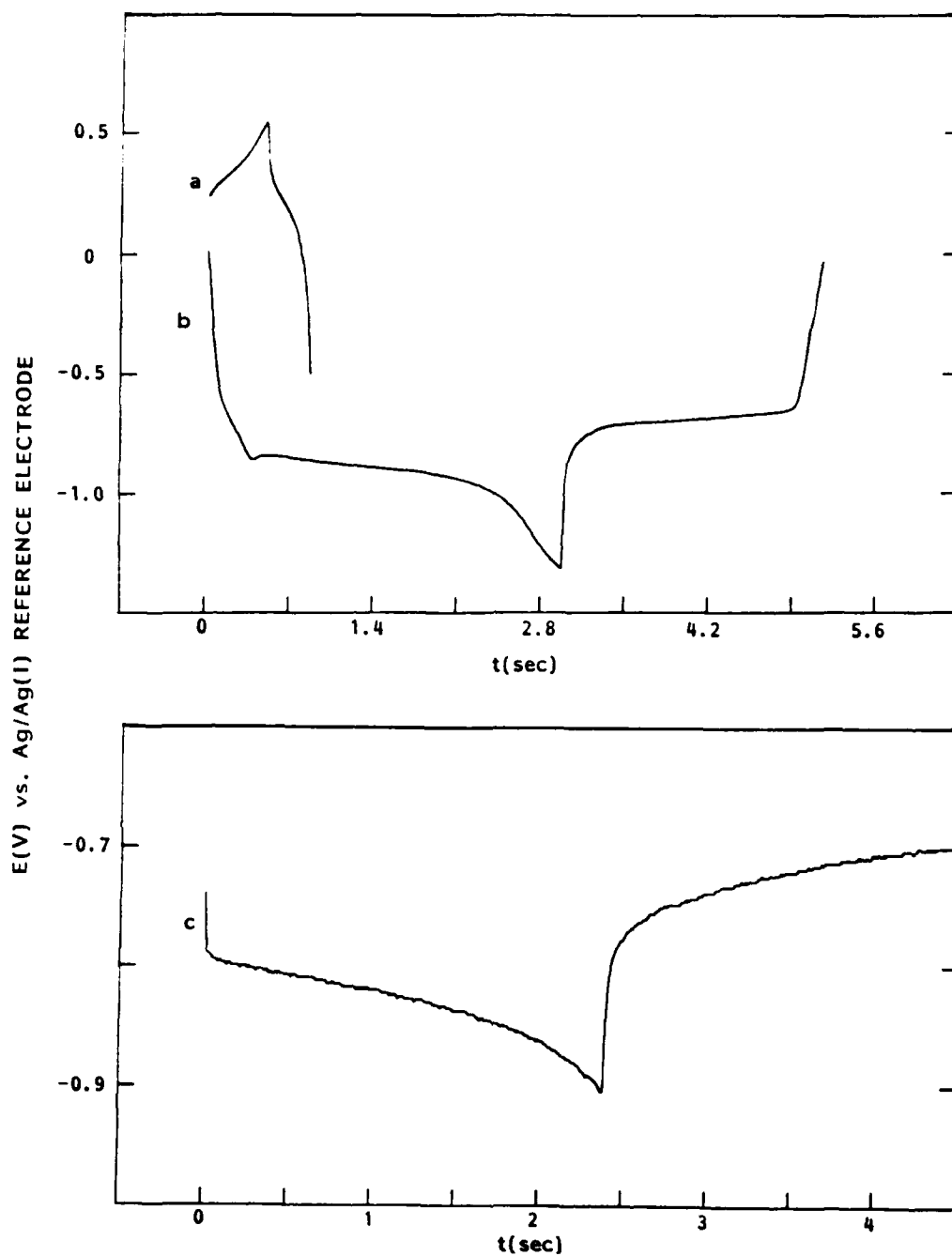


Fig. 12. Current reversal chronopotentiograms for the oxidation (a) and reduction (b,c) of Cr(II) in LiCl-KCl eutectic at 425°C on a gold electrode (0.43 cm²) (a,b) and on a chromium coated copper electrode (0.5 cm²). Concentration of Cr(II) - (a,b) 8.8 mM and (c) 13 mM; current (a,b) 2 mA, (c) 7 mA.

TABLE 3

CYCLIC VOLTAMMETRIC DATA ON GOLD
ELECTRODES AT 7 mM Cr(II) at 425°C

a. Reduction $E_i = -0.745\text{V}$ versus Ag reference

v V/s	Current mA	$-E_p$ volts	$\Delta E_p/2$ volts	$i_p/v^{1/2}$ mA (s/V) ^{1/2}
0.020	1.13	0.850	0.014	7.99
0.050	1.75	0.853	0.015	7.83
0.100	2.75	0.857	0.018	8.13
0.200	3.75	0.865	0.020	7.98
1.00	8.15	0.880	0.025	8.15
2.00	12.0	0.890	0.040	8.49
5.00	20.5	0.910	0.050	9.17
10.00	28.9	0.950	0.130	9.13

b. Oxidation $E_i = -0.738\text{V}$ versus Ag reference

v V/s	Current mA	E_p volts	$\Delta E_p/2$ volts	$E^{1/2}$ volts	$(i_b/i_f)_p$	$i_p/v^{1/2}$ mA (s/V) ^{1/2}
0.050	0.347	0.350	0.143		1.04	1.55
0.050	0.395	0.340	0.133	0.275	1.02	1.77
0.100	0.470	0.347	0.143		1.06	1.49
0.100	0.555	0.345	0.145	0.275	1.03	1.76
0.150	0.635	0.350	0.146	0.275	1.04	1.64
0.200	0.770	0.350	0.149		1.05	1.72
0.300	0.905	0.350	0.150		1.06	1.65
Mean		0.347	0.144	0.275	1.04	1.65
Standard Deviation		0.004	0.006	-	0.02	0.11

TABLE 4

CHRONOPOTENTIOMETRIC DATA ON GOLD ELECTRODES
AT 7 mM Cr(II) AT 425°C

a. Reduction $E_i = -0.755V$ versus Ag reference

<u>Current</u> <u>mA</u>	<u>τ</u> <u>sec</u>	<u>$-E\tau/4$</u> <u>volts</u>	<u>τ_b/τ_f</u>	<u>$i\tau^{1/2}$</u> <u>$\text{mAs}^{1/2}$</u>
2.0	1.00	0.820	1.11	2.00
2.0	1.10	0.830	1.14	2.10
4.0	0.376	0.780	1.47	2.45
4.0	0.401	0.787	0.91	2.53
6.0	0.195	0.862	1.39	2.65
6.0	0.108	-	0.72	-
8.0	0.105	-	2.01	2.59
8.0	0.069	-	1.42	-

b. Oxidation $E_i = -0.753V$ versus Ag reference

<u>Current</u> <u>mA</u>	<u>τ</u> <u>sec</u>	<u>$E\tau/4$</u> <u>volts</u>	<u>$E.22\tau$</u> <u>volts</u>	<u>$+E_{rp}$</u> <u>volts</u>	<u>τ_b/τ_f</u>	<u>$i\tau^{1/2}$</u> <u>$\text{mAs}^{1/2}$</u>
0.50	1.075	0.280	-	0.191	-	0.52
0.50	1.065	0.285	0.285	0.191	0.77	0.52
0.50	0.985	-	-	0.188	0.51	-
0.65	0.540	0.285	0.275	0.200	0.97	0.48
0.65	0.490	-	-	0.200	0.67	-
0.80	0.405	0.285	0.275	0.188	0.82	0.51
0.80	0.400	0.280	0.269	0.192	0.70	0.51
0.90	0.335	0.286	0.269	0.190	0.82	0.52
0.90	0.333	0.285	-	0.193	-	0.52
0.90	0.300	-	0.263	0.193	0.64	-
1.00	0.580	0.280	0.280	0.187	0.76	0.76
1.00	0.588	0.280	0.280	0.190	0.81	0.77
1.20	0.534	0.288	0.266	0.203	0.70	0.88
1.20	0.510	0.291	0.278	0.203	0.90	0.71
1.20	0.294	-	0.238	0.203	0.90	-

TABLE 5

CYCLIC VOLTAMMETRIC DATA ON GOLD ELECTRODES
 AT 7 mM Cr (II) AT 425°C 17-24 HOURS AFTER
 DATA TAKEN IN TABLE 3

a. Reduction $E_i = -0.769\text{V}$ versus Ag reference

v V/s	Current mA	$-E_p$ volts	$\Delta E_p/2$ volts	$i_p/v^{1/2}$ mA (s/V) ^{1/2}
0.020	0.588	0.905	0.025	4.15
0.050	0.988	0.903	0.010	4.42
0.100	1.52	0.910	0.016	4.80
0.200	2.19	0.920	0.030	4.89

b. Oxidation $E_i = -0.768\text{V}$ versus Ag reference

v V/s	Current mA	E_p volts	$\Delta E_p/2$ volts	$E^{1/2}$ volts	$(i_b/i_f)_p$	$i_p/v^{1/2}$ mA (s/V) ^{1/2}
0.020	0.149	0.345	0.150	0.265	1.22	1.05
0.050	0.230	0.340	0.150	0.263	1.07	1.03
0.100	0.327	0.340	0.143	0.263	1.08	1.03
0.200	0.460	0.340	0.160	0.260	1.10	1.03
Mean		0.341	0.151	0.263	1.12	1.03
Standard Deviation		0.003	0.007	0.002	0.07	0.01

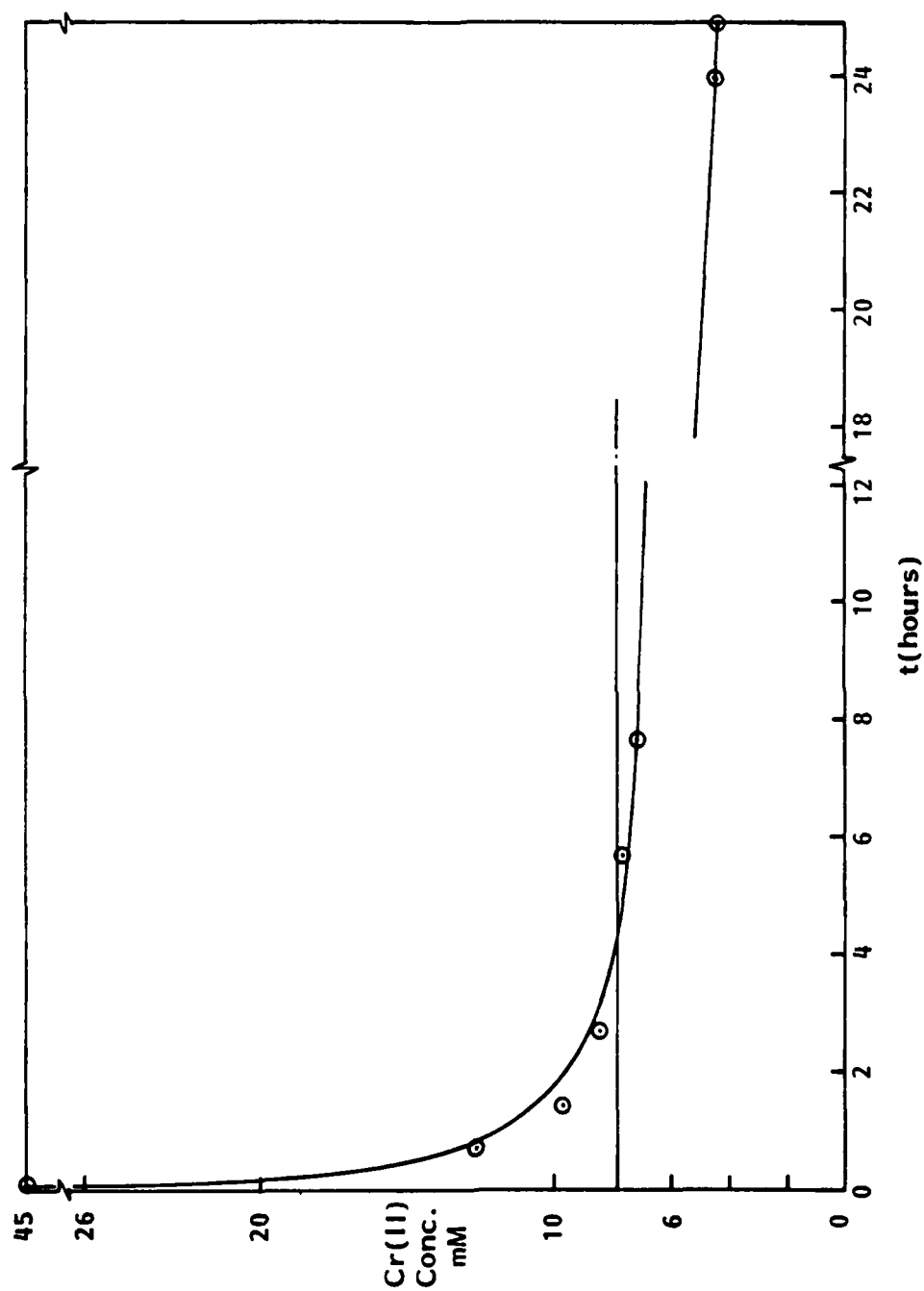


Fig. 13. Change in Cr(II) ion concentration after electrolytic generation of Cr(II) as measured by a Cr²⁺/Cr indicator electrode in LiCl-KCl at 425°C.

TABLE 6

ANODIC/CATHODIC CYCLIC VOLTAMMETRY DATA FOR Cr^{2+} (24 mM) IN LiCl-KCl AT 450°C

ANODIC PROCESS		$\text{Cr}^{2+} \rightarrow \text{Cr}^{3+} + e$		CATHODIC PROCESS		$\text{Cr}^{2+} + 2e \rightarrow \text{Cr}$					
GOLD ELECTRODE (0.26 cm ²)											
Scan Rate V/s	E(Peak) vs. Ref	Ep-Ep/2 volts	I(C)/I(A)	Ip/v ^{1/2}	Q(P)/v ^{1/2}	E(Peak) vs. Ref	Ep-Ep/2 volts	Q(A)/Q(C)	Q(P)v ^{1/2}	Ip/v ^{1/2}	Ip/v ^{1/2}
0.05	0.411	0.152	0.903	0.0117	1871.42	-0.802	-0.017	0.963	949.47	0.0466	0.0452
0.2	0.402	0.147	1.027	0.0116	1904.10	-0.811	-0.018	1.142	890.99	0.0430	0.0448
0.5	0.394	0.154	1.013	0.0115	1993.50	-0.816	-0.018	1.081	807.73	0.0408	0.0445
1	0.397	0.147	1.007	0.0116	1907.69	-0.839	-0.021	1.007	1038.46	0.0385	0.0448
2	0.396	0.146	1.031	0.0117	1892.87	-0.854	-0.027	0.969	1202.08	0.0353	0.0452
5	0.399	0.148	1.025	0.0112	1960.06	-0.868	-0.038	0.991	1290.04	0.0323	0.0433
Mean	0.399	0.149	1.001	0.0115	1921.74			1.03			0.0446
Theory		0.137	1.000			-0.741	-0.024	1.000			
PLATINUM ELECTRODE (0.23 cm ²)											
Scan Rate V/s	E(Peak) vs. Ref	Ep-Ep/2 volts	I(C)/I(A)	Ip/v ^{1/2}	Q(P)/v ^{1/2}	E(Peak) vs. Ref	Ep-Ep/2 volts	Q(A)/Q(C)	Q(P)v ^{1/2}	Ip/v ^{1/2}	Ip/v ^{1/2}
0.05	0.399	0.136	0.911	0.0112	1924.00	-0.784	-0.016	1.001	909.98	0.0518	0.0433
0.2	0.386	0.152	0.978	0.112	2049.00	-0.787	-0.015	1.236	612.49	0.0445	0.0434
0.5	0.378	0.144	0.991	0.0113	2125.00	-0.794	-0.018	1.176	747.07	0.0435	0.0437
1	0.394	0.155	1.001	0.0114	2365.00	-0.812	-0.018	1.088	899.57	0.0420	0.0443
2	0.389	0.155	0.996	0.0117	2275.00	-0.821	-0.022	1.029	885.42	0.0390	0.0452
5	0.384	0.156	0.994	0.0128	2867.00	-0.831	-0.028	1.005	923.59	0.0358	0.0496
Mean	0.388	0.151	0.9785		2267.50			1.09			
Theory		0.137	1.000			-0.741	-0.024	1.000			

*Based on Anodic Au

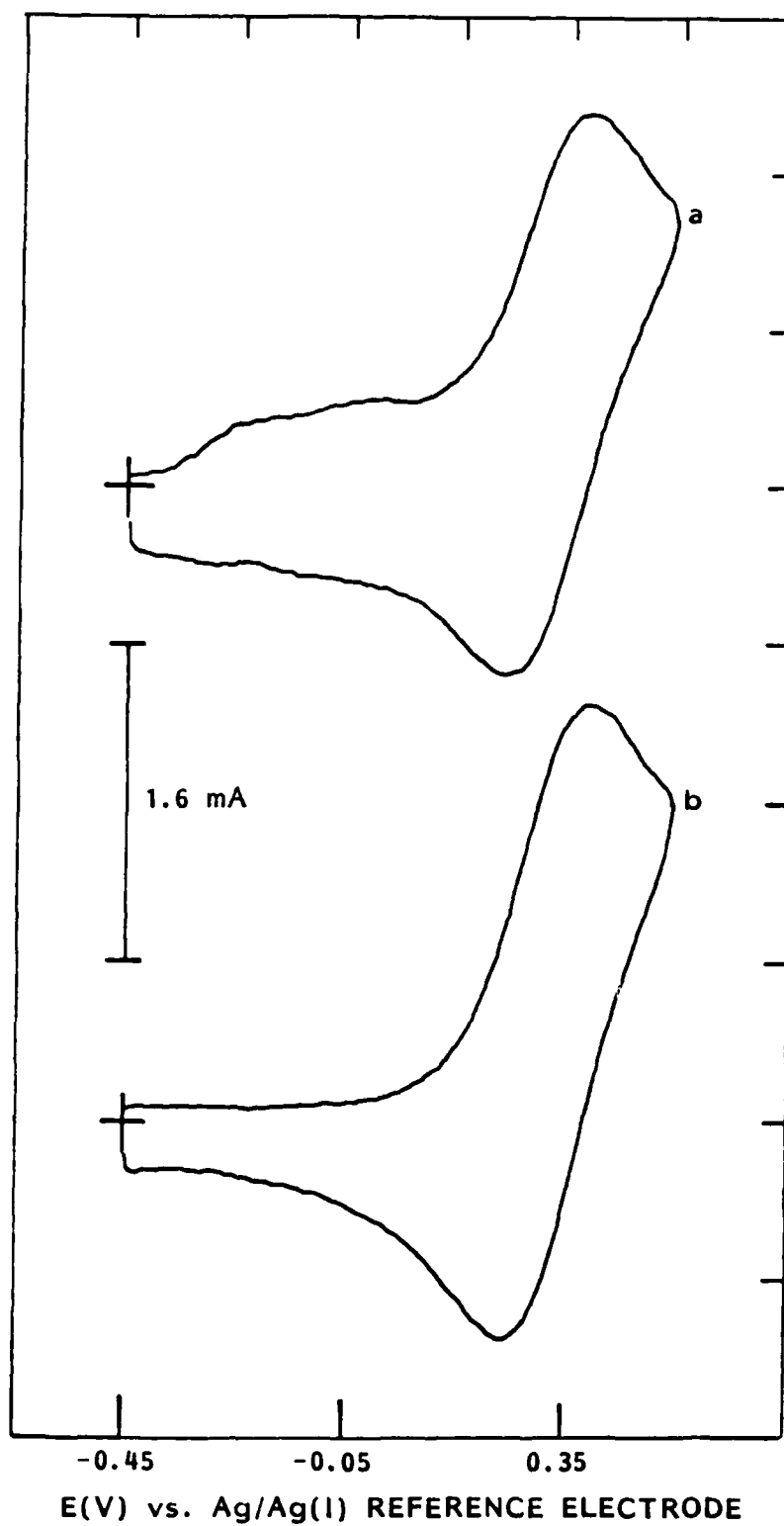


Fig. 14. Cyclic voltammograms acquired at a scan rate of 0.5 V/s for the electro-oxidation of Cr(II) (24 mM) in LiCl-KCl eutectic at 450°C on (a) Pt and (b) gold (0.26 cm²) electrodes.

Anodic chronoamperometry was also carried out on the dilute solutions and the results are summarized later in the context of the nucleation and growth studies relating to chromium deposition.

3.2.2 Solutions of Cr(III) in Lithium Bromide - Potassium Bromide - Caesium Bromide Eutectic Mixture

This solvent, with a melting point in the region of 236°C, was selected because of the interest in reducing the operating temperature for chromium plating. A wide range of temperature conditions were explored in this little investigated solvent. The chromium (III) bromide was available commercially in pure form and was used initially. The solution chemistry was examined at temperatures below those readily accessed with the LiCl-KCl eutectic mixture. An addition of CrBr₃ was made to a sample of the bromide eutectic mixture contained in a Pyrex tube. The sample was sealed off under vacuum before raising the temperature to 450°C. The melt was dark green in color and cooled to a green solid.

Electrochemical studies of solutions of chromium (III) bromide in the ternary eutectic were made. A differential pulse voltammogram acquired on a gold electrode is shown in Figure 15. Three peaks are visible in the potential range +0.52 to -1.30V vs. the Ag/Ag⁺ reference electrode. Normal pulse voltammograms, on the other hand, show the presence of only two limiting currents, Figure 16. Cyclic voltammetric measurements which show three reduction peaks support the differential pulse measurements. Comparison of the cyclic voltammograms, Figure 17, obtained for the bromide solvent and the solutions containing Cr(III) ions show that the peak at around -0.45V is present in the solvent.

The peak at around +0.43 was investigated briefly. Figure 18 shows voltammograms for this reduction process as a function of scan rate. Data were analyzed in terms of the recent theory of Fasang et al. (28) and extended by numerical solution of their differential equation for the voltammetric current by Sasahira and Yokokawa (29). Table 7 gives some typical experimental results for the reduction of Cr(III) ions. When the switching potential was extended to -1.4V, data for the second reduction process involving chromium (II) to metal was accessed. Table 8 summarizes some results for this consecutive reduction process.

Single and double pulse potential step measurements were also made on this system at a nominal concentration of 31.7 mM at 380°C. The current time curves were integrated using Bascom-Turner 8120 software. The response to a typical potential step experiment is illustrated in Figure 19. Ten points were read from each current time and charge time curve and analyzed according to a simple diffusion model for the electrochemical processes. Table 9 shows the results for a step to the limiting current region for the reduction of Cr(III) to Cr(II) for pulse lengths of 2 and 5 seconds. Table 10 shows a single pulse stepped to -1.5V, i.e., in the limiting current region for the reduction of Cr(III) to Cr metal. The results of these measurements are summarized in Table 11.

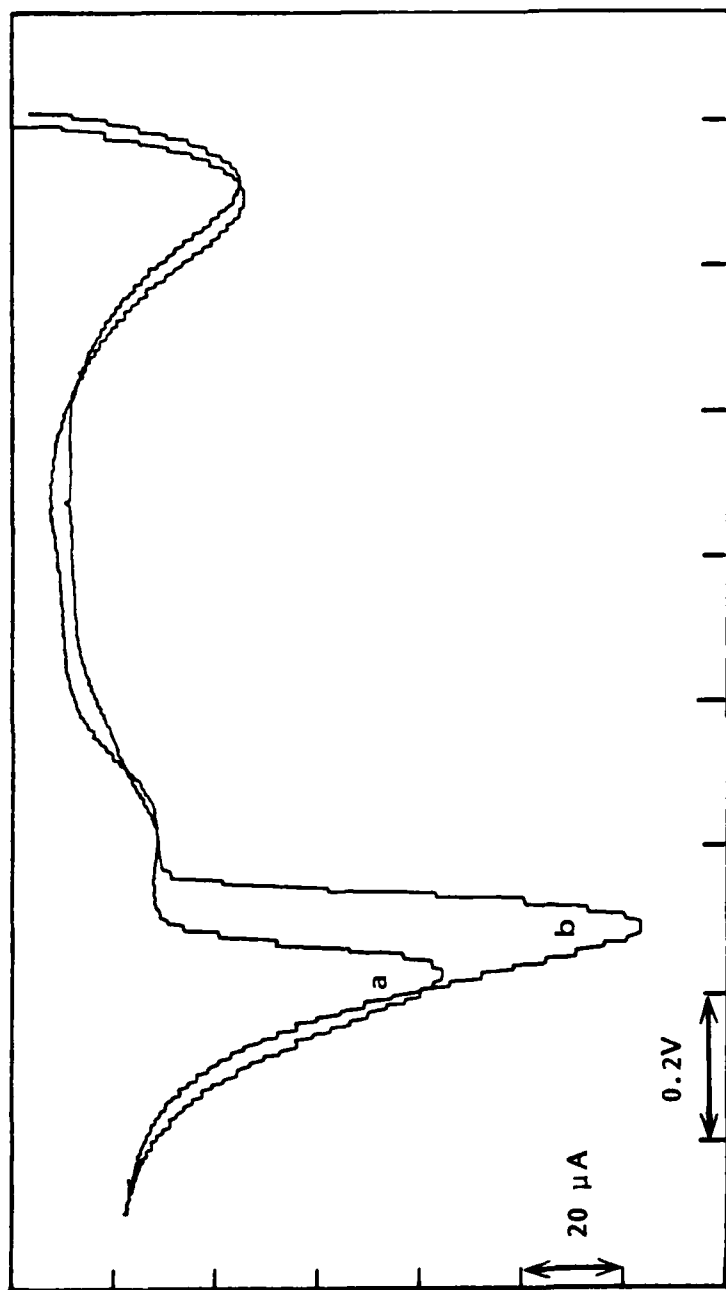


Fig. 15. Differential pulse voltammograms acquired on a gold electrode (0.121 cm^2) in a solution of CrBr_3 in LiBr-KBr-CsBr at 381°C . (a) 7.9×10^{-3} molal; (b) 12.7×10^{-3} molal. Sweep rate, 2 mVs^{-1} ; pulse height, 25 mV . Initial potential: (a) $\sim 521 \text{ mV vs. Ag/Ag(I)}$; (b) $\sim 537 \text{ mV vs. Ag/Ag(I)}$.

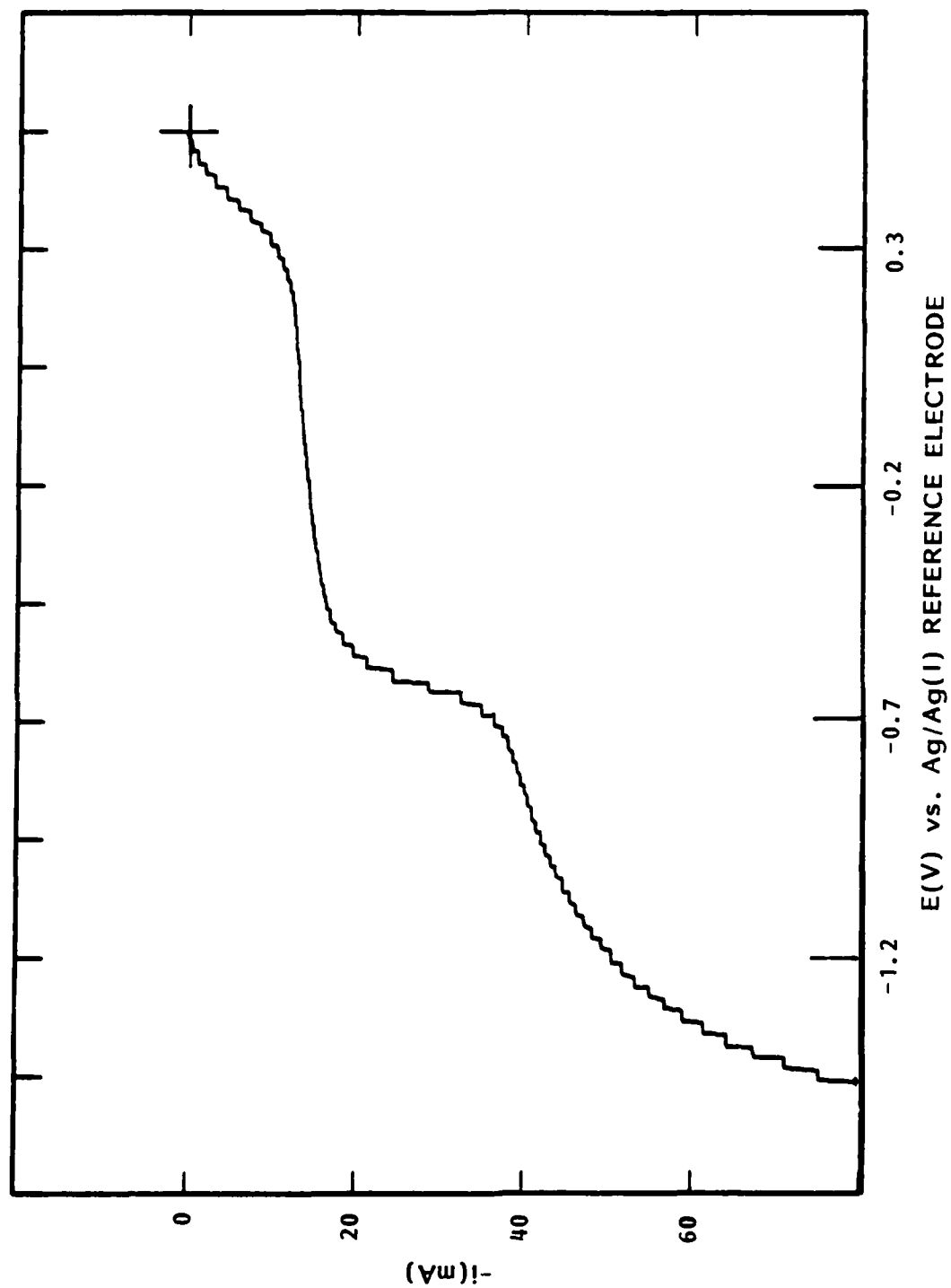


Fig. 16. Normal pulse voltammograms for the electroreduction of Cr(III) in LiBr-KBr-CsBr eutectic mixture at 374°C on a gold electrode (0.12 cm^2).

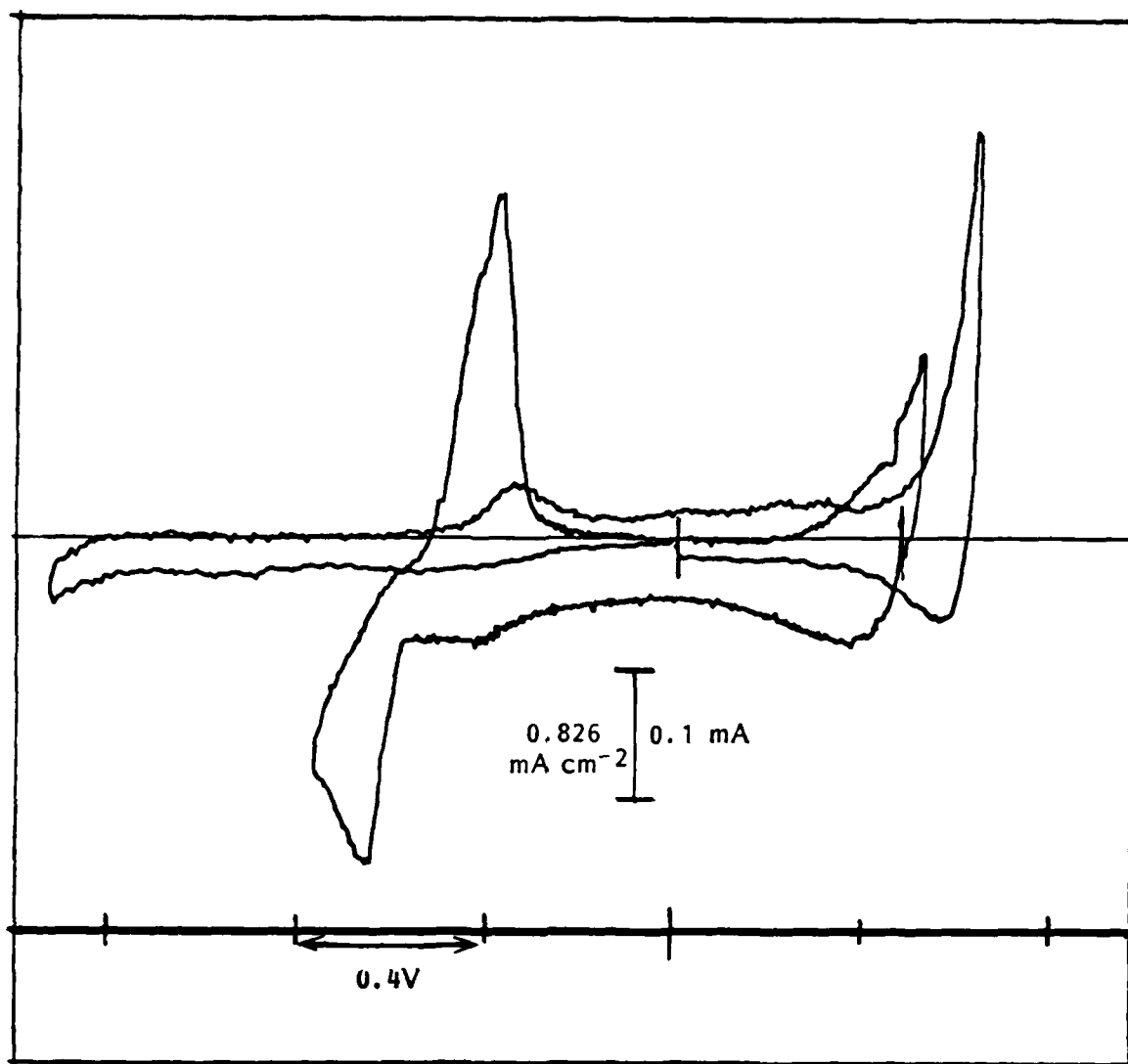


Fig. 17. Cyclic voltammograms for (a) the LiBr-KBr-CsBr eutectic and (b) the eutectic with an addition of nominally 7.88×10^{-3} molal CrBr_3 . Scan rate = 50 mVs^{-1} ; gold microelectrode ($A = 0.121 \text{ cm}^2$). Rest potential:

- (a) +26 mV vs. Ag/AgBr (0.141M) eutectic; $T = 325^\circ\text{C}$.
- (b) +526 mV vs. Ag/AgBr (0.141M) eutectic; $T = 385^\circ\text{C}$.

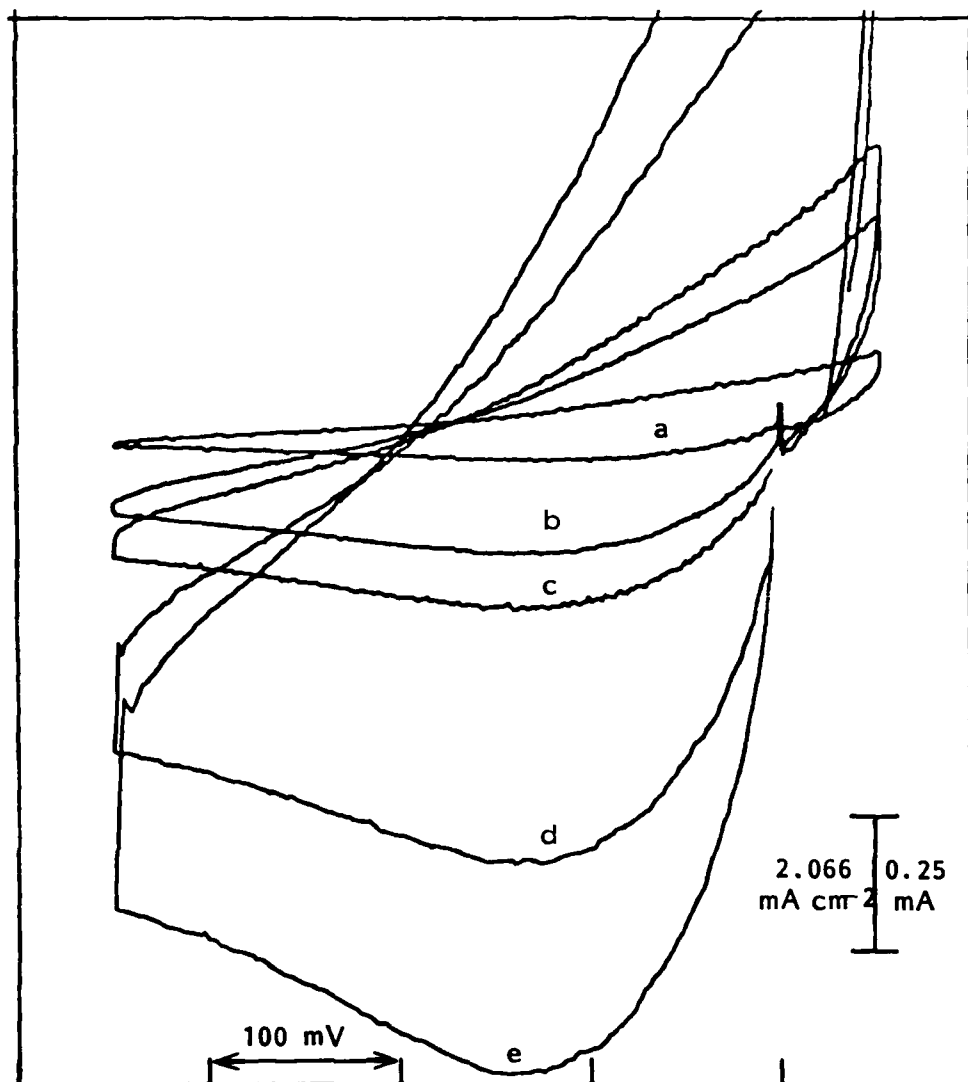


Fig. 18. Cyclic voltammograms acquired at a gold electrode (0.121 cm²) in a solution of 7.9×10^{-3} molal CrBr₃ in LiBr-KBr-CsBr eutectic at 381°C. Scan rates: a) 0.050 Vs⁻¹; b) 0.500 Vs⁻¹; c) 1.00 Vs⁻¹; d) 5.00 Vs⁻¹; e) 10.0 Vs⁻¹. R.P. = 0.520V vs. Ag/Ag(I) reference electrode.

TABLE 7

ANALYSIS OF CYCLIC VOLTAMMETRIC DATA FOR REV/SOL BOTH OX AND RED IN SOLUTION

Temperature 3810C
 Electrode Area 0.121 cm²
 Switching Potential -0.35 volts
 Initial Potential 0.00 volts
 Rest Potential 0.523 volts vs. ref electrode Ag/Ag⁺ (0.39M) in Bromide melt

Scan Rate	Current 10 ⁶ Amps	Peak Pot ⁿ Volts	E(p)-Ep/2	E(p)-E(i) *nF/RT	(CD ^{1/2} /2)OX (CD ^{1/2} /2)RED	$\pi^{1/2}$ $\chi(i)$	i(p) $AV^{1/2}$	(CD ^{1/2} /2)OX mol.cm ⁻² s ^{-1/2}	CAIC E(1/2) Volts
0.2000	16200	-0.125	-0.112	2.2168	2.5714	0.4918	0.00298	1.49 x 10 ⁻⁸	-0.0538
0.5000	253	-0.125	-0.115	2.2168	2.5714	0.4918	0.00296	1.48 x 10 ⁻⁸	-0.0533
1.0000	358	-0.125	-0.115	2.2168	2.5714	0.4918	0.00296	1.48 x 10 ⁻⁸	-0.0533
2.0000	512	-0.125	-0.115	2.2168	2.5714	0.4918	0.00299	1.50 x 10 ⁻⁸	-0.0533
5.0000	834	-0.125	-0.115	2.2168	2.5714	0.4918	0.00308	1.54 x 10 ⁻⁸	-0.0533
10.0000	1240	-0.125	-0.115	2.2168	2.5714	0.4918	0.00323	1.62 x 10 ⁻⁸	-0.0533
0.2000	159	-0.125	-0.105	2.2168	2.5714	0.4918	0.00293	1.47 x 10 ⁻⁸	-0.0533
10.0000	1230	-0.130	-0.120	2.3054	2.8565	0.4885	0.00322	1.62 x 10 ⁻⁸	-0.0592
0.0500	79.8	-0.120	-0.115	2.1281	2.3012	0.4995	0.00295	1.46 x 10 ⁻⁸	-0.0470
0.0200	48.8	-0.120	-0.110	2.1281	2.3012	0.4955	0.00285	1.42 x 10 ⁻⁸	-0.0470
0.0500	78.5	-0.1200	-0.1100	2.1281	2.3012	0.4955	0.00290	1.44 x 10 ⁻⁸	-0.0470
Average				2.52	0.493		0.00301	1.50 x 10 ⁻⁸	
Standard Deviation				0.166	0.00216		0.000123	6.63 x 10 ⁻¹⁰	

TABLE 8

ANALYSIS OF CYCLIC VOLTAMMETRIC DATA FOR
REV/SOL BOTH OX AND RED IN SOLUTION

Temperature = 385°C
 Area of Au Electrode = 0.121 cm²
 Switching Potential = -1.400V
 Initial Potential = 0V
 Rest Potential = 0.541V vs. reference electrode Ag/Ag⁺
 (0.39M) in Bromide melt

Scan Rate	Current Amps	Peak Pot ⁿ Volts	E _(1/2) Expn	Ep-Ep/2	Ep-E ₁ nF/RT	(CD ^{1/2}) _{OX} (CD ^{1/2}) _{RED}	n ^{1/2} X(i)	I _p /v ^{1/2} _A AV ^{-1/2} s ^{1/2} cm ⁻²	(CD ^{1/2}) _{OX}	E _(1/2) Calc
0.0200	5.10 × 10 ⁻⁵	-0.1000	-0.0500	-0.0875	1.7626	1.3459	0.5154	2.96 × 10 ⁻³	1.43 × 10 ⁻⁸	-0.0169
0.0500	8.00 × 10 ⁻⁵	-0.1000	-0.0500	-0.0875	1.7626	1.3459	0.5154	2.96 × 10 ⁻³	1.42 × 10 ⁻⁸	-0.0169
0.0500	8.20 × 10 ⁻⁵	-0.1125	-0.0410	-0.0880	1.9830	1.8914	0.5025	3.03 × 10 ⁻³	1.49 × 10 ⁻⁸	-0.0362
0.0500	8.00 × 10 ⁻⁵	-0.1125	-0.0520	-0.1000	1.9830	1.8914	0.5025	2.96 × 10 ⁻³	1.45 × 10 ⁻⁸	-0.0362
0.0500	8.20 × 10 ⁻⁵	-0.1160	-0.0625	-0.0950	2.0446	2.0607	0.4994	3.03 × 10 ⁻³	1.50 × 10 ⁻⁸	-0.0410
0.1000	1.20 × 10 ⁻⁴	-0.1000	-0.0500	-0.0875	1.7626	1.3459	0.5154	3.14 × 10 ⁻³	1.50 × 10 ⁻⁸	-0.0169
0.2000	1.75 × 10 ⁻⁴	-0.1120	-0.0530	-0.0940	1.9741	1.8678	0.5029	3.23 × 10 ⁻³	1.59 × 10 ⁻⁸	-0.0354
0.5000	3.00 × 10 ⁻⁴	-0.1160	-0.0580	-0.0910	2.0446	2.0607	0.4994	3.51 × 10 ⁻³	1.73 × 10 ⁻⁸	-0.0410
0.5000	2.90 × 10 ⁻⁴	-0.1200	-0.0580	-0.1070	2.1152	2.2631	0.4961	3.39 × 10 ⁻³	1.69 × 10 ⁻⁸	-0.0463
1.0000	4.30 × 10 ⁻⁴	-0.1250	-0.0660	-0.1000	2.2033	2.5294	0.4924	3.55 × 10 ⁻³	1.78 × 10 ⁻⁸	-0.0526
2.0000	6.30 × 10 ⁻⁴	-0.1380	-0.0740	-0.1130	2.4324	3.2911	0.4843	3.68 × 10 ⁻³	1.86 × 10 ⁻⁸	-0.0676
5.0000	1.11 × 10 ⁻³	-0.1550	-0.0875	-0.1250	2.7321	4.4383	0.4763	4.10 × 10 ⁻³	2.13 × 10 ⁻⁸	-0.0845
Mean						1.68	0.508	3.05 × 10 ⁻³	1.48 × 10 ⁻⁸	
Standard Deviation						0.317	0.00738	1.03 × 10 ⁻⁴	5.78 × 10 ⁻¹⁰	

Reduction Cr(II) → Cr(0)

I _p mAmps	i _p /v ^{1/2} _A AV ^{-1/2} s ^{1/2} cm ⁻²	Ep V	Ep-Ep/2 V	(CD ^{1/2}) _{RE}
0.236	1.37 × 10 ⁻²	-1.1100		1.97 × 10 ⁻⁸
0.408	1.51 × 10 ⁻²	-1.1120	-0.0200	2.16 × 10 ⁻⁸
0.408	1.51 × 10 ⁻²	-1.1140	-0.0180	2.16 × 10 ⁻⁸
0.391	1.45 × 10 ⁻²	-1.1180	-0.0200	2.07 × 10 ⁻⁸
0.426	1.57 × 10 ⁻²	-1.1180	-0.0180	2.25 × 10 ⁻⁸
0.630	1.65 × 10 ⁻²	-1.1150	-1.1160	2.36 × 10 ⁻⁸
0.995 × 10 ²	1.65 × 10 ⁻²	-1.1300		2.37 × 10 ⁻⁸
1.34	1.57 × 10 ⁻²	-1.1150		2.24 × 10 ⁻⁸
1.20	1.40 × 10 ⁻²	-1.1630		2.01 × 10 ⁻⁸
1.49	1.23 × 10 ⁻²	-1.1950		1.77 × 10 ⁻⁸
1.86	1.09 × 10 ⁻²	-1.2750		1.56 × 10 ⁻⁸
2.48	9.17 × 10 ⁻³	-1.2800		1.31 × 10 ⁻⁸

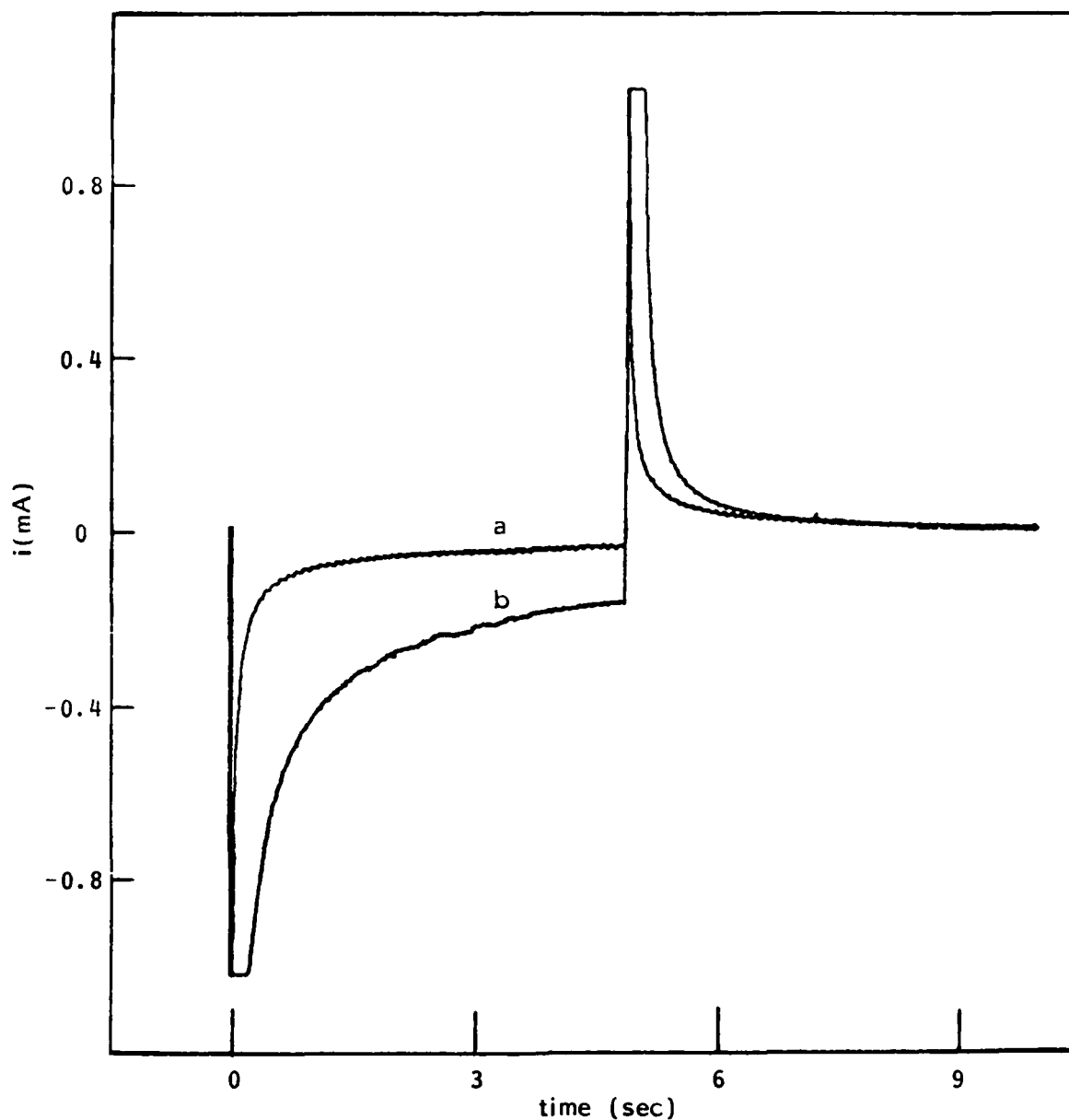


Fig. 19. Current time transient acquired at gold electrode (0.12 cm^2) for the electroreduction of Cr(III) in LiBr-KBr-CsBr eutectic mixture at 377°C for the potential step a) -600 mV and b) -1.5V from the rest potential 0.543V vs. $\text{Ag}/\text{Ag(I)}$ reference electrode.

TABLE 9

ANALYSIS OF REPRESENTATIVE DOUBLE STEP CHRONOAMPEROMETRIC
DATA FOR THE REDUCTION OF Cr(III) TO Cr(II) IN ALKALI
METAL BROMIDE MELT AT 382°C

Gold Electrode Area = 0.121 cm²

Cr(III) Concentration ~ 32 mM

Switching Time τ = 4.87 sec

Switching Charge = 0.382 mC

Rest Potential Gold WE = 0.534V vs. Ag reference

Applied Forward Step = -0.600V

Forward t sec	Current Amps	Charge 10 ⁴ C	Qt ^{-1/2} 10 ⁴ C s ^{-1/2}	Diff Coef 10 ⁷ cm ² s ⁻¹	it ^{1/2} 10 ⁵ As ^{1/2}	Diff Coef 10 ⁷ cm ² s ⁻¹	$\frac{Q(t < \tau_f)}{Q(t_f)}$	$\frac{Q(t < \tau_f)}{Q(t_f)}$	10 ² ΔQ
0.5	13.0	1.44	2.03	2.36	8.84	1.79	0.320	0.376	-5.6
1.0	8.40	1.95	1.95	2.17	8.40	1.62	0.453	0.510	-5.7
1.5	6.60	2.31	1.89	2.04	8.08	1.50	0.555	0.606	-5.1
2.0	5.55	2.61	1.85	1.95	7.85	1.41	0.641	0.684	-4.3
2.5	5.00	2.87	1.82	1.89	7.91	1.43	0.716	0.752	-3.6
3.0	4.50	3.11	1.80	1.85	7.79	1.39	0.785	0.815	-3.0
3.5	4.25	3.32	1.77	1.81	7.95	1.45	0.848	0.870	-2.2
4.0	3.85	3.52	1.76	1.78	7.70	1.36	0.906	0.923	-1.6
4.5	3.50	3.70	1.74	1.74	7.42	1.27	0.916	0.969	-0.7
4.87	3.05	3.82	1.73	1.71	6.73	1.04	1.00	1.00	0.0

Mean 1.83x10⁴ 1.93x10⁻⁷ 7.87x10⁻⁵ 1.43x10⁻⁷

Standard Deviation 9.65x10⁻⁶ 2.07x10⁻⁸ 5.58x10⁻⁶ 2.00x10⁻⁸

Reverse t, sec	θ sec ^{1/2}	10δ sec ^{1/2}	Reverse Current 10 ⁵ A	Reverse Charge 10 ⁴ C	$\frac{10^4 Q(R)}{\theta}$	Diff Coef 10 ⁷ cm ² s ⁻¹	$\frac{10^5 i(R)}{\delta}$	Diff Coef 10 ⁷ cm ² s ⁻¹	$\frac{Q(t < \tau_f)}{Q(t_f)}$ 10X	$\frac{Q(t < \tau_f)}{Q(t_f)}$ 10X	10 ² ΔQ
5.37	0.60	9.83	8.65	1.24	2.07	2.46	8.80	1.78	7.30	6.76	5.31
5.87	0.78	5.87	4.85	1.55	1.98	2.24	8.26	1.57	6.45	5.94	5.10
6.37	0.91	4.20	3.35	1.74	1.91	2.10	7.97	1.46	5.89	5.45	4.3
6.87	1.00	3.26	2.65	1.89	1.89	2.04	8.14	1.52	5.47	5.06	4.1
7.37	1.07	2.64	2.00	2.00	1.86	1.99	7.57	1.32	5.14	4.76	3.8
7.87	1.13	2.21	1.65	2.10	1.85	1.96	7.47	1.28	4.86	4.51	3.6
8.37	1.18	1.89	1.45	2.17	1.83	1.93	7.68	1.35	4.63	4.31	3.2
8.87	1.23	1.64	1.25	2.24	1.82	1.90	7.61	1.33	4.43	4.14	2.9
9.37	1.27	1.45	1.05	2.30	1.81	1.88	7.26	1.21	4.26	3.98	2.7
9.87	1.30	1.29	0.80	2.34	1.80	1.86	6.21	8.84	4.10	3.87	2.4

Mean 1.80x10⁻⁴ 2.04x10⁻⁷ 7.70x10⁻⁵ 1.37x10⁻⁷

Standard Deviation 8.51x10⁻⁶ 1.89x10⁻⁸ 6.91x10⁻⁶ 2.38x10⁻⁸

TABLE 10

ANALYSIS OF REPRESENTATIVE CHRONOAMPEROMETRIC DATA FOR THE REDUCTION
OF Cr(III) TO Cr(0) IN THE ALKALI METAL BROMIDE MELT AT 382°C

Gold Electrode area = 0.121cm^2 Cr(III) concentration ~ 32 mM
 Switching time = 4.87 sec Switching charge $Q(t) = 1.65\text{ mC}$
 Rest Potential of gold WE = 0.534 vs. Ag reference
 Applied potential step = -1.500V

Time Sec	Current 10^4Amps	Charge Q 10^3C	$Qt^{-1/2}$ $10^4\text{C s}^{-1/2}$	Diff Coef $10^7\text{cm}^2\text{s}^{-1}$	$it^{1/2}$ $10^4\text{Amps}^{1/2}$	Diff Coef $10^7\text{cm}^2\text{s}^{-1}$	$Q(t < t_f)$ $Q(t_f)$	$Q(t < t_f)$ $Q(t_f)$	$10^3\Delta Q$
5.00	6.66	0.44	6.28	2.51	4.71	5.66	0.320	0.268	52.0
1.00	4.34	0.71	7.10	3.21	4.34	4.80	0.453	0.429	24.0
1.50	3.40	0.90	7.38	3.47	4.16	4.42	0.555	0.547	8.4
2.00	2.84	1.05	7.45	3.54	4.02	4.11	0.641	0.637	3.6
2.50	2.46	1.19	7.51	3.60	3.89	3.86	0.716	0.718	-1.8
3.00	2.26	1.31	7.54	3.63	3.91	3.91	0.785	0.790	-4.7
3.50	2.00	1.41	7.55	3.63	3.74	3.57	0.848	0.854	-5.9
4.00	1.84	1.51	7.53	3.62	3.68	3.45	0.906	0.911	-4.2
4.50	1.72	1.59	7.50	3.59	3.65	3.40	0.961	0.963	-1.3
4.87	1.62	1.66	7.50	3.59	3.58	3.26	1.00	1.00	-1.2
Mean			7.3×10^{-4}	3.44×10^{-7}	3.97×10^{-4}	4.04×10^{-7}			
Standard Deviation			3.95×10^{-5}	3.28×10^{-8}	3.54×10^{-5}	7.44×10^{-8}			

TABLE 11

SUMMARY OF CHRONOAMPEROMETRIC AND COULOMETRIC RESULTS FOR
LiBr-KBr-CsBr EUTECTIC AT 385°CConcentration of Cr(III) $\approx 32 \times 10^{-6}$ mol cm $^{-3}$ Area of gold electrode = 0.121 cm 2

Rest potential of gold = +0.534V vs. Ag reference

FIRST REDUCTION PROCESS $\text{CrBr}_3 + e = \text{CrBr}_2 + \text{Br}^-$

	$10^4 Q_f t^{-1/2}$ (C s $^{-1/2}$)	$10^6 D(\text{Cr}^{3+})$ (cm 2 s $^{-1}$)	$10^4 Q_f t^{-1/2}$ (C s $^{-1/2}$)	$10^6 D(\text{Cr}^{3+})$ (cm 2 s $^{-1}$)	Pot n (mv)	$i_f t^{1/2}$ (As $^{1/2}$)	$10^6 D_f(\text{Cr}^{3+})$ (cm 2 s $^{-1}$)	$i_f t^{1/2}$ (As $^{1/2}$)	$10^6 D_r(\text{Cr}^{3+})$ (cm 2 s $^{-1}$)	$Q_C - Q_E^*$
5s pulse	1.54 + 0.066	0.136 + 0.012	1.64 + 0.081	0.155 + 0.016	-400	0.687 + 0.032	0.109 + 0.010	0.707 + 0.040	0.115 + 0.013	-ve for forward +ve for reverse
2s pulse	1.90 + 0.079	0.208 + 0.017	1.78 + 0.291	0.187 + 0.48	-600	0.845 + 0.072	0.165 + 0.029	0.822 + 0.050	0.155 + 0.020	-ve for forward +ve for reverse
5s pulse	1.83 + 0.097	0.193 + 0.021	1.88 + 0.085	0.204 + 0.019	-600	0.787 + 0.056	0.143 + 0.020	0.770 + 0.069	0.137 + 0.024	-ve for forward +ve for reverse

FIRST AND SECOND REDUCTION PROCESSES $\text{CrBr}_3 + 3e = \text{Cr} + 3\text{Br}^-$

	$10^4 Q_f t^{-1/2}$ (C s $^{-1/2}$)	$10^6 D(\text{Cr}^{3+})$ (cm 2 s $^{-1}$)	$10^4 Q_f t^{-1/2}$ (C s $^{-1/2}$)	$10^6 D(\text{Cr}^{3+})$ (cm 2 s $^{-1}$)	Pot n (mv)	$i_f t^{1/2}$ (As $^{1/2}$)	$10^6 D_f(\text{Cr}^{3+})$ (cm 2 s $^{-1}$)	$i_f t^{1/2}$ (As $^{1/2}$)	$10^6 D_r(\text{Cr}^{3+})$ (cm 2 s $^{-1}$)	$Q_C - Q_E^*$
2s pulse	8.93 + 0.184	0.509 + 0.021	-	-	-1500	4.31 + 0.462	0.478 + 0.107	-	-	-ve for forward
5s pulse	7.34 + 0.395	0.344 + 0.035	-	-	-1500	3.97 + 0.354	0.404 + 0.074	-	-	50% +ve 50% -ve

$$*Q_C - Q_E = \frac{Q(t < \tau)(\text{calc})}{Q_T} - \frac{Q(t < \tau)(\text{exp})}{Q_T}$$

3.2.3 Solutions of Cr(III) in Lithium Bromide - Potassium Bromide - Caesium Bromide Eutectic Mixture

The solutions of Cr(III) ions in the bromide melt were reduced by the addition of chromium metal. A well defined peak for the reduced product Cr(II) was observed voltammetrically after the solution was raised to 450°C. The stepwise cooling of the solution to 272°C is shown in Figure 20. No dramatic changes in the electrochemical response was observed above 292°C. At the lowest temperature of 272°C, the anodic response at potentials positive to that of the silver reference was not that expected for the oxidation of Cr(II) to Cr(III). The shapes of the voltammetric responses indicated the formation of an insoluble product which might indicate low solubility of the Cr(III) at this low temperature. This aspect of the chemistry was not explored further. The range of electroactivity of the melt containing Cr(II) ions is illustrated for three different temperatures in Figure 21. A window of between 3.2 and 3.3V is expected on the basis of thermodynamic data (20) for the individual melts. The measured values of around 2.5V probably reflect activity effects associated with the use of a mixed melt and perhaps some under-potential effects on the gold and chromium coated gold electrode.

The reduction of Cr(II) ions to Cr metal is demonstrated by the shape of the voltammograms at all the temperatures explored in this work. Figure 22 illustrates that the sharp anodic peak arises as a result of the presence of the cathodic peak. The charge in the anodic peak depends upon the switching potential for the cathodic sweep. The linear relationship between the measured i_p for the reduction peak at different scan rates is reported for five of the temperatures examined in Figure 23. Some curvature above 2 V/s may reflect uncompensated IR effects. When the more sensitive plot of $i_p v^{-1/2}$ vs. v is made, some decrease in the current function at low scan rates is detected. This could reflect spherical diffusion due to the metal nucleation and growth in the early stages of the reduction process. At the lower temperatures, a prepeak is visible prior to the main reduction peak. Although Figure 17 shows the presence of a peak in a similar potential range initially in the melt, the introduction of chromium metal reducing agent should have reduced all species more noble than chromium. A similar feature is apparent at 450°C in LiCl-KCl melt for the reduction of Cr^{2+} ions on the gold substrate. It is possible, therefore, that the prepeak is due to some aspect of the chromium (II) ion reduction process. At 292°C, the peak is well defined and grows with scan rate as illustrated in Figure 24. A corresponding anodic oxidation process can be detected after the sharp stripping peak and the correspondence of charge was confirmed by integration of the voltammogram as shown in Figure 25. The charge measured for scan rates between 2 and 20 V/s was constant corresponding to $600 \mu C cm^{-2}$. Such a value represent close to monolayer coverage of the electrode. The potential excursion for this process is some 0.2V corresponding to times ranging between 10 and 100 ms. It can be noted that a predeposition process for Zn^{2+} reduction on gold is also seen in the $ZnCl_2$ -KCl (see Section 3.4). Thus, some predeposition feature is common to metal forming processes on gold. These observations are particularly relevant to the studies of metal deposition presented in Section 3.3.

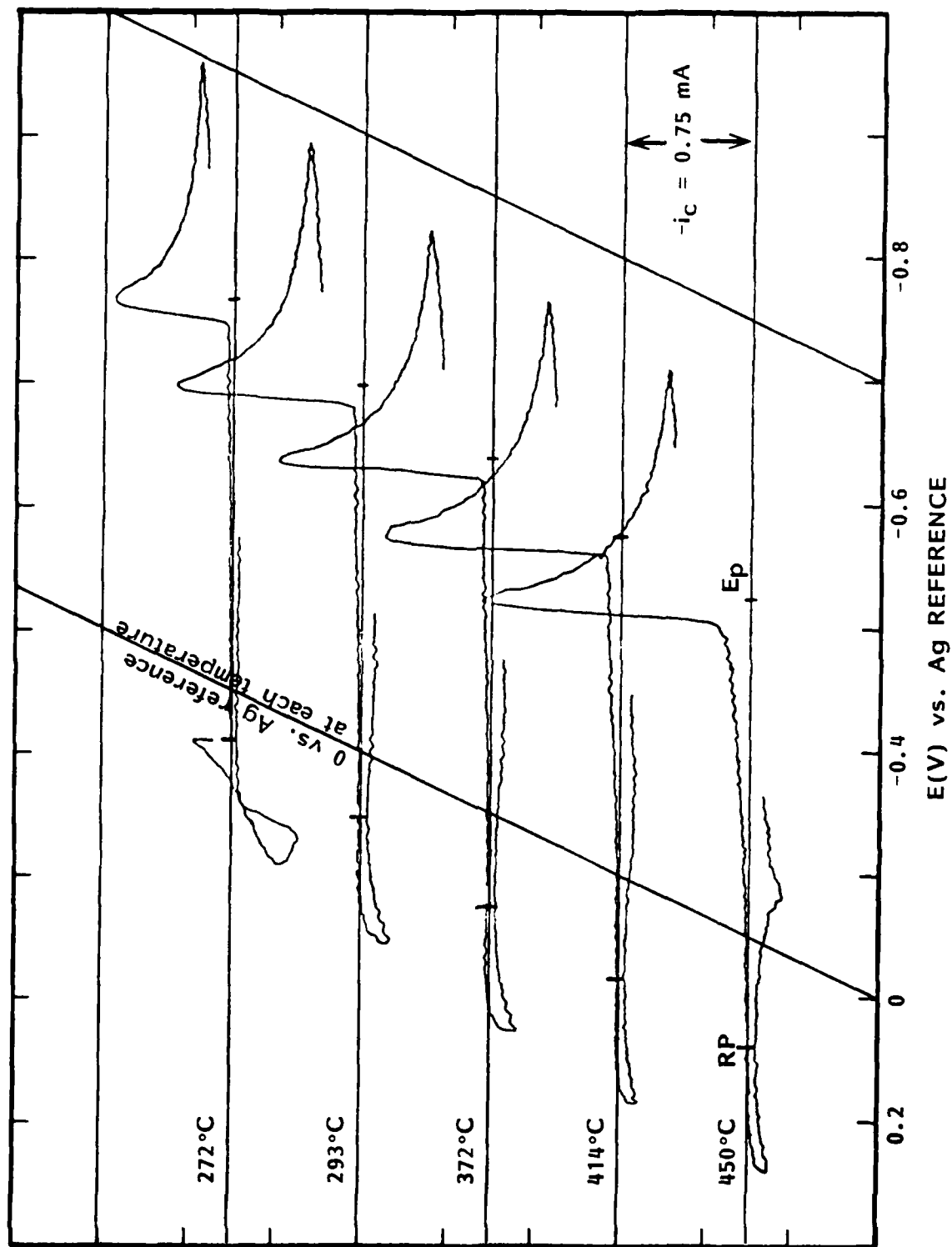


Fig. 20. The influence of temperature on the voltammetric reduction peak on gold for Cr(II) ions in the ternary alkali bromide eutectic acquired at 50 mVs⁻¹. The reverse metal oxidation peak has been omitted for clarity.

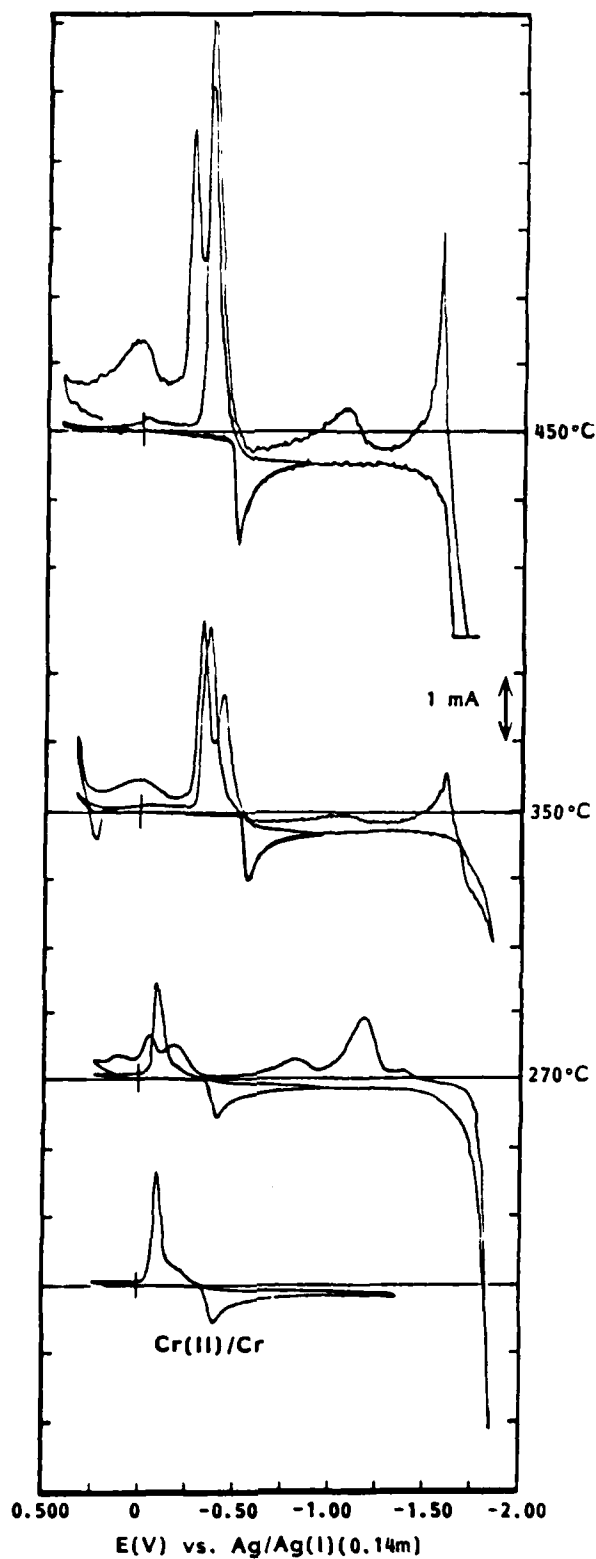


Fig. 21. Comparison of Cr(II) ion reductions relative to the solvent window at three different temperatures in the ternary bromide eutectic. Scans acquired at 50 mVs^{-1} . Gold electrode ($A = 0.088 \text{ cm}^2$).

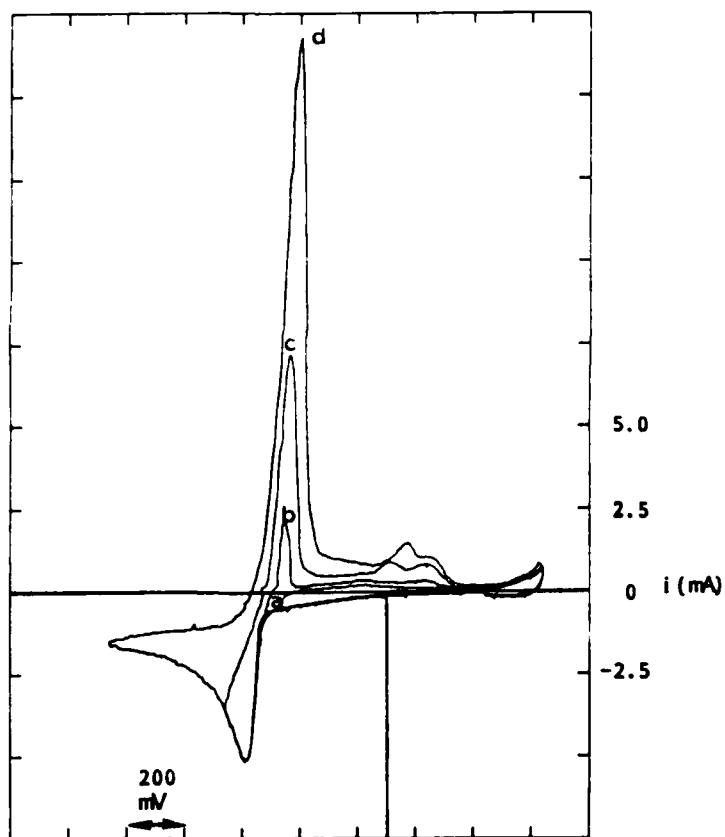
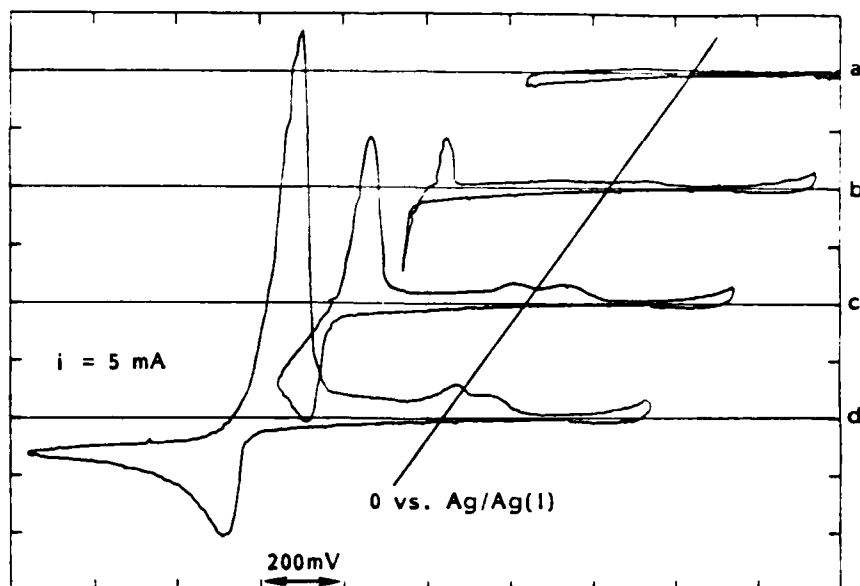


Fig. 22. Influence of switching potential on the deposition and stripping of Cr on gold from ternary bromide melt at 450°C and scan rate of 1 Vs^{-1} .

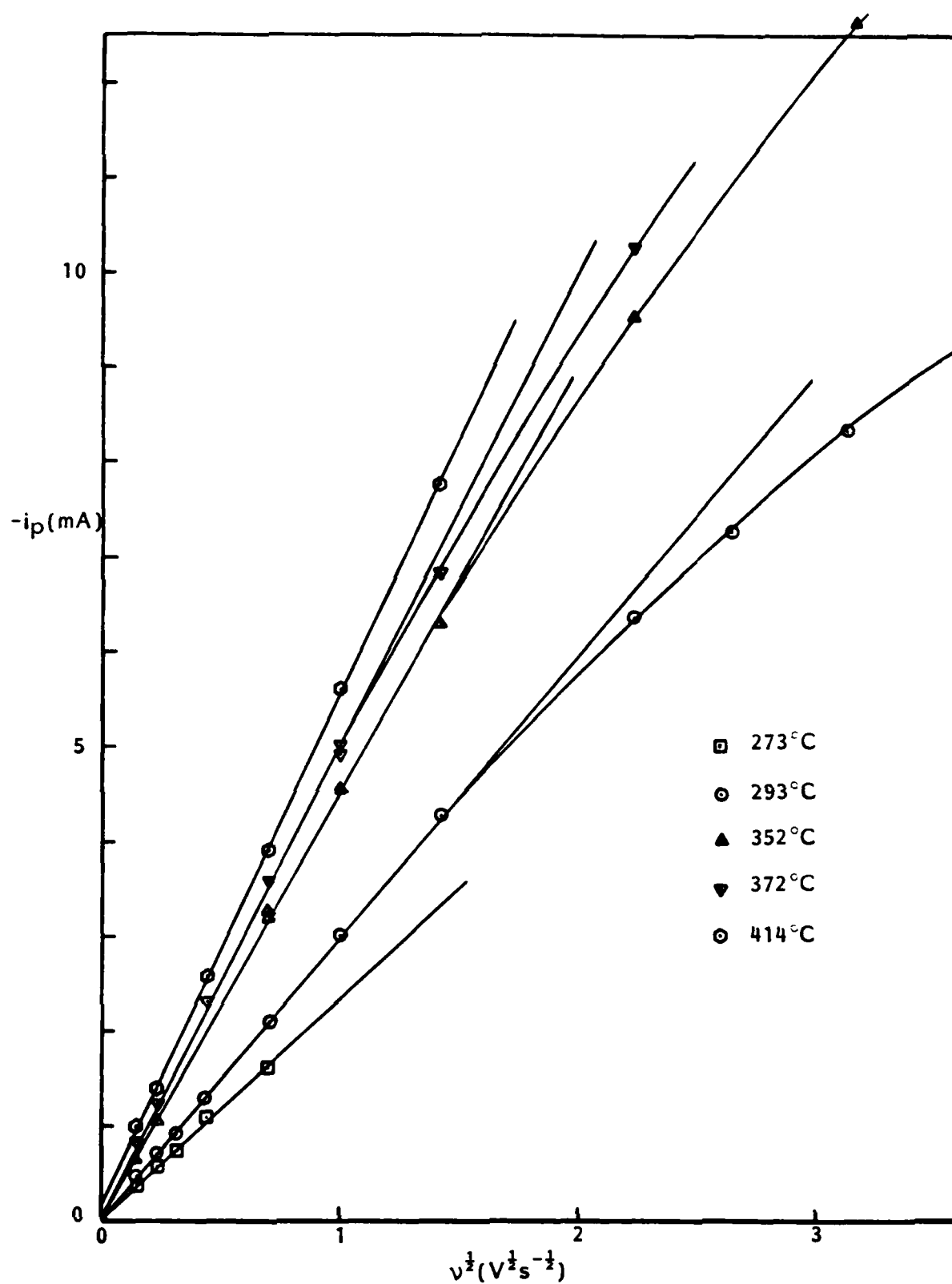


Fig. 23. Plots of the peak current for the reduction of Cr(II) ions in the ternary alkali metal bromide melt at five different temperatures as a function of the square root of the scan rate.

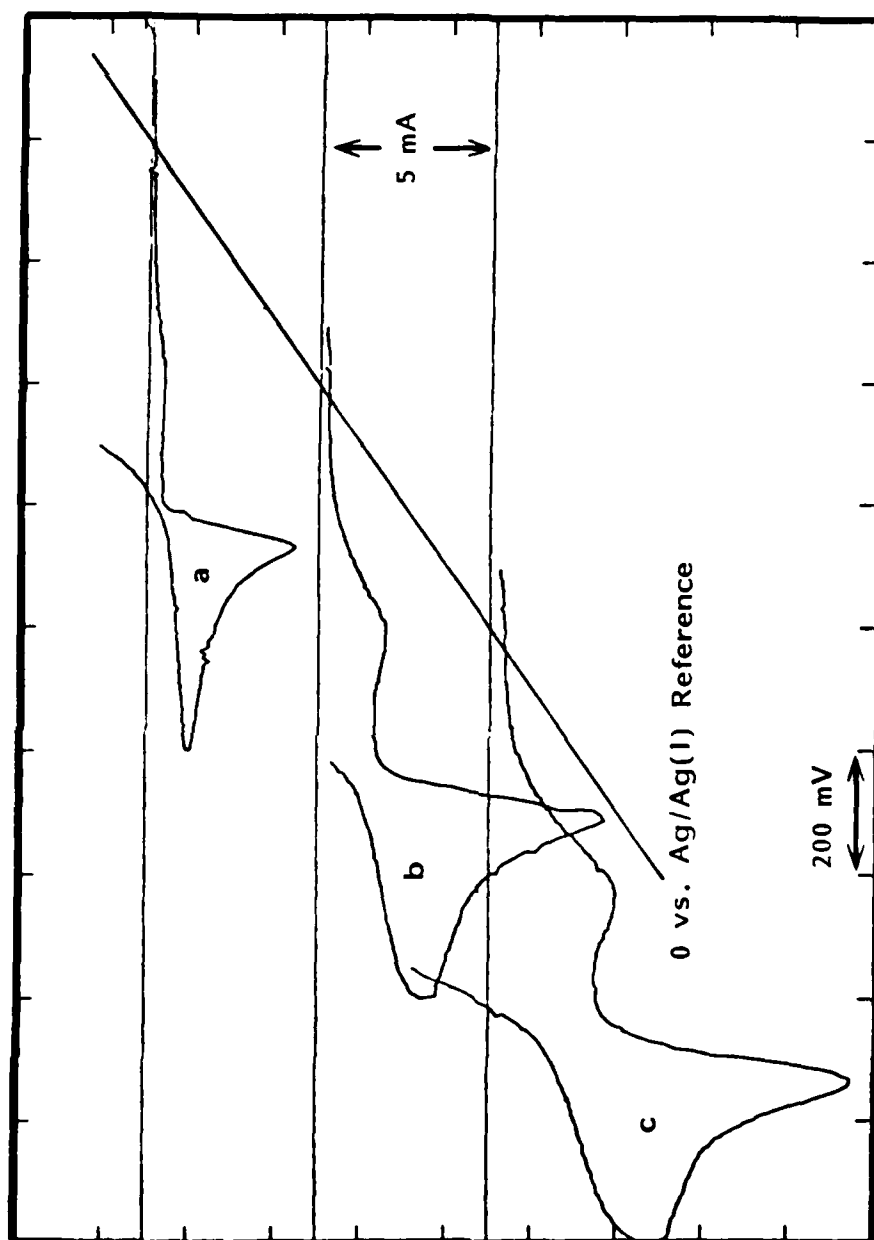


Fig. 24. The influence of sweep rate on the development of the prepeak during the reduction of Cr(II) on a gold substrate in the ternary alkali bromide eutectic at 293°C. a) 2 Vs⁻¹; b) 10 Vs⁻¹; c) 20 Vs⁻¹. The reverse sweep is omitted for clarity.

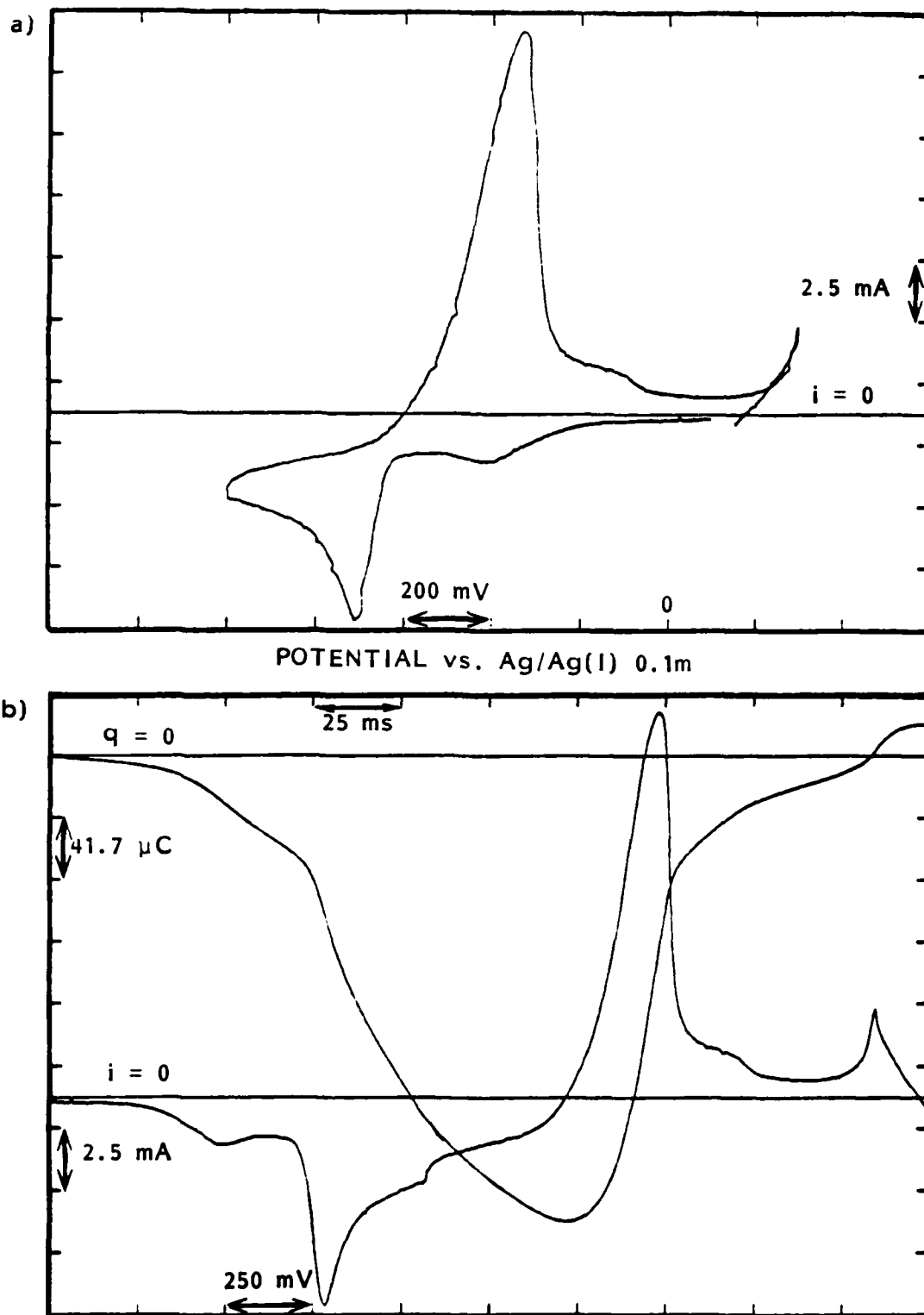


Fig. 25. Analysis of prepeak for the reduction of Cr(II) in the ternary alkali bromide eutectic at 295°C, gold substrate. a) Potential relationships between cathodic and anodic processes; b) voltammogram and its integral showing charge for prepeak and post stripping peak. Scan rate = 10 Vs⁻¹.

3.2.4 Discussion of Chromium Solution Chemistry

Table 12 shows a summary of studies made in recent years on the electrochemistry of chromium in fluorides, chlorides, bromides, and aluminum chloride containing melts. The major focus of attention has been on the use of chloride melts. However, it was shown that fluoride melts operating at temperatures in excess of 800°C will produce coherent deposits of chromium (4,30). The solution chemistry of these melts has been difficult to resolve in spite of efforts by both Senderoff (30) and Yoko and Bailey (31), and it is unclear at this time whether the electroactive species present in the solution of the molten fluoride is a chromium (IV) or a chromium (II) species. In contrast to the fluoride electrolytes, chloride and bromide melts containing chromium (III) or (II) ions have been investigated and shown to possess a considerably simpler solution chemistry, although it is clear from the studies here that maintaining low concentrations of chromium (II) ions in solution without some oxidative loss (see below) requires exceptional care in cell seals and gas purification. Nevertheless, chromium metal has been plated from both of these electrolytes (32-34), and it is pertinent to explore the reasons for the apparent ease by which these melts yield coherent metal.

The chemistry of chromium (III) and chromium (II) halides dissolved in alkali metal chlorides and bromides is relatively straightforward. Spectroscopic studies suggest that chromium (II) ions are present in alkali metal chloride (and bromide) melts as octahedral complexes $[\text{CrX}_6]^{-3}$. Spectroscopic studies of chromium (II) ions in the same melts show a band at 9800 cm^{-1} , but the nature of the configuration responsible for this spectrum has not been identified (35). However, it has been suggested that on the basis of other first row transition metal divalent ions that the chromium (II) halocomplex present in the melts is a distorted tetrahedral species (22). Chromium (II) ions are readily reduced by a two electron transfer to metal in both alkali chloride (32,33) and bromide (34) solutions. On the other hand, oxidation of chromium (II) takes place in these melts via a one electron process to the chromium (III) species at 450°C. This latter oxidation process would allow the measurement of the diffusion coefficients of chromium (II) ions in chloride and bromide melts without the complications associated with electrocrystallization phenomena which normally arise in the reduction process to metal. However, the uncertainty in the concentration of Cr(II) ions in solution has resulted in poor precision for this quantity. In addition to these difficulties in the case of the bromide melt, the density of the ternary mixture has not been measured so that only approximate values based upon additivity of the densities of the pure salts must be used. The magnitude of the diffusion coefficient of Cr(II) of $0.2 \times 10^{-5}\text{ cm}^2\text{s}^{-1}$ estimated for the bromide at 273°C suggests that this melt is quite suitable for the electrodeposition of chromium metal.

Consequently, it is to be concluded that chromium (II) ions in molten alkali chloride or bromide solutions are relatively easy to use

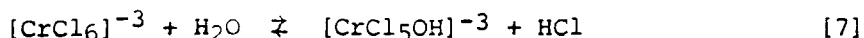
TABLE 12

SUMMARY OF THE ELECTROCHEMISTRY OF CHROMIUM

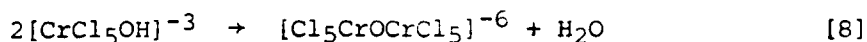
Melt	Solute and/or Mean Valency	Temp. (°C)	Reduction Pathway	No. of Electrons (n)	Deposit Form	Ref.
LiF-KF-NaF	CrF ₄	900	Cr(IV) → Cr(O)	4	Coherent	[30]
LiCl-KCl	Cr anodization to Cr(III) & oxidation to Cr(III) and CrCl ₂ addn.	450-500	Cr(III) → Cr(II) Cr(II) → Cr(O) (irr.)	1 2	Coherent	[33, 36]
LiCl-KCl NaBr, KBr	CrCl ₂	550-750	Cr(II) → Cr(O)		Dendrite	[37]
LiCl-KCl LiBr-KBr-CsBr	Cr anodization Cr(III)	450 270-450	Cr(II) → Cr(II) Cr(II) → Cr(O) Rev.	2	Coherent	[32] [34]
LiCl-KCl	CrCl ₃	500	Cr(III) → Cr(II) Cr(II) + 2Cl ⁻ → CrCl ₂ (insoluble) and Cr(II) → Cr(O)	1 2		[38]
LiF-NaF-KF	CrF ₃	550-1000	Cr(III) → Cr(II) Cr(II) → Z Z → (x/2)Cr(O) Z → Cr(III)	1 (x)	Coherent above 900°C	[39]
NaCl-AlCl ₃ 1:1 1:2	CrCl ₃	175	Cr(III) → Cr(II) Cr(III) → Cr(II) ndsp Cr(II) → Cr(O) Cr(I)ads → Cr(O)	1 1 2	No deposit	[39]
LiCl-KCl	CrCl ₃	450	Cr(III) → Cr(II) Cr(III) → Cr(O)	1 2		[40]
NaCl-KCl		700	Cr(III) + 2e → Cr(II) Cr(III) + 2e → Cr(O) irr	1 2		[41]
LiCl-KCl	CrCl ₃	450	Cr(III) → Cr(II) [CrCl ₅ OH] ³⁻ → [CrCl ₅ OH] ⁴⁻	1 1		[41, 42]
NaCl	CrCl ₂	815-1015	Cr(II) → Cr(O) rev.	2		[43]
NaF-CaF ₂	CrF ₂	1050-1100	Cr(II) → Cr(M)		Chromium	[44]
LiF-NaF-KF	CrF ₂ CrF ₃ TaF ₅	800-900			Coherent Cr & Cr/Ta alloy	[45]

for metal deposition because in these solutions chemical processes involve simple complex ions whose transitions are rapid and transport controlled in contrast to molybdenum (vide ultra). However, for plating where more stringent conditions are required of the deposition process several complications have been identified, particularly as more detailed studies are made which still require complete resolution. Three areas are significant in the development of a high temperature (H.T.) chromium plating process. The first already touched upon, in regard to solution stability, concerns the interaction of the system with atmospheric components. The other two are concerned with the intrinsic properties of the electrode/electrolyte system. These are then (1) chemistry coupled to the electrode process and (2) adsorption phenomena and their relationship to metal nucleation.

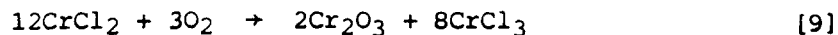
The sensitivity of chromium (II) and chromium (III) ions to moisture and oxygen is of some significance to the design of a chromium plating process. The results of this work show that the dilute solutions of Cr(II) ions are subject to loss of soluble chromium species. Indeed, in the bromide melts some insoluble material was visible on the salt surface. Laitinen et al. (22) showed that when melts containing chromium (III) were exposed to moist hydrogen chloride, the formation of hydroxychloro complexes took place:



The subsequent coupling of the hydroxypentachloro complex ions to form an oxygen bridge compound appears to take in an irreversible manner and ultimately leads to an insoluble product:



Although these reactions are not necessarily a direct problem with chromium (II) baths, it is known that chromium (II) species are sensitive to oxygen so that it might be expected that reaction will lead to the formation of chromium chloride as well as Cr_3O_3 :



Thus, the presence of small amounts of chromic chloride in a bath in contact with moist atmospheres will ensure the formation of these oxygen bridge species. It is likely that oxide occlusions experienced with deposited metal from chromium (II) plating baths may arise because of parallel reduction of the hydroxy species formed by the mechanisms indicated above. Traces of oxygen in the inert cover gas could be a problem when long term usage of flowing gas is necessary which would explain much of the difficulties experienced with varying Cr(II) concentrations in the present work and would account for the green oxides recovered from the salt baths.

Reactions which follow the electrochemical step have been identified when chromium (III) ions are reduced to chromium (II) ions. Levy (3c), and Laitinen and co-workers (22) reported that the peak current for the reoxidation process divided by the peak current for the reduction process was less than unity at low scan rates. Levy et al. interpreted their results as due to the insolubility of chromium (II) chloride (38). It is reported that chromium (II) chloride is soluble in the lithium chloride - potassium chloride solvent (42) and no evidence to the contrary was obtained in the present work. An alternative explanation is necessary. It has been suggested that the results can be explained by considering the geometric changes which are possible when chromium (II) ions in the octahedral coordination are reduced to chromium (II) ions which require some modified tetrahedral coordination. Results from experiments in this work for the oxidation of chromium (II) ions to chromium (III) ions on vitreous carbon electrodes show no evidence for follow-up chemistry which might be expected on the basis of a model requiring a change in the coordination geometry (22). It is possible that the differences between the work of Laitinen and co-workers and the present studies is to be found in the lability associated with different chromium complexes (14).

Reactant adsorption has been reported to occur during the reduction of chromium (II) ions on a chromium substrate (36). Present studies on foreign substrates employing both cyclic voltammetry and chronopotentiometry has not detected the influence of adsorption, although this could be because of the masking effect of the electrocrystallization phenomena (loc. cit.). Analysis of potential time data for the reduction of chromium (II) ions onto a chromium coated copper electrode showed the expected behavior for a unit activity surface, Figure 26. It can be concluded that under these conditions, reactant adsorption does not play a role in the reduction of chromium (II) ions. Nevertheless, the ramp observed during the reduction of Cr(II) on gold in the chloride and the bromide melts are consistent with adsorption of product, i.e., Cr ad-atoms. Such observations are of importance in understanding the stages of metal formation prior to growth of critical nuclei.

The present studies have shown that the reduction of chromium (II) to chromium metal requires a considerable overpotential at foreign cathodes. Evidence for these overpotentials has been obtained on copper, nickel, gold, platinum and tungsten. Figure 27a shows the cyclic voltammetric response on a nickel electrode when the switching potential is made more negative. The crossover of the current on the reverse sweep corresponds to a process associated with nucleation (46), and similar results for copper are shown in Figure 27. Correspondingly, substantial overpotentials are observed in the initial portion of chronopotentiograms obtained on these substrates. These effects make the study of the reduction of chromium (II) somewhat more difficult than had earlier been recognized and show that the solution properties of Cr(II) ions are more reliably measured in their oxidative chemistry. The nature of the processes associated with metal formation will be addressed in the next section.

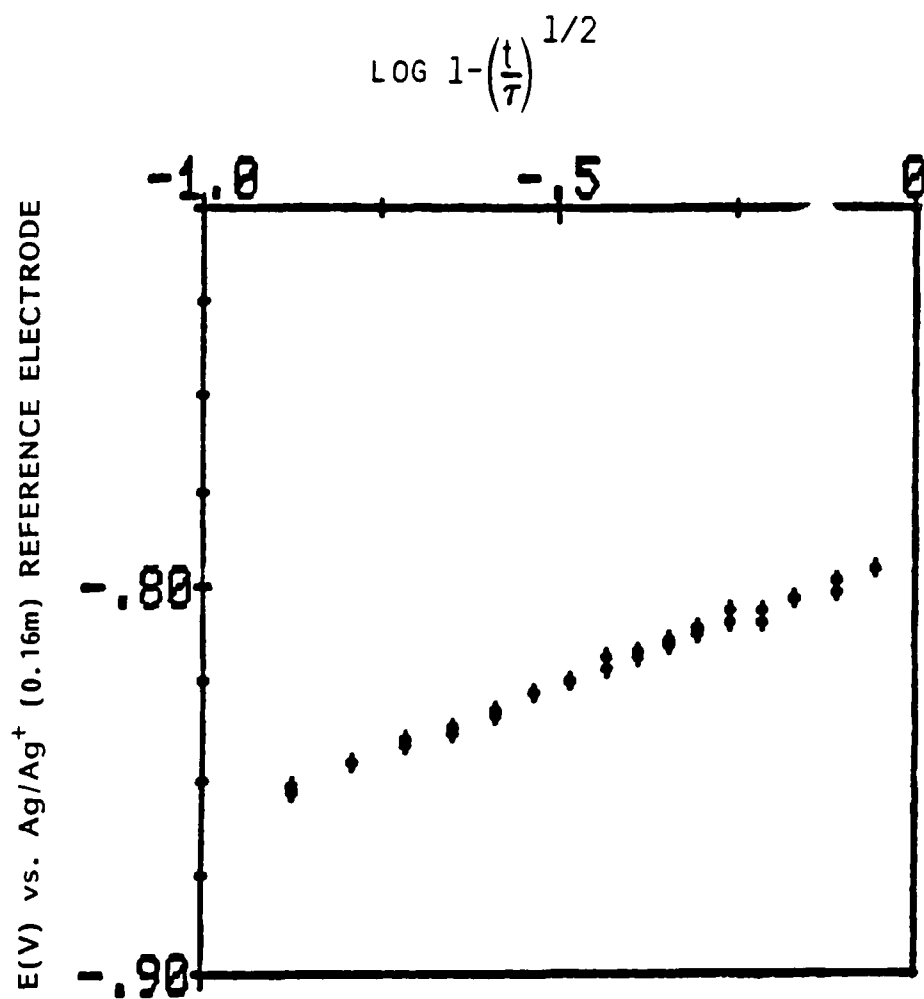


Fig. 26. Potential time analysis of galvanostatic transient for Cr deposited on chromium coated copper. The slope gives $n = 1.999$ and from the intercept $E_{\tau/4}$ is calculated to be -0.811 mV vs. reference. $E_{\tau/4} = 0.763$ V based upon E° and concentration.

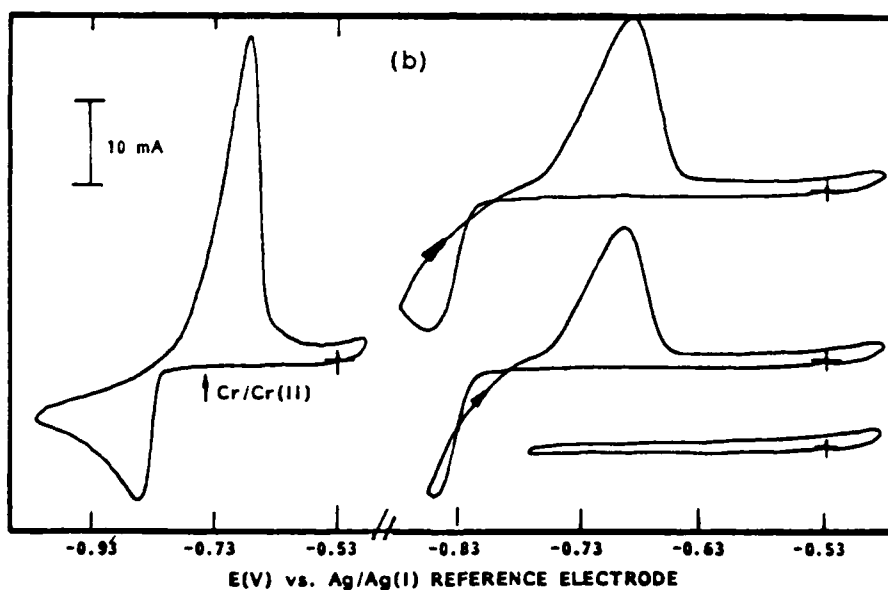
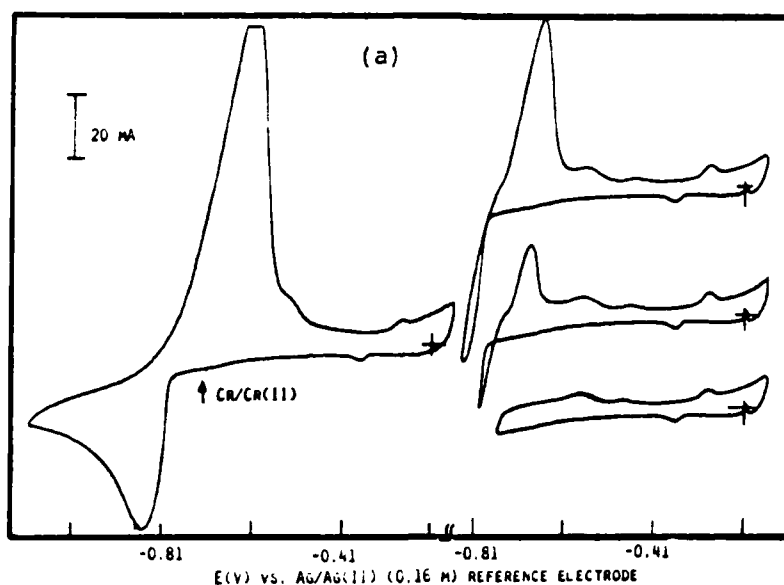


Fig. 27. Cyclic voltammograms illustrating overpotential deposition of Cr and the influence of switching potential on "nucleation cross-over effect" in the return current sweep for (a) nickel and (b) copper substrates in LiCl-KCl containing 13 mM Cr(II) at 450°C.

3.3 Electronucleation and Growth of Chromium on Different Substrates

The initial stages of the formation of a new phase upon a cathode substrate are now recognized to be important in the subsequent development of epitaxial and polycrystalline deposits (47-50). Little is known about such processes in aprotic solutions based upon molten salt solvents. The present studies have investigated these initial stages of metallic phase formation on four different substrates, using both potentiostatic and galvanostatic pulse techniques. Measurements on gold substrates were made both in the LiCl-KCl eutectic as well as the ternary alkali metal bromide melt LiBr-KBr-CsBr. In these experiments, the working electrode surface was prepared by electropolishing sheet material, and for the case of the gold electrode in the bromide melt, the electrode was prepared in the form of a sphere by melting and cooling. Well developed crystal faces were observable in this case. Control of the surface properties of the electrode substrates is an important aspect of electrocrystallization studies, but it has usually been neglected, particularly in molten salts. In this work, some attempt was made to control this factor albeit in a rather elementary way.

The earlier discussion of the solution chemistry of chromium in the chloride and bromide melts suggest that the control of exact solution composition is difficult, and thus the values of the diffusion coefficient of the chromium (II) ions cannot be obtained precisely. Under these circumstances, the values of $CAD^{1/2}$ were obtained from either anodic potential step measurements into the limiting current region for the oxidation of the Cr(II) ions, by stepping negative into the limiting current region for the reduction process where metal deposition is under control by linear diffusion or from other transient measurements. In contrast to this disadvantageous circumstance concerning solution composition, the rather low potential for Cr(II) reduction ensures a wide range of inactivity for the working electrode materials studied, thus enabling the rest potential of the working electrode to be selected in a way which ensured complete removal of the deposited chromium from the electrode surface after the cathodic pulse. In the galvanostatic experiments, a reverse current pulse was used to assure that this was achieved by matching of the cathodic and anodic charges followed by open circuit conditions.

3.3.1 Potential Step Measurements

● Platinum. Measurements were made on platinum at 450°C at three different concentrations of Cr(II) ions in the LiCl-KCl eutectic. The chromium chloride was introduced by anodic dissolution. Figure 28 shows a cyclic voltammogram prior to the potential step measurements. It illustrates the relative position of the reduction process to the potential of the Cr/Cr²⁺ and the range of the potential steps employed in the experiments. Figure 29 shows a series of current time curves observed in response to the applied potential steps. A characteristic shaped response can be seen with the current passing through a minimum as well as a maximum

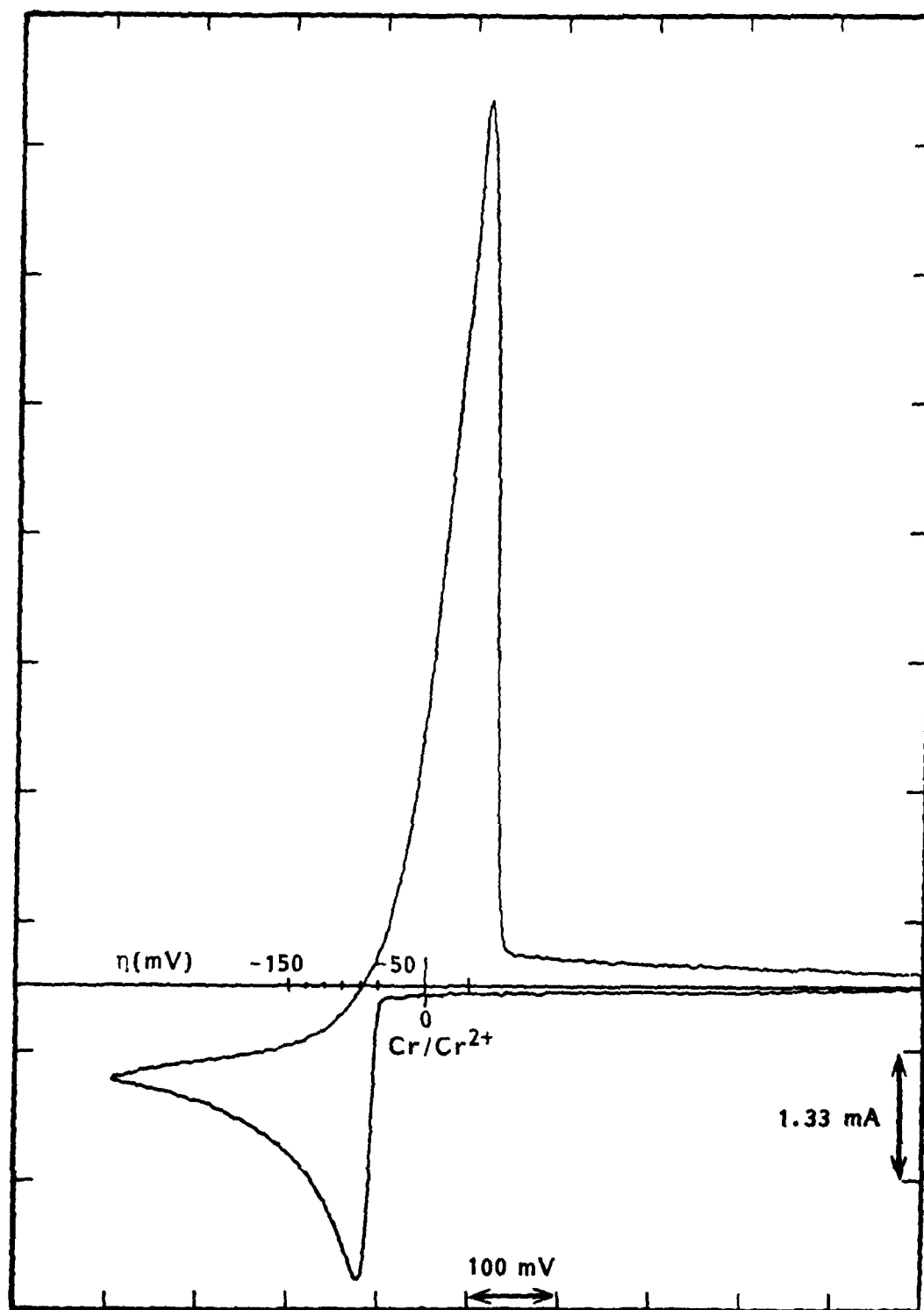


Fig. 28. Cyclic voltammogram acquired on Pt electrode in LiCl-KCl containing 24 mM of Cr(II) at 100 mVs⁻¹.

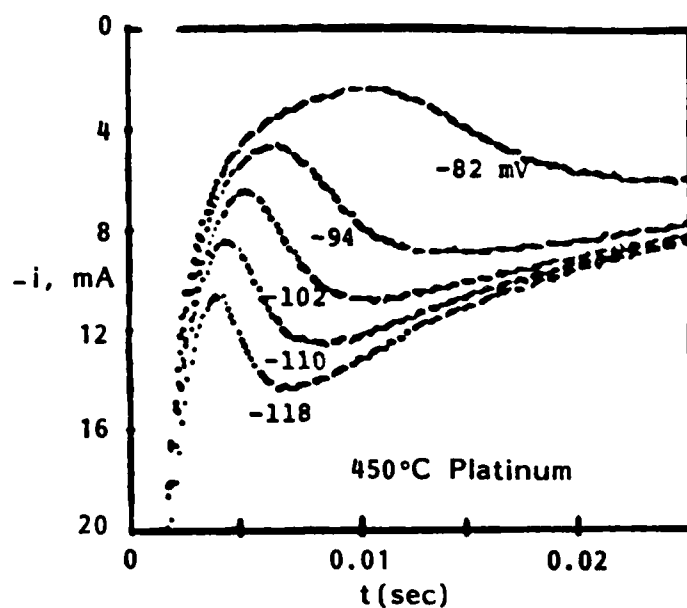


Fig. 29. Current time transients from potential step experiments for the deposition of chromium on a platinum substrate from a solution of Cr(II) ions (24 mM) in LiCl-KCl eutectic mixture (450°C).

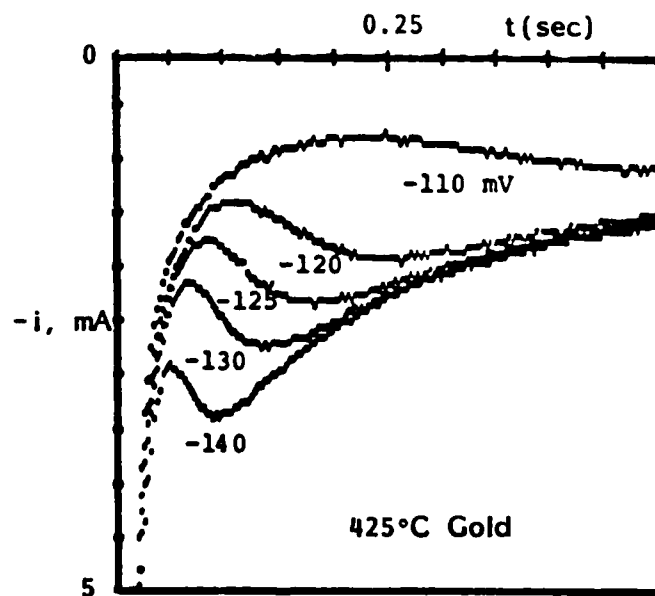


Fig. 30. Current time transients from potential step experiments for the deposition of chromium on a gold substrate from a solution of Cr(II) ions (8 mM) in LiCl-KCl eutectic mixture (425°C).

before decaying monotonically. Tables 13-15 record the measured maximum currents as well as the corresponding time at i_{\max} for each applied potential step from the rest potential. The overpotential, η , is calculated from the measured Cr/Cr(II) potential, the rest potential and the potential step. These values of η are included in the tables for the three concentrations employed.

The measured values of $CAD^{\frac{1}{2}}$ obtained from potential step measurements into the limiting current regions for oxidation and reduction of the Cr(II) ions are reported in Table 16 at the three corresponding concentrations. The values predicted for $i_m^2 t_m$ for the nucleation and growth and instantaneous nucleation and growth models of hemispherical nuclei (47,51) are included in Table 16.

- Gold. Because of the electrochemical stability of gold and its lack of susceptibility to oxide formation, it was used extensively in the study of chromium both in potential step and other electrochemical measurements. In the exploratory studies with the bromide melt, it was used exclusively.

Alkali Metal Chloride Solutions. Potential step measurements were made with planar gold electrodes at 425 and 450°C in the LiCl-KCl eutectic melt. Typical current time curves are shown in Figure 30. Measurements which were obtained at three concentrations in different melt batches are reported in Tables 17-19 together with the relevant derived parameters. Table 20 reports the values of $CAD^{\frac{1}{2}}$ obtained from anodic chronoamperometric measurements together with the values of $i_m^2 t_m$ calculated from this data.

Alkali Metal Bromide Solutions. Potential step measurements were made with a spherical gold electrode in the ternary LiBr-KBr-CsBr eutectic melt at 450 and 292°C. At the higher temperature, the transients were poorly defined and extensive measurements were not made. At 292°C, well developed transients were observed and results are reported in Table 21 together with the derived parameters. Table 20 shows values of $CAD^{\frac{1}{2}}$ obtained from cathodic potential steps into the limiting current region for the reduction of Cr(II) ions and the corresponding values calculated for $i_m^2 t_m$.

- Copper and Nickel. A preliminary study of copper and nickel as substrates was made in view of their likely importance as flash coatings in plating more active metals as mandrels in electroforming and as components of stainless steels and nimonic alloys. From a fundamental point of view, these metals should alloy with depositing chromium, and the effect of such a process is of significance in understanding electronucleation and growth under these circumstances. Careful control of the rest potential of these substrates is required on the one hand to prevent dissolution of the metal, but on the other ensure that deposited chromium is removed after the cathodic pulse and the surface returned to its original condition.

TABLE 13

POTENTIAL STEP RESULTS FOR PLATINUM SUBSTRATE (0.23 cm²)
 IN LiCl-KCl EUTECTIC AT 450°C
 FIRST CONCENTRATION CHROMIUM II

Concentration Cr ²⁺	= 7.84 x 10 ⁻⁶ molcm ⁻³
Atomic Weight Cr	= 51.99 gmol ⁻¹
Density of Cr	= 7.1 gcm ⁻³
Diffusion Coefficient of Cr ²⁺	= 1.14 x 10 ⁻⁵ cm ² s ⁻¹
Rest Potential of Pt	= -0.15V vs. Ag reference
Rest Potential of Cr ²⁺ /Cr	= -0.736V vs. Ag reference

10 ³ i (max) Amps	t(max) sec	Overpot ⁿ η (V)	10 ⁷ i _{mt} ² A ² s	Nuclei Density	N x Rate AN ₀
0.588	0.360	-0.074	1.513	2.69 x 10 ⁶	2.1 x 10 ⁷
0.600	0.196	-0.078	0.837	4.92 x 10 ⁶	7.0 x 10 ⁷
0.675	0.255	-0.078	1.378	3.78 x 10 ⁶	4.1 x 10 ⁷
0.850	0.176	-0.082	1.472	5.46 x 10 ⁶	8.7 x 10 ⁷
0.875	0.164	-0.084	1.444	5.83 x 10 ⁶	9.9 x 10 ⁷
0.975	0.142	-0.086	1.539	6.72 x 10 ⁶	1.3 x 10 ⁸
1.060	0.128	-0.088	1.625	7.44 x 10 ⁶	1.6 x 10 ⁸
1.230	0.098	-0.092	1.651	9.68 x 10 ⁶	2.8 x 10 ⁸
1.130	0.095	-0.094	1.341	9.97 x 10 ⁶	2.9 x 10 ⁸
1.130	0.104	-0.094	1.468	9.10 x 10 ⁶	2.4 x 10 ⁸
1.260	0.090	-0.094	1.580	1.05 x 10 ⁷	3.3 x 10 ⁸
1.330	0.084	-0.094	1.643	1.13 x 10 ⁷	3.7 x 10 ⁸
1.160	0.105	-0.096	1.552	9.00 x 10 ⁶	2.4 x 10 ⁸
1.420	0.078	-0.098	1.718	1.21 x 10 ⁷	4.3 x 10 ⁸
1.530	0.069	-0.100	1.754	1.37 x 10 ⁷	5.5 x 10 ⁸
1.550	0.066	-0.100	1.722	1.43 x 10 ⁷	6.0 x 10 ⁸
1.660	0.056	-0.104	1.659	1.68 x 10 ⁷	8.4 x 10 ⁸
1.700	0.057	-0.104	1.771	1.65 x 10 ⁷	8.1 x 10 ⁸
1.710	0.058	-0.104	1.823	1.62 x 10 ⁷	7.8 x 10 ⁸
1.800	0.053	-0.108	1.830	1.77 x 10 ⁷	9.3 x 10 ⁸
1.800	0.050	-0.108	1.726	1.88 x 10 ⁷	1.0 x 10 ⁹
1.930	0.045	-0.112	1.772	2.08 x 10 ⁷	1.3 x 10 ⁹
2.000	0.043	-0.114	1.812	2.18 x 10 ⁷	1.4 x 10 ⁹
2.040	0.042	-0.116	1.836	2.23 x 10 ⁷	1.5 x 10 ⁹
2.040	0.043	-0.116	1.857	2.20 x 10 ⁷	1.4 x 10 ⁹
2.130	0.038	-0.118	1.805	2.46 x 10 ⁷	1.8 x 10 ⁹
2.140	0.039	-0.120	1.864	2.39 x 10 ⁷	1.7 x 10 ⁹
2.180	0.037	-0.120	1.836	2.52 x 10 ⁷	1.9 x 10 ⁹
2.250	0.035	-0.124	1.840	2.66 x 10 ⁷	2.1 x 10 ⁹
2.250	0.036	-0.124	1.906	2.57 x 10 ⁷	2.0 x 10 ⁹
2.310	0.035	-0.124	1.939	2.66 x 10 ⁷	2.1 x 10 ⁹
2.240	0.037	-0.128	1.893	2.55 x 10 ⁷	1.9 x 10 ⁹
2.380	0.034	-0.128	1.991	2.74 x 10 ⁷	2.2 x 10 ⁹
2.410	0.032	-0.128	1.921	2.91 x 10 ⁷	2.5 x 10 ⁹
2.450	0.031	-0.132	1.916	3.00 x 10 ⁷	2.7 x 10 ⁹
2.490	0.030	-0.132	1.915	3.10 x 10 ⁷	2.9 x 10 ⁹
2.560	0.028	-0.134	1.886	3.32 x 10 ⁷	3.3 x 10 ⁹
2.560	0.028	-0.136	1.883	3.32 x 10 ⁷	3.3 x 10 ⁹
2.580	0.027	-0.136	1.844	3.44 x 10 ⁷	3.6 x 10 ⁹
2.720	0.026	-0.144	1.962	3.57 x 10 ⁷	3.8 x 10 ⁹
2.800	0.023	-0.144	1.839	4.03 x 10 ⁷	4.9 x 10 ⁹

TABLE 14

POTENTIAL STEP RESULTS FOR PLATINUM SUBSTRATE (0.23 cm^2)
 IN LiCl-KCl EUTECTIC AT 450°C
 SECOND CONCENTRATION CHROMIUM II

Concentration Cr^{2+} = $2.41 \times 10^{-5} \text{ mol cm}^{-3}$
 Atomic Weight Cr = 51.99 gmol^{-1}
 Density of Cr = 7.1 g cm^{-3}
 Diffusion Coefficient of Cr^{2+} = $1.14 \times 10^{-5} \text{ cm}^2 \text{ s}^{-1}$
 Rest Potential of Pt = $-0.55 \text{ V vs. Cr reference}$

$10^3 i_1$ (max) Amps	t(max) sec	Overpot ⁿ η (V)	$10^7 i_1^2 t_{\text{max}} L^{-2}$ A ² s	Nuclei Density	N x Rate AN _O	t^* ms
0.63	0.7000	-0.054	4.100	8.30×10^5	3.3×10^6	
1.17	0.5000	-0.058	9.597	1.15×10^6	6.4×10^6	135.40
1.20	0.5000	-0.058	10.095	1.15×10^6	6.4×10^6	
1.70	0.2350	-0.062	9.114	2.41×10^6	2.9×10^7	65.00
2.40	0.1275	-0.066	9.489	4.41×10^6	9.6×10^7	
2.40	0.1400	-0.066	10.420	4.01×10^6	8.0×10^7	
2.55	0.1140	-0.066	9.578	4.93×10^6	1.2×10^8	
2.95	0.0930	-0.068	10.282	6.02×10^6	1.8×10^8	
3.20	0.0750	-0.070	9.604	7.43×10^6	2.8×10^8	
3.30	0.0375	-0.070	5.107	1.49×10^7	1.1×10^9	
3.35	0.0420	-0.070	5.895	1.33×10^7	8.8×10^8	
3.20	0.0420	-0.070	5.379	1.33×10^7	8.8×10^8	
3.30	0.0750	-0.070	10.214	7.43×10^6	2.8×10^8	
3.30	0.0750	-0.070	10.214	7.43×10^6	2.8×10^8	
3.50	0.7125	-0.070	10.915	7.82×10^6	3.1×10^8	
4.40	0.0475	-0.074	11.179	1.17×10^7	6.8×10^8	
4.10	0.0525	-0.074	10.729	1.05×10^7	5.6×10^8	
4.10	0.0525	-0.074	10.729	1.05×10^7	5.6×10^8	
5.13	0.0375	-0.078	11.706	1.47×10^7	1.1×10^9	
5.13	0.0345	-0.078	10.770	1.59×10^7	1.3×10^9	
5.10	0.0365	-0.078	11.261	1.51×10^7	1.2×10^9	
6.15	0.0265	-0.082	11.638	2.07×10^7	2.2×10^9	
6.15	0.0250	-0.082	10.979	2.19×10^7	2.4×10^9	
6.15	0.0266	-0.082	11.682	2.06×10^7	2.2×10^9	
7.20	0.0200	-0.086	11.817	2.72×10^7	3.8×10^9	
7.17	0.0206	-0.086	12.070	2.64×10^7	3.6×10^9	6.10
8.00	0.0179	-0.090	12.811	3.04×10^7	4.7×10^9	
8.02	0.0175	-0.090	12.622	3.10×10^7	4.9×10^9	
9.06	0.0150	-0.094	13.613	3.60×10^7	6.7×10^9	
9.00	0.0143	-0.094	12.762	3.79×10^7	7.4×10^9	3.82
10.00	0.0123	-0.098	13.378	4.4×10^7	1.0×10^{10}	
10.00	0.0125	-0.098	13.651	4.31×10^7	9.6×10^9	
10.35	0.0110	-0.100	12.796	4.89×10^7	1.2×10^{10}	
10.50	0.0110	-0.100	13.170	4.89×10^7	1.2×10^{10}	
10.90	0.0105	-0.102	13.477	5.12×10^7	1.4×10^{10}	
10.95	0.0109	-0.102	14.086	4.94×10^7	1.3×10^{10}	2.56
10.95	0.0110	-0.102	14.248	4.89×10^7	1.2×10^{10}	
10.82	0.0100	-0.102	12.647	5.37×10^7	1.5×10^{10}	
11.75	0.0090	-0.106	13.297	5.96×10^7	1.8×10^{10}	
11.80	0.0098	-0.106	14.528	5.50×10^7	1.6×10^{10}	
12.63	0.0080	-0.110	13.543	6.69×10^7	2.3×10^{10}	
12.63	0.0085	-0.110	14.390	6.30×10^7	2.1×10^{10}	
12.70	0.0088	-0.110	14.978	6.12×10^7	1.9×10^{10}	
13.60	0.0078	-0.114	15.103	6.89×10^7	2.5×10^{10}	
14.40	0.0070	-0.118	15.196	7.62×10^7	3.0×10^{10}	0.66
17.00	0.0065	-0.130	19.378	8.17×10^7	3.5×10^{10}	

* t^* = Induction time

TABLE 15

POTENTIAL STEP RESULTS FOR PLATINUM SUBSTRATE (0.23 cm^2)
 IN LiCl-KCl EUTECTIC AT 450°C
 THIRD CONCENTRATION CHROMIUM II

Concentration Cr^{2+}	$= 3.53 \times 10^{-5} \text{ molcm}^{-3}$
Atomic Weight Cr	$= 51.99 \text{ gmol}^{-1}$
Density of Cr	$= 7.1 \text{ gcm}^{-3}$
Diffusion Coefficient of Cr^{2+}	$= 1.14 \times 10^{-5} \text{ cm}^2\text{s}^{-1}$
Rest Potential of Pt	$= 0\text{V vs. Ag reference}$
Rest Potential of Cr^{2+}/Cr	$= -0.535\text{V vs. Ag reference}$

$10^3 i$ (max) Amps	t (max) sec	Overpot ⁿ η (V)	$10^7 i_m^2 t_m L^{-2}$ A^2s	Nuclei Density	$N \times \text{Rate}$ AN_0	τ'^* ms
1.10	1.00	-0.045	20.728	4.98×10^5	1.4×10^6	
1.23	1.24	-0.045	31.876	4.02×10^5	9.0×10^5	260.1
3.40	2.0×10^{-1}	-0.055	33.825	2.38×10^6	3.3×10^7	40.0
7.25	5.0×10^{-2}	-0.065	34.263	9.31×10^6	5.2×10^8	
7.25	5.0×10^{-2}	-0.065	34.263	9.31×10^6	5.2×10^8	10.4
6.75	5.5×10^{-2}	-0.065	32.670	8.46×10^6	4.3×10^8	
11.1	2.5×10^{-2}	-0.075	37.205	1.83×10^7	2.0×10^9	
11.1	2.5×10^{-2}	-0.075	36.870	1.83×10^7	2.0×10^9	4.3
16.1	1.5×10^{-2}	-0.085	43.768	3.05×10^7	5.8×10^9	
15.3	1.3×10^{-2}	-0.085	35.276	3.40×10^7	7.2×10^9	2.5
19.3	9.8×10^{-3}	-0.095	39.817	4.58×10^7	1.3×10^{10}	
25.7	6.1×10^{-3}	-0.115	42.553	7.20×10^7	3.3×10^{10}	

* τ' = Induction time

TABLE 16

MEASUREMENTS OF $\text{CAD}^{1/2}$ FOR THE PLATINUM ELECTRODE (0.23 cm^2) AND THE CALCULATED VALUES OF $i_m^{2t_m}$ PREDICTED FOR INSTANTANEOUS AND PROGRESSIVE NUCLEATION

	Red $10^9 \text{ CAD}^{1/2}$ $\text{mol s}^{-1/2}$	Ox $10^9 \text{ CAD}^{1/2}$ $\text{mol s}^{-1/2}$	Mean $10^9 \text{ CAD}^{1/2}$ $\text{mol s}^{-1/2}$	Progr.		Instantaneous	
				$i_m^{2t_m}$ A^2S	$i_m^{2t_m}$ A^2S	$i_m^{2t_m}$ A^2S	D cm^2s^{-1}
$C_1 = 7.84 \times 10^{-6}$ mol cm^{-3}	- 4.41	4.80 -	4.80 4.41	2.23×10^{-7} 1.88×10^{-7}	1.37×10^{-7} 1.16×10^{-7}	0.7×10^{-5}	
$C_2 = 24.1 \times 10^{-6}$ mol cm^{-3}	-	13.60	13.60	17.9×10^{-7}	11.0×10^{-7}	0.6×10^{-5}	
$C_3 = 35 \times 10^{-6}$ mol cm^{-3}	..	27.2	27.2	71.6×10^{-7}	44.0×10^{-7}	1.14×10^{-5}	

TABLE 17

POTENTIAL STEP RESULTS FOR GOLD SUBSTRATE
IN LiCl-KCl EUTECTIC AT 425°C

Concentration Cr^{2+}	= $8.3 \times 10^{-6} \text{ mol cm}^{-3}$
Area Au electrode	= 0.4 cm^2
Atomic Weight Cr	= 51.99 gmol^{-1}
Density of Cr	= 7.1 g cm^{-3}
Diffusion Coefficient of Cr^{2+}	= $1.0 \times 10^{-5} \text{ cm}^2 \text{ s}^{-1}$
Rest Potential of Au	= 0V vs. Cr^{2+}/Cr reference
Rest Potential of Cr^{2+}/Cr	= -0.750V vs. Ag reference

$10^3 i_{\text{max}}$ Amps	t_{max} sec	Overpot ⁿ η (V)	$10^7 i_{\text{max}}^2 t_{\text{max}} L^{-2}$ $\text{A}^2 \text{ s}$	Nuclei Density	$N \times \text{Rate}$ AN_0
0.55	3.000	-0.100	9.766	3.47×10^5	3.2×10^5
0.56	2.000	-0.100	6.749	5.21×10^5	7.3×10^5
1.15	0.500	-0.110	6.968	2.07×10^6	1.2×10^7
1.11	0.450	-0.110	5.842	2.30×10^6	1.4×10^7
1.11	0.500	-0.110	6.491	2.07×10^6	1.2×10^7
1.91	0.240	-0.120	9.089	4.30×10^6	5.0×10^7
1.89	0.250	-0.120	9.270	4.13×10^6	4.6×10^7
1.96	0.230	-0.120	9.172	4.49×10^6	5.4×10^7
1.91	0.220	-0.120	8.332	4.69×10^6	6.0×10^7
2.30	0.182	-0.125	9.937	5.66×10^6	8.7×10^7
2.80	0.130	-0.130	10.468	7.92×10^6	1.7×10^8
2.80	0.130	-0.130	10.468	7.92×10^6	1.7×10^8
2.73	0.140	-0.130	10.717	7.36×10^6	1.5×10^8
2.74	0.130	-0.130	10.024	7.92×10^6	1.7×10^8
3.39	0.090	-0.140	10.543	1.14×10^7	3.5×10^8
3.33	0.094	-0.140	10.625	1.09×10^7	3.2×10^8
3.30	0.095	-0.140	10.545	1.08×10^7	3.2×10^8

TABLE 18

POTENTIAL STEP RESULTS FOR GOLD SUBSTRATE
IN LiCl-KCl EUTECTIC AT 450°C

Concentration Cr^{2+}	$= 2.41 \times 10^{-5} \text{ mol cm}^{-3}$
Area Au electrode	$= 0.26 \text{ cm}^2$
Atomic Weight Cr	$= 51.99 \text{ gmol}^{-1}$
Density of Cr	$= 7.1 \text{ g cm}^{-3}$
Diffusion Coefficient of Cr^{2+}	$= 1.14 \times 10^{-5} \text{ cm}^2 \text{ s}^{-1}$
Rest Potential of Au	$= 0.55 \text{ V vs. Ag reference}$
Rest Potential of Cr^{2+}/Cr	$= -0.75 \text{ V vs. Ag reference}$

$10^3 i$ (max) Amps	t (max) sec	Overpot ⁿ η (V)	$10^7 i_m^2 t_m L^{-2}$ $\text{A}^2 \text{ s}$	Nuclei Density	$N \times \text{Rate}$ AN_0
0.78	2.5000	-0.074	16.642	2.46×10^5	3.1×10^5
1.08	1.3000	-0.078	17.986	4.23×10^5	9.1×10^5
1.42	0.6700	-0.082	15.687	8.17×10^5	3.4×10^6
1.85	0.3850	-0.086	15.018	1.42×10^6	1.0×10^7
1.90	0.3650	-0.094	14.568	1.48×10^6	1.1×10^7
2.33	0.2250	-0.090	13.698	2.41×10^6	3.0×10^7
2.40	0.2150	-0.090	13.887	2.52×10^6	3.3×10^7
3.45	0.1080	-0.098	14.038	4.99×10^6	1.3×10^8
3.50	0.1000	-0.098	13.378	5.39×10^6	1.5×10^8
3.85	0.0900	-0.100	14.487	5.98×10^6	1.9×10^8
3.75	0.0900	-0.100	13.744	5.98×10^6	1.9×10^8
4.15	0.0760	-0.102	14.140	7.07×10^6	2.6×10^8
4.20	0.0750	-0.102	14.292	7.17×10^6	2.7×10^8
4.40	0.0700	-0.102	14.640	7.68×10^6	3.1×10^8
5.05	0.0550	-0.106	15.010	9.75×10^6	4.9×10^8
5.73	0.0440	-0.110	15.332	1.22×10^7	7.7×10^8
6.40	0.0370	-0.114	15.968	1.44×10^7	1.1×10^9
7.00	0.0375	-0.118	19.237	1.42×10^7	1.1×10^9
7.05	0.0300	-0.118	15.610	1.78×10^7	1.7×10^9
8.05	0.0275	-0.122	18.553	1.94×10^7	2.0×10^9
8.90	0.0215	-0.126	17.644	2.47×10^7	3.2×10^9
9.80	0.0200	-0.134	19.740	2.65×10^7	3.7×10^9
10.7	0.0175	-0.138	20.523	3.03×10^7	4.8×10^9
12.0	0.0150	-0.146	22.004	3.53×10^7	6.6×10^9
20.5	0.0050	-0.200	21.081	1.06×10^8	5.9×10^{10}

TABLE 19

POTENTIAL STEP RESULTS FOR GOLD SUBSTRATE
IN LiCl-KCl EUTECTIC AT 450°C

Concentration Cr^{2+}	= $3.53 \times 10^{-5} \text{ mol cm}^{-3}$
Area Au electrode	= 0.26 cm^2
Atomic Weight Cr	= 51.99 gmol^{-1}
Density of Cr	= 7.1 g cm^{-3}
Diffusion Coefficient of Cr^{2+}	= $1.14 \times 10^{-5} \text{ cm}^2 \text{ s}^{-1}$
Rest Potential of Au	= 0V vs. Ag reference
Rest Potential of Cr^{2+}/Cr	= -0.535V vs. Ag reference

$10^3 i$ (max) Amps	t (max) sec	Overpot ⁿ η (V)	$10^7 i_m^2 t_m L^{-2}$ $\text{A}^2 \text{ s}$	Nuclei Density	$N \times \text{Rate}$ AN_0	τ^* ms
0.290	8.0000	-0.055	9.794	5.98×10^4	2.1×10^4	
1.125	2.2500	-0.065	37.125	2.07×10^5	2.6×10^5	
2.740	0.5500	-0.075	49.874	8.30×10^5	4.2×10^6	
2.850	0.5400	-0.075	52.978	8.45×10^5	4.4×10^6	50.6
5.400	0.1700	-0.085	56.748	2.65×10^6	4.3×10^7	15.6
8.850	0.0650	-0.095	56.105	6.86×10^6	2.9×10^8	2.7
9.300	0.0559	-0.095	53.282	7.98×10^6	4.0×10^8	
16.300	0.0200	-0.115	55.893	2.20×10^7	3.1×10^9	0.73
16.400	0.0194	-0.115	54.884	2.27×10^7	3.3×10^9	

* τ' = induction time

TABLE 20

MEASUREMENTS OF $\text{CAD}^{1/2}$ FOR GOLD ELECTRODES IN DIFFERENT HALIDE SOLVENTS AND THE CALCULATED
VALUES OF $i_m^{2t_m}$ PREDICTED FOR INSTANTANEOUS AND PROGRESSIVE NUCLEATION

	Red	Ox	Mean	Instantaneous		
				$10^9 \text{ CAD}^{1/2}$	$i_m^{2t_m}$	$\frac{D}{A^2 s}$
	$10^9 \text{ CAD}^{1/2}$	$10^9 \text{ CAD}^{1/2}$	$10^9 \text{ CAD}^{1/2}$	$i_m^{2t_m}$	$i_m^{2t_m}$	$\frac{D}{A^2 s}$
	$\text{mol s}^{-1/2}$	$\text{mol s}^{-1/2}$	$\text{mol s}^{-1/2}$	$\text{A}^2 \text{s}$	$\text{cm}^2 \text{s}^{-1}$	$\text{A}^2 \text{s}$
<u>LiCl-KCl Eutectic Mixture</u>						
$t = 450^\circ\text{C}$						
$C_1 = 7.84 \times 10^{-6}$ mol cm^{-3} $A = 0.26 \text{ cm}^2$	-	5.66	5.66	3.10×10^{-7}	1.91×10^{-7}	0.77×10^{-5}
$C(\text{ii}) = 8.75 \times 10^{-6}$ mol cm^{-3} $A = 0.4 \text{ cm}^2$	9.3 10.7	13.1 9.3		14.7×10^{-7} 7.4×10^{-7} 9.8×10^{-7}	10.2×10^{-7} 5.1×10^{-7} 6.8×10^{-7}	
$C_2 = 24.1 \times 10^{-6}$ mol cm^{-3} $A = 0.26 \text{ cm}^2$	-	15.36	15.36	22.8×10^{-7}	14.1×10^{-7}	0.60×10^{-5}
$C_3 = 35 \times 10^{-6}$ mol cm^{-3} $A = 0.26 \text{ cm}^2$	-	30.4	30.4	89.4×10^{-7}	55.0×10^{-7}	1.12×10^{-5}
<u>LiBr-KBr-CsBr Eutectic Mixture</u>						
$t = 292^\circ\text{C}$						
Nominal conc. $C_N = 54 \times 10^{-6}$ mol cm^{-3} $A = 0.0882 \text{ cm}^2$	44.8	-	-	1.94×10^{-7}	1.20×10^{-7}	-

TABLE 21

POTENTIAL STEP RESULTS FOR GOLD SUBSTRATE IN THE
TERNARY ALKALI METAL BROMIDE EUTECTIC AT 292°C

Concentration Cr^{2+}	$= 5.46 \times 10^{-5} \text{ mol cm}^{-3}$
Atomic Weight Cr	$= 51.99 \text{ g mol}^{-1}$
Density of Cr	$= 7.1 \text{ g cm}^{-3}$
Diffusion Coefficient of Cr^{2+} *	$= 4.1 \times 10^{-6} \text{ cm}^2 \text{ s}^{-1}$
Rest Potential of Au	$= 0\text{V}$ vs. Ag reference
Rest Potential of Cr^{2+}/Cr	$= -0.63\text{V}^\dagger$ vs. Ag reference

$10^3 i$ (max) Amps	t (max) sec	Overpot ⁿ η (V)	$10^7 i_m^2 t_m L^{-2}$ $\text{A}^2 \text{s}$	Nuclei Density	$N \times \text{Rate}$ AN_0
0.650	0.1800	-0.050	1.001	8.52×10^6	1.3×10^8
1.200	0.2350	-0.060	4.043	6.37×10^6	5.1×10^7
0.720	0.1700	-0.065	1.017	8.73×10^6	9.7×10^7
0.950	0.110	-0.070	1.115	1.34×10^7	2.3×10^8
0.860	0.1200	-0.070	0.997	1.23×10^7	1.9×10^8
1.350	0.0610	-0.080	1.200	2.39×10^7	7.4×10^8
0.900	0.1200	-0.085	1.034	1.21×10^7	1.9×10^8
1.240	0.0600	-0.085	0.981	2.42×10^7	7.7×10^8
1.840	0.0316	-0.090	1.125	4.59×10^7	2.8×10^9
1.400	0.0560	-0.090	1.154	2.59×10^7	8.8×10^8
1.565	0.0420	-0.095	1.072	3.45×10^7	1.6×10^9
2.280	0.0254	-0.100	1.365	5.69×10^7	4.2×10^9
1.730	0.0340	-0.100	1.052	4.25×10^7	2.4×10^9
2.550	0.0190	-0.105	1.269	7.59×10^7	7.6×10^9
2.200	0.0300	-0.110	1.484	4.80×10^7	3.0×10^9

Two assumptions:

* D calc from $D_{4500} \text{Cl}^-$ melt by assuming $0.4\%/1^\circ\text{C}$.

† Cr/ Cr^{2+} potⁿ adjusted until $i_m^2 t_m L^{-2} \sim \text{constant}$.

Potential step experiments were successful and the results are recorded in Tables 22-24. The values of $CAD^{\frac{1}{2}}$ were obtained from various transient measurements and are presented in Table 25.

3.3.2 Discussion of Potential Step Results

The transient response to a potential step into the limiting current region for the reduction of Cr(II) ions to chromium metal shows a monotonous decay of current with time as is illustrated for the reduction on a copper substrate at 450°C in Figure 31. As the potential is increased (overpotential decreased), the shape of the transient changes and well defined current maxima are observed as is illustrated for each substrate material in Figures 29 and 30. The transient contains three major regions. At the shortest times, a rapid decreasing current is observed which contains the convolution of charging current and nuclei formation. In the region where the current is increasing, nuclei grow and may continue to be created. During this growth period the diffusion layers around the nuclei expand and overlap ultimately resulting in one dimensional diffusion (perpendicular to the surface) to become predominant. Under these latter conditions, the decay of current becomes monotonous according to the Cottrell relationship (52).

The analysis of these transients is based upon several assumptions. It is postulated that nucleation takes place at particular sites on the electrode surface and the number of these sites depends upon the overpotential (53). In addition, the nucleation process is statistical (48) in nature and the formation of nuclei at any time, t , is described by the rate law:

$$N(t) = N_0[1 - \exp(-At)] \quad [10]$$

where N_0 is the number of available sites and A is the rate of nucleus formation at a particular site. In formulating a description of the growth of the nuclei, equation [10] has been used in two limiting forms:

a) where At is large in which case

$$N(t) = N_0[1 - 1/\exp(At)] = N_0 \quad [11]$$

i.e., all sites at a given overpotential are immediately nucleated, and this case is known as instantaneous nucleation;

b) where $At \rightarrow 0$ in which case

$$N(t) = N_0[1 - \{1 - At\}] = N_0At \quad [12]$$

and the number of sites are progressively consumed at a given overpotential.

TABLE 22

POTENTIAL STEP RESULTS FOR COPPER SUBSTRATE
IN LiCl-KCl EUTECTIC AT 425°C

Concentration Cr^{2+}	$= 12.3 \times 10^{-6} \text{ mol cm}^{-3}$
Area of Cu electrode	$= 0.5 \text{ cm}^2$
Atomic Weight Cr	$= 51.99 \text{ gmol}^{-1}$
Density of Cr	$= 7.1 \text{ g cm}^{-3}$
Diffusion Coefficient of Cr^{2+}	$= 1.03 \times 10^{-5} \text{ cm}^2 \text{ s}^{-1}$
Rest Potential of Cu Electrode	$= -0.530 \text{ V vs. Ag reference}$
Rest Potential of Cr^{2+}/Cr	$= -0.739 \text{ V vs. Ag reference}$

$10^3 i_{\text{max}}$ Amps	t_{max} sec	Overpot ⁿ η (V)	$10^7 i_{\text{max}}^2 t_{\text{max}} L^{-2}$ $\text{A}^2 \text{ s}$	Nuclei Density	$N \times \text{Fate}$ AN_0
11.50	0.1275	-0.091	186.271	6.56×10^6	1.4×10^8
35.50	0.0220	-0.121	287.463	3.74×10^7	4.7×10^9
45.50	0.0125	-0.131	265.562	6.56×10^7	1.5×10^{10}
51.30	0.0095	-0.141	254.683	8.62×10^7	2.5×10^{10}
52.00	0.0095	-0.141	261.681	8.62×10^7	2.5×10^{10}
69.00	0.0040	-0.161	192.258	2.04×10^8	1.4×10^{11}
71.00	0.0067	-0.161	340.972	1.22×10^8	5.1×10^{10}
72.00	0.0059	-0.161	308.776	1.39×10^8	6.5×10^{10}

TABLE 23

POTENTIAL STEP RESULTS FOR COPPER SUBSTRATE
IN LiCl-KCl EUTECTIC AT 450°C

Concentration Cr^{2+}	= $21.7 \times 10^{-6} \text{ molcm}^{-3}$
Area of Cu electrode	= 0.5 cm^2
Atomic Weight Cr	= 51.99 gmol^{-1}
Density of Cr	= 7.1 gcm^{-3}
Diffusion Coefficient of Cr^{2+}	= $1.14 \times 10^{-5} \text{ cm}^2\text{s}^{-1}$
Rest Potential of Cu Electrode	= -0.550V vs. Ag reference
Rest Potential of Cr^{2+}/Cr	= -0.720V vs. Ag reference

$10^3 i_{\text{max}}$ Amps	t_{max} sec	Overpot ⁿ η (V)	$10^7 i_{\text{max}}^2 t_{\text{max}} \text{L}^{-2}$ A^2s	Nuclei Density	$N \times \text{Rate}$ AN_0
17.50	0.1400	-0.070	536.188	4.19×10^6	8.3×10^7
45.50	0.0225	-0.100	505.846	2.52×10^7	3.1×10^9
75.50	0.0100	-0.130	588.024	5.59×10^7	1.6×10^{10}
75.50	0.0110	-0.130	646.827	5.08×10^7	1.3×10^{10}
75.70	0.0110	-0.130	650.258	5.08×10^7	1.3×10^{10}

TABLE 24

POTENTIAL STEP RESULTS FOR NICKEL SUBSTRATE
IN LiCl-KCl EUTECTIC AT 450°C

Concentration Cr^{2+}	= $21.7 \times 10^{-6} \text{ mol cm}^{-3}$
Area of Nickel electrode	= 0.6 cm^2
Atomic Weight Cr	= 51.99 gmol^{-1}
Density of Cr	= 7.1 g cm^{-3}
Diffusion Coefficient of Cr^{2+}	= $1.14 \times 10^{-5} \text{ cm}^2 \text{ s}^{-1}$
Rest Potential of Ni Electrode	= -0.210 V vs. Ag reference
Rest Potential of Cr^{2+}/Cr	= -0.723 V vs. Ag reference

$10^3 i$ (max) Amps	t (max) sec	Overpot ⁿ η (V)	$10^7 i_m^2 t_m L^{-2}$ $\text{A}^2 \text{ s}$	Nuclei Density	$N \times \text{Rate}$ AN_0
16.40	0.2150	-0.067	740.774	2.74×10^6	3.6×10^7
15.00	0.2500	-0.067	720.580	2.36×10^6	2.6×10^7
23.50	0.1250	-0.077	823.623	4.64×10^6	1.0×10^8
33.40	0.0750	-0.087	949.519	7.63×10^6	2.8×10^8
33.40	0.0725	-0.087	917.868	7.89×10^6	3.0×10^8
54.00	0.0375	-0.107	1167.634	1.50×10^7	1.1×10^9
76.00	0.0240	-0.127	1434.551	2.33×10^7	2.7×10^9

TABLE 25

MEASUREMENTS OF $\text{CAD}^{1/2}$ FOR COPPER AND NICKEL ELECTRODES IN LiCl-KCl EUTECTIC AND THE CALCULATED VALUES OF $i_m^{2t_m}$ PREDICTED FOR INSTANTANEOUS AND PROGRESSIVE NUCLEATION

	$10^0 \text{ CAD}^{1/2}$ from Cathodic	$10^9 \text{ CAD}^{1/2}$ from Cathodic	$10^9 \text{ CAD}^{1/2}$ from Cathodic	CP	Progr. $i_m^{2t_m}$ 10^{-7}	Instantaneous $i_m^{2t_m}$ 10^{-7}
	CA	CV				
<hr/>						
$t = 425^\circ\text{C}$						
Copper #1	-	55		43	259	180
					158	110
Area 0.5 cm^2						
Conc. $\sim 13 \times 10^{-6}$ mol cm^{-3}						
<hr/>						
$t = 450^\circ\text{C}$						
Copper #2	119				1212	843
		81		111	562	391
					1054	734
Area $\sim 0.5 \text{ cm}^2$						
Conc. $\sim 23 \times 10^{-6}$ mol cm^{-3}						
<hr/>						
$t = 450^\circ\text{C}$						
Nickel	-	139		-	1653	1150
Area $\sim 0.6 \text{ cm}^2$						
Conc. 23×10^{-6} mol cm^{-3}						

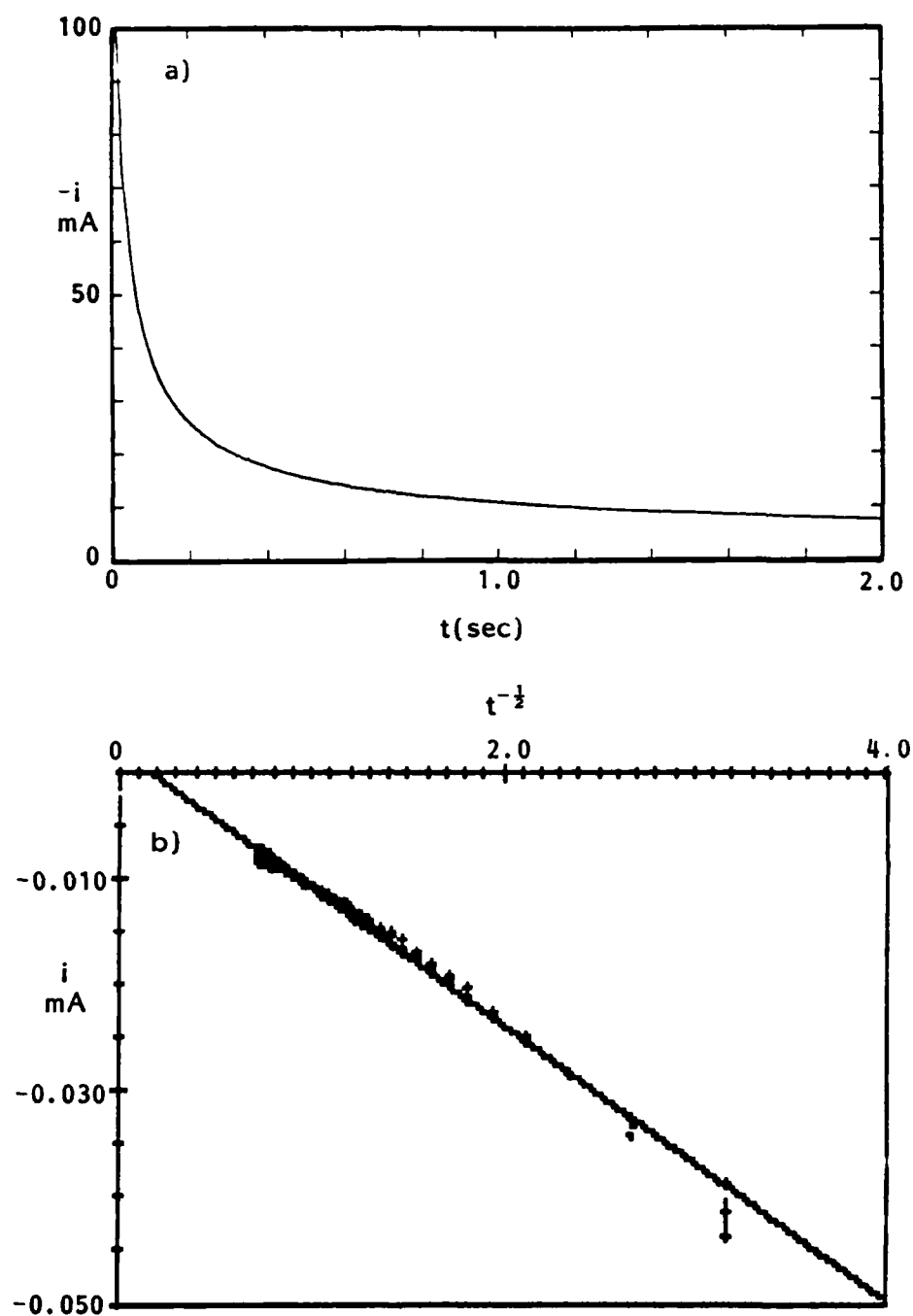


Fig. 31. (a) Chronoamperogram for the reduction of Cr(II) ions on a copper substrate (0.5 cm^2). Potential step -180 mV vs. Cr^{2+}/Cr electrode. (b) Plot of i vs. $t^{-1/2}$ for data (450 pts) in (a) showing diffusion control to $<0.1 \text{ se}$.

Descriptions of three dimensional growth mechanisms have been given for the case of linear diffusion (47,48). Electron microscopical analysis of the earliest stages of metal deposition suggest that the nuclei have a hemispherical shape and, therefore, the current associated with the growth of the nuclei should be described for hemispherical diffusional growth. (If the nuclei can be regarded as point sources, then their geometric shape is rather unimportant in the theoretical description.) The growth of N isolated nuclei in terms of linear diffusion was elaborated by Astley et al. (54). Hills and co-workers have presented the results for the two cases of a) and b) above for spherical diffusion (55) which for instantaneous nucleation is

$$i(t) = zFN_0\pi(2DC)^{3/2}V_m^{-1/2}t^{1/2} \quad [13]$$

and progressive nucleation is

$$i(t) = 1.33'zFAN_0\pi(2DC)^{3/2}V_m^{-1/2}t^{3/2} \quad [14]$$

and more recently have taken account of the overlap of the expanding diffusion fields around the nuclei (51). For the case where the overvoltage is insufficient for the surface concentration to be reduced to zero, the correction term $L = 1 - \exp(zF\eta/RT)$ must be applied to the concentration term in their equations. The current under conditions of instantaneous nucleation is given by:

$$i_g(t) = zFCLD^{1/2}\{\pi t\}^{-1/2}[1 - \exp(-N_0\pi kDt)] \quad [15]$$

Such a current exhibits a maximum at

$$i_m = 0.6382zFDCL(kN)^{1/2} \quad [16]$$

which occurs at a time given by

$$t_m = 1.2564(\pi NkD)^{-1} \quad [17]$$

where

$$k = \{8\pi CLV_m\}^{1/2} \quad [18]$$

In a similar manner, the results for progressive nucleation are given by the equations:

$$i_g(t) = zFCLD^{1/2}\{\pi t\}^{-1/2}[1 - \exp(-0.5AN_0k'Dt^2)] \quad [19]$$

with a maximum given by:

$$i_m = 0.4615zFD^{3/4}CL(k'AN_0)^{1/4} \quad [20]$$

which occurs at a time given by:

$$t_m = \{4.6733(\pi AN_0k'D)^{-1}\}^{1/2} \quad [21]$$

with $k' = 1.333k$.

The products $i_m^2 t_m$ for the two cases depends only upon the solution conditions and differ by numerical constants. Thus the measured i_m and t_m enable the two cases to be distinguished for particular metal deposition conditions. In the limits that $N_t \rightarrow 0$ and $AN_0 t \rightarrow 0$, equations [15] and [19] take the form:

$$i(t) = \{zFCLNk\pi^{1/2} D^{3/2}\} t^{1/2} \quad [22]$$

and

$$i(t) = \{zFCLK'\pi^{1/2} D^{3/2} AN_0 t\} t^{1/2} \quad [23]$$

When the rate of nucleus formation remains unchanged, i.e., in the steady state, equation [23] shows a $t^{1/2}$ rather than a $t^{3/2}$ dependence since $AN_0 t$ remains constant.

These equations have been shown to apply to results obtained from a number of aqueous systems involving mercury deposition on vitreous carbon and silver on VC and platinum (51,55-57). Lantelme and Chevalet (58) reported that copper deposition on vitreous carbon from LiCl-KCl at 410°C could be described in terms of instantaneous nucleation.

The present experimental data for the different substrates in the two melts were analyzed with the aid of the theories summarized above and are now presented. Figure 32 shows the plot of the observed current as a function of $t^{1/2}$ over the whole transient at different overpotentials for the platinum substrate at two different Cr(II) concentrations. Clearly defined linear regions are observed whose slope varies with overpotential as predicted by equation [22]. The lines extrapolated to zero current cut the time axis in the positive quadrant. Such times have been related to the duration of the nucleation process and the double layer charging (58) (vide infra). The results for gold substrates presented in Figure 33 for the same solutions show some differences. At the lower concentration and the shorter times, the linear region extrapolates to cut the time axis in the negative quadrant. At the higher concentration, the extrapolated line cuts the positive time axis similar to the results for the platinum substrate. The behavior of gold in the bromide melt is similar to that for this substrate in the chloride solutions at the lower concentration. In the case of nickel at the single concentration studied, the $i-t^{1/2}$ plots intersect the time axis in the negative quadrant. At the same Cr(II) concentration and temperature as in the nickel experiment, the copper substrate results in $i-t^{1/2}$ where the intersections are at positive values of time, Figure 34. However, at a lower concentration and temperature, their behavior is similar to nickel and gold, Figure 35.

The initial portions of the rising part of the transients obtained for platinum were examined for their time dependence. A typical set of data is presented in Table 26 in the form of a $\log i$ vs. $\log t$ analysis. The slope which corresponds to ~ 1.6 indicates a $t^{3/2}$ dependence.

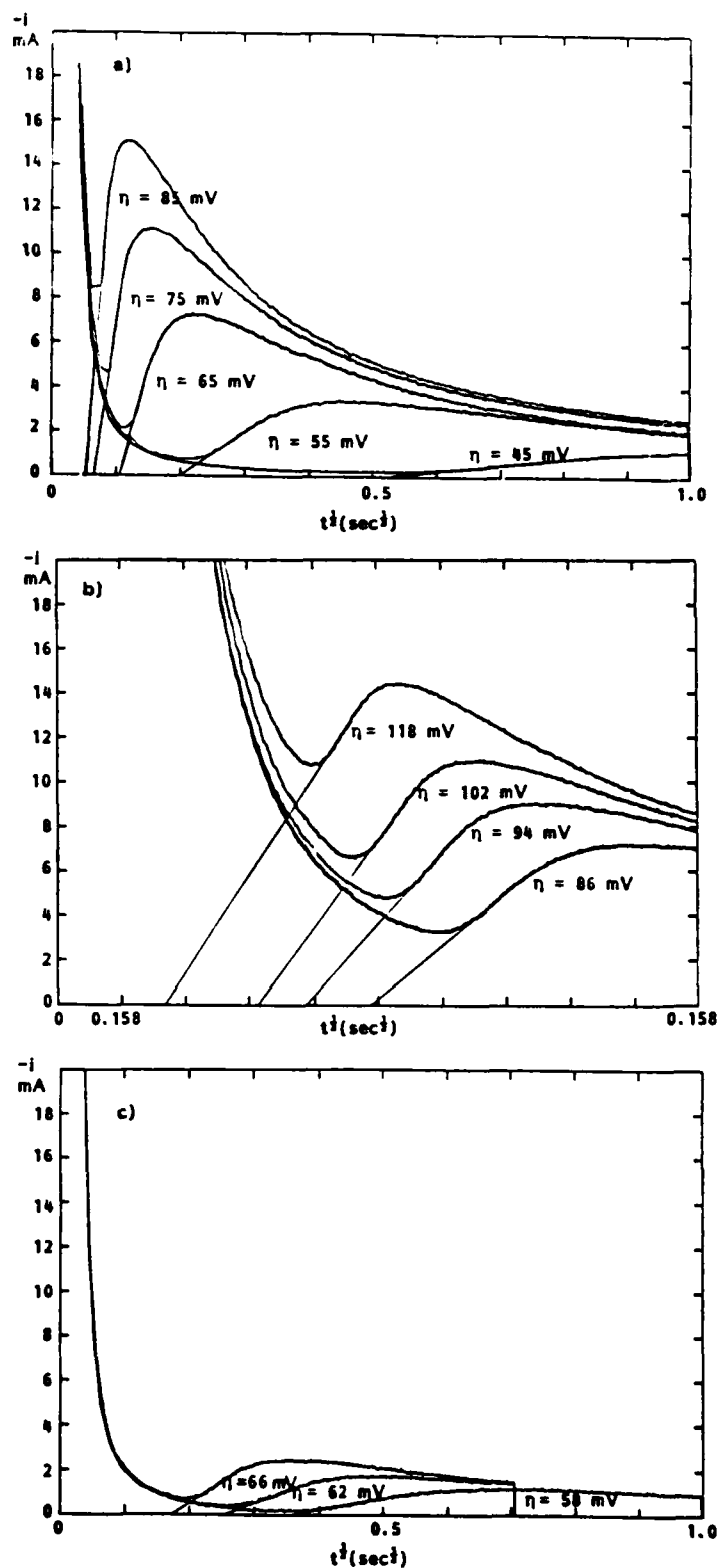


Fig. 32. Current $t^{1/2}$ plots of potential step transients showing linear region for and induction times for platinum substrate in LiCl-KCl eutectic at 450°C . (a) Concentration 34 mM Cr(II); (b)-(c) Concentration 24 mM Cr(II).

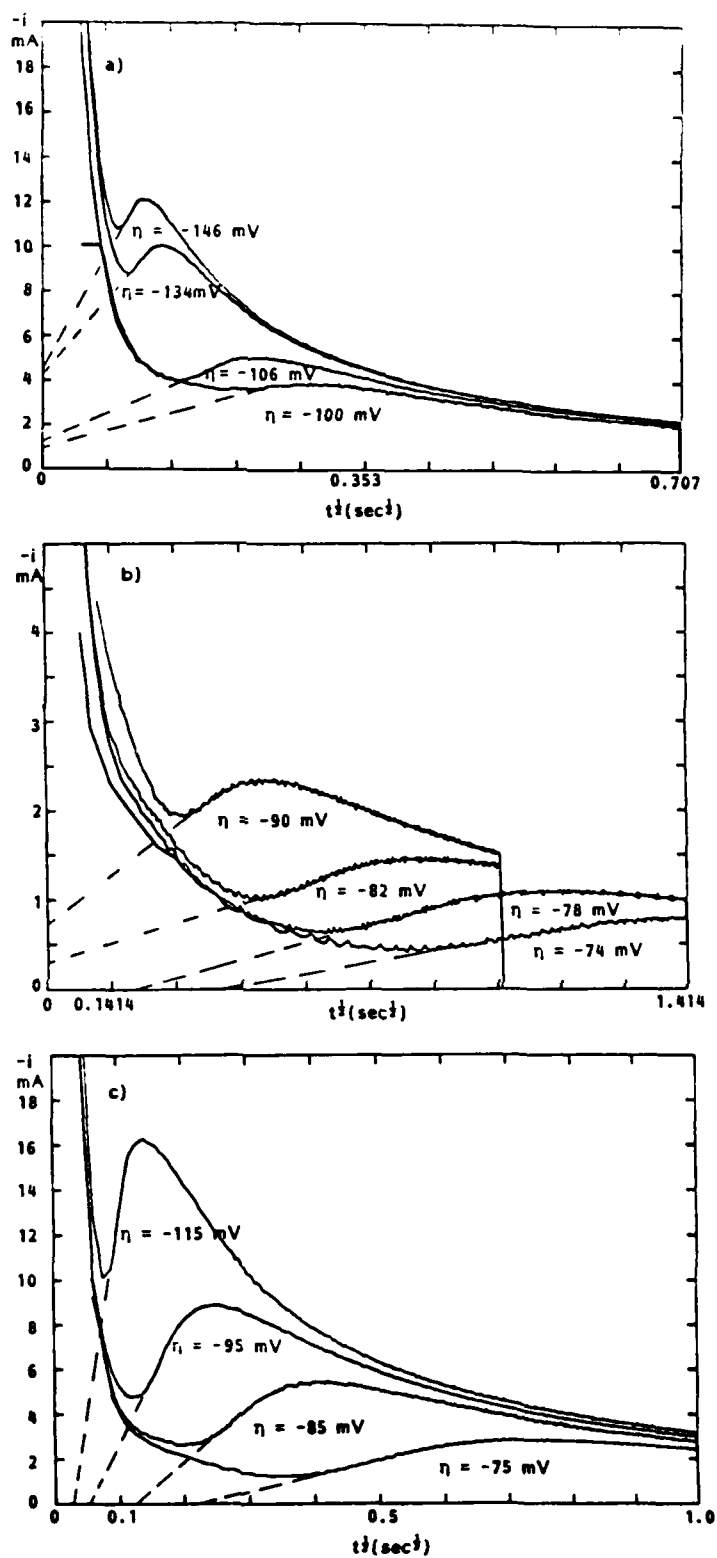


Fig. 33. Current time $^{1/2}$ plots of potential step transients showing linear region for gold substrate in LiCl-KCl eutectic at 450°C. Concentration of Cr(II) for (a)-(b) 24 mM; (c) is 34 mM.

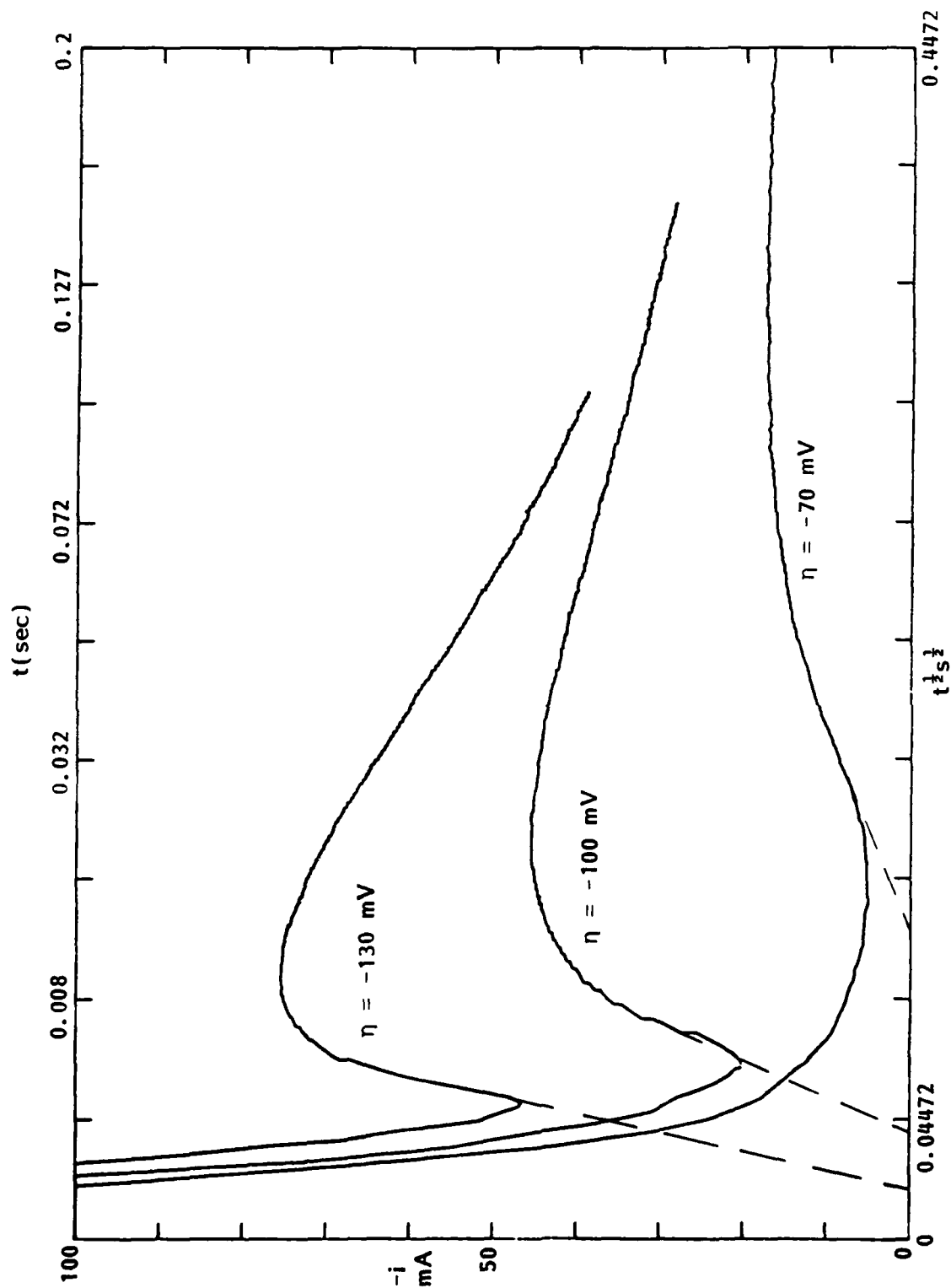


Fig. 34. Current time^{1/2} plots of potential step transients showing linear region and induction times for copper substrate in LiCl-KCl eutectic at 450°C. Concentration = 21.7 mM Cr(II).

TABLE 26

TIME DEPENDENCE OF EARLY PART OF GROWTH
TRANSIENT FOR Cr DEPOSITION ON PLATINUM
SUBSTRATE IN LiCl-KCl AT 450°C

Concentration Cr^{2+} = $24 \times 10^{-6} \text{ mol cm}^{-3}$
 Area of Pt Electrode = 0.23 cm^2
 Applied Pulse = -0.650V
 Rest Potential of Pt = -0.150V vs. Ag ref.
 500 data points taken
 First Point 125
 Last Point 175

<u>Points</u>	<u>Log(t)</u>	<u>Log(i)</u>	<u>$10^3 \Delta i$</u>
1	-2.2041	-2.3372	-0.320
4	-2.1938	-2.3233	-2.470
7	-2.1838	-2.3054	-0.279
10	-2.1739	-2.2924	2.676
13	-2.1643	-2.2798	-5.107
16	-2.1549	-2.2636	-3.566
19	-2.1457	-2.2480	-2.298
22	-2.1367	-2.2291	2.420
25	-2.1278	-2.2111	6.645
28	-2.1992	-2.2041	0.126
31	-2.1107	-2.1871	3.900
34	-2.1024	-2.1739	4.056
37	-2.0942	-2.1612	4.069
40	-2.0862	-2.1518	0.884
43	-2.0783	-2.1427	-2.270
46	-2.0706	-2.1308	-2.450
49	-2.0630	-2.1220	-5.602

Intercept = 1.1062
 Standard Deviation Intercept = 0.0219
 Slope = 1.5621
 Standard Deviation Slope = 0.0103
 Correlation Coefficient = 0.998648

This was confirmed by plots of i vs. $t^{3/2}$ at various overpotentials. That a good fit to this time dependence is obtained can be judged from the correlation coefficients in Table 27. The values of AN_0 and N_{sat} derived from the slopes are also included. When the diffusion zones extend outward from the nuclei, these areas are excluded for nucleation (51,59), and the number of sites nucleated is reduced and ultimately becomes constant. At this point, the nucleation process is arrested. The nuclear number density under these conditions will be different from the maximum available sites. The saturated number density can be related to the AN_0 by the expression (56):

$$N(sat) = \{AN_0/2k'D\}^{1/2} \quad [24]$$

These values, reported in Table 27, are lower than those obtained from t_m as expected.

In the case of gold electrodes, no evidence for progressive nucleation in the initial stages of the growth process could be detected from an examination of the early part of the current time curve. Log i -log t plots gave slopes of one half indicative of instantaneous nucleation. Analysis of the i_m , t_m data in Tables 17 to 19 and comparison with the values of $i_m^2 t_m$ calculated from the experimental CAD² for each electrode, Table 20, also indicated that the nucleation process at longer times was instantaneous for gold, and in the case of platinum had become arrested. The data for copper and nickel at 450°C may be consistent with instantaneous nucleation, but at the lower temperature and concentration, Table 20, the magnitudes of $i_m^2 t_m$ suggest that nucleation is progressive. The number of nuclei formed have been calculated on the basis of t_m (because it is less likely to be distorted by the convolution of charging and nucleation currents at the shortest times), and in all cases it is clear that the number of nuclei formed is strongly dependent upon the overpotential. AN_0 also shows a strong overpotential dependence, see Figure 36. The magnitudes of the number densities are reasonable and are consistent with values reported in the literature for aqueous ambient temperature systems and with recent results for copper deposition on vitreous carbon in this chloride melt at 450°C.

The discussion has so far been concerned with the mechanism of growth of the nuclei albeit necessarily taking account of the primary nucleation process. Classical nucleation theory applied to the electrochemical situation enables some correlation between the quantities AN_0 , N and the overpotential to be written. From the theory of Volmer (60) for three dimensional nucleation, the quantity AN_0 can be related to overpotential by an equation of the form:

$$\ln J = [\log J_0 - B\eta^{-2}] = \ln AN_0 \quad [25]$$

and

$$B = \frac{8\pi V_m^2 \phi \sigma^3}{3 (zF)^2 kT} \quad [26]$$

AD-A171 410

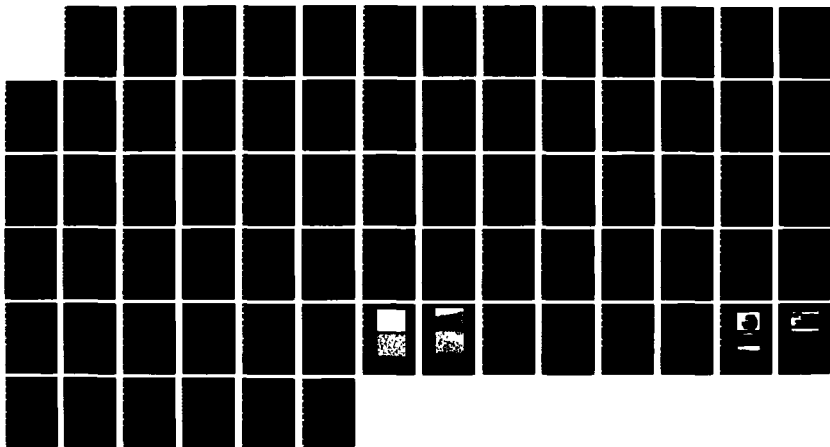
AN INVESTIGATION OF THE ELECTRODE KINETICS AND
ELECTROCHEMISTRY OF REFRAC (U) EIC LABS IN NORWOOD MA
S H WHITE ET AL JUL 86 C-674(F) ARO-19354 3-MS-5
DAG029-82-C-0013

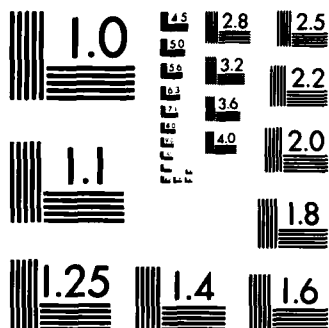
2/2

UNCLASSIFIED

F/G 13/8

NL





MICROCOPY RESOLUTION TEST CHART
NATIONAL BUREAU OF STANDARDS-1963-A

TABLE 27

POTENTIAL STEP RESULTS

ANALYSIS AS i VS. $t^{3/2}$ OF INITIAL PORTION OF GROWTH TRANSIENT ON
PLATINUM SUBSTRATE IN LiCl-KCl EUTECTIC AT 450°C

Concentration of Cr^{2+} = $24 \times 10^{-6} \text{ mol cm}^{-3}$
 Area of Pt Electrode = 0.23 cm^2
 Rest Potential of Pt Electrode = $+0.55\text{V}$ vs. Cr^{2+}/Cr
 Rest Potential of Cr^{2+}/Cr = -0.55V vs. Ag reference
 Diffusion coefficient for Cr^{2+} = $1.14 \times 10^{-5} \text{ cm}^2 \text{ s}^{-1}$
 L = $(1 - \exp \eta \cdot 2F/RT)$

Overpot ⁿ $-\eta$ (V)	η^{-2} V^{-2}	$L^{-3/2}$	Measured Slope	Corr Coef	10^{-8} AN_0	10^{-6} N(sat)
0.070	204.082	1.183	0.3350	0.9857	0.4337	4.4401
0.074	182.615	1.158	0.6397	0.9957	0.8107	6.1032
0.078	164.366	1.137	1.3909	0.9982	1.7305	8.9582
0.082	148.721	1.119	2.5107	0.9977	3.0741	11.9875
0.086	135.208	1.103	4.2437	0.9971	5.1241	15.5306
0.090	123.457	1.090	5.8000	0.9975	6.9186	18.1013
0.094	113.173	1.078	7.8682	0.9979	9.2865	21.0272
0.098	104.123	1.068	10.7119	0.9964	12.5261	24.4776
0.098	104.123	1.068	7.6944	0.9906	8.9975	20.7455
0.102	96.117	1.060	9.8390	0.9817	11.4124	23.4116
0.106	89.000	1.052	14.8860	0.9989	17.1444	28.7458
0.110	82.645	1.046	16.2300	0.9983	18.5764	29.9688
0.114	76.947	1.040	19.0095	0.9972	21.6396	32.3895
0.118	71.818	1.035	17.6432	0.9983	19.9887	31.1666

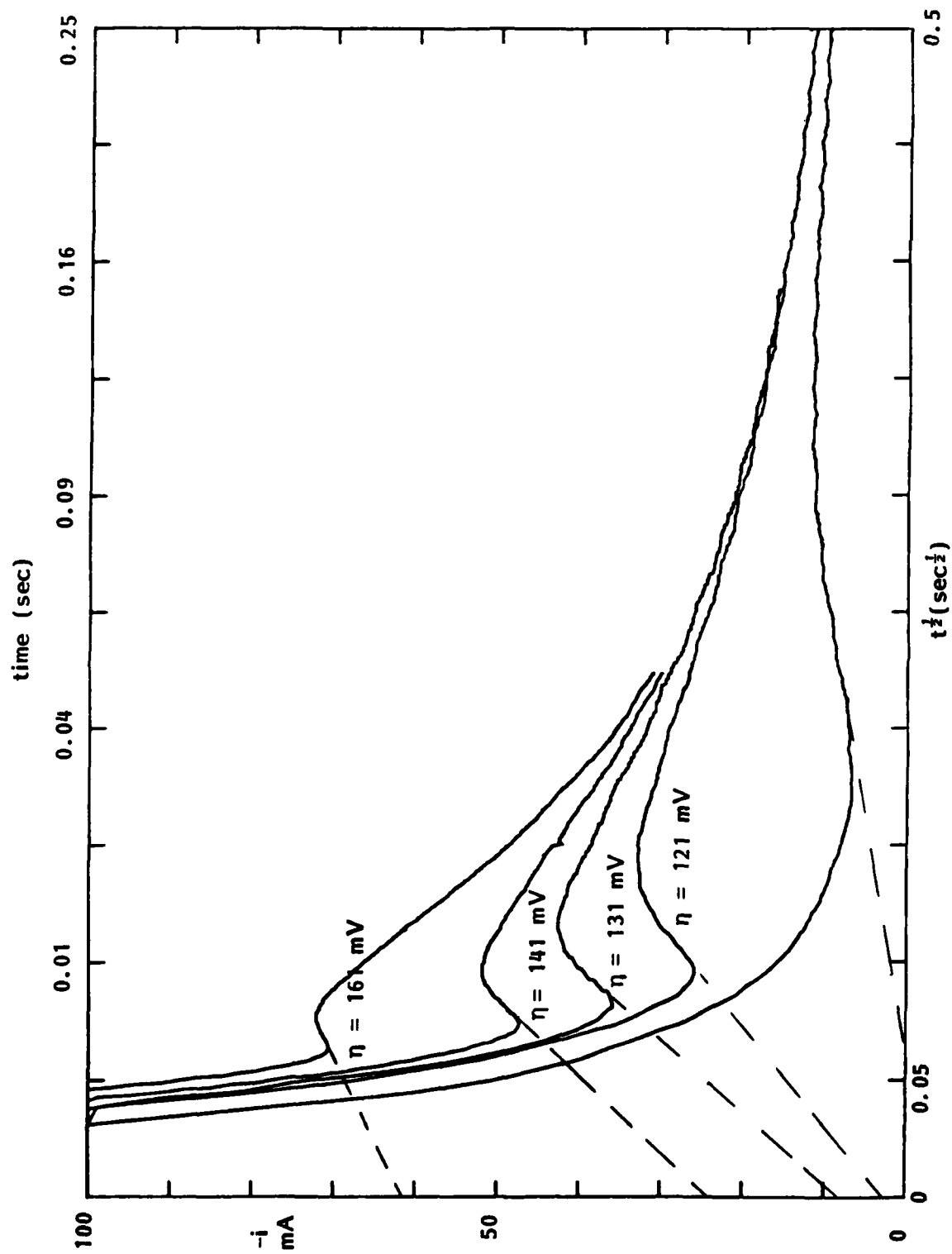


Fig. 35. Current time $^{1/2}$ plots of potential step transients showing linear region and induction times for copper substrate in LiCl-KCl eutectic at 425°C. Concentration 12.5 mM Cr(II).

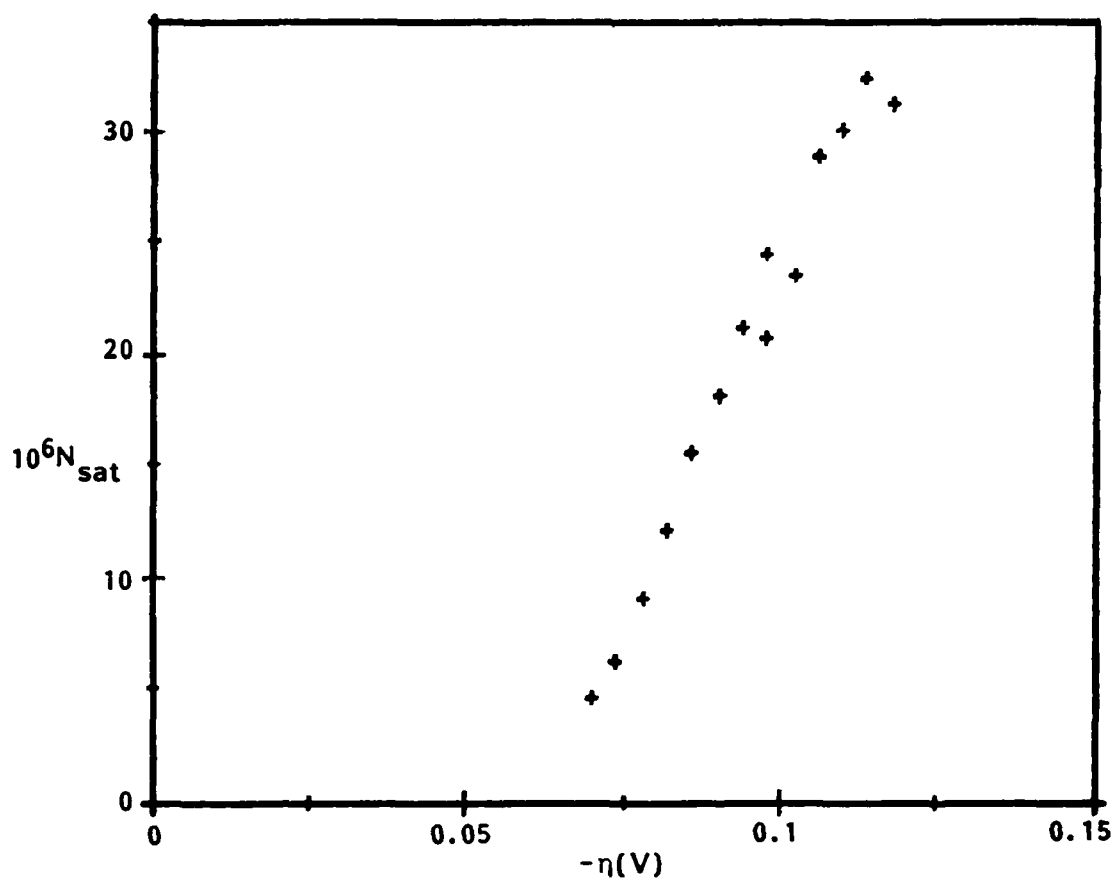


Fig. 36. A plot showing the dependence of N_{sat} on overpotential for reduction of Cr(II) on platinum in LiCl-KCl containing Cr(II) at 24 mM.

and J and J_0 are related to the nucleation rate, S is the substrate surface area, k is Boltzmann's constant, V_m is the molar volume of Cr, c is a function of the interfacial energy between depositing metal and substrate and ϕ is a value between 0 and 1 which allows for the interaction of the substrate and the depositing metal (61). The form of B is developed from thermodynamic arguments using the Gibbs Thompson description of surface tension of small drops. The number of atoms in the nuclei can be obtained in the form:

$$n_{3c} = \frac{16\pi V_m^2 \sigma^3}{3(zF\eta)^2 (ze\eta)} \quad [27]$$

where e is the electronic charge. Lantelme and Chevalet (58) expressed the relationship for the nuclear density N when nucleation is instantaneous:

$$\ln N = \frac{1}{2} [\ln(J_0 S^2 / 2\alpha D) - B\eta^{-2}] \quad [28]$$

where α is a dimensionless constant. Noting equation [25], equation [28] can be obtained from equation [24]. In this case, the constant α of Lantelme is simply the constant k' given above.

Plots of the logarithm of the measured N values as a function of $1/\eta^2$ are linear, Figure 37, as is the plot for AN_0 , Figure 38; Table 28 reports the derived value from the slopes and intercepts. The derived interfacial surface energies together with the number of atoms in the nucleus are also included. The results on platinum substrate are compared in Figure 38 with recent results obtained by Vargas (62) for platinum in the same melt at 0.396M. The derived quantities from the two sets of results shown in Table 29 are in excellent agreement.

The magnitude of the interfacial energy product is of the same order as the surface energies of liquid metals at ambient temperature (24) and is dependent upon the substrate material and temperature. The number of atoms in the nucleus is not large but suggest that at the lower values of the overpotentials employed the classical theory may be applicable. The quantity J_0/α obtained from the intercepts is reported, the magnitude of which is consistent with theoretical values and those reported in the literature in aqueous solutions (63).

An alternative view of the steady state nucleation process for high overpotentials has been derived with the aid of the atomistic approach of Walton (64) who considered the critical nucleus to comprise of a small number of atoms. Kaishev and co-workers (65) have elaborated this theory and express the resultant relationship between the steady state rate of nucleation and the overpotential as:

$$J = K_1 \exp[-\phi(n)/kT] \exp[(n + 1 - a) \{ze/kT\}\eta] \quad [29]$$

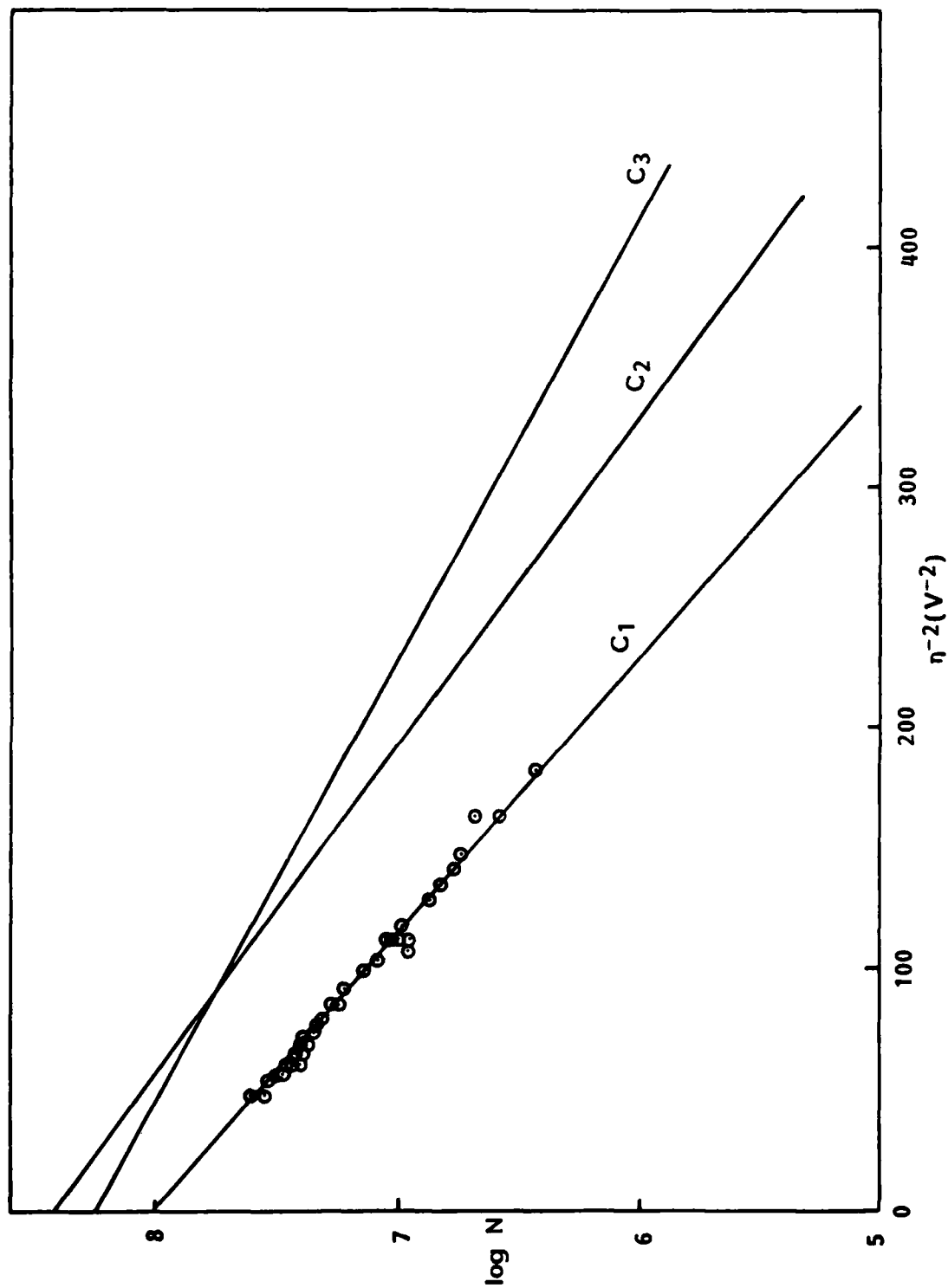


Fig. 37. Plots of the arrested nucleus density as a function of measured overpotential according to the classical nucleation theory. (a) Substrate platinum 8.75 mM; (b) 24 mM; (c) 34 mM Cr(II) ions in LiCl-KCl eutectic mixture at 450°C.

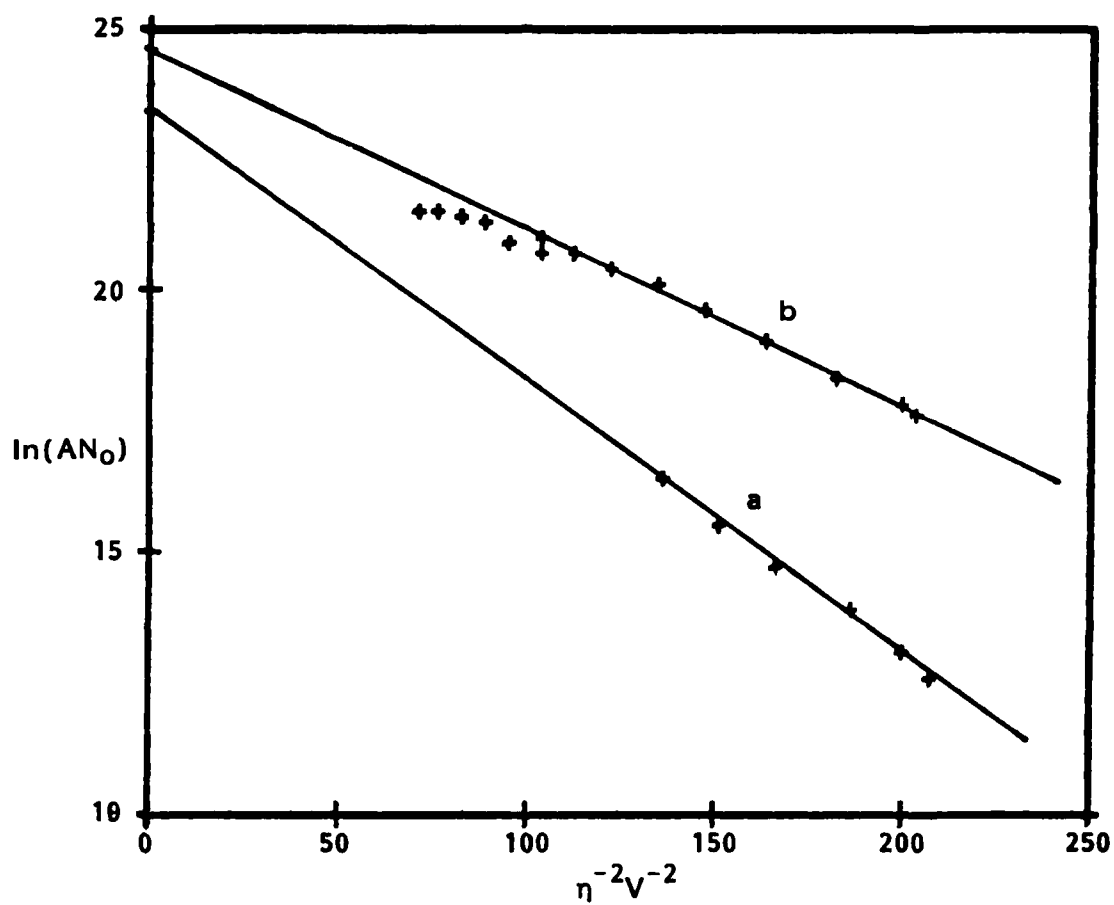


Fig. 38. Comparison of data of (a) Vargas (Ref. 62) with (b) the present work.

TABLE 28

SURFACE ENERGIES AND NUCLEATION RATES FROM POTENTIAL STEP DATA
ACCORDING TO CLASSICAL NUCLEATION THEORY

Substrate	Platinum		Gold		Gold	Copper		Nickel
Temperature, °C	450		425	450		425	450	450
Electrode Area, cm ²	0.23		0.40	0.26		#1 0.5	#2 0.5	0.6
Diff Coef CrII cm ² s ⁻¹	1.13x10 ⁻⁵		1x10 ⁻⁵	1.13x10 ⁻⁵		1x10 ⁻⁵	1.13x10 ⁻⁵	1.13x10 ⁻⁵
10 ⁶ Conc CrII, mM	7.6	24	35	8.3	24	35	12.3	21.7
Solvent	A		A	A		B	A	A
10 ³ B V ²	40.4	33.9	25.1	113	81.3	66.3	74.2	29.3
10 ⁻¹² J/α Nuclei, cm ⁻² s ⁻¹	4.5	30.0	13.7	53	39	26.7	11.6	0.21
σ mN m ⁻¹	321	304	275	449	406	380	390	289
η _{3c} (0.05V)	20	17	13	55	40	33	36	15
E, V	0.201	0.184	0.158	0.336	0.285	0.257	0.292	0.171
J Nuclei cm ⁻² s ⁻¹	3.4x10 ¹⁴		0.336		4.4x10 ¹⁴	0.23x10 ¹⁴		0.02x10 ¹⁴

A = LiCl-KCl: 41:59 mol %.

B = LiBr-KBr-CaBr: 56:19:25 mol %.

TABLE 29

COMPARISON OF RESULTS OF CLASSICAL NUCLEATION THEORY FOR DEPOSITION
 OF CHROMIUM ON A PLATINUM SUBSTRATE IN LiCl-KCl AT 450°C.
 PLOT OF $\ln AN_0$ vs. η^{-2}

<u>Source</u>	<u>This Work</u>	<u>Vargas [62]</u>
CrII Conc mM	24	386
Slope	-0.0299	-0.0514
Intercept	23.85	23.32
σ mN m ⁻¹	466	539
Corr Coeff	0.9983	0.9981
SEE	0.076	0.104
No. Pts.	8	5

where K_1 is a constant independent of overvoltage, n is the number of atoms in the critical nucleus, a is the symmetry factor and $\phi(n)$ measures the difference in energy of n atoms in the bulk and in a cluster of atoms on the substrate. Thus $\ln AN_0$ is a linear function of overpotential since:

$$\ln AN_0 = \ln K_1 - \phi(n)/kT + (n + 1 - a)\{ze/kT\} \eta \quad [30]$$

and

$$\ln N_S = 0.5[\ln K_1 - \ln 2k'D - \phi(n)/kT] + (n + 1 - a)\{2ze/kT\} \eta \quad [31]$$

Plot of $\log AN_0$ for the case of platinum substrate in Table 27 are shown in Figure 39, and for the values of N_S for platinum and gold at 24 mM are shown in Figure 40. The plots show two linear regions as was found for aqueous systems [56,57,65) and the number of atoms constituting the critical nucleus is small. In the case of the platinum and gold data, for example, the number was 7.5 and 7.4, respectively. That there are significant differences between gold and platinum is apparent from the data presented here. Thus, the application of the atomistic model in these cases may not be appropriate. Similar difficulties in the choice and applications of these models has been reported in the literature and by the authors (66) themselves suggesting that more elaborate calculations are required to accommodate the new experimental data becoming available.

The cyclic voltammogram (Figure 41) show that an overpotential of not less than 45 mV is required to initiate chromium metal deposition on the platinum substrate. This was confirmed in the potential step experiments. Overpotentials in the range 0.045-0.150V were required for the transients measured; lower overpotentials gave only monotonic decay curves mainly associated with charging. The need for a critical overpotential is consistent with the presence of an induction time in the growth transients observed with, for example, platinum. The values of the intercept on the time axis at different overpotentials are some measure of the critical induction time, since logarithmic plots of their values as a function of overpotential show similar form to induction times measured by the double pulse technique (67). It is clear in Figure 42 that a critical overpotential is necessary. The relationship between the induction time and overpotential has not been resolved for metal deposition to account for the experimental data in spite of some exacting theory attempting to do so. In view of this and the fact that induction times were not measured directly, the results here must await further study, suffice to say that the presence of a critical overvoltage in chromium deposition from the melts is consistent with recent findings in other systems (55,58). In contrast, the results for gold, copper and nickel under particular circumstances show negative intercepts which suggest that the nucleation process is modified in some way perhaps by surface alloying which must be deconvoluted in order to obtain authentic induction times. More detailed study of the role of substrate composition in the nucleation/phase forming steps is clearly required.

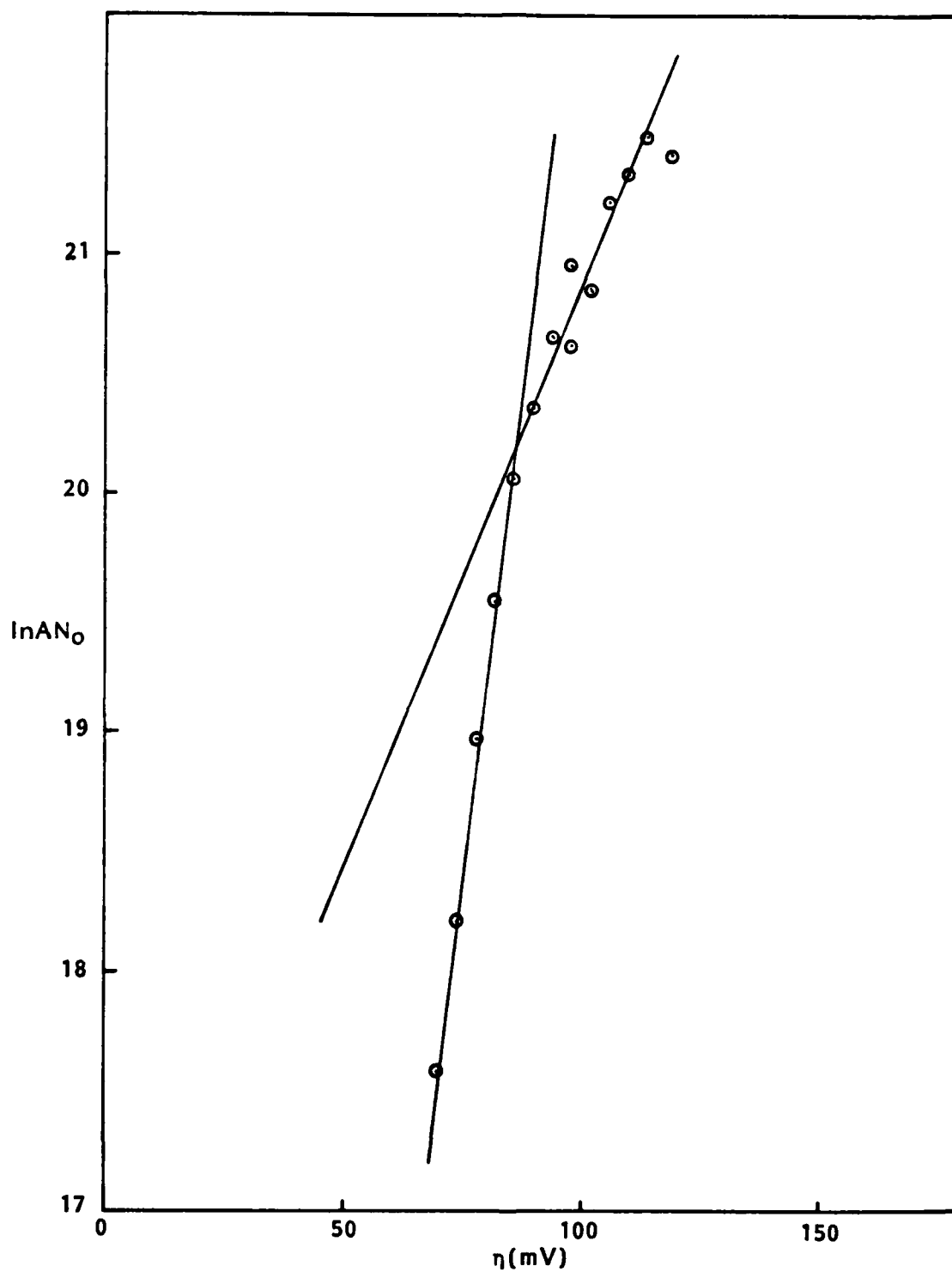


Fig. 39. Plot of steady state nucleation rate for chromium deposition on platinum substrate in LiCl-KCl-Cr(II) 24 mM at 450°C as a function of applied overpotential according to atomistic theory.

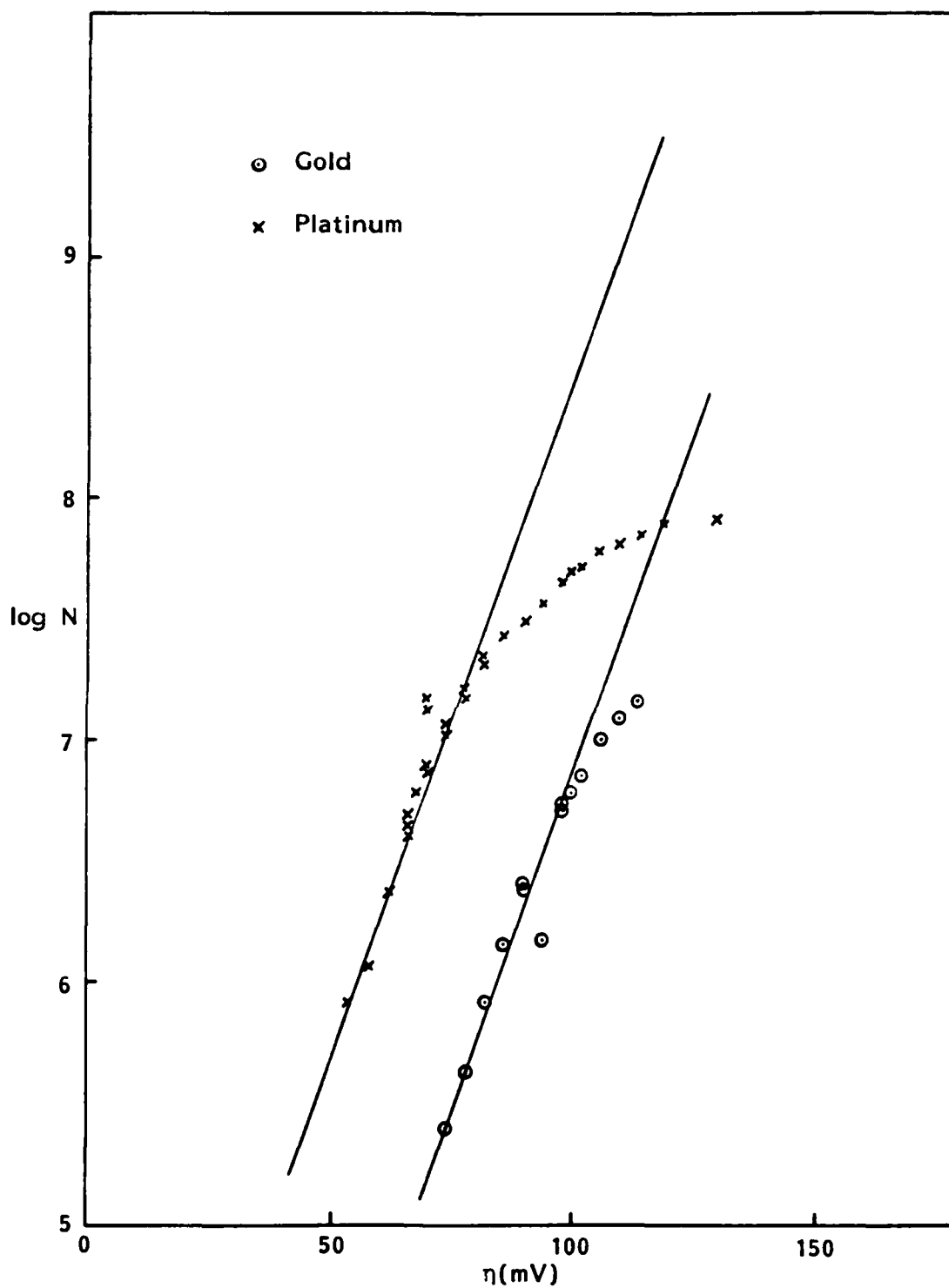


Fig. 40. Plot of the steady state nucleation rate vs. the overpotential for the deposition of chromium metal on gold and platinum substrates according to the atomistic theory.

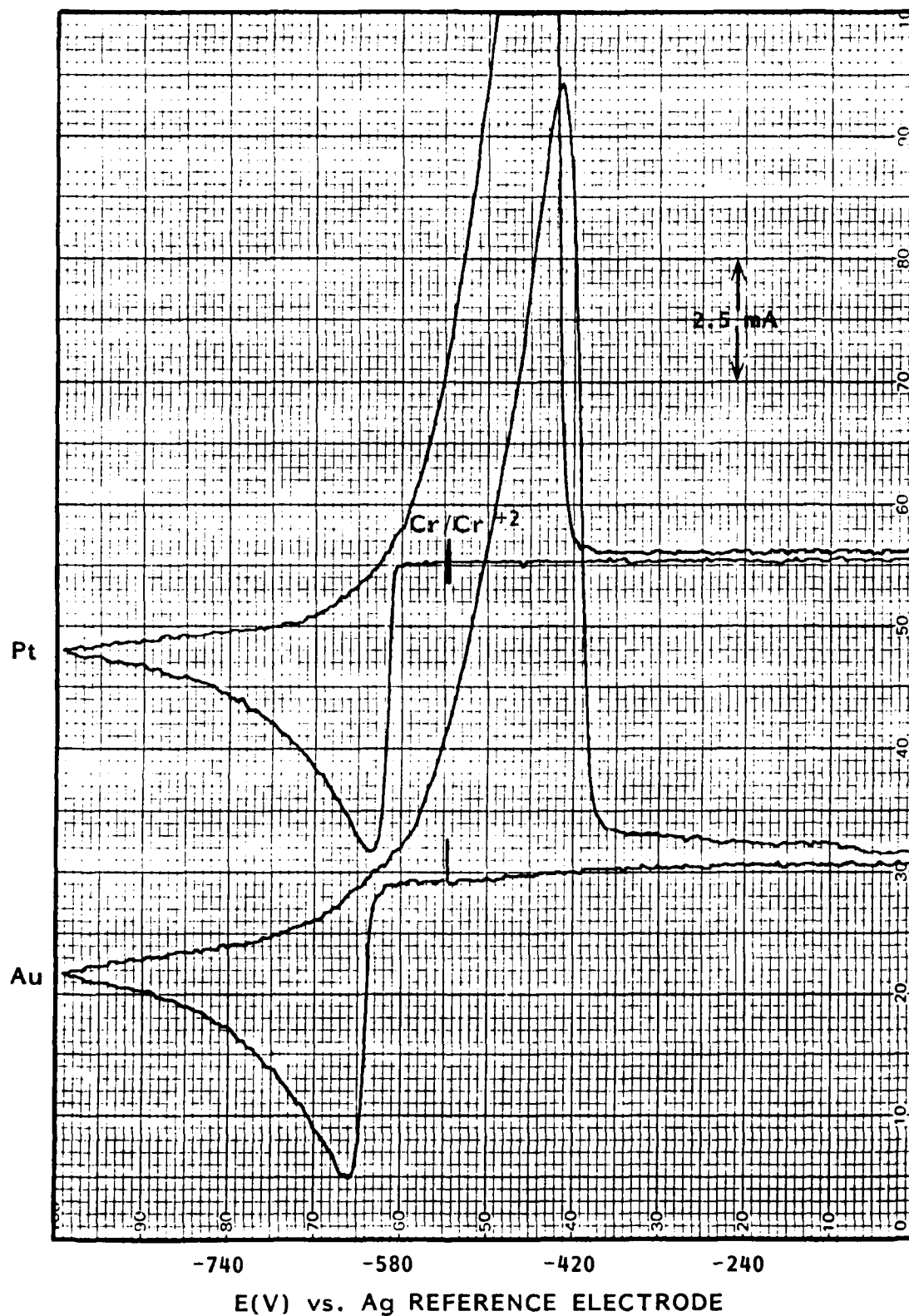


Fig. 41. Cyclic voltammograms acquired at 100 mVs^{-1} illustrating the differences in overpotential required at (a) gold and (b) platinum to initiate the reduction of Cr^{2+} ions to chromium metal on these different substrates in LiCl-KCl ($Cr(II) \sim 34 \text{ mM}$) at 450°C .

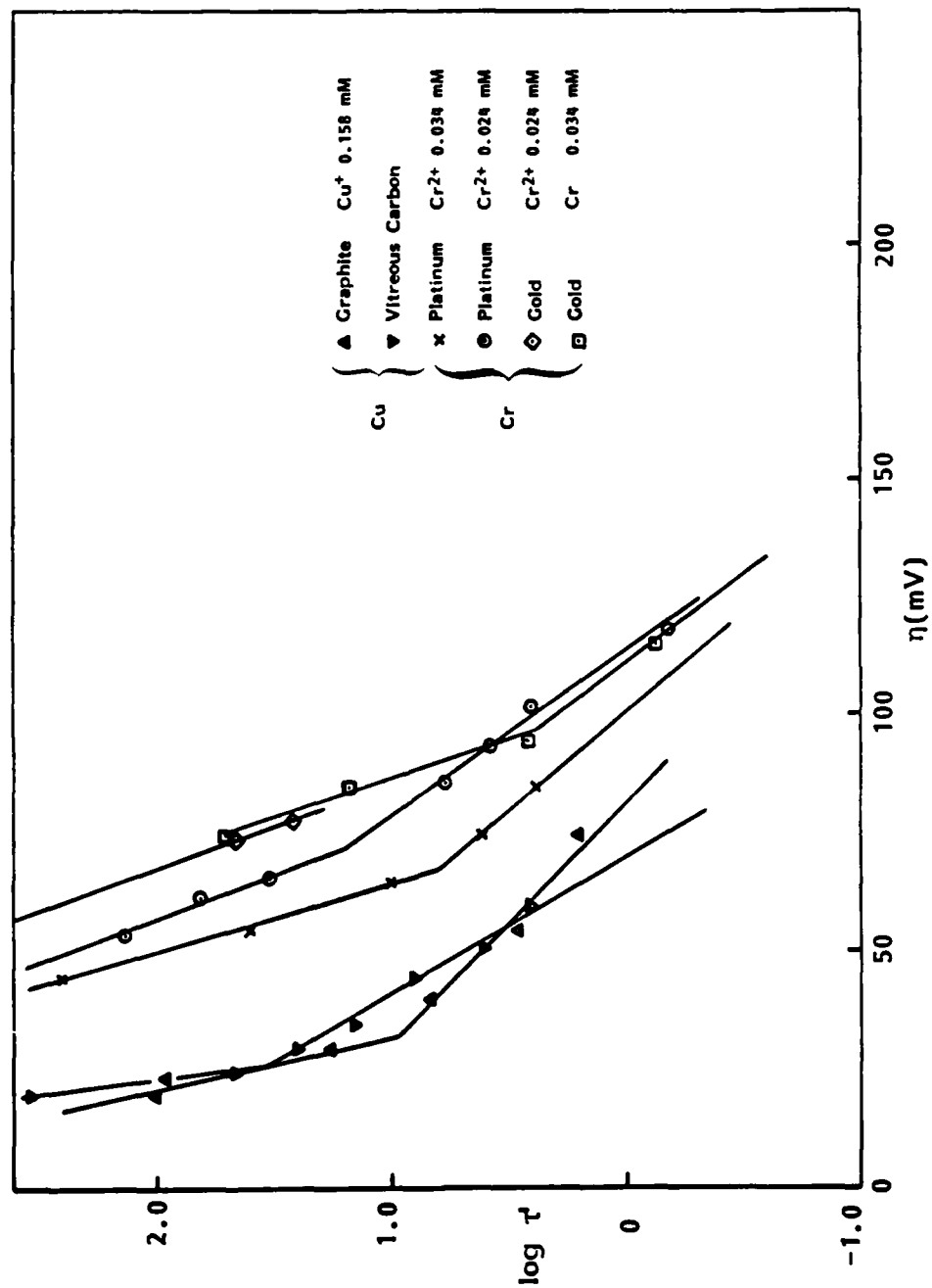


Fig. 42. Plots of "induction time" τ' as a function of overpotential for deposition of chromium on (a) gold and (b) platinum at 450°C in LiCl-KCl-Cr(II); deposition of copper (58) on vitreous carbon and graphite at 410°C in LiCl-KCl-Cu(I).

3.3.3 Current Step Measurements

The same electrode substrates, namely platinum, gold, copper and nickel have been used in current step experiments to study the reduction of Cr(II) ions in the chloride and bromide eutectics elaborated earlier. In the case of the bromide melt, measurements as a function of temperature were obtained in the range 292 to 450°C on the gold substrate. The surface condition was controlled by using a reverse pulse of duration equal to the forward pulse. Under these conditions, the rest potential of the electrodes were generally some several hundred millivolts anodic of the Cr/Cr²⁺ potential. Current pulse lengths and amplitudes were varied to establish Sand's law behavior at higher charge densities, as well as examining the potential response at lower charge densities. A typical current reversal chronopotentiogram is given in Figure 43. A representative set of data, Table 30, for the reduction of Cr(II) on a substrate illustrates that the process at long times is consistent with the Sand equation. The potential at a quarter of the transition time is clearly not expressed by the simple relationship:

$$E_{\tau/4} = E^{\circ} + RT/zF \ln C_0/2 \quad [32]$$

derived by Delahay, assuming unit activity of deposited metal on the surface (27). However, if chromium is not stripped from the surface then the measured $E_{\tau/4}$ is closely expressed by [32], see Figure 26. For measurements made at shorter times and smaller charge densities, the representative data for the gold substrate in the ternary bromide and the binary chloride melts at 450°C are given in Table 31 and illustrative potential time curves are shown in Figures 44 and 45.

3.3.4 Discussion of Galvanostatic Results

In general, the potential time transients showed a distinctive maximum in the potential after initial charging of the electrode. The difference between this maximum potential and the equilibrium potential of the corresponding Cr/Cr(II) electrode varies with the applied current density, the substrate composition, the temperature, and the melt composition. The influence of current density on a particular substrate at 450°C in LiCl-KCl containing 35 mM Cr(II) ions is illustrated in Figure 45. Such maxima have been observed for other metal deposition reactions in aqueous solutions and have been ascribed to nucleation of new phase materials (68). Rudoi and co-workers (69) presented a simple analysis of the effect in terms of classical nucleation theory. Since at the potential maximum, the rate of change of potential is zero, the overpotential at this point with respect to the M/M^{n+} equilibrium potential must represent the nucleation overpotential and the constant applied current is the nucleation current. On this basis and the Volmer equation [25], the nucleation current is:

$$i_n = \{32\pi\sigma^3 V_m^2 / 3(zF)^2 \eta^3\} J_0 \exp -B'/\eta^2 \quad [33]$$

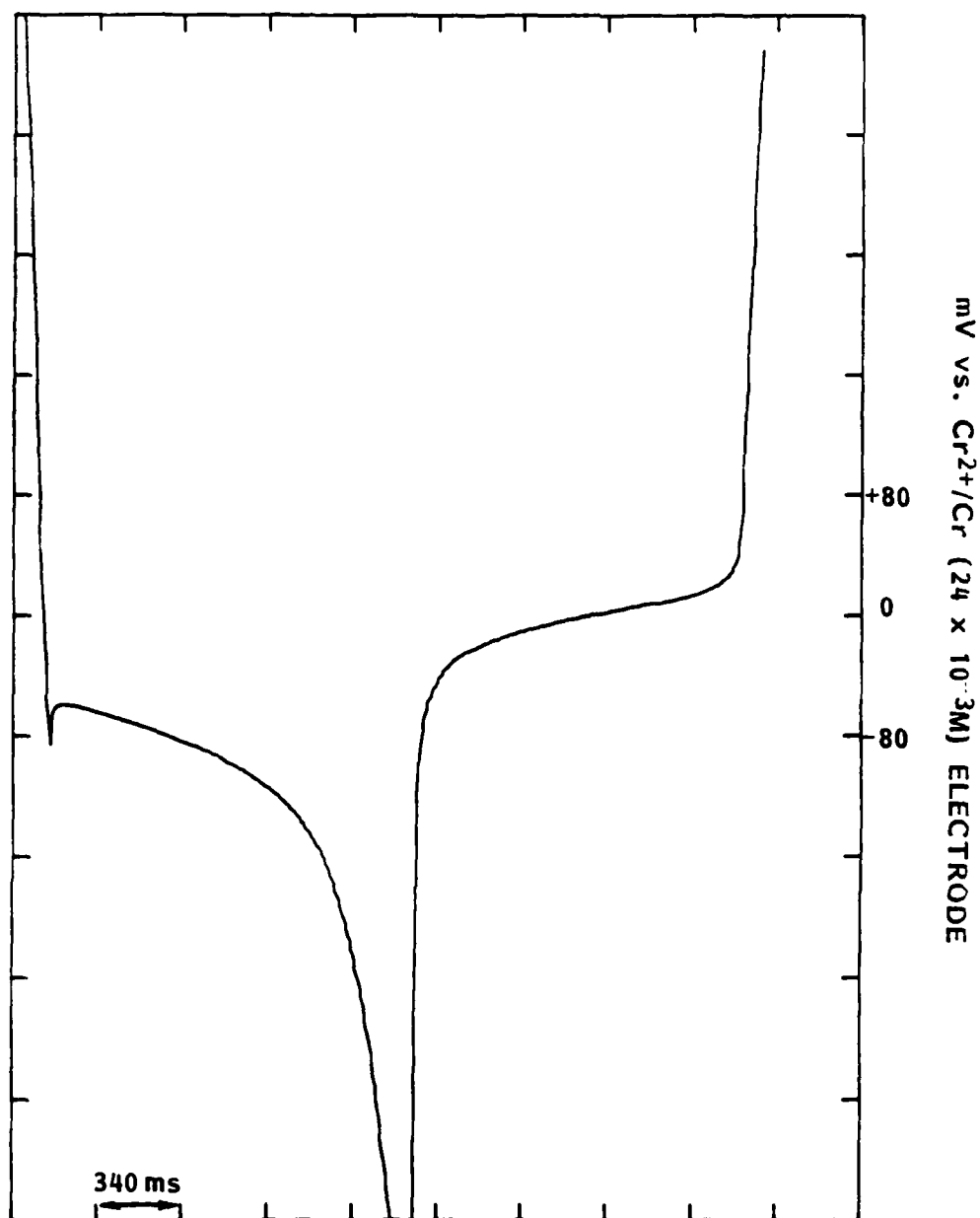


Fig. 43. Current reversal chronopotentiogram for the reduction of Cr(II) ions at a platinum electrode in LiCl-KCl containing $24 \times 10^{-3}\text{M}$ Cr(II) at 450°C . Applied current density = 8.7 mA cm^{-2} .

TABLE 30

TYPICAL CHRONOPOTENTIOMETRIC DATA FOR CHROMIUM (II)
REDUCTION ON COPPER AT 425°C

Concentration Cr(II) = 22 mM

Area of Cu W.E. = 0.5 cm²

i mA	τ sec	$10^3 i \tau^{1/2}$ A s ^{1/2}	τ_R/τ_f	t sec
8.0	1.632	10.22	1.03	-
	-	-	0.93	0.89
10.0	0.834	9.13	1.02	-
12.0	0.666	9.79	1.01	-
	-	-	0.97	0.42
14.0	0.488	9.78	1.05	-
	-	-	0.98	0.238
14.0	0.479	9.69	1.06	-
14.0	0.478	9.68	1.08	-
18.0	0.276	9.46	1.08	-
18.0	-	-	1.06	0.127

REPRESENTATIVE GALVANOSTATIC DATA FOR THE REDUCTION OF Cr(II) IONS ON DIFFERENT SUBSTRATES IN ALKALI HALIDE MELTS BETWEEN 295 AND 450°C

98

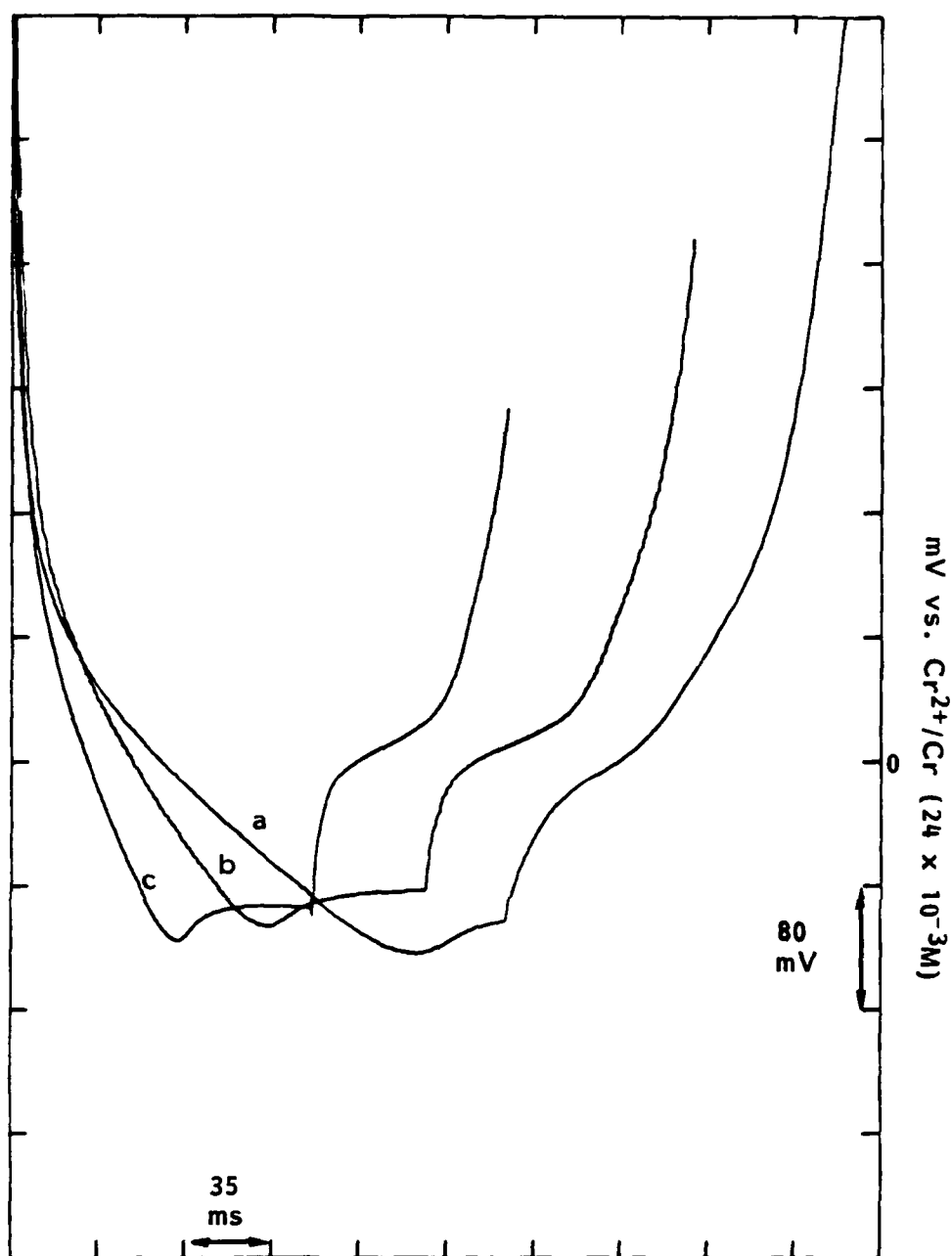


Fig. 44. Double pulse galvanostatic transients for a gold substrate in LiCl-KCl containing $24 \times 10^{-3} \text{ M}$ Cr(II) at 450°C . Applied current densities: (a) 7.69 mA cm^{-2} ; (b) 11.54 mA cm^{-2} ; (c) 16.35 mA cm^{-2} . Rest potential: (a) 398 mV; (b) 640 mV; (c) 608 mV vs. Cr^{2+}/Cr .

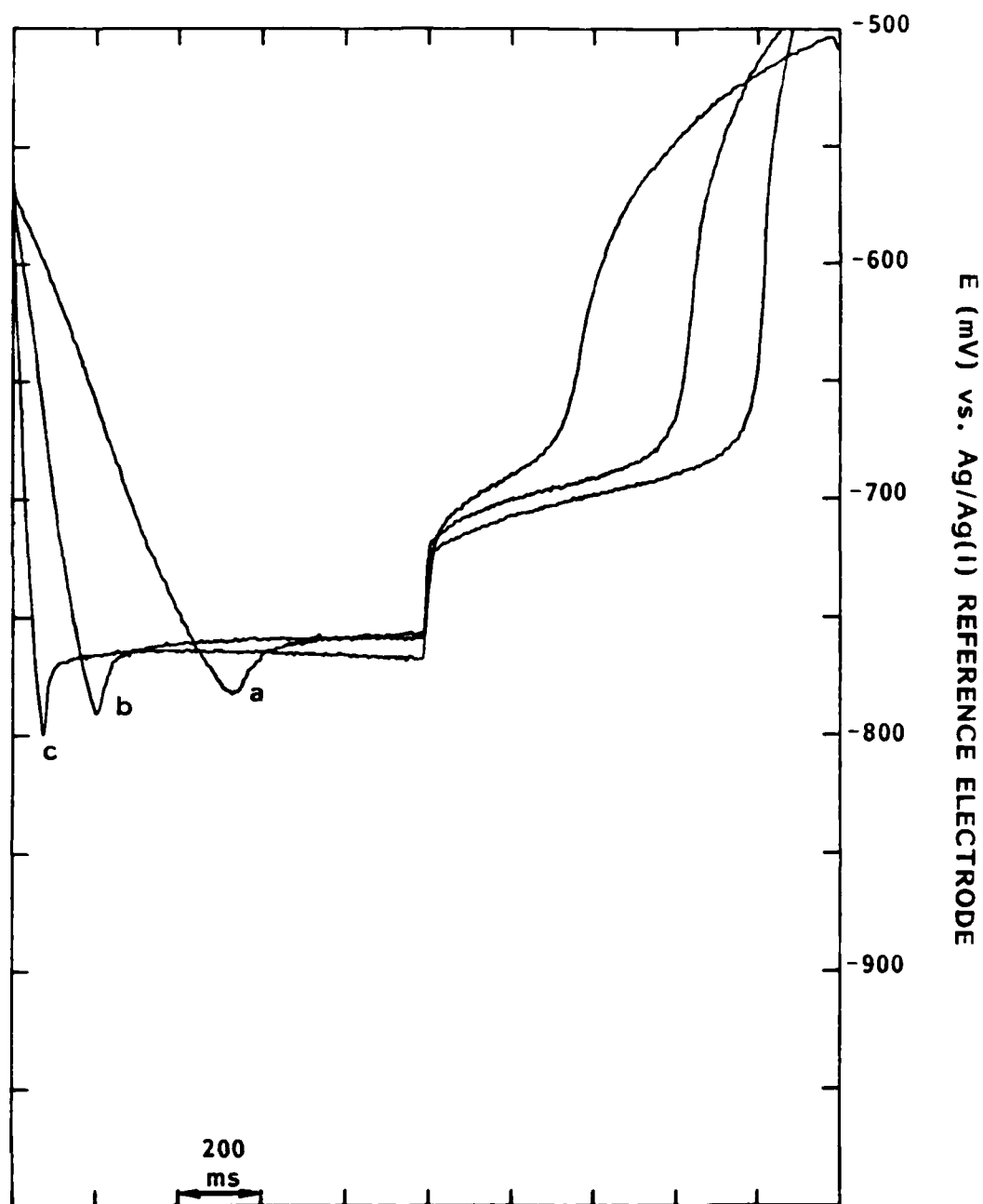


Fig. 45. Double pulse galvanostatic transients recorded for the reduction of Cr(II) at a copper electrode in LiCl-KCl containing $47 \times 10^{-3} \text{ M Cr(II)}$ at 450°C . Applied current densities: (a) 2 mA cm^{-2} ; (b) 4 mA cm^{-2} ; (c) 8 mA cm^{-2} . Rest potential: (a) 564 mV; (b) 560 mV; (c) 560 mV vs. Ag/Ag^+ (0.162m).

where $B' = B^2$, then

$$\ln i_{\eta}^3 = \ln J_0 + \ln 2B'^2 kT - B'^2 \eta^2 \quad [34]$$

The data obtained from the current pulse measurements were analyzed according to this relationship. Figure 46 compares the log plots for four different substrates in LiCl-KCl at 450°C, and Figure 47 compares results for three different temperatures for the gold substrate in the ternary alkali metal bromide melt. Since B' is known from the slope, and the explicit form of B is given by equation [26], the values for the nucleation rate J_0 and the surface energy term can be calculated. This data is summarized in Table 32. Tables 33 and 34 compare the effects of temperature and substrate, respectively, upon the values of J_0 and $\phi\sigma$. The surface energy term for the Cr-Au-bromide melt system increases as the temperature decreases in much the same way as the surface tension of liquid metals does, see Table 33. When the solvent is changed from chloride to bromide at 450°C and the substrate is gold, the surface energy term increases. This cannot simply be due to the change of solution surface tension, since according to Young's equation,

$$\sigma_{SL} = \sigma_{SD} + \sigma_{DL} \cos \theta \quad [35]$$

where θ is the wetting angle, two interfacial tension terms are affected. On the other hand, the changes in the measured surface energy term as a function of substrate composition probably reflects the changes in σ_{SD} . Similar differences are found in this quantity calculated from the potential step results in that σ_{gold} is greater than σ_{platinum} or σ_{nickel} is less than σ_{copper} . The magnitudes of the surface energies are higher in the case of the results from potentiostatic measurements. Comparison of the steady state nucleation rate constants determined by the two different techniques give values in fair agreement and typical of values reported for metal deposition processes (58,63). Energies of nucleation (given in volts) are somewhat lower when determined by the galvanostatic method than those obtained by potentiostatic method.

The results here show that properties such as interfacial energies which describe the interaction between deposit of substrate can be measured as well as the nucleation rates. In this particular set of experiments, copper and nickel are the most likely substrates to alloy with depositing chromium and the cyclic voltammograms for nickel electrodes do show evidence of this at 450°C, Figure 27. At 425°C, cyclic voltammograms for the reduction of chromium on copper also suggest some metal-metal interaction based upon the shape of the metal stripping peaks. In addition, the reduction on gold involves a predeposition process which is not observed in the voltammograms for a platinum electrode in the same solution. This latter observation is supported by corresponding ramps in the galvanostatic transient responses. The unlikely presence of impurity is ruled out by the difference in behavior on the two substrates. Thus refinement of the potentiostatic and galvanostatic pulse measurements

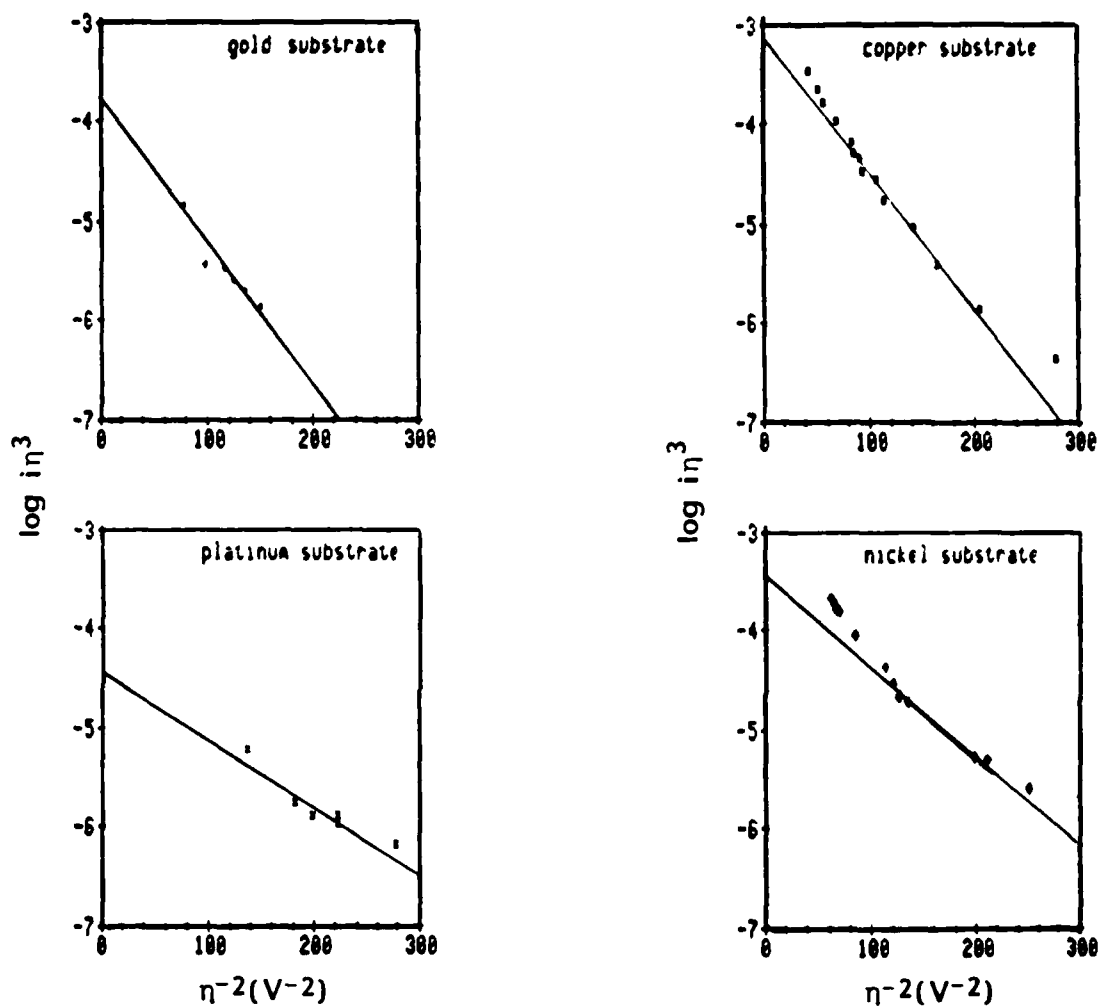


Fig. 46. Comparison of nucleation kinetics for the deposition of Cr on different substrates at 450°C in LiCl-KCl.

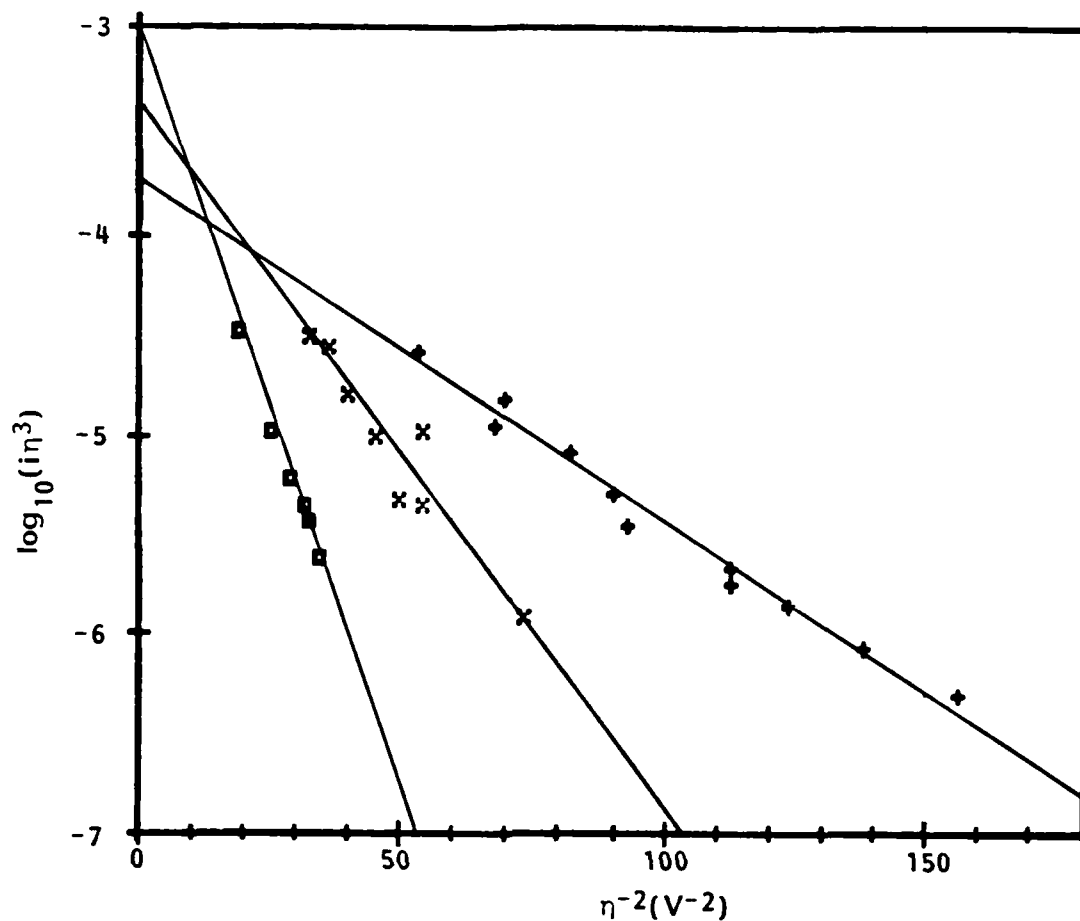


Fig. 47. Temperature dependence on nucleation kinetics for the deposition of chromium on gold from the ternary bromide eutectic mixture at: +, 455°C; x, 370°C; □, 295°C.

TABLE 32

GALVANOSTATIC RESULTS FOR CHROMIUM DEPOSITION ON DIFFERENT SUBSTRATES
AS A FUNCTION OF MELT COMPOSITION AND TEMPERATURE

Substrate	LiCl-KCl				LiBr-KBr-CsBr	T, °C
	Nickel	Copper	Platinum	Gold	Gold	
Conc Cr(II), mM B' V $10^{-16} J_O \text{ s}^{-1} \text{ cm}^{-2}$ $\sigma \text{ mNm}^{-1}$	-	-	-	-	~50 0.416 273 383	295
Conc Cr(II), mM B' V $10^{-16} J_O \text{ s}^{-1} \text{ cm}^{-2}$ $\sigma \text{ mNm}^{-1}$	-	-	-	-	~50 0.282 350 308	370
Conc Cr(II), mM B' V $10^{-16} J_O \text{ s}^{-1} \text{ cm}^{-2}$ $\sigma \text{ mNm}^{-1}$	-	~13 0.222 251 270	-	~13 0.252 430 294	-	425
Conc Cr(II), mM B' V $10^{-16} J_O \text{ s}^{-1} \text{ cm}^{-2}$ $\sigma \text{ mNm}^{-1}$	22 0.144 103 205	22 0.178 247 236	24 0.133 15 194	24 0.180 41 237	~50 0.198 273 253	450
Conc Cr(II), mM B' V $10^{-16} J_O \text{ s}^{-1} \text{ cm}^{-2}$ $\sigma \text{ mNm}^{-1}$			34 0.122 42 184	34 0.181 97 238	-	450

TABLE 33

INFLUENCE OF TEMPERATURE ON THE NUCLEATION PROCESS
FOR CHROMIUM DEPOSITION ON GOLD IN THE
TERNARY BROMIDE MELT

Temp., °C	455	370	295
Nucleation rate cm ⁻² s ⁻¹	273 x 10 ¹⁶	350 x 10 ¹⁶	442 x 10 ¹⁶
Interfacial surface Energy, mNm ⁻¹	253	308	383
Energy of Nucleation volts	0.198	0.282	0.416
Surface Tension Liquid Tin, mNm ⁻¹	528	534	540

TABLE 34

THE INFLUENCE OF SUBSTRATE COMPOSITION UPON THE NUCLEATION
OF Cr METAL FROM LiCl-KCl SOLUTIONS AT 450°C

	Gold	Platinum	Copper	Nickel
Nucleation Rate $\text{cm}^{-2}\text{s}^{-1}$	41×10^{16}	15×10^{16}	247×10^{16}	103×10^{16}
Interfacial Energy mNm^{-1}	238	194	236	205
Energy of Nucleation volts	0.180	0.133	0.178	0.144

would provide an entrée into the elucidation of these interactions between the substrate metals and the depositing metal, particularly since the chromium system provides a relatively simple solution chemistry and enables a wide range of substrates with different possible interactions with depositing metal to be examined. The ability to control these interactions by change of temperature is also possible by suitable solvent selection.

3.4 Solution Chemistry of Molybdenum in Alkali Metal Chloride Containing Melts

3.4.1 Electrochemistry of Molybdenum in Zinc Chloride - Potassium Chloride Mixtures

Introduction. The development of low melting electrolytes based upon mixtures of zinc chloride with alkali metal chlorides for molybdenum plating requires a knowledge of at least the following basic properties:

- The magnitude of the electrochemical window of the solvent in terms of melt composition, temperature and electrode substrate composition.
- The stability of the molybdenum precursor.
- The concomitant solubilization of molybdenum metal at the anode to maintain optimal bath composition.

The experimental results now reported sought to provide knowledge about these three aspects for the two zinc chloride - potassium chloride mixtures.

Solvent Behavior at Different Microelectrode Substrates. Rubel and Gross (70) concluded from their results that Mo(III) ions formed in the melt by anodic dissolution are reduced to molybdenum metal at a platinum cathode, "according to the universal mechanism proposed by Senderoff for LiCl-KCl." Susic (71) demonstrated that in pure zinc chloride the electrochemical window on a platinum electrode was about 1V, whereas on vitreous carbon the range was 1.5V. Flengas and co-workers showed that the reduction to metal of a number of metal cations could be achieved in mixtures of zinc chloride-caesium chloride (72).

Figure 48 illustrates the overall voltammograms acquired at three different substrates (Pt, Au, vitreous carbon) in the $2\text{ZnCl}_2\text{-KCl}$ mixture. At the platinum electrode, the voltammogram exhibits an anodic passivation peak at 0.9V vs. the Ag reference electrode and its corresponding cathodic peak. The charge under the cathodic peak is less than that measured for the anodic peak suggesting that the passive layer has a finite solubility in the electrolyte, Table 35. The cathodic limit involves a current which, on the reverse scan, shows a typical cathodic

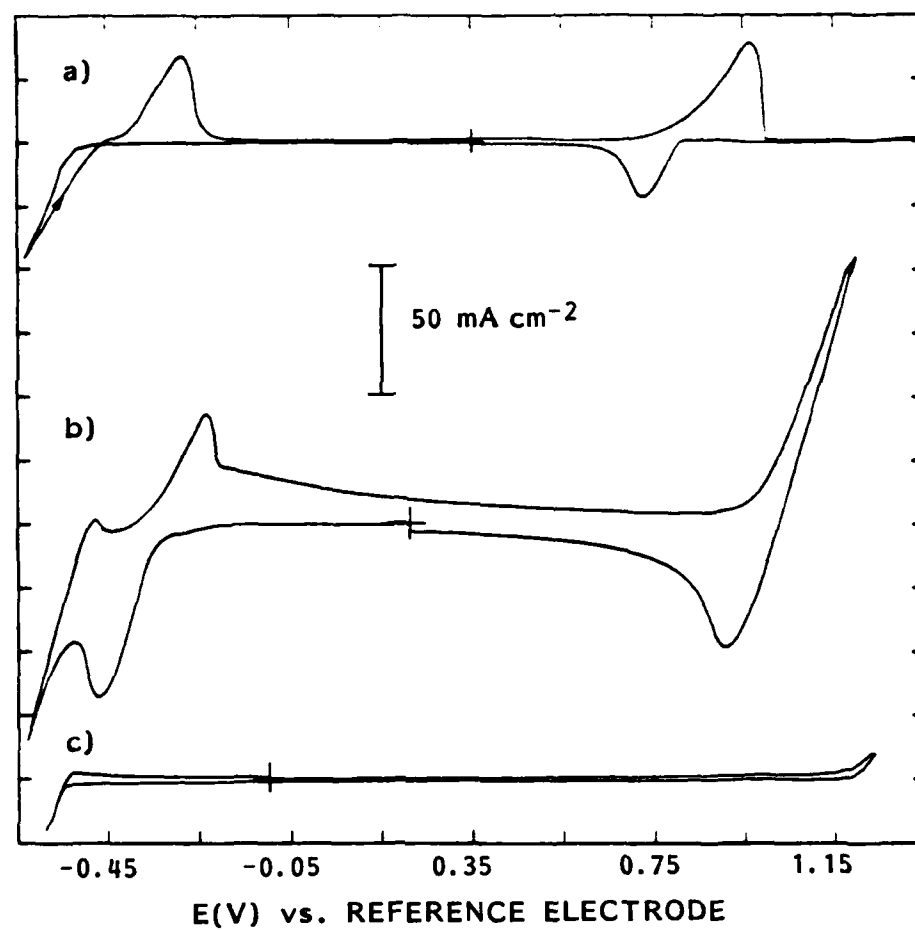


Fig. 48. Cyclic voltammetric background of a molten 2:1 ZnCl_2 -KCl mixture of 320°C at scan rate 0.1 V/s on (a) platinum; (b) gold; and (c) glassy carbon electrodes.

TABLE 35

TYPICAL CYCLIC VOLTAMMETRIC DATA FOR THE ANODIC FORMATION OF THE PASSIVATION FILM AND
CATHODIC REDUCTION OF THAT FILM IN MOLTEN $\text{ZnCl}_2\text{-KCl}$ MIXTURE AT Pt ELECTRODE

Melt Composition $\text{ZnCl}_2\text{-KCl}$	Temp. $^{\circ}\text{C}$	Scan Rate V/s	E_p^a V	E_p^c V	i_p^a mA cm^{-2}	$Q^a \times 10^2$ C cm^{-2}	$Q^c \times 10^2$ C cm^{-2}	$\frac{Q^c}{Q^a}$
1 : 1	290	0.1	0.84	0.66	76.5	5.84	4.55	0.70
1 : 1	320	0.1	0.89	0.64	76.5	9.29	6.86	0.74
2 : 1	320	0.1	0.97	0.73	79.0	10.00	4.00	0.40
2 : 1	320	1.0	1.12	0.63	165.7	3.67	2.87	0.78

current crossover (characteristic of a nucleation process)(46) followed by a corresponding stripping peak. At more anodic potentials, there is observed an additional peak with a smaller current density. This peak is not observed when the cathodic sweep is reversed prior to the deposition process, see Figure 49. This suggests that the anodic process involves a reoxidation of a surface alloy. Susic (71) reported a similar peak in the pure zinc chloride melt and several peaks corresponding to alloy reoxidations were observed (73) in a study of zinc chloride in LiCl-KCl at 450°C. The background for the 1:1 mixture exhibited identical features to those described for the 2:1 mixture, see Figure 50.

At a gold electrode, the voltammogram shows characteristic features. The anodic limit corresponds to the oxidation of gold. The cathodic limit is preceded by a diffusion controlled peak and its corresponding anodic stripping peak. On the anodic shoulder of the stripping peak, the current decays in an almost linear fashion over the whole potential range prior to the oxidation of the gold, Figure 51. The cathodic peak depends both upon the melt composition and temperature. When the ratio ZnCl_2/KCl and the temperature increases, the height of the peak increases, see Table 36. This diffusion controlled peak is preceded by a prepeak which is symmetrical about the current axis and possesses properties characteristic of an adsorption process. Some typical data are presented in Table 37 and illustrated in Figure 52.

Within the same potential ranges explored for the Pt and Au electrodes, vitreous carbon and graphite show no electrochemical activity. The range expected on the basis of the thermodynamic data (20) for zinc chloride is between 1.68 and 1.71V, close to that observed at 320°C and consistent with overvoltage effects known to occur on these substrates (58).

The oxidation process of the molybdenum electrode in molten $\text{ZnCl}_2\text{-KCl}$ mixtures is illustrated in the cyclic voltammograms shown in Figure 53. Two distinct anodic peaks are visible. Some data for the first anodic peak during the oxidation of molybdenum are shown in Table 38. The oxidation of metal under voltammetric conditions often shows a simple increasing current. When the solubility of the product is small, a passivation peak is observed (see Figure 49), and the post peak current is some measure of the solubility. The complex behavior observed here may find an explanation in the control of the anodic reaction by diffusion of species (ligands) present in the solution. The first anodic peak shifts anodic with increasing scan rate. An explanation for this behavior and that observed for the reduction peak on gold may be expressed in terms of a common solution species present in the solvent. Entities such as ZnCl_4^{-2} , ZnCl_3^- , ZnCl^+ have been advocated by several workers (74,75). Knowing that the overall oxidation of molybdenum involves three electrons per atom of metal (70), stoichiometric arguments which make use of the measured current function

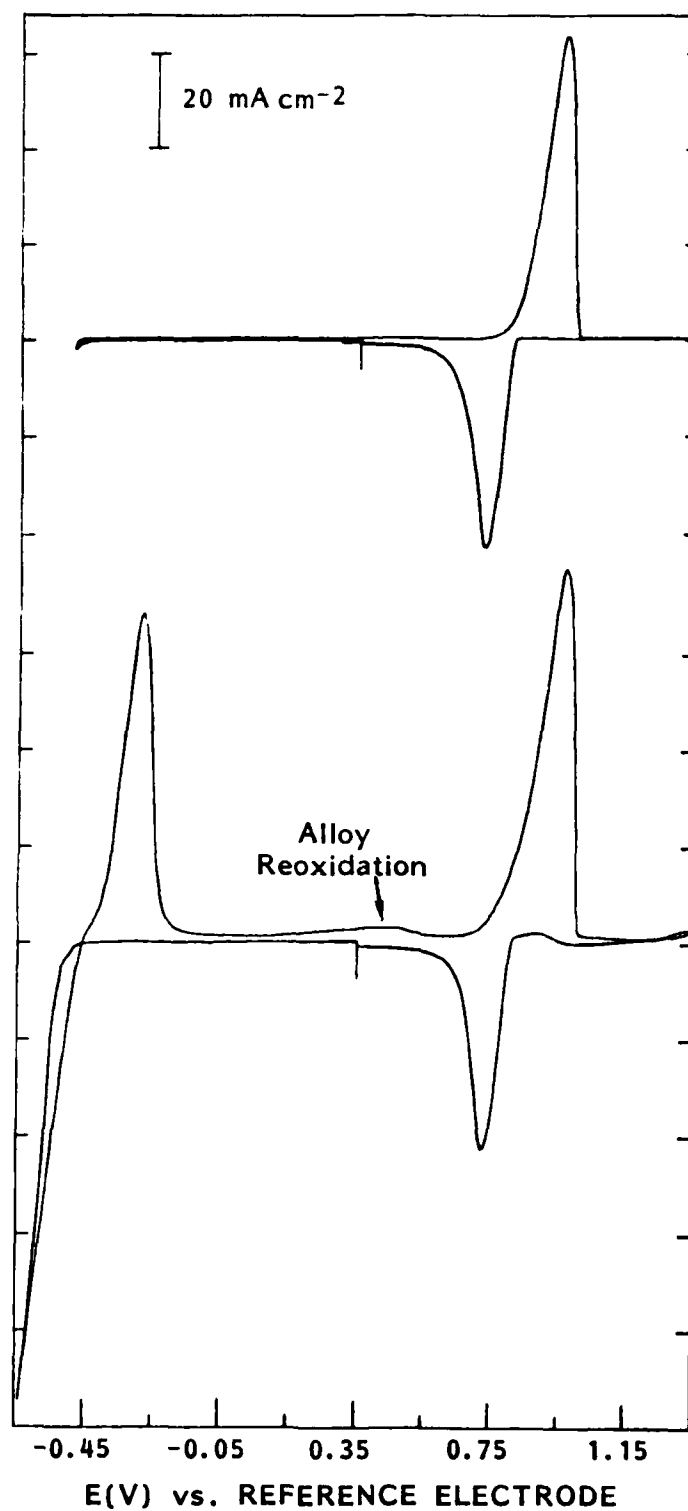


Fig. 49. Cyclic voltammograms acquired at scan rate 0.1 V/s on a platinum electrode in molten $\text{ZnCl}_2\text{-KCl}$ (2:1) mixture at 320°C. Switching potential prior to zinc deposition.

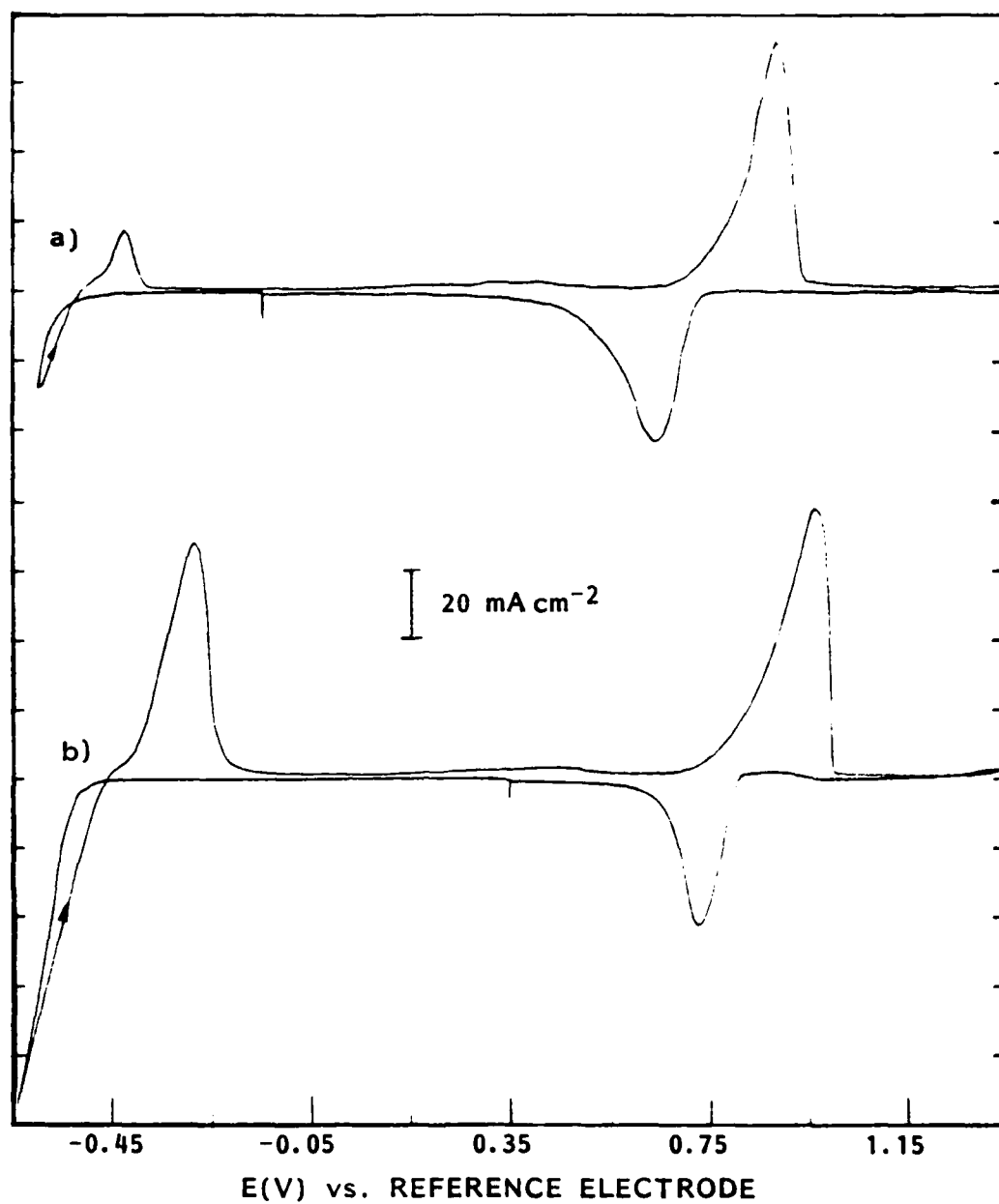


Fig. 50. Cyclic voltammetric backgrounds acquired at scan rate 0.1 V/s on a platinum electrode in molten $\text{ZnCl}_2\text{-KCl}$ mixtures: a) 1:1 mixture; b) 2:1 mixture at 320°C .

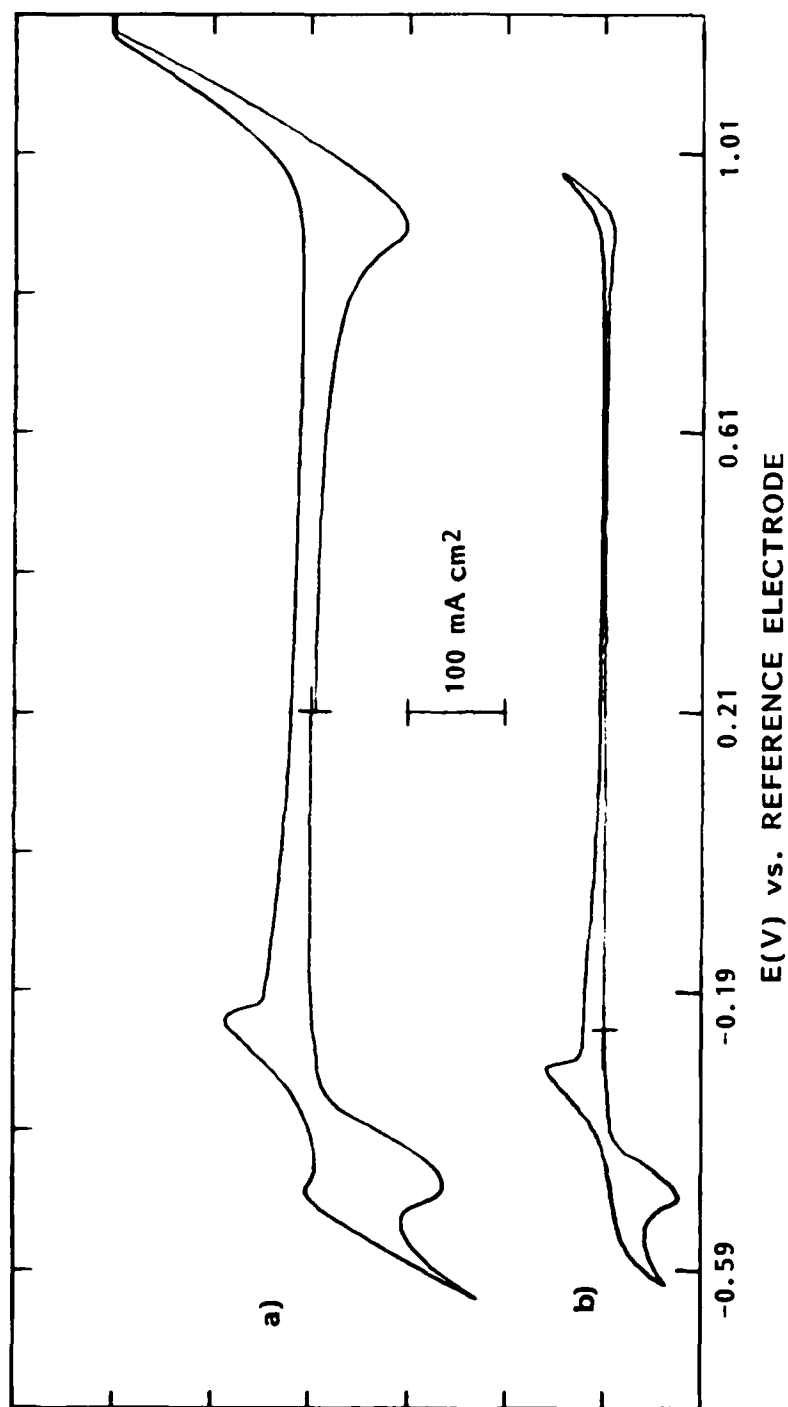


Fig. 51. Cyclic voltammetric backgrounds acquired at scan rate 0.1 V/s for a gold electrode at temperature 320°C in ZnCl_2 -KCl mixtures: a) 2:1 and b) 1:1.

TABLE 36

TYPICAL CYCLIC VOLTAMMETRIC DATA FOR THE REDUCTION AND REOXIDATION
PROCESSES IN MOLTEN $\text{ZnCl}_2\text{-KCl}$ AT GOLD ELECTRODE AT SCAN RATE 0.1 V/S

Melt Composition $\text{ZnCl}_2\text{-KCl}$	Temp. $^{\circ}\text{C}$	E_p^c V	E_p^a V	i_p^c mAcm^{-2}	$\Delta E_{p/2}$ mV	2.2RT/2F mV	0.77RT/2F mV
1 : 1	290	-0.53	-0.30	39.8	55	53	19
1 : 1	320	-0.49	-0.31	72.3	65	56	20
2 : 1	320	-0.47	-0.24	128.0	75	56	20

TABLE 37

TYPICAL CYCLIC VOLTAMMETRIC DATA FOR THE PRE-CATHODE PROCESS AT
GOLD ELECTRODE IN MOLTEN $\text{ZnCl}_2\text{-KCl}$ (2:1) MIXTURE AT 320°C

Scan Rate Vs^{-1}	E_p^c V	E_p^a V	i_p^c mAcm^{-2}	i_p^c/v $\text{mA V}^{-1}\text{s cm}^{-2}$	Q^c μC	Q^a μC	$\frac{Q^a}{Q^c}$
0.1	0.02	0.02	0.09	0.90	216	220	0.98
1.0	0.01	0.03	0.88	0.88	182	190	0.96
10	0.00	0.04	8.80	0.88	183	180	1.01

TABLE 38

CYCLIC VOLTAMMETRIC DATA FOR THE ANODIC OXIDATION OF THE MOLYBDENUM
ELECTRODE IN MOLTEN $\text{ZnCl}_2\text{-KCl}$ (2:1) AT 320°C

Scan Rate v Vs^{-1}	E_p^{a1} V	E_p^{a2} V	E_p^c V	i_p^{a1} mAcm^{-2}	$i v^{-1/2} A^{-}$ $\text{mA V}^{-1/2}\text{s cm}^2$	$\Delta E_{p/2}$ mV
0.01	0.46	plateau	-	5.47	54.7	50
0.10	0.52	0.74	0.15	17.84	56.4	80
1.00	0.70	0.97	0.13	66.67	66.7	170
10.00	0.92	1.18	0.07	203.33	54.3	-

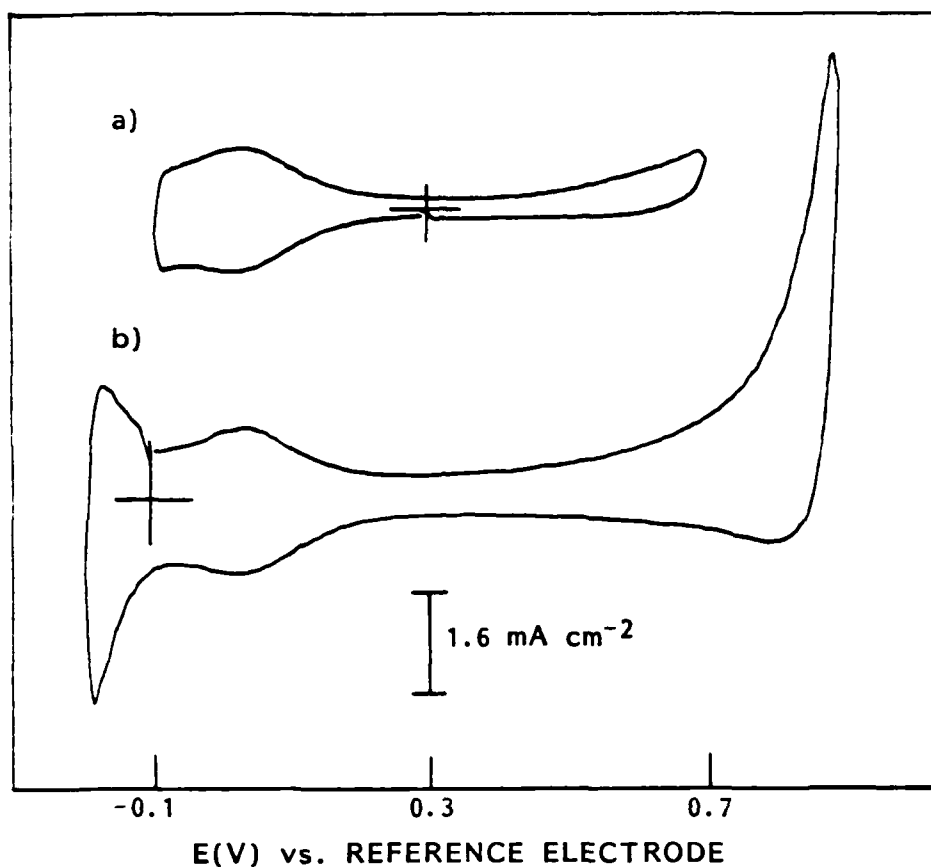


Fig. 52. Cyclic voltammetric backgrounds acquired at a scan rate of 1 V/s on a gold electrode in $\text{ZnCl}_2\text{-KCl}$ (2:1) mixture at temperature 320°C : a) Initial scan direction cathodic from the starting potential 0.3V vs. reference electrode; b) initial scan direction anodic from the starting potential -0.1V vs. reference electrode.

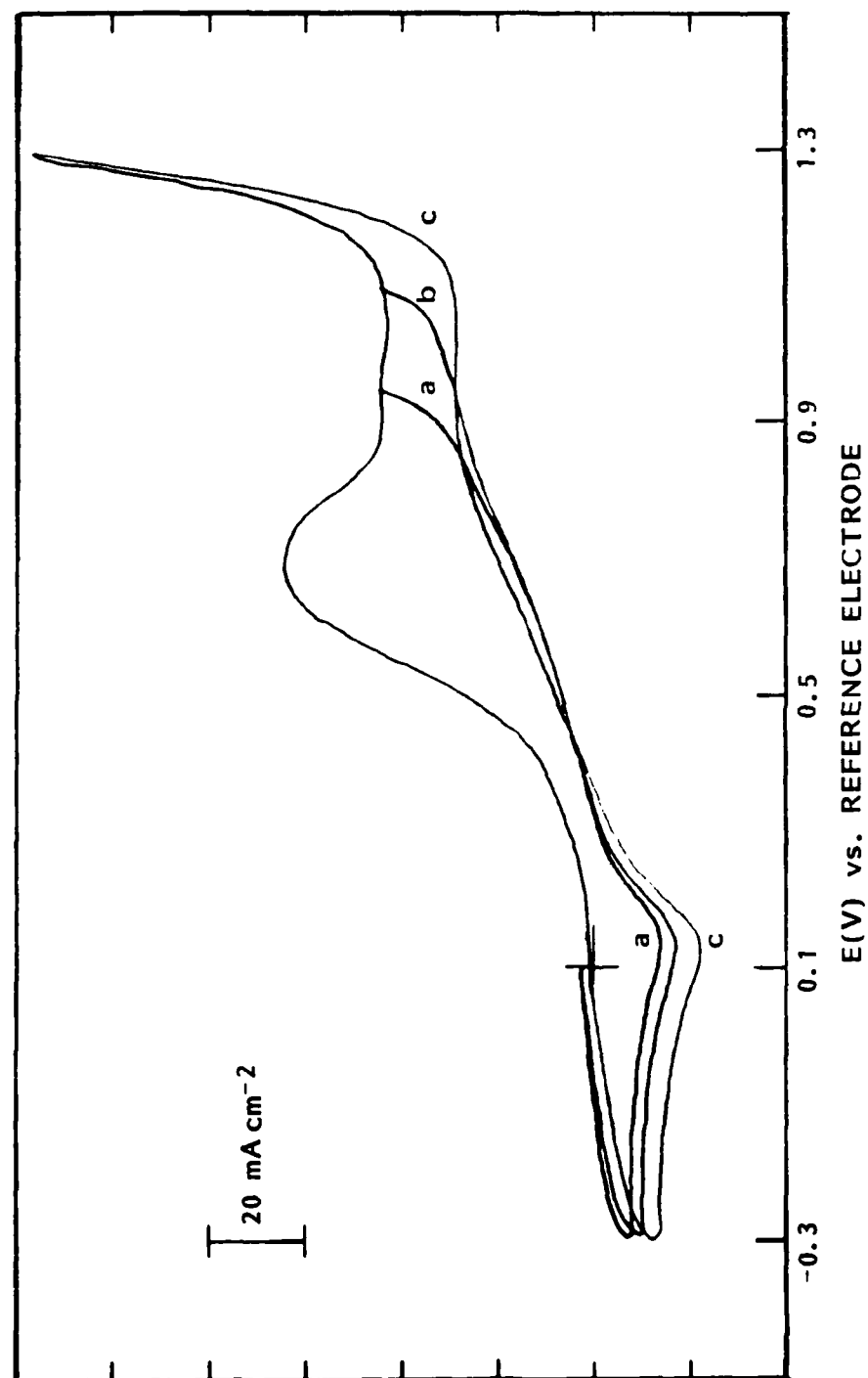
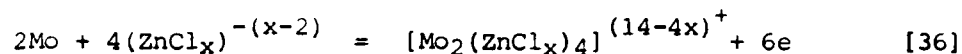


Fig. 53. Cyclic voltammograms acquired at a scan rate of 1 V/s at molybdenum electrode in molten $\text{ZnCl}_2\text{-KCl}$ (2:1) mixture at 320°C to different anodic potential: a) 0.95V; b) 1.2V; and c) 1.3V.

for the cathodic reduction process on gold and the current function for the anodic process of interest suggest that the overall reaction for the oxidation of molybdenum in ZnCl_2 -KCl mixtures is:



Although the chemistry of molybdenum (III) species is extensive, a compound of similar stoichiometry (to product described above) with triple M-M bond is described in literature with the ligand $(\text{HPO}_4)^{-2}$ whose structure is tetrahedral (15). In ZnCl_2 -KCl mixture, the $(\text{ZnCl}_4)^{2-}$ is tetrahedral, which implies that the product is $[\text{Mo}(\text{ZnCl}_4)_4]^{2-}$.

The second oxidation peak is strongly affected by the magnitude of the scan rate. For values higher than 5 Vs^{-1} , no second peak is observed. As the scan rate is decreased, the second peak is detected. At the lowest scan rates ($\sim 10 \text{ mVs}^{-1}$), the second peak is spread out over 0.5V, see Figure 54. Such behavior might be expected for an E_1CE_2 mechanism in which $\text{E}_1 < \text{E}_2$. Following the switch of scan direction, the major cathodic peak is around 0.1V. When the scan direction is reversed in the potential range after second anodic process, the net current is anodic during the reduction of the product of the second anodic process. This arises because the first oxidation reaction is still proceeding at a sufficient rate that it exceeds the reduction current for the product of the second reaction. The cathodic peak at 0.1V cannot be attributed to the six electron reduction of the product generated in the first reaction [36]. The reverse of reaction [36] would require the peak to be exceedingly sharp, i.e., the half peak width would be of the order of $\sim 10 \text{ mV}$. It must be concluded that the reduction of the product formed during the first process proceeds via different routes. The identification of this electrochemical reduction reaction, the electrochemical reaction for the second oxidation process, as well as the chemical reaction following the first oxidation process was derived from the electrochemical study of solutions of the molybdenum (III) species added as K_3MoCl_6 in ZnCl_2 -KCl melts.

Electrochemistry of K_3MoCl_6 in Zinc Chloride - Potassium Chloride Mixtures. When the initial scan direction is cathodic from the open circuit potential, voltammograms for this solution exhibit two cathodic peaks. The current function for each peak increases with increase in the concentration of K_3MoCl_6 (see Figure 55). The ratio of the height of the first peak to the height of the second peak depends upon melt composition (see Figure 56) as well as the temperature (see Figure 57). The first peak is predominant in 2:1 (ZnCl_2 -KCl) mixture. For the 1:1 mixture, the height of the first peak is significantly lower than that of the second peak. Increasing the temperature not only results in a change in the relative height of the peaks but the resolution of the two peaks decreases. This behavior is not consistent with a simple consecutive reaction scheme. This implies that two different species exist in the melt in the same oxidation state. The half peak width for the first cathodic peak in the 2:1 mixture is slightly smaller than that

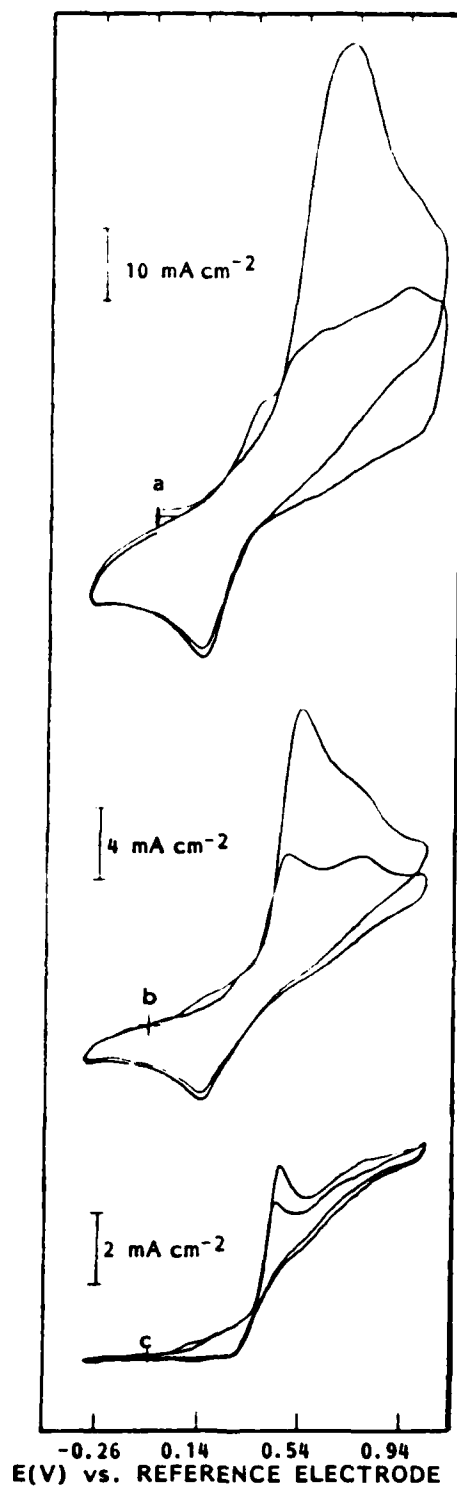


Fig. 54. Multicyclic voltammograms acquired at molybdenum electrode in molten $\text{ZnCl}_2\text{-KCl}$ (2:1) at 320°C of scan rates of a) 1 V/s; b) 0.1 V/s; and c) 0.01 V/s.

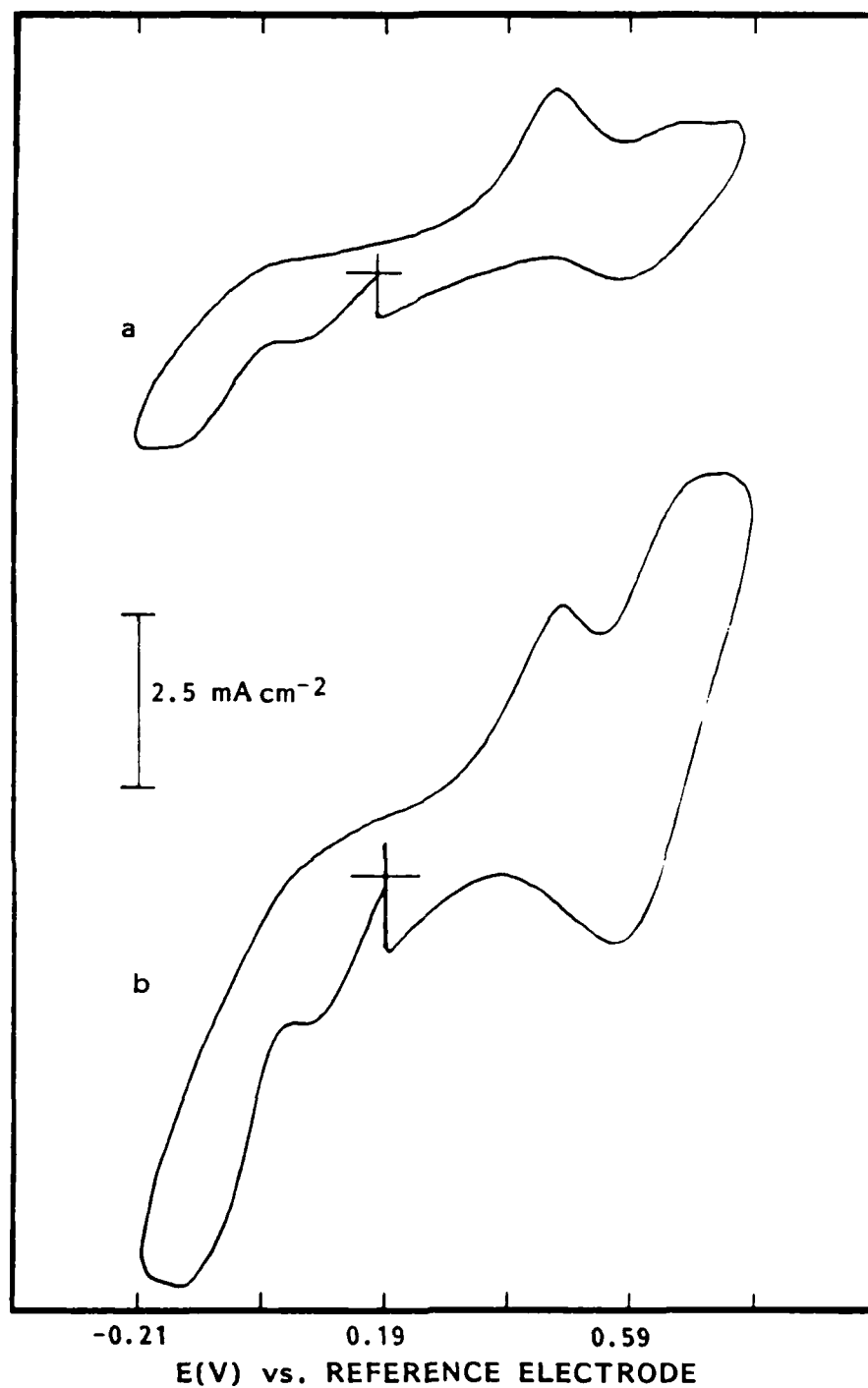


Fig. 55. Cyclic voltammograms acquired at gold electrode at scan rate 0.1 V/s in a 1:1 ZnCl_2 -KCl melt at temperature 320°C containing K_3MoCl_6 at concentrations of a) 0.028 mol/kg; b) 0.129 mol/kg.

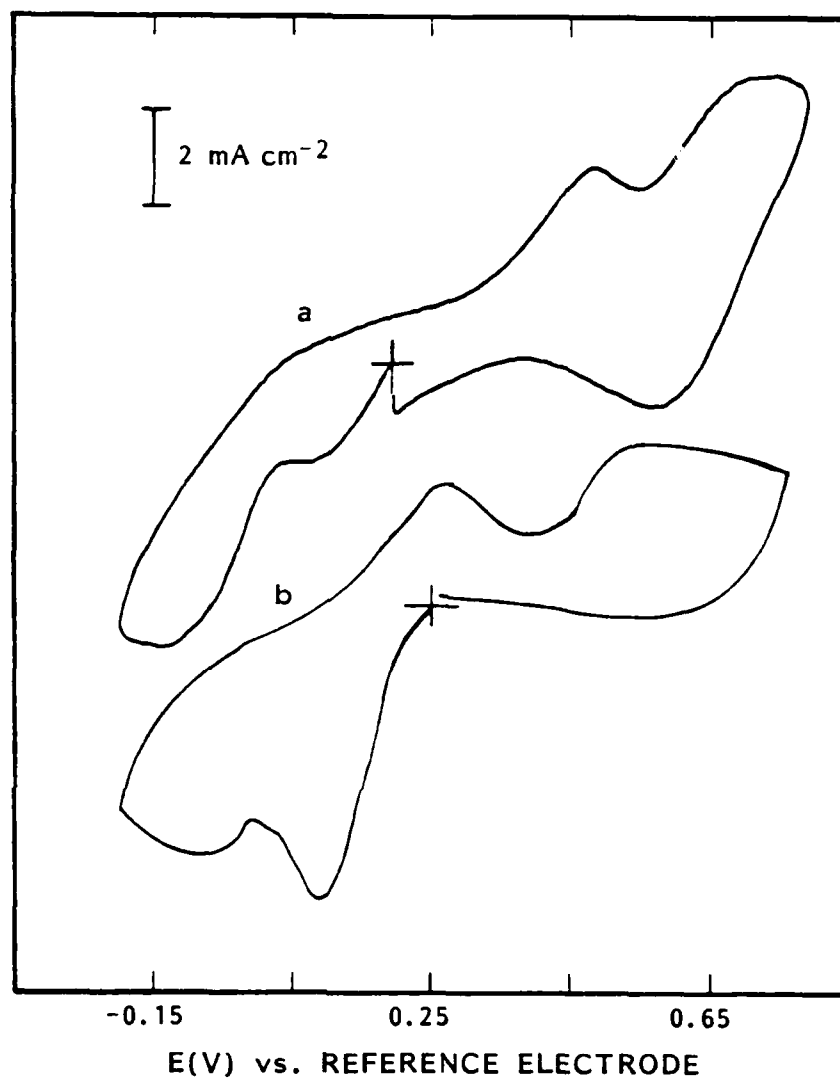


Fig. 56. Cyclic voltammograms acquired at 0.1 V/s on a gold electrode for solutions of K_3MoCl_6 in molten ZnCl_2 -KCl mixtures a) 1:1 and b) 2:1 at a temperature of 320°C .

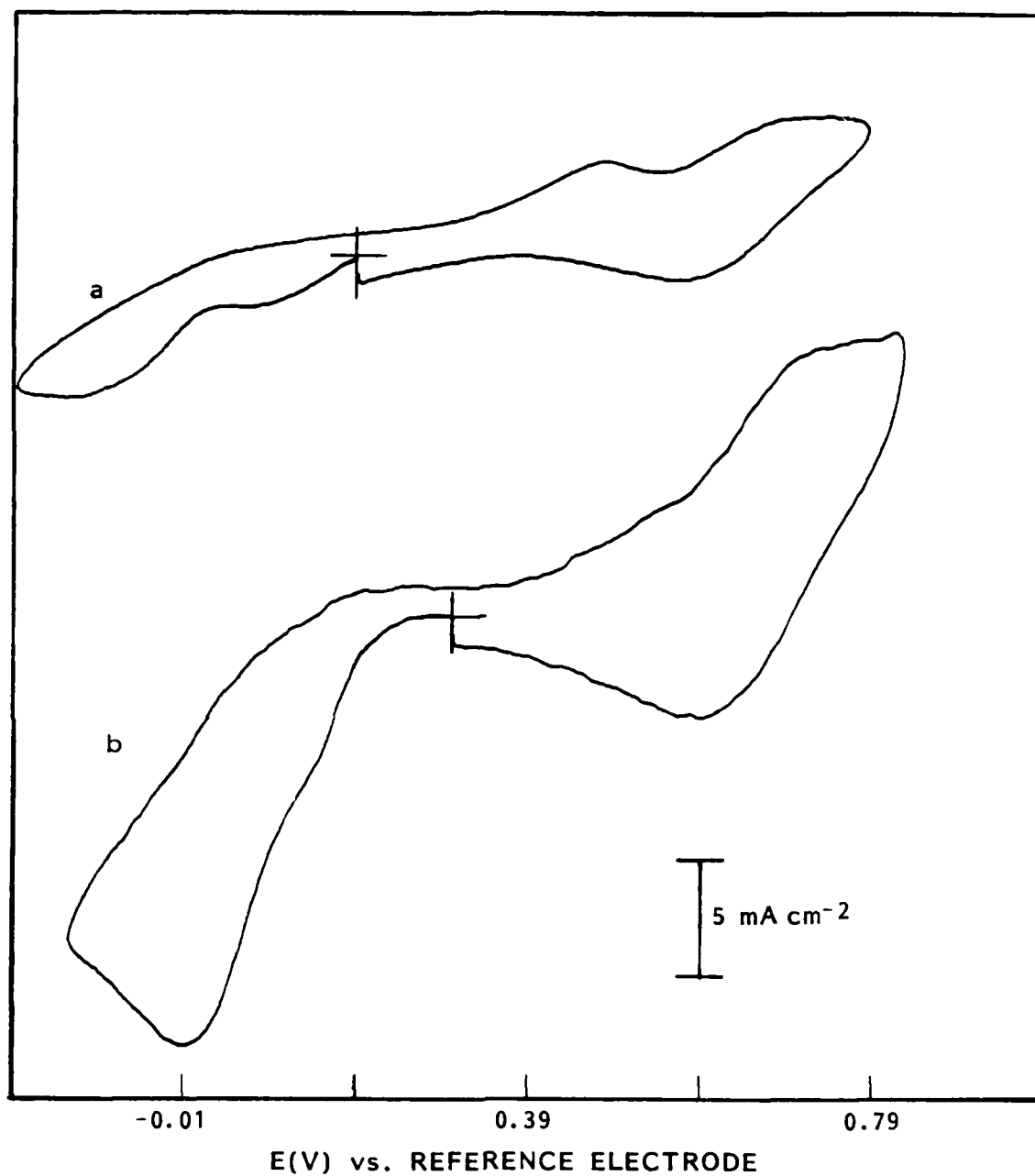
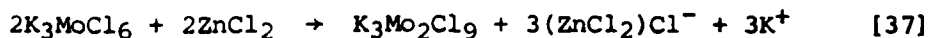


Fig. 57. Cyclic voltammograms of 0.129 molal K_3MoCl_6 in 1:1 ZnCl_2 -KCl melt acquired on gold electrode at scan rate 0.1 V/s at temperature a) 320°C and b) 400°C.

predicted for a two electron process involving a soluble product. The increase in the peak current function with increasing scan rate is accompanied by the cathodic shift of the peak potential, Table 39. These facts derived from the voltammograms are characteristic for a two electron transfer process followed by reversible homogeneous reaction (52).

Before discussion of the property of the second cathodic peak, it is more convenient to present the voltammetric responses obtained in the same solution when the initial scan direction is anodic from the open circuit potential. The voltammograms exhibit a single well defined anodic peak (B) with the corresponding cathodic peak which is still anodic from the open circuit potential (see Figure 58). The properties of these cyclic voltammograms are characteristic for a diffusion controlled one electron transfer process forming a soluble product (see Table 40). When the initial scan direction is cathodic from the open circuit potential and the potential scan direction is reversed at a potential in the region of the first cathodic peak (C), the anodic peak (B) on the subsequent anodic scan is unchanged. When the switching potential is cathodic of the second peak (D), then on the subsequent anodic scan, a new peak appears anodic of the open circuit potential and preceding the peak B. Concomitant with this, the current for peak B is lowered in comparison to the current when the initial scan direction is anodic or cathodic but with the switching potential anodic to the second cathodic peak D. This is strong evidence that the species which are oxidized in the potential range of peak B (when the initial scan direction is anodic) are also reduced in the potential range for the second cathodic peak D. In addition, the common species are not completely regenerated after potential switching in the region of the second cathodic peak, since there is a new peak preceding peak B and a lowering of the peak current for B. This can be explained by postulating that the product of the second reduction process undergoes chemical reaction to form a moiety which is oxidized prior to peak B. Table 41 shows that the half peak width ($E_{p/2} - E_p$) and the current function for the second cathodic peak are not inconsistent with a one electron transfer process followed by irreversible chemical reaction.

A reaction scheme which takes into account this electrochemistry is as follows. When K_3MoCl_6 is added to the zinc chloride containing melts on the basis of the electrochemistry described above, it is proposed that an acid base reaction initially converts the Mo(III) monomer into the chloride bridged dimer by the reaction:



The Mo(III) dimer may undergo additional reactions with the $ZnCl_4^{2-}$ species present in the melt compositions used to form a triple metal-metal bonded complex; for example,

TABLE 39

REPRESENTATIVE NUMERICAL DATA FOR THE FIRST REDUCTION PEAK (c)
 OF THE VOLTAMMOGRAMS ACQUIRED IN A SOLUTION OF K_3MoCl_6 IN
 MOLTEN $ZnCl_2-KCl$ (2:1) AT 320°C ON A GOLD ELECTRODE

Scan Rate ν (V/s)	Peak Potential E_p^c (V)	Peak Current Function $i_p \nu^{-1/2} A^{-1}$ ($mA \nu^{-1/2} s^{1/2} cm^{-2}$)	Peak Width $E_{p/2}^c - E_p^a$ (mV)
0.050	0.069	10.25	49
0.075	0.068	10.77	46
0.100	0.065	10.90	47
0.150	0.056	11.66	47
0.200	0.054	11.96	50

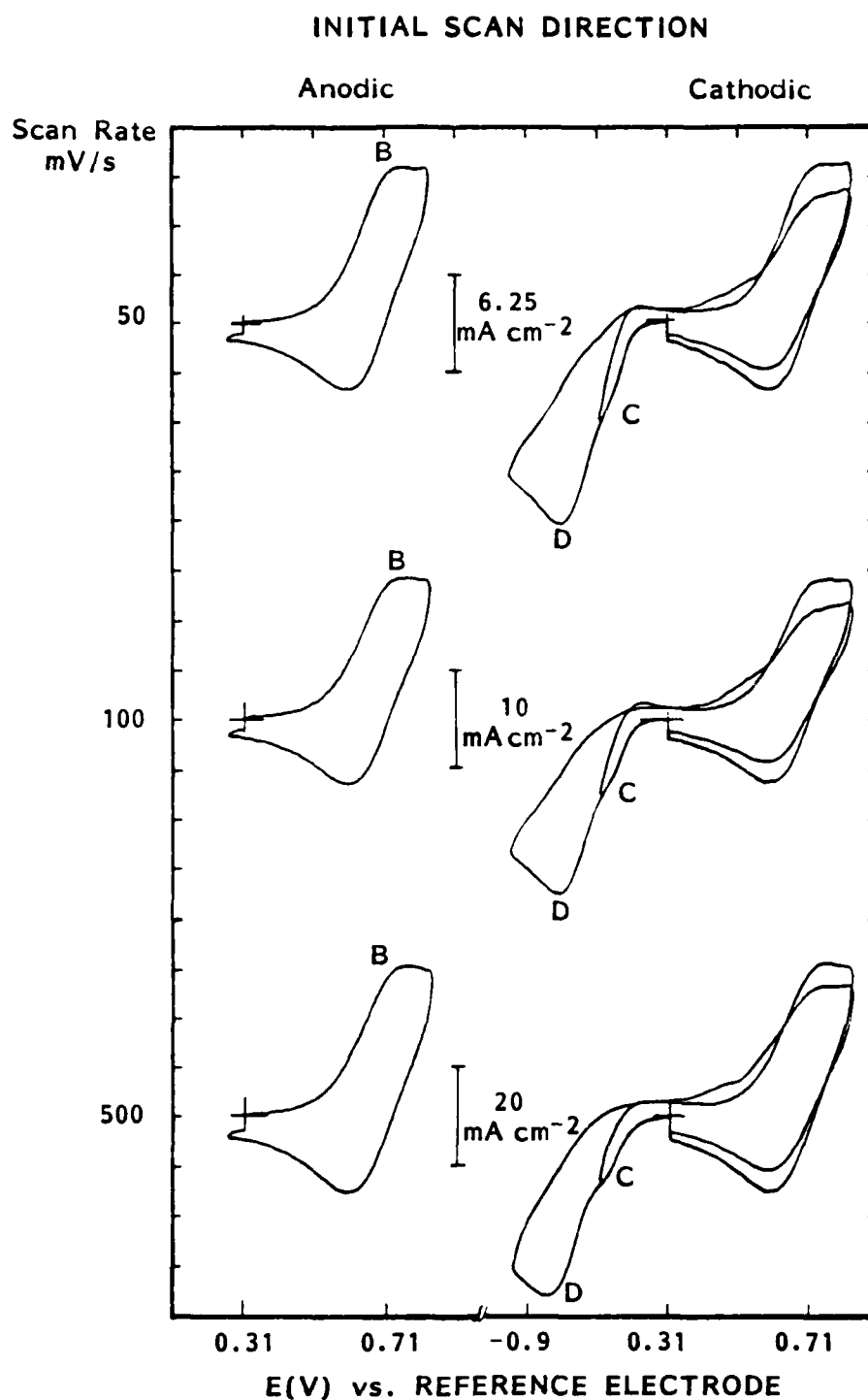


Fig. 58. Cyclic voltammograms obtained at different initial scan directions and rates at a gold electrode in a solution of 0.129 molal K_3MoCl_6 in 1:1 $ZnCl_2$ -KCl melt at 400°C.

TABLE 40

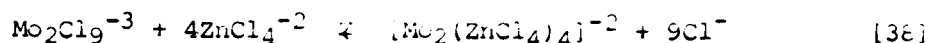
CYCLIC VOLTAMMETRIC DATA FOR THE OXIDATION AND CORRESPONDING
REDUCTION PROCESS OF THE SOLUTION OF $K_3Mo_3Cl_6$ IN
MOLTEN $ZnCl_2-KCl$ (1:1) AT 400°C AT GOLD ELECTRODE

Scan Rate v (V/s)	Anodic Peak Potential E_p^a (V)	Anodic Peak Potential E_p^c (V)	Anodic Peak Current Function ($mA v^{-1/2} s^{1/2} cm^{-2}$)	Anodic Peak Width (mV)
0.050	0.756	0.596	43.0	136
0.100	0.756	0.596	43.1	136
0.150	0.746	0.596	42.3	131
0.200	0.751	0.600	42.2	131
0.300	0.751	0.596	42.4	135
0.500	0.751	0.586	42.2	131
0.750	0.766	0.600	42.6	140
1.000	0.777	0.587	43.0	150

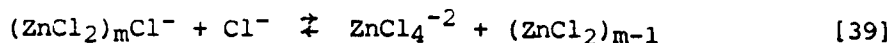
TABLE 41

REPRESENTATIVE NUMERICAL DATA FOR THE SECOND REDUCTION PROCESS
 OF THE VOLTAMMOGRAMS ACQUIRED IN A SOLUTION OF K_3MoCl_6
 IN MOLTEN $ZnCl_2-KCl$ (1:1) at 400°C IN GOLD ELECTRODE

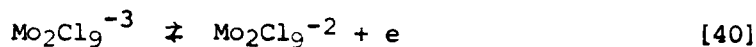
Scan Rate (V/s)	Peak Potential E_p^c (V)	Peak Current $i_p v^{-1/2} A^{-1}$ ($mA v^{-1/2} s^{1/2} cm^{-2}$)	Peak Width $E_{p/2} - E_p$ (mV)
0.05	0.008	54.56	115
0.10	0.003	53.76	107
0.15	-0.013	51.80	112
0.20	-0.016	51.05	108
0.30	-0.023	50.48	110
0.50	-0.033	49.41	115
0.75	-0.048	48.69	120
1.00	-0.053	48.19	120



where ZnCl_4^{-2} arises in the solvent (74,75) via reaction such as:

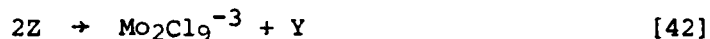


On the basis of such solution chemistry, the oxidation reaction (peak B) is:

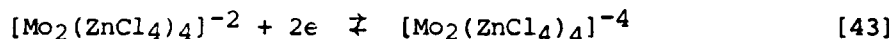


Such mixed oxidation state complexes have been identified in ambient temperature systems (15).

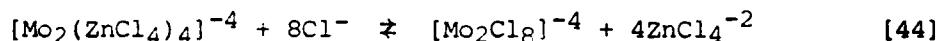
In the case of the reduction reactions, the second peak D, which involves the same electroactive species is of the form:



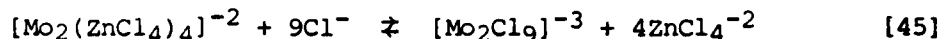
The first process (peak C) then involves the reduction of the triple metal bonded dimer, see equation [38], to form a quadruple metal bonded complex:



The coupled equilibrium most likely involves a ligand exchange reaction:



Returning to the question of the anodic dissolution of molybdenum the identity of the following chemical reaction and the second scan rate dependent oxidation reaction now become clearly identified as being due to the reverse of reaction [38], i.e.:



and the chloro bridged dimer is oxidized according to reaction [40].

Discussion in Relationship to Plating Molybdenum. The purpose of this study was to establish whether the low melting zinc chloride containing mixtures could be utilized for the electroplating of molybdenum metal. The complex results discussed above indicate that the formation of metal-metal bonded compounds mitigate against simple metal forming reduction reactions within the electrochemical window of these solvents.

3.4.2 Electrochemistry of Molybdenum in Lithium Chloride - Potassium Chloride Eutectic Mixture

Senderoff and Brenner (76) demonstrated that molybdenum can be plated from lithium chloride-potassium chloride mixtures containing potassium hexachloromolybdate at temperatures in the range 600-800°C. Subsequently, Senderoff and Mellors (77) reported that molybdenum could also be plated from the molten alkali fluoride electrolytes containing molybdenum (III)/(IV) prepared by reduction of MoF_6 with Mo metal. They proposed that in the chloride (78) melt two molybdenum (III) species were present, in a equilibrium coupled to a disproportionation reaction involving Mo(III) and Mo(V). To achieve the conditions whereby good quality plating products can be produced at economic rates, at temperatures where the cathode substrate is stable, the details of the solution chemistry in low melting solvents (other than fluorides) as well as the electrodic processes must be quantified. The results from the present study serve to emphasize the problems associated with the deconvolution of the solution chemistry from the nucleation and growth processes involved in the metal forming reactions.

The investigation of the solution chemistry by electrochemical techniques is complicated by the fact that in chronopotentiometric measurements, see Figure 59, the initial part of the transients contains information related to the electrocrystallization of the molybdenum upon a foreign substrate in addition to the concentration overpotential. Likewise, the chronoamperometric measurement, even when the potential is stepped into the limiting current region, requires the separation of the electrocrystallization component from that due to concentration overvoltages arising from mass transfer and/or reaction overvoltages at short times. In the case of cyclic voltammetry, it must be expected that similar complications will also exist in any quantitative analysis of the experimental data. Furthermore, the chemistry of the molybdenum (III) species in this melt undoubtedly involves an equilibrium between monomer and dimer species, and this complication has not been fully expressed in theoretical analyses of these dynamic electrochemical techniques. Nevertheless, it might be useful to make some first approximation type calculations based upon the voltammetric results.

Typical cyclic voltammograms obtained at different temperatures are illustrated in Figure 60. The effects of nucleation are seen clearly in the voltammogram at 550°C where the "current crossover" effect is detected. The current function, calculated as the measured peak current divided by the square root of the scan rate, is seen to decrease as the scan rate is increased, Table 42. At the same time, the peak width increases. At the lower temperature, the peak becomes wave shaped. These features might be expected for an electrochemical process modified by a preceding chemical reaction. The expected anodic shift with increasing scan rate must be seriously modified by the electrocrystallization

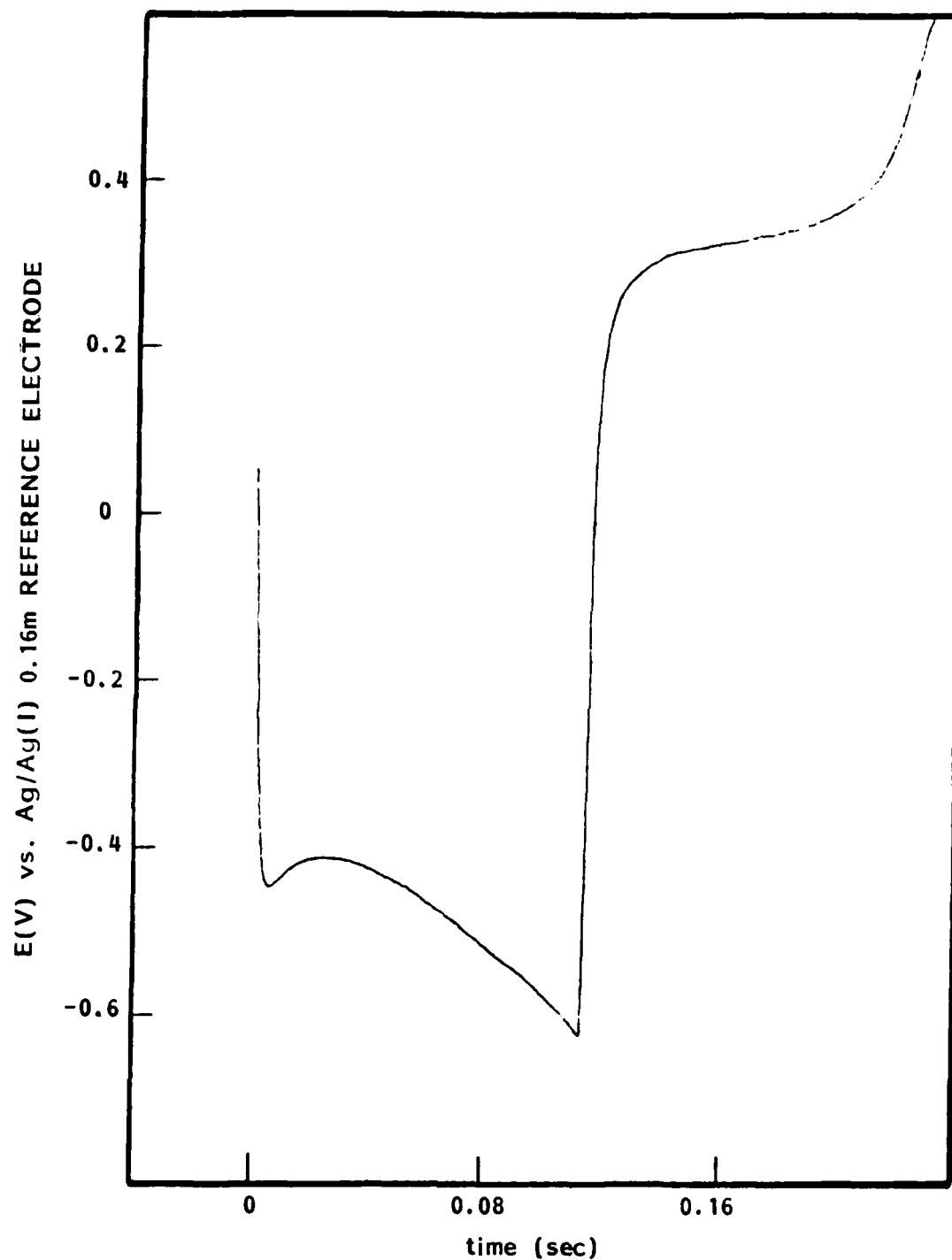


Fig. 59. Current reversal chronopotentiogram acquired at gold electrode in LiCl-KCl containing 0.0197 molal K_3MoCl_6 at $450^\circ C$, current pulses $\pm 70 \text{ mA cm}^{-2}$.

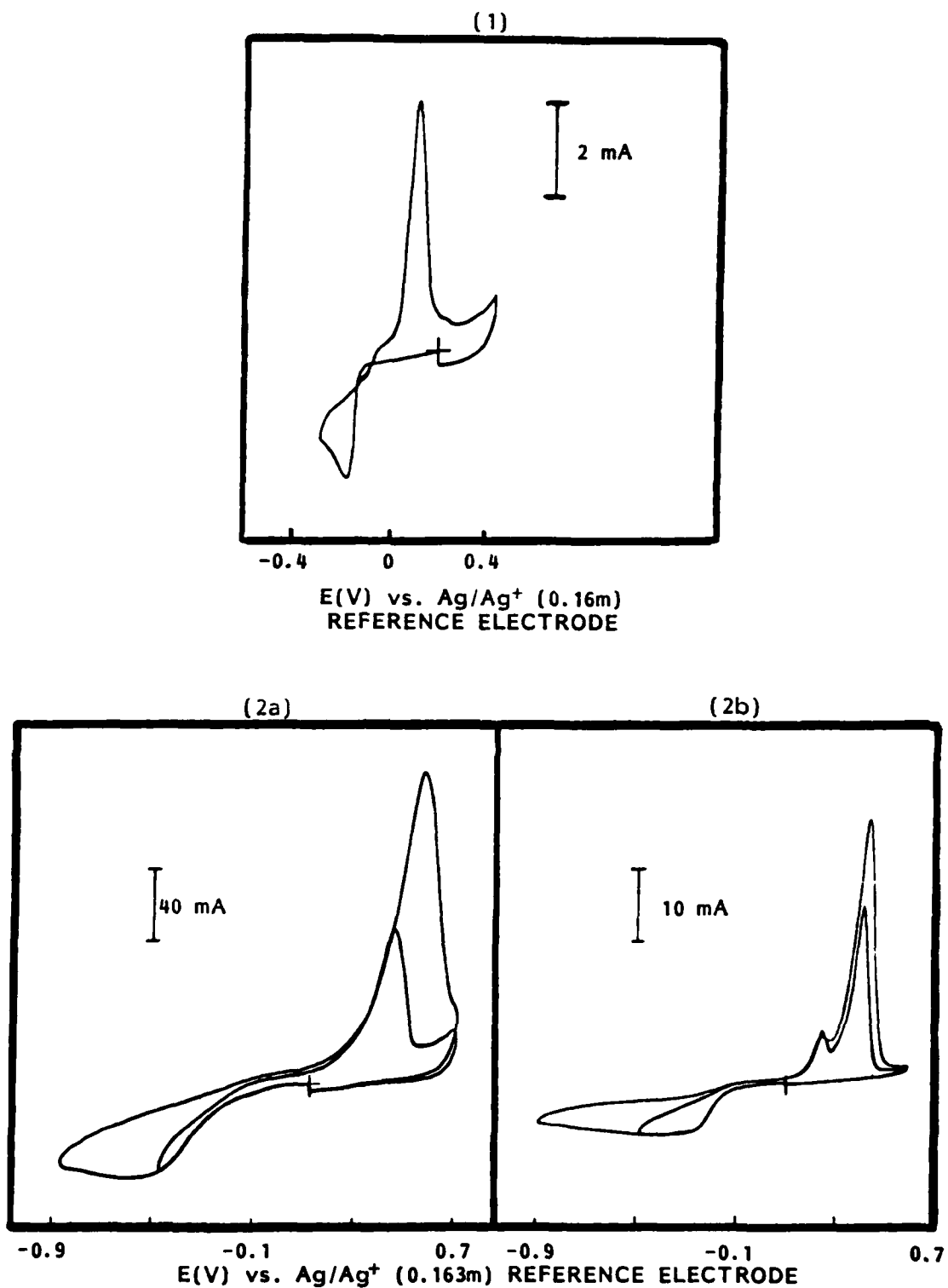


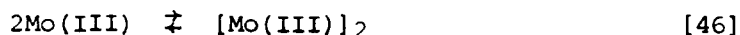
Fig. 60. Cyclic voltammograms acquired on gold electrodes in LiCl-KCl containing K_3MoCl_6 at (1) 550°C , area = 0.6 cm^2 and $\nu = 0.05 \text{ Vs}^{-1}$, $c = 5.06 \times 10^{-3} \text{ mol kg}^{-1}$ and (2) 450°C , area 0.43 cm^2 , (a) $\nu = 10 \text{ Vs}^{-1}$, (b) $\nu = 0.1 \text{ Vs}^{-1}$, $c = 19.7 \times 10^{-3} \text{ mol kg}^{-1}$.

TABLE 42

REPRESENTATIVE NUMERICAL VOLTAMMETRIC DATA ACQUIRED AT A GOLD
ELECTRODE IN MOLTEN LiCl-KCl MIXTURE CONTAINING K_3MoCl_6
a) 5.06×10^{-3} mol/Kg at 550°C b) 19.7×10^{-3} mol/Kg at 450°C

Scan Rate ν (V/s)	E_p^c (V)	E_p^{a1} (V)	E_p^{a2} (V)	$i_p \nu^{-1/2}$ ($mA \nu^{-1/2} s^{1/2} cm^{-2}$)	ΔE_p^c (mV)
a)					
0.020	-0.165	0.110	-	21.935	25
0.050	-0.185	0.120	0.235	19.938	40
0.075	-0.200	0.120	0.245	18.705	40
0.100	-0.204	0.120	0.250	17.261	45
0.150	-0.215	0.115	0.240	15.833	47
0.200	-0.225	0.120	0.250	15.130	55
0.500	-0.250	0.140	0.280	13.900	70
1.000	-0.280	0.160	0.300	13.200	85
2.000	-0.340	0.165	0.300	13.200	145
b)					
0.010	-0.198	0.177	0.310	52.273	35
0.100	-0.268	0.180	0.360	39.530	80
1.000	Plateau	-	0.390	31.818	

processes. If it is postulated that at the highest scan rates, the measured value of the current function reflects the equilibrium concentration of electroactive species and that the equilibrium can be written as:



The equilibrium constant K is

$$K = C_{\text{Mo(III)}}^2 / C_{[\text{Mo(III)}]_2} \quad [47]$$

Table 43 shows the corresponding values of K and the monomer and dimer equilibrium concentrations calculated on the assumption that $D = 8.88 \times 10^{-6} \text{ cm}^2\text{s}^{-1}$ at 450°C obtained from potential step measurement and assuming $D = 1 \times 10^{-5} \text{ cm}^2\text{s}^{-1}$ at 550°C .

3.5 Electrocrystallization of Molybdenum from Lithium Chloride-Potassium Chloride Eutectic Mixture at 450°C

Some details of the formation of new molybdenum phase upon the gold substrate have been obtained by potential step experiments. The gold substrate was 100% gold sheet material previously electropolished by the supplier. Significant overvoltages, in the range -300 to -650 mV vs. a molybdenum electrode in the same solution, were required to observe the nucleation and growth transients. Some typical examples of these transients are shown in Figure 61. Table 44 summarizes the i_{max} and t_{max} values obtained from these transients as a function of the overpotential. Values of i_{mtm}^2 at each overpotential are given in the table and plotted as a function of the overpotential in Figure 62. This figure shows the tenfold increase in i_{mtm}^2 as the overpotential decreases. According to the theory of Hills et al. (51) changes in this quantity due to changes in the nucleation process, i.e., from instantaneous to progressive nucleation would only result in a 1.6 times increase. The time ranges of the measurements preclude charging current effects as well as the fact that for the chromium system such an effect causes positive deviations in the measured current maximum when i_{m} is plotted vs. $t_{\text{m}}^{-1/2}$ in contrast to the negative deviations observed for the molybdenum data, see Figure 63. In view of the solution chemistry of Mo(III) in this melt (see above), these results can be rationalized in terms of the effect of the preceding reaction [46]. Indeed, on the basis of this model the data enable the equilibrium constant to be evaluated. At the shortest times (high overvoltage), the growth of the nuclei is controlled by the equilibrium concentration of the electroactive species in the melt in contrast to the situation at long times where the rate of chemical reaction is sufficient to convert dimer into monomer so that the growth depends on the total concentration of Mo(III) species added to the solution. Under these circumstances, the diffusion coefficient can be calculated from the value of i_{mtm}^2 and is found to be $8.9 \times 10^{-6} \text{ cm}^2\text{s}^{-1}$. The value of the equilibrium constant K for reaction [46] is

TABLE 43

EQUILIBRIUM CONSTANTS DETERMINED FOR THE MONOMER DIMER EQUILIBRIUM
INVOLVING Mo(III) SPECIES IN LiCl-KCl EUTECTIC

<u>T</u> <u>°C</u>	<u>Method</u>	<u>C_T × 10⁶</u> <u>molcm⁻³</u>	<u>C_M^E × 10⁶</u> <u>molcm⁻³</u>	<u>C_D^E × 10⁶</u> <u>molcm⁻³</u>	<u>K × 10⁶</u> <u>molcm⁻³</u>
550	CP	2.0605	4.448	1.809	10.93
550	CV	8.0605	4.819	1.623	14.30
450	CV	32.447	11.553	10.447	12.78
450	PS	32.447	11.254	10.596	11.95

CP = Chronopotentiometry

CV = Cyclic Voltammetry

PS = Potential Step

C_M^E = Equilibrium concentration of monomer

C_D^E = Equilibrium concentration of dimer

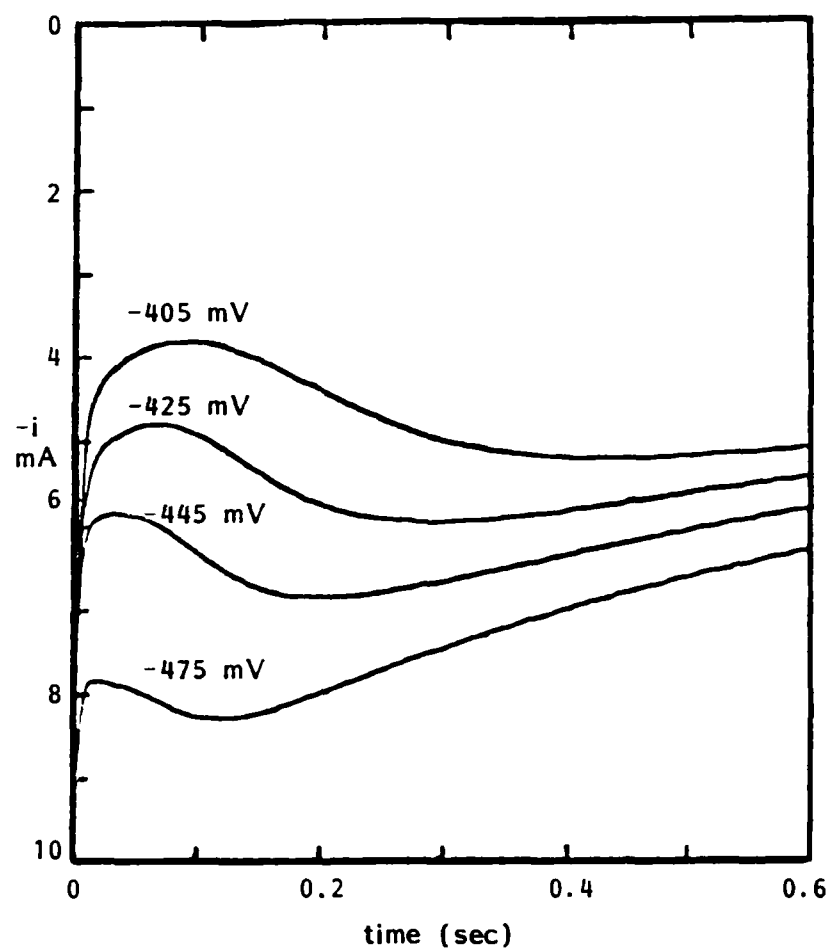


Fig. 61. Current time transients acquired at gold electrode (0.43 cm^2) in molten LiCl-KCl mixture at 450°C for the reduction of Mo(III) at different overpotentials vs. Mo^{3+}/Mo .

TABLE 44

POTENTIAL STEP RESULTS FOR GOLD SUBSTRATE
IN LiCl-KCl EUTECTIC AT 450°C

Concentration Mo ³⁺	= 32.5 x 10 ⁻⁶ molcm ⁻³
Area Au electrode	= 0.43 cm ²
Atomic Weight Mo	= 95.94 gmol ⁻¹
Density of Mo	= 10.2 gcm ⁻³
Diffusion Coefficient of Mo ³⁺	= 8.88 x 10 ⁻⁶ cm ² s ⁻¹
Rest Potential of Au Electrode	= -0.025V vs. Mo reference
Rest Potential of Mo	= 0.120V vs. Ag reference

10 ³ i (max) Amps	t(max) sec	Overpot ⁿ η (V)	10 ⁷ i _m ² t _m L ⁻² A ² s	Nuclei Density	N x Rate AN _O	AN _O from N(sat)
1.880	6.5600	-0.305	231.857	8.88 x 10 ⁴	3.8 x 10 ⁴	1.64 x 10 ⁴
2.250	4.3200	-0.315	218.700	1.35 x 10 ⁵	8.7 x 10 ⁴	3.77 x 10 ⁴
2.520	3.2400	-0.325	205.753	1.80 x 10 ⁵	1.5 x 10 ⁵	6.70 x 10 ⁴
2.860	2.4000	-0.335	196.310	2.43 x 10 ⁵	2.8 x 10 ⁵	1.22 x 10 ⁵
3.220	1.8000	-0.345	186.631	3.24 x 10 ⁵	5.0 x 10 ⁵	2.17 x 10 ⁵
3.220	1.8000	-0.345	186.631	3.24 x 10 ⁵	5.0 x 10 ⁵	2.17 x 10 ⁵
3.850	1.1200	-0.365	166.012	5.20 x 10 ⁵	1.3 x 10 ⁶	5.61 x 10 ⁵
4.250	0.0000	-0.375	144.500	7.28 x 10 ⁵	2.5 x 10 ⁶	1.10 x 10 ⁶
4.660	0.6150	-0.385	133.551	9.47 x 10 ⁵	4.3 x 10 ⁶	1.86 x 10 ⁶
4.550	0.6700	-0.385	138.707	8.69 x 10 ⁵	3.6 x 10 ⁶	1.57 x 10 ⁶
5.230	0.4350	-0.405	118.985	1.34 x 10 ⁶	8.6 x 10 ⁶	3.72 x 10 ⁶
5.970	0.2850	-0.425	101.577	2.04 x 10 ⁶	2.0 x 10 ⁷	8.66 x 10 ⁶
6.850	0.2000	-0.445	93.845	2.91 x 10 ⁶	4.1 x 10 ⁷	1.76 x 10 ⁷
7.520	0.1540	-0.455	87.088	3.78 x 10 ⁶	6.8 x 10 ⁷	2.97 x 10 ⁷
8.370	0.1150	-0.465	80.565	5.06 x 10 ⁶	1.2 x 10 ⁸	5.32 x 10 ⁷
8.280	0.1200	-0.475	82.270	4.85 x 10 ⁶	1.1 x 10 ⁸	4.89 x 10 ⁷
8.150	0.1320	-0.475	87.678	4.41 x 10 ⁶	9.3 x 10 ⁷	4.04 x 10 ⁷
8.600	0.1100	-0.485	81.356	5.29 x 10 ⁶	1.3 x 10 ⁸	5.82 x 10 ⁷
9.200	0.0900	-0.495	76.176	6.47 x 10 ⁶	2.0 x 10 ⁸	8.69 x 10 ⁷
9.600	0.0825	-0.505	76.032	7.06 x 10 ⁶	2.4 x 10 ⁸	1.03 x 10 ⁸
9.400	0.080	-0.510	70.688	7.28 x 10 ⁶	2.5 x 10 ⁸	1.10 x 10 ⁸
10.900	0.0500	-0.525	59.405	1.16 x 10 ⁷	6.5 x 10 ⁸	2.82 x 10 ⁸
12.300	0.0180	-0.545	27.232	3.24 x 10 ⁷	5.0 x 10 ⁹	2.17 x 10 ⁹
15.100	0.0120	-0.575	27.361	4.85 x 10 ⁷	1.1 x 10 ¹⁰	4.89 x 10 ⁹
18.000	0.0090	-0.625	29.160	6.47 x 10 ⁷	2.0 x 10 ¹⁰	8.69 x 10 ⁹

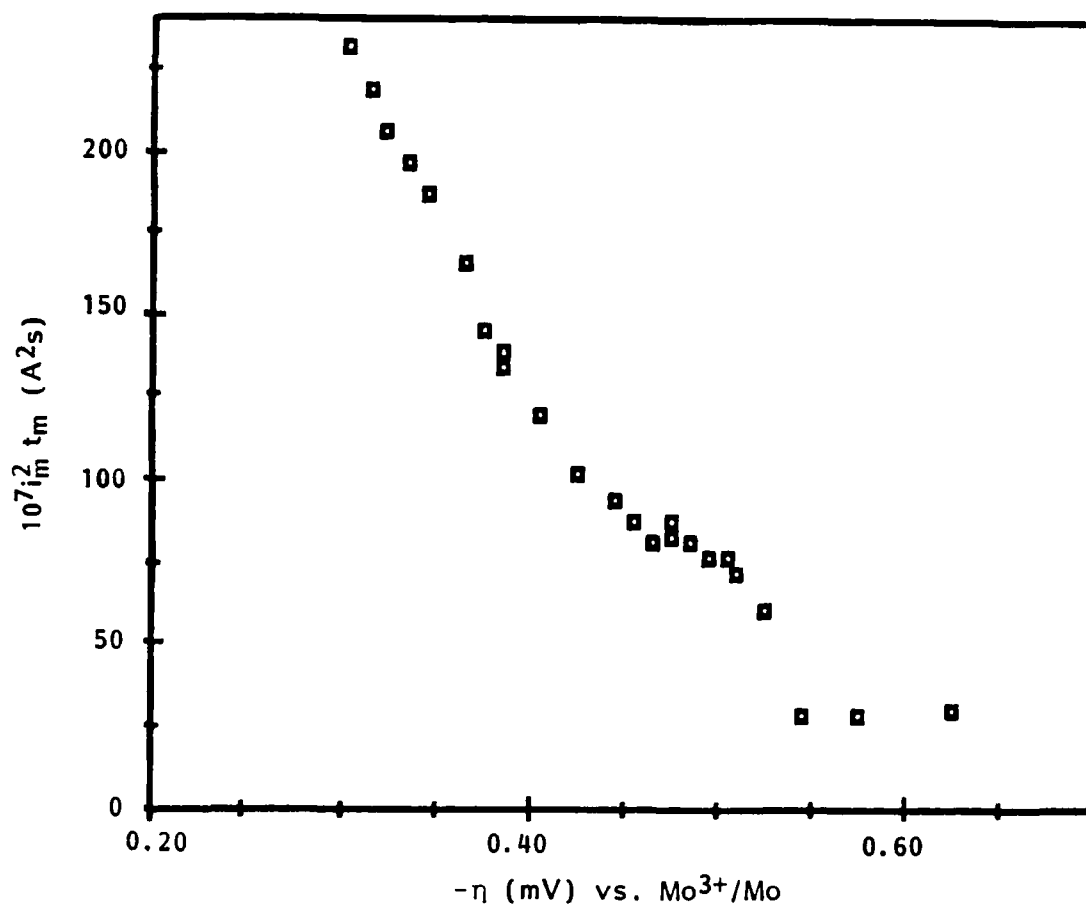


Fig. 62. Plot of $i_m^2 t_m$ vs. applied overpotential for molybdenum metal deposition on a gold substrate in LiCl-KCl eutectic mixture at 450°C.

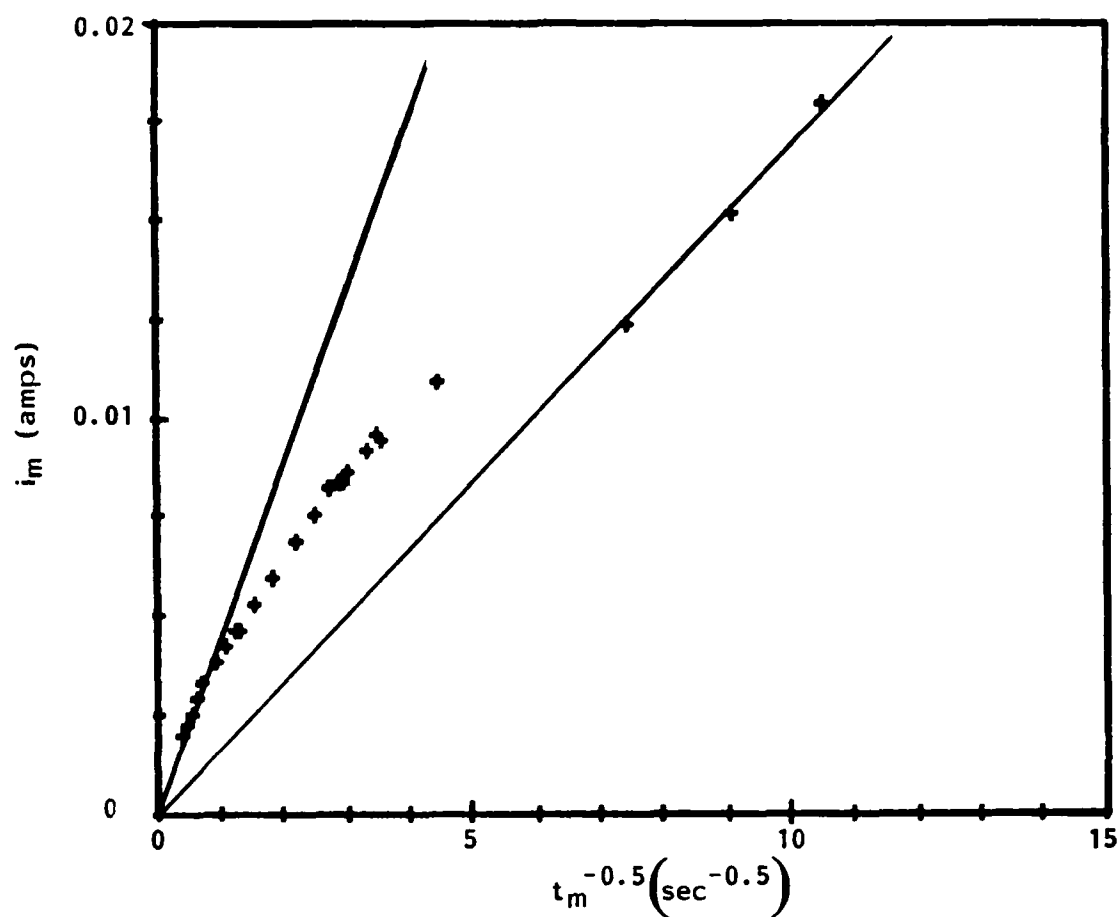


Fig. 63. Current maximum from potential step measurements as a function of $t_m^{-1/2}$ for Mo deposition on a gold substrate from LiCl-KCl at 450°C.

included in Table 43 for comparison with values calculated from chronopotentiometry and cyclic voltammetry.

3.5.1 Discussion

The voltammograms for the reduction of the molybdenum (III) species in solution at 550°C are rather sharp at scan rates below 100 mVs⁻¹, see Table 42, showing that the response is dominated by the metal deposition process ($0.77RT/nF = 0.018V$) and that the concentration of electroactive species is not controlled by the kinetics of the equilibrium between Mo(III) species in solution. This can be contrasted with the voltammograms for solutions at 450°C where a plateau-like response is observed consistent with reaction controlled overvoltage. Thus, at potentials lower than -0.15V vs. the silver reference electrode, molybdenum metal is produced.

The value of the equilibrium constant calculated on the basis of the voltammetric measurements and the potential step measurements are in remarkably good agreement and represent the first measurement of this important equilibrium constant in lithium chloride-potassium chloride mixture. The concentration of monomer and dimer are seen to be of the same order of magnitude concentration in the temperature range 450-550°C.

The nature of the nucleation process is not readily determined from the present data since an independent value of the diffusion coefficient is not available. Values of the nucleus density are calculated for progressive nucleation assuming that at these high overpotentials the nucleation is arrested, see Table 44. These values must be regarded as order of magnitude in view of the need to use the total Mo(III) concentration in evaluating these numbers from the t_m data. At the highest overpotentials, the nucleus densities are too small. Nevertheless, the values are similar order of magnitude to those obtained for chromium deposition. From classical nucleation theory, the value of the surface energy for molybdenum on gold is 1040 mNm⁻¹. The number of atoms in the nucleus is 3 at an overvoltage of 0.25V where nucleation is first detected. The rate of nucleation is 2.1×10^{16} cm²s⁻¹. On the other hand, for the low values of overpotential the atomistic theory gives $n = >0$ which means that all sites are nucleated (65). The magnitudes of the surface energy and the nucleation rate are significantly different from those reported in Table 28 for chromium deposition on gold at 450°C which may be attributed to the influence of the preceding reaction on the electrocrystallization.

4.0 PLATING OF CHROMIUM AND MOLYBDENUM FROM LOWER MELTING HALIDE ELECTRODES

The preparation of coherent deposits of chromium and molybdenum for corrosion and erosion protection applications is of current interest. Although chromium can be plated from aqueous electrolytes, the properties of the deposit are not satisfactory for certain more demanding applications in energy and military technology. Molybdenum cannot be plated from aqueous solution, and only molten alkali metal halide electrolytes operating at temperatures in excess of 700°C have been found to produce satisfactory plates. At such high temperatures, the cathode substrate is limited in composition, and in addition, the plating baths themselves are somewhat unstable. The coating is also rather soft. Mixtures of alkali metal chlorides and bromides containing caesium cations provide electrolytes which melt in the region 200-300°C; thus, there is an opportunity to operate plating baths at much reduced temperatures if conditions can be found for the production of coherent plates. This program has attempted to develop a better understanding of the solution chemistry of both chromium and molybdenum precursors in such electrolytes as well as providing insight into the nucleation and growth processes of the metals on foreign substrates so that the plating conditions may be chosen based upon a scientific rather than an ad hoc approach.

The recent success in the application of pulse plating and the more detailed understanding of the electrolysis processes themselves suggested that such an approach might be beneficial in the case of the present metals. In this section, preliminary results of the application of single pulsed current plating for these metals from two different solvents are reported.

Table 45 contains results of some plating experiments for chromium from LiCl-KCl at 450°C. The results showed that coherent thin coatings could be obtained on copper with good throwing power. In view of the interest expressed in lower melting solvents, this work was not pursued further. Table 46 reports some results obtained for the deposition of chromium from the ternary alkali bromide melt at 335°C. Coatings were obtained which were bright and coherent. Examination of them at high magnification in the SEM showed them to be made up of rather granular chromium crystals as illustrated in Figures 64 and 65. The formation of nuclei during the initial pulses is shown in the SEM photograph taken for a copper electrode after removal from the electrolysis cell (see Figure 65b). Corresponding potential time curves for the sequence of current pulses are presented in Figure 66. The presence of an initial maximum is clearly seen corresponding to the nucleation process, and these transients show that the nucleation process decays away rapidly with pulse number. After the fourth pulse, the nucleation maximum has disappeared, but a significant overpotential remains when the

TABLE 45

ELECTROPLATING EXPERIMENTS CHROMIUM DEPOSITION FROM A LITHIUM CHLORIDE-POTASSIUM CHLORIDE-CHROMOUS CHLORIDE SOLN (0.27 wt %) AT 450°C

Electrode Material	W.E. Area cm^2	Current Density mA/cm^2	Modulation	Delay Time ms	Electrolysis Time hours	Wt Change grams	Efficiency %	Comments
Copper 1	0.98	107	DC		0.18			Patchy deposit. Alkali metal deposited. Electrode fizzed in water.
Copper 2	0.91	11	DC		1.88			Patchy deposit. Alkali metal deposited. Electrode fizzed in water.
Copper 3	0.91	0.76	DC		7.41	0.0459	>>100	Deposit was continuous.
Copper 4	0.92	105	2 ms current pulse	22				Electrolysis discontinued since potential goes to alkali. Waiting time too short.
Copper 5	1.17	77	6 ms current pulse	194	3.67	0.0092	96	Continuous deposit. Dendrites at edges. Cross-section shows thin, continuous coating. Thickness rather irregular, throwing power good.
Copper 6	0.46	82	6 ms current pulse	1954	35.9	wt loss		Patchy on one side, continuous on other. Poor throwing power, one side blocked by crucible.
Copper 7	1.00	92	6 ms current pulse	969	19.8	wt loss		Patchy deposit, one side better than other.
Copper 8	1.04	91	6 ms current pulse	489	9.17	0.0089	84	Continuous deposit.
Nickel 1	0.91	108	6 ms current pulse	484	10.09	0.0014	11	Deposit on Cr but green oxide on surface?
Nickel 2	0.93	103	8 ms current pulse	489	7.88	0.0091	70	As above.
Nickel 3	0.89	106	8 ms current pulse	967	15.61	0.0055	42	Patchy deposit.

TABLE 46

ELECTROPLATING EXPERIMENTS - CHROMIUM DEPOSITION FROM A LITHIUM BROMIDE-POTASSIUM
BROMIDE CESIUM BROMIDE-CHROMIUM(II) BROMIDE SOLUTION AT $335 \pm 5^\circ\text{C}$

Substrate	Current mA	$t_{\text{off}}/t_{\text{on}}$	Total Charge		Current Efficiency	Method	Comments
			C	C			
Copper	2.4	-	31	-	-	DC	Slight wt loss. Dark loose material.
Copper	5.2	-	75	-	-	DC	Dark nodular poorly adherent deposit.
Copper	250	89	-	-	-	P	Surface initially stripped. Net loss granular coating, dendrites at edges.
Copper	200	89	515	60	-	P	Black coating copper bright above 3-phase boundary.
Copper	200	87	204	64	-	P	Anodic clean with first two pulses.
Copper	210	87	0.005	-	-	P	Single pulse - look for nuclei with SEM.
Nickel	140	87	368	15	-	P	Grey black deposit.
Copper	199	87	0.05	-	-	P	Ten pulses - look for nuclei SEM.
Stainless steel	250	87	227	71	-	P	Silvery white coating after water rinse.
Stainless steel	264	87	260	-	-	P	Grey deposit.
Stainless steel	284	87	260	46	-	P	Grey deposit, white grey after water rinse.

a)



b)

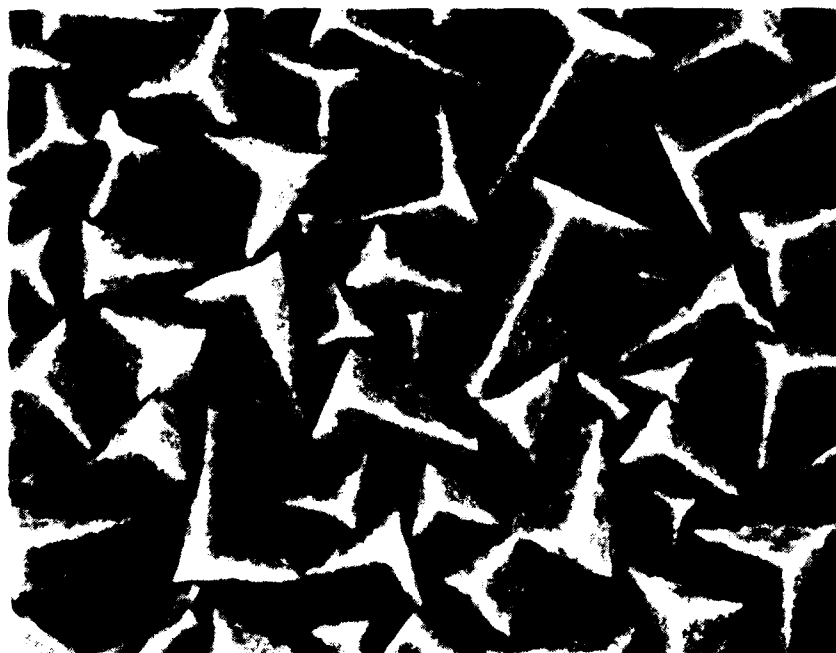
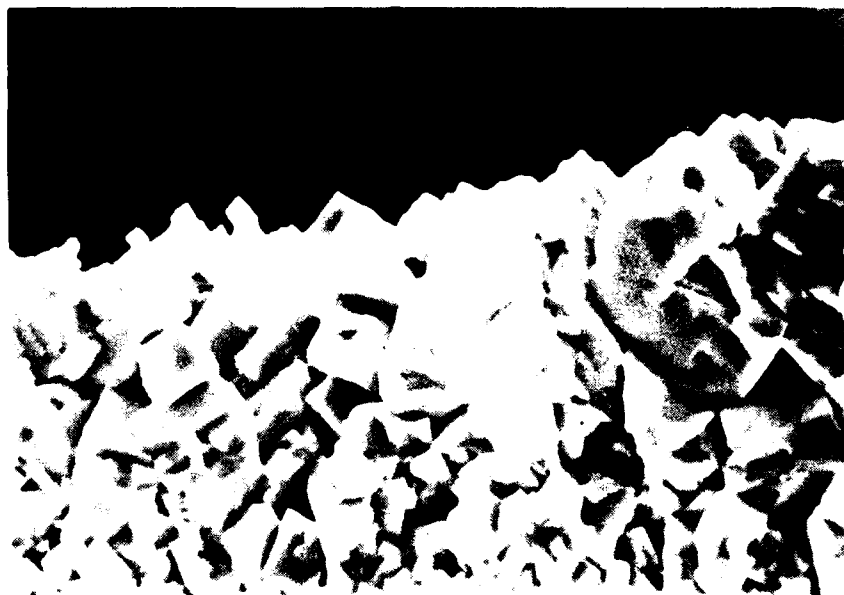


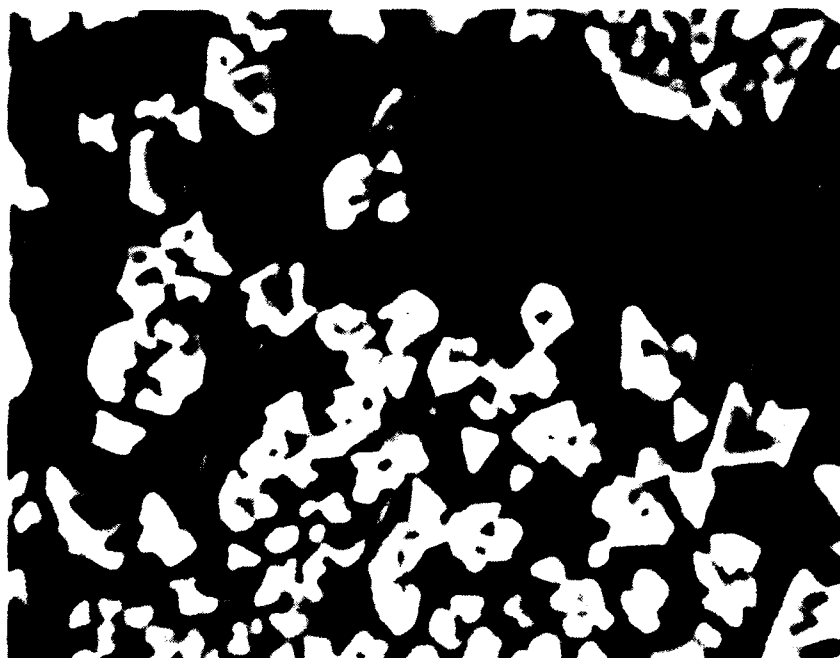
Fig. 64. SEM of chromium deposit from the ternary alkali metal bromide melt at 340°C. (a) 500X; (b) 2000X.

a)



2000X

b)



1000X

Fig. 65. (a) SEM of cross section of chromium deposition on stainless steel obtained from bromide melt at 340°C.

(b) Nuclei formed and grown on copper substrate during 10 current pulses, $t_{\text{off}}/t_{\text{on}} = 90$, $j = 110 \text{ mA cm}^{-2}$.

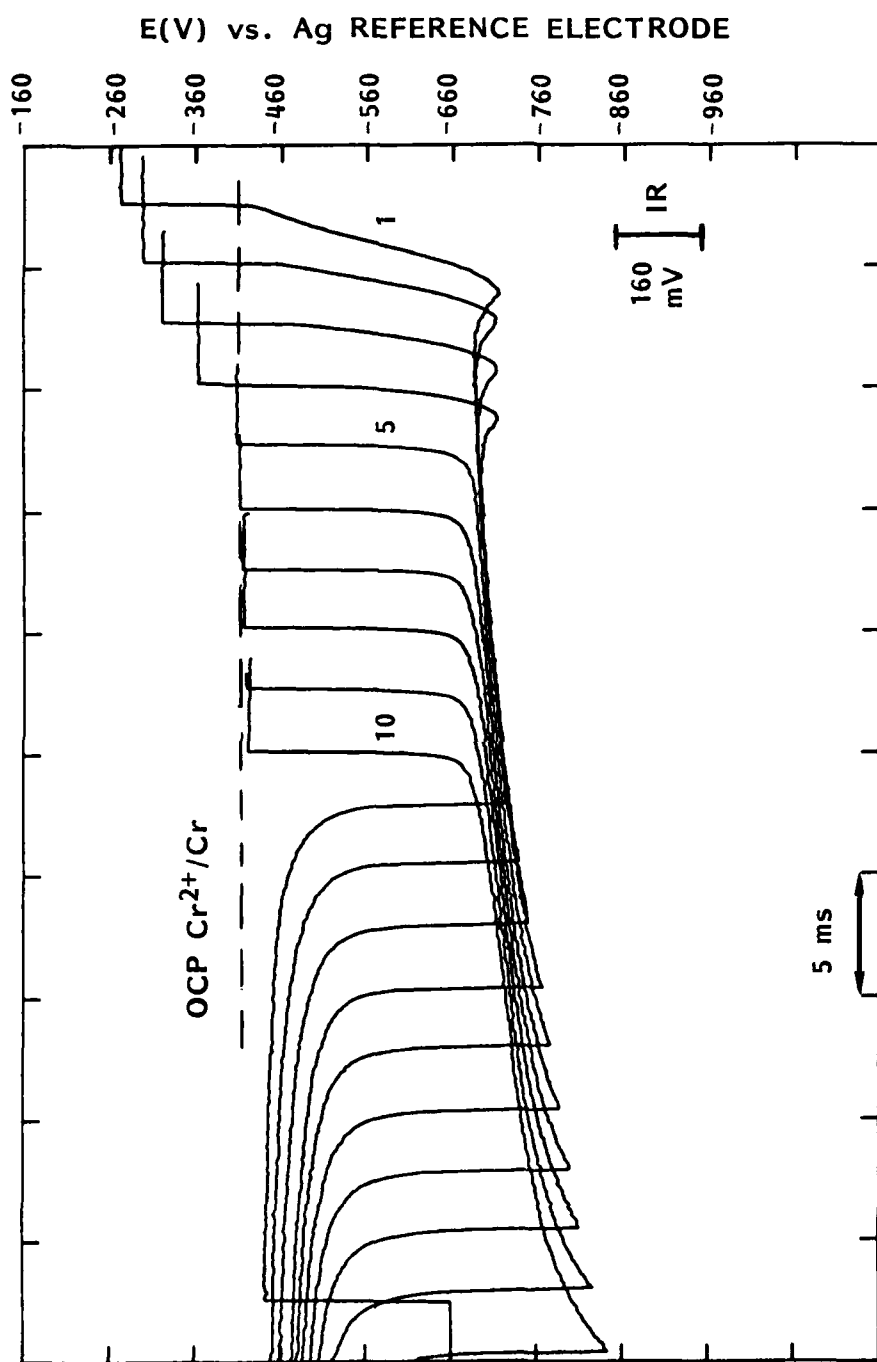


Fig. 66. Ten potential time curves acquired during the galvanostatic pulsing of a copper substrate to deposit Cr metal nuclei from a ternary bromide melt at 335°C. Applied current density = 110 mA cm⁻².

potential is corrected for iR effects of the magnitude shown in Figure 66. Contributions due to concentration polarization do not completely account for this overpotential, and it must be concluded that overpotential corresponding to the development as well as the formation of nuclei must continue to contribute at this early stage. It can be seen from the interpulse period that by the end of the fifth pulse the open circuit potential of the electrode has reached that of the Cr^{2+}/Cr rest potential which implies that the activity of chromium at the copper surface is close to unity. After subsequent pulses, the potential during the interpulse period decays to this same value within a few millivolts which suggests that the interpulse period is sufficient to allow the concentration gradients developed during the current pulse to decay away justifying control of concentration polarization by the ratio of $t_{\text{off}}/t_{\text{on}}$. In contrast, the deposition on nickel and stainless steel showed no evidence for an initial nucleation process, although well into the plating a sharp prepeak was seen in the transient for deposition on nickel. Current efficiencies were satisfactory for such preliminary studies where plating conditions were far from optimal.

Table 47 compares results from this work with other data for chromium in the literature. It is clear that the low melting bromide electrolyte offers advantages from chromium plating and refining, particularly under pulsed conditions. The development of such processes requires a detailed study of the relationship between plating conditions and deposit structure. Such work also needs concomitant support from continued fundamental studies on the mechanism of nucleation and growth of metal.

Molybdenum coating from lower melting electrolytes are highly desirable for many commercial applications. Previous workers had emphasized the need for high temperature to obtain coherent deposits by direct current procedures. In addition, it was suggested that the electrolytes were unstable at lower temperatures. The electrolytes based upon lithium chloride-potassium chloride, prepared and operated here, were found to be stable at 450-550°C, and preliminary experiments (see Table 48) showed that pulse plating could yield coherent coatings as illustrated in Figures 67 and 68.

These preliminary results have demonstrated that high rate, high current efficiency, low temperature molten salt plating processes for chromium and molybdenum are realistic goals using pulsed techniques. The knowledgeable application of alkali metal chloride and bromide electrolyte baths will ensure that substrates currently excluded by thermal effects can be utilized in these baths operating at low temperatures (<450°C). The next stage in their development is the establishment of the optimal conditions required for plating which will be based upon studies of the relationship between the electrochemical parameters in pulsed plating and the structure and properties of the coatings so formed. Successful achievement of these goals will lead to processes which will provide both chromium and molybdenum plates with and without interstitial elements as well as alloy coatings of chromium and molybdenum.

TABLE 47

COMPARISON OF CONDITIONS FOR THE ELECTRODEPOSITION OF CHROMIUM
FROM DIFFERENT ELECTROLYTES

Plating Bath	Aqueous	FLiNak	LiCl-KCl	LiCl-KCl	LiBr-KBr-CsBr
M Pt OC	<4	454	362	362	236
Solute salt	H ₂ SO ₄ CrO ₃	CrF ₃	CrCl ₂	CrCl ₂	CrBr ₂
Conc. wt %		15	0.2-15	0.25	0.6
Operating Temp., °C	20-60	800	450-500	450	300-340
DC plating j (Adm ⁻²)	10-50	2-3	0.1-1	0.08	1-2
Pulse plating Potentiostatic j _{av} (Adm ⁻²)	-	-	2	-	
Galvanostatic j _{av} (Adm ⁻²)	-	-	-	0.23	3.2
Current efficiency	10-30	65	80	90	70
Plating Rate (microns/hr)	3-70	15	28	13	20-60
Substrate compn.	Cu/Ni flash	Steel	Steel	Cu, Ni	Cu, Ni, steel
Deposit adhesion	Good	Good	Poor	Good	Good/poor
Surface fluxing		Very good		unknown	
Reference	[79,80]	[30]	[33]	[32]	[34]

TABLE 48

ELECTROPLATING EXPERIMENTS - MOLYBDENUM DEPOSITION FROM A LITHIUM CHLORIDE-POTASSIUM CHLORIDE-POTASSIUM HEXACHLOROMOLYBDATE SOLUTION AT 455°C

Substrate	Current mA	$t_{\text{off}}/\text{ton}$	Total		Method	Comments
			Charge C	Current Efficiency		
Nickel	6	-	86	46	DC	Powdery.
Nickel	6	-	86	100	D	Grey deposit. Wing formed at 3-phase boundary.
Nickel	20	-	132	66	DC	Grey deposit. Wing formed at 3-phase boundary.
Nickel	40	-	150	58	DC	Grey dendritic.
Nickel	50	10	207	58	P	Dark grey deposit.
Nickel	100	11	297	81	P	Dark grey coating covering electrode.
Nickel	200	44	266	95	P	Dark coating - some dendrites at edges.
Nickel	400	44	1322	100	P	Clean dendrite free surface with good coverage.
Nickel	800	88	482	100	P	Grey deposit - no loose material.
Nickel	400	11	935	-	P	Black deposit - loose powder.
Nickel	1000	110	472	100	P	Grey deposit - no loose material.
Nickel	1000	110	458	> 100	P	Dark, poorly coherent deposit.
Stainless steel	1000	110	456	> 100	P	Large angular collar at 3-phase boundary, poorly coherent.
Stainless steel	1000	440	61	-	P	Three-phase boundary deposit.

a)



b)

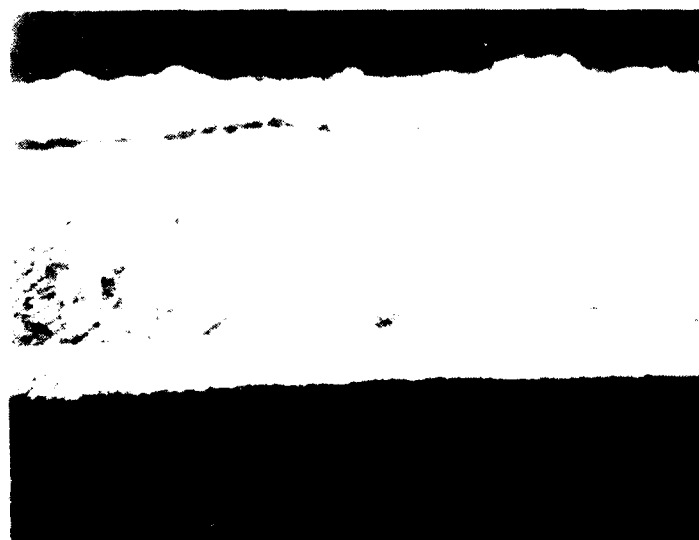


Fig. 67. Micrographs of molybdenum deposit on nickel: (a) 10.5X; (b) 100X (longitudinal section).



Analysis of Cross Section of Molybdenum
on Nickel using EDAX

<u>Area</u>	<u>Elemental Ni Wt%</u>	<u>Analysis Mo Wt%</u>
A	100	-
B	100	-
C	100	-
D	4.5	95.5
E	4.5	95.5

Fig. 68. Robinson backscattered electron image of cross section of a molybdenum deposit on nickel from LiCl-KCl bath at 450°C. Points A to E analyzed for elemental content.

5.0 REFERENCES

1. C. L. Mantell, Electrochemical Engineering (McGraw Hill, 1960).
2. S. Senderoff, *Metall. Rev.*, 1, 97 (1966).
3. D. Inman and S. H. White, *J. Applied Electrochem.*, 8, 375 (1978).
4. G. W. Mellors and S. Senderoff, Canadian Patent 688,546 (1964).
5. S. Senderoff, in Modern Electroplating, ed. F. A. Lowenheim (New York: Wiley, 1974), p. 473.
6. B. L. Davis and C. H. R. Gentry, *Metallurgia*, 53, 3 (1956).
7. A. N. Baraboshkin, K. A. Kaliev and A. B. Aksent'sev, *Elektrokhimiya*, 14, 1836 (1978).
8. K. H. Stern and S. T. Gadomski, Proc. Fourth International Symposium on Molten Salts (New Jersey: The Electrochemical Society, 1984), p. 611.
9. C. L. Hussey and T. M. Laher, in Proc. Third International Symposium on Molten Salts (New Jersey: The Electrochemical Society, 1981), p. 256.
10. T. B. Scheffer, C. L. Hussey, K. R. Seddon, C. M. Kear and P. D. Armitage, *Inorg. Chem.*, 22, 2099 (1983).
11. D. L. Brotherton, Ph.D. Dissertation, The University of Tennessee (1974).
12. J. L. Meyer and R. E. McCarley, *Inorg. Chem.*, 17, 1867 (1978).
13. G. Mamantov et al., Proc. First International Symposium on Molten Salts (New Jersey: The Electrochemical Society, 1976), p. 234.
14. F. A. Cotton and G. Wilkinson, Advanced Inorganic Chemistry (New York: Interscience, 1980).
15. F. A. Cotton and R. A. Walton, Multiple Bonds Between Metal Atoms (New York: Wiley, 1982).
16. S. H. White and U. M. Twardoch, unpublished work, 1985.
17. A. D. Graves, G. J. Hills and D. Inman, in Advances in Electrochemistry and Electrochemical Engineering, ed. P. Delahay (Interscience, 1966), p. 117.

18. S. H. White, in Ionic Liquids, eds. D. Inman and D. L. Lovering (London: Plenum, 1981).
19. S. H. White, in Molten Salt Techniques, eds. D. L. Lovering and R. J. Gale (Plenum, 1983), Vol. 1, p. 19.
20. W. J. Hamer, M. S. Malmberg and B. Rubin, *J. Electrochem. Soc.*, 103, 8 (1956); 112, 750 (1965).
21. N. K. Gupta, *Rev. Sci. Instr.*, 42, 1368 (1971).
22. H. A. Laitinen, Y. Yamamura and I. Uchida, *J. Electrochem. Soc.*, 125, 1450 (1978).
23. J. P. Hoare, *Electrochim. Acta*, 27, 1751 (1982); *J. Electrochem. Soc.*, 131, 1808 (1984).
24. C. J. Smithells, Metals Reference Book, 5th Edition (Butterworths, 1978).
25. C. R. Wolfe and R. D. Caton, *Anal. Chem.*, 43, 663 (1971).
26. L. Yang and R. G. Hudson, *Trans. AIME*, 215, 589 (1959).
27. T. Berzins and P. Delahay, *J. Amer. Chem. Soc.*, 75, 555 (1953).
28. G. Fasang, B. Rozsondai and L. Tomesanyi, *Magy. Kem. Foly.*, 76, 233 (1970).
29. A. Sasahira and T. Yokokawa, *Electrochim. Acta*, 29, 533 (1984).
30. G. W. Mellors and S. Senderoff, in Appl. Fund. Thermod. Metal Processing, Proc. Conf. Therm. Properties Mat. (Univ. Pittsburgh, 1967), p. 81.
31. T. Yoko and R. A. Bailey, *J. Electrochem. Soc.*, 131, 2590 (1984).
32. S. H. White and U. M. Twardoch, Proc. Fourth International Symposium on Molten Salts (New Jersey: The Electrochemical Society, 1984), p. 559.
33. D. Inman, T. Vargas, S. Duan and P. G. Dudley, in Proc. Fourth International Symposium on Molten Salts (New Jersey: The Electrochemical Society, 1984), p. 545.
34. S. H. White and U. M. Twardoch, unpublished work, 1985.
35. G. P. Smith, in Molten Salt Chemistry, ed. M. Blander (New York: Interscience, 1964), p. 427.
36. D. Inman, J. C. Legey and R. Spencer, *J. Electroanal. Chem.*, 61, 289 (1975).

37. K. P. V. Lei, J. M. Hiegel and T. A. Sullivan, *J. Less-Common Metals*, 27, 353 (1972).
38. S. C. Levy and F. W. Reinhardt, *J. Electrochem. Soc.*, 122, 200 (1975).
39. C. L. Hussey, L. A. King and J. K. Erbacher, *J. Electrochem. Soc.*, 125, 561 (1978).
40. I. I. Naryshkin, V. P. Yurinskii and P. T. Stangrit, *Elektrokhimiya*, 5, 1043 (1969).
41. K. Cho and T. Kuroda, *Denki Kagaku*, 39, 206 (1971).
42. H. A. Laitinen, C. H. Liu and W. S. Ferguson, *Anal. Chem.*, 30, 1266 (1958).
43. G. Stehle, J. J. Duruz and D. Landolt, *J. Appl. Electrochem.*, 12, 591 (1982).
44. P. Bowles and P. C. Newdick, *Electroplating and Metal Finishing*, (Jan, 1971).
45. I. Ahmad, W. A. Spiak and G. J. Janz, *J. Appl. Electrochem.*, 11, 291 (1981).
46. S. Fletcher et al., *J. Electroanal. Chem.*, 159, 267 (1983).
47. S. Fletcher, *J. Chem. Soc. Faraday Trans. 1*, 79, 467 (1983).
48. M. Fleischmann and H. R. Thirsk, in Advances in Electrochemistry and Electrochemical Engineering, ed. P. Delahay (New York: Wiley, 1963), Vol. 3.
49. J. A. Harrison and H. R. Thirsk, in Electroanalytical Chemistry, ed. A. J. Bard (New York: Marcel-Dekker, 1971), Vol. 5, p. 68.
50. T. Vitanov, A. Popov and E. Budevski, *J. Electrochem. Soc.*, 121, 207 (1974).
51. G. Gunawardena, G. J. Hills, I. Montenegro and B. Scharifker, *J. Electroanal. Chem.*, 138, 225 (1982).
52. D. D. MacDonald, Transient Techniques in Electrochemistry (Plenum, 1977).
53. R. Kaischew and B. Mutaftschiew, *Electrochim. Acta*, 10, 643 (1965).
54. D. J. Astley, J. A. Harrison and H. R. Thirsk, *Trans. Faraday Soc.*, 64, 192 (1968).

55. G. J. Hills, D. J. Schriffin and J. Thompson, *Electrochim. Acta*, 19, 657,671 (1974).
56. G. Gunawardena, G. J. Hills, I. Montenegro and B. Scharifker, *J. Electroanal. Chem.*, 138, 255 (1982).
57. G. Gunawardena, G. J. Hills and I. Montenegro, *J. Electroanal. Chem.*, 138, 241 (1982).
58. F. Lantelme and J. Chevalet, *J. Electroanal. Chem.*, 121, 311 (1981).
59. M. Y. Abyaneh and M. Fleischmann, *Electrochim. Acta*, 27, 1513 (1982).
60. T. Erdey-Gruz and M. Volmer, *Z. Physik. Chem.*, 157, 165 (1931).
61. R. Kaishev, *Fortschr. Miner.*, 38, 7 (1960).
62. T. Vargas, private communication, 1986.
63. K. J. Vetter, *Electrochemical Kinetics* (Academic Press, 1967).
64. D. Walton, *J. Chem. Phys.*, 37, 2182 (1962).
65. A. Milchev, S. Stoyanov and R. Kaishev, *Thin Solid Films*, 22, 255, 267 (1974).
66. A. Milchev and S. Stoyanov, *J. Electroanal. Chem.*, 72, 33 (1976).
67. R. Kaishev, A. Schelu'dko and G. Bliznakov, *Ber. Bulg. Akad. Wiss. Physik. Ser.* 1.137 (1950); see also Ref. 56.
68. G. A. Gunawardena, G. J. Hills and I. Montenegro, *Faraday Symp. Chem. Soc.*, 12, 90 (1977).
69. V. M. Rudoi, V. N. Samoilenko, E. V. Kantsler and A. I. Levin, *Elektrokhimiya*, 11, 566 (1975).
70. G. Rubel and M. Gross, *Corr. Sci.*, 15, 261 (1975).
71. M. V. Susic, Extended Abstract, ISE Meeting, Trondheim (1979), 190.
72. H. S. Ray, N. K. H. Tumanova and S. N. Flengas, *Can. J. Chem.*, 55, 656 (1977).
73. S. H. White, unpublished work, 1978.
74. J. R. Moyer, J. C. Evans and G. Y-S. Lo, *J. Electrochem. Soc.*, 113, 158 (1966).

75. H. Bloom, The Chemistry of Molten Salts (New York: Benjamin, 1967), p. 122.
76. S. Senderoff and A. Brenner, J. Electrochem. Soc., 101, 16,38,31 (1954).
77. S. Senderoff and G. W. Mellors, J. Electrochem. Soc., 114, 586 (1967).
78. S. Senderoff and G. W. Mellors, J. Electrochem. Soc., 114, 556 (1967).
79. G. Dubpernell, in Modern Electroplating, ed. F. F. Lowenheim (New York: Wiley, 1974), p. 87.
80. Canning Handbook on Electroplating, E&F.N. Spon (1978).

END

10-86

DTIC